Statistical properties of single and multiple active particles

A thesis submitted to

Tata Institute of Fundamental Research, Mumbai, India
for the degree of
Doctor of Philosophy
in
Physics

By

Prashant Singh

International Centre for Theoretical Sciences
Tata Institute of Fundamental Research
Bangalore 560089, India

November, 2022

Declaration

This thesis is a presentation of my original research work. Wherever contributions of others are involved, every effort is made to indicate this clearly, with due reference to the literature, and acknowledgement of collaborative research and discussions.

The work was done under the guidance of Prof. Anupam Kundu, at International Centre for Theoretical Sciences, Tata Institute of Fundamental Research (ICTS-TIFR), Bangalore.

Prashant Singh

Prashant Singh

In my capacity as supervisor of the candidates thesis, I certify that the above statements are true to the best of my knowledge.

Anupam Kundu

Anupam Kundu

Date: November 17, 2022

Acknowledgements

I would like to thank my advisor Dr. Anupam Kundu for his guidance and support during my PhD. Discussions with him have mostly helped me in gaining a wider understanding about the problems. Two qualities that I find most attractive about him: first, he is very professional and second, he is very intuitive. I hope to instill these qualities even in my research. Thank you for giving me the privilege of being your first student. I would also like to convey my best regards to his family.

I benefitted a lot through my discussions with Dr. Abhishek Dhar and Dr. Sanjib Sabhapandit. Also, they were kind enough to be a part of my thesis monitoring committee. I would like to express my gratitude towards them. Recently, I also got to collaborate with Dr. Satya N. Majumdar. I have learned a great deal from his papers and review articles. I would like to thank him for this. I am also grateful to Dr. Arnab Pal with whom I have had the opportunity to collaborate on different projects. He has been very kind towards me and guided me at different times of my PhD. Working with him has always been a joyful experience. I also thank Dr. Urna Basu for various discussions and for being a part of the committee that evaluated my synopsis.

My stay at ICTS has been a pleasant one. This, in retrospect, is partly because of my friends. I believe our batch (constituted by Arnab, Soummyadip, Monica, Pronobesh, Sugan, Srikanth, Pinak, Shashank and myself) was a set of most hardworking people at ICTS. In future, I would like to be as intuitive as Arnab, as knowledged as Soummyadip, as perseverant as Monica, as sharp as Pronobesh, as disciplined as Sugan, as rigorous as Srikanth, as computationally-skilled as Pinak and as balanced as Shashank. Apart from them, I also thank my other friends from ICTS, namely, Santhosh, Joydeep, Akhil, Varun, Manisha, Kohinoor, Saikat, Jitendra, Basudeb, Saurav, Suman da, Debarshee da, Subhajit da, Soumi, Dipankar and all other students and postdocs. They have always been very amicable towards me. In particular, discussions with Suman da on various academic and non-academic matters are always eye-opening. I also cherish my friendship with Kanaya, Arghya da, Subhadip da, Amit da and Aritra da who were there when I had joined ICTS. I remember how Kanaya had taught me (a novice) simulations of run and tumble particles. I extend my best wishes to her. I would also like to thank all professors, academic and non-academic staffs at ICTS for making it a best place to work at.

Before coming to ICTS, I was fortunate to have very supportive teachers in my life. Right from my schooling at Sonada Model school and St. Robert's School till my bachelors at St.

Joseph's college, Darjeeling, I owe a great deal to my teachers. In particular, I would like to acknowledge Mr. Kaushal Chettri, Prof. Debarghya Goswami and Dr. Pragati Pradhan who were very instrumental for my entry into research. During my masters at IIT, Kanpur, I got to know many new people who subsequently became good friends. Out of them, I still share a great camaraderie with Manika and Soummyadip. Both of them are my favourites.

Finally and most importantly, I would like to thank my parents and my family for constantly nurturing me. I dedicate this thesis to them.

Publications [1]

1* Generalised 'Arcsine' laws for run-and-tumble particle in one dimension, Prashant Singh and Anupam Kundu, *J. Stat. Mech.* 083205 (2019).

2* Run-and-tumble particle in inhomogeneous media in one dimension, Prashant Singh, Sanjib Sabhapandit and Anupam Kundu, *J. Stat. Mech.* 083207 (2020).

3* Local time for run and tumble particle, Prashant Singh and Anupam Kundu, *Phy. Rev. E* 103 042119 (2021).

4* Crossover behaviours exhibited by fluctuations and correlations in a chain of active particles, Prashant Singh and Anupam Kundu, *J. Phys. A: Math. Theor.* 54 305001 (2021).

5* Mean area of the convex hull for a run and tumble particle in two dimensions, Prashant Singh, Anupam Kundu, Hendrik Schawe and Satya N. Majumdar *J. Phys. A: Math. Theor.* 55 225001 (2022).

Other publications which are not part of this thesis.

6 Random acceleration process under stochastic resetting, Prashant Singh, *J. Phys. A: Math. Theor.* 53 405005 (2020).

7 Extremal statistics for stochastic resetting systems, Prashant Singh and Arnab Pal, *Phy. Rev. E* 103 052119 (2021).

8 Extreme value statistics and arcsine laws for heterogeneous diffusion processes, Prashant Singh *Phys. Rev. E* 105 024113 (2022).

9 Coarse-grained Stochastic Model of Myosin-Driven Vesicles into Dendritic Spines, Youngmin Park, Prashant Singh and Thomas G. Fai, *SIAM J. Appl. Mat.* 82(3) 793-820 (2022).

10 First-passage Brownian functionals with stochastic resetting, Prashant Singh and Arnab Pal, *J. Phys. A: Math. Theor.* 55 234001 (2022).

[1] $*$ part of this thesis

Contents

Chapter 1

Overview

Broadly speaking, out-of-equilibrium behaviour in a statistical system commonly arises in three ways: First by suitably quenching a system below certain temperature such that physical observables take experimentally unachievable time to relax to their equilibrium value. Such systems belong to a widely-studied state of matter called glass [1]. Second class of non-equilibrium systems are the ones that are driven from the boundary by maintaining a difference in the chemical potential or the temperature at the two ends [2–4]. Consequently, there is a flow of particle current or energy current through the system and one is often interested in the transport properties of these currents. Finally, in the third class, the energy drive is maintained at the local scale and every individual unit of the system experiences a chemical difference or a temperature difference [5–10]. This thesis presents a theoretical and numerical study on the third class of non-equilibrium systems which are known as "active systems" in the literature.

In equilibrium, the detailed balance and the fluctuation dissipation relations are known to be valid [11–16]. While detailed balance is a statement about the probabilistic current balance between every pair of microscopic states, the fluctuation-dissipation relation gives the linear response of the system in terms of its equilibrium correlations [16]. We refer to appendix 8.1 for a brief discussion on these equilibrium conditions. For a diffusing particle in presence of a confining potential $V(\vec{r})$ [17–20], the position $\vec{r}(t)$ is often described the following evolution equation:

$$\frac{d\vec{r}}{dt} = -\vec{\nabla}V(\vec{r}) + \sqrt{2k_BT}\ \vec{\eta}(t), \tag{1.1}$$

where $\vec{\eta}(t) = (\eta_x(t), \eta_y(t), \eta_z(t))$ is the Gaussian white noise with zero mean and correlation $\langle \eta_i(t)\ \eta_j(t') \rangle = \delta_{i,j}\ \delta(t - t')$. For this model, one can rigorously prove that all equilibrium conditions mentioned above are satisfied [21–25]. However, our interest, in this thesis, are active systems whose constituent particles violate these conditions and thus are intrinsically driven out-of-equilibrium right at the microscopic scale [5, 8, 26–28]. These particles can, individually, consume the supplied energy and generate a systematic movement out of it. Observe that this behaviour is intrinsically different than that of a diffusing particle where the motion is generated due to the thermal bombardments from the surrounding molecules. Here, instead, motion is an autonomous property of the particle itself.

Mechanisms for generating this autonomous motion vary from system to system. For example, some species of bacteria like E. Coli swim through the medium by rotating a collection of flagella emanating out of their body [29]. When these helical-shaped flagella bundle together and rotate in the counter-clockwise direction, the cell experiences a push that gives rise to the motion in the forward direction. This mode of motion is called a 'run'. After a random time, some of the flagella disassemble out and start rotating in the clockwise direction. During this event, known as 'tumble', the cell simply rotates and does not move forward appreciably. Bacteria, thus, move in a series of runs and tumbles. Experimentally, the typical run duration in a uniform medium without nutrient-gradient is found to be $\sim$ 1s while the tumbling duration is $\sim$ 0.1s [30]. Moreover, the run time is found to be exponentially distributed in some types of E. Coli [29,30].

Even though, historically, the subject of active matter began as a description for the biological systems, active motion has been realised experimentally in synthetic objects also. For instance, asymmetric chemical reaction around the surface of a spherical particle (known as Janus particle) coated with some catalysis generates self-propulsion due to the mechanism of diffusiophoresis [31, 32]. Other examples include granular matter subjected to shaking [33–35], magnetic colloids with DNA linkers [36] and janus particles in a laser beam [37]. Designing synthetic objects to generate controlled active motion is an active area of research [38]. Recent focus has been on tuning this motion for various potential applications like targeted delivery of drug and biomarking [39]. Due to their autonomous motion, active particles offer advantageous functionality for delivery actions compared to the thermal particles.

When many of these self-propelling particles are put together, they exhibit several intriguing emergent phenomena which are otherwise absent in their passive counterparts. Paradigmatic example is the collective coherrent motion as seen in flocks of birds and schools of fish [40–43]. A

minimal model that captures this behavour is the Vicsek model where every particle moves with a constant speed and also interacts with the surrounding particles to align its direction along the average direction of motion of the surrounding particles [41]. This model gives a transition as a function of density between two states: one where particles move randomly (low density) and the other where particles move in the same direction (high density). Another fascinating phenomenon in active systems is the motility-induced phase separation where particles with purely repulsive interactions undergo phase separation into dilute and dense regions [44–47]. Note that such phase separation can occur in thermal systems only in presence of attractive interaction [27, 44]. Similarly, one observes other exotic collective phenomena like non-existence of the equation of state in pressure [48] and active turbulence [49–51]. The last example is particularly intriguing because these systems typically occur at low Reynold's number ($\sim 10^{-5}$) where turbulent behaviour is not anticipated [52].

Research on active matter in the last two decades has mostly focused on unravelling and understanding these collective behaviours. However, various recent studies have revealed that active systems also show distinct non-thermal behaviours even at the level of a single particle or few particles. For example, the probability distribution of finding the particle in position $\vec{r}(t)$ at time t is strictly non-Gaussian with far tails characterised by interesting large deviation functions [53–71]. Also, contrarily to the thermal particles, the steady-state distributions are found to have non-Boltzmann forms both experimentally and theoretically [53, 70, 72–82] with non-zero entropy productions [83–90]. Also, the first-passage properties are very different than that of a Brownian particle [54, 70, 71, 91–96]. Escape problems for a self-propelled particle also exhibit unusual beaviours like escape through a higher potential barrier instead of the lower one and so on [97–100]. Thus, studying non-interacting active particles has also garnered significant interest in the last few years.

Most of these studies have been performed in the context of three archetypal models of an active particle - active Brownian particle, run and tumble particle and active Ornstein-Uhlenbeck particle. We will refer to them as ABP, RTP and AOUP respectively. If $\vec{r}(t)$ denotes the position of the particle, then the time evolution equation in the overdamped limit reads

$$\frac{d\vec{r}}{dt} = \sqrt{2D}\ \vec{\eta}(t) + \vec{F}^A(t). \tag{1.2}$$

The first term $\sqrt{2D}\ \vec{\eta}(t)$ is the translational diffusion term with $\vec{\eta}(t) = (\eta_x(t), \eta_y(t), \eta_z(t))$ being the Gaussian white noise. It is characterized by the zero mean and correlation $\langle \eta_i(t)\eta_j(t')\rangle =$

$\delta_{i,j}\delta(t-t')$. On the other hand, the second term $\vec{F}^A(t)$ is the active part to the dynamics and its precise form depends on the choice of model. For the three models mentioned above, it has the following forms:

ABP: In this model, the particle performs the rotational diffusion in two dimensions in addition to the translational diffusion [10,34]. The particle moves along a direction ϕ with respect to the x-axis which itself performs the Brownian motion. Exact form of $\vec{F}^A(t)$ in Eq. (6.1) for this model is

$$\vec{F}^A(t) = v_A\,(\cos\phi, \sin\phi)\,, \qquad \text{with} \tag{1.3}$$

$$\frac{d\phi}{dt} = \sqrt{2D_{rot}}\;\xi(t), \tag{1.4}$$

where v_A (>0) is the speed of the ABP and D_{rot} (>0) is the rotational diffusion constant. Also, here $\xi(t)$ is the usual Gaussian white noise with zero mean and delta correlation. Experimentally janus particles are known to perform active Brownian motion [31].

RTP: Another well-studied model for the active motion is the run and tumble particle (RTP) where the particle runs ballistically with speed v_0 along some direction. In two dimensions, this direction may be represented by an angle $\phi \in [0, 2\pi]$ with respect to the x-axis [27]. At a constant rate γ, the particle tumbles during which it chooses a new direction ϕ' uniformly between $[0, 2\pi]$ for the next run. Thus, the particle moves in a series of runs interspersed by tumbles. For this case, $\vec{F}^A(t)$ in Eq. (6.1) takes the form

$$\vec{F}^A(t) = v_0\,(\cos\phi, \sin\phi)\,. \tag{1.5}$$

As discussed before, certain species of bacteria like E. Coli perform this kind of motion [29]. Moreover, since the typical duration for a run is large compared to the tumbling duration, we assume tumbles to be instantaneous throughout this thesis. Generalisations of RTP with non-instantaneous tumbles can be found in [81, 93].

AOUP: The third class of model for the active motion is the active Ornstein Uhlenbeck particle where $\vec{F}^A(t)$ follows the dynamics [101]

$$\frac{d\vec{F}^A}{dt} = -\zeta\vec{F}^A + \sqrt{2D_{OU}}\;\vec{\psi}(t), \tag{1.6}$$

where $\vec{\psi}(t)$ is the Gaussian white noise with $\langle\vec{\psi}(t)\rangle = 0$ and $\langle\psi_i(t)\psi_j(t')\rangle = \delta_{i,j}\delta(t-t')$.

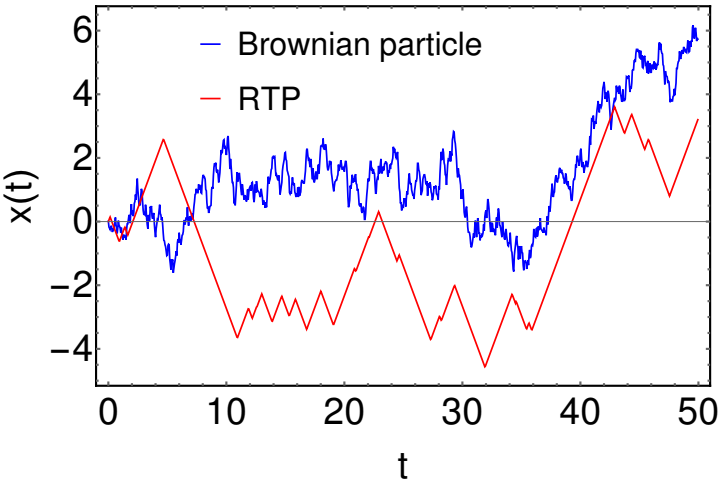

Figure 1.1: Typical trajectories of a run and tumble particle and a Brownian particle. For Brownian particle, the trajectory is more random and changes its direction very frequently. On the other hand, the RTP displays a persistent behaviour whereby it has non-vanishing likeability to move along a given direction.

To illustrate more precisely the effect of activity in these models, we present below a brief discussion on the statitical properties of the position of a single RTP. This will be relevant for the later parts of this thesis as most of our results are based on the run and tumble motion.

1.1 Position distribution of a run and tumble particle

Historically, the first account of the run and tumble model appeared in the works of Fürth [102] and Taylor [103]. Taylor considered the discrete run and tumble model as a simple way to introduce correlations between movements of a particle at two different time steps. Later Goldstein and Kac studied the probability distribution of this model and showed that it obeys the Telegrapher equation [104,105]. Over the course of time, this model has found applications in chromatography [106], in electromagnetic theory [107] and also in transport theory [108] [see [109] and references therein]. Particularly, in the random walk literature, this model was known as the persistent random walker and a number of results were already derived for them [109–113]. The present day interest arose due to its biological applications in mimicking the motion of some species of bacteria like E. coli [29,30].

The evolution of the position $x(t)$ of a RTP in one dimension is governed by the equation

$$\frac{dx}{dt} = v_0\sigma(t), \tag{1.7}$$

where $\sigma(t)$ is the telegraphic or dichotomous noise that alternates between ± 1 with some rate γ. The noise $\sigma(t)$ at different times are exponentially correlated as $v_0^2\langle\sigma(t)\sigma(t')\rangle = v_0^2 e^{-2\gamma|t-t'|}$. Due to this history dependence, the run and tumble motion is a non-Markovian process. However, in the limit $v_0 \to \infty$ and $\gamma \to \infty$ keeping the ratio $D_R = v_0^2/2\gamma$ fixed, the noises become delta correlated and the RTP dynamics becomes indistinguishable from the Brownian motion (atleast for the typical fluctuations in x). On the other hand, for $\gamma \to 0$, the noise $\sigma(t) = \sigma_0$ is just a constant and from Eq. (1.7), it follows that the particle performs the ballistic motion. Hence, one can interpolate between ballistic and diffusive motions by appropriately tuning the parameter γ

In Figure 1.1, we have compared the typical trajectories of a RTP and a Brownian particle by numerically simulating Eq. (1.7). Compared to the Brownian motion, we see that the trajectory of a RTP is more regular and show non-vanishing persistence along a given direction. By persistence, we mean the ability of the particle to continue moving along the same direction. This drastically changes the behaviour of the particle. For example, the mean-squared displacement of $x(t)$ reads as [70]

$$\langle x^2(t)\rangle = \frac{v_0^2}{\gamma}t - \frac{v_0^2}{2\gamma^2}\left(1 - e^{-2\gamma t}\right). \tag{1.8}$$

We see that for $t \ll \gamma^{-1}$, the MSD scales ballistically as $\sim t^2$ which is different than the diffusive scaling at $t \gg \gamma^{-1}$. This time scale $\tau_A = \gamma^{-1}$ which sets the time scale for the crossover will be referred to as the activity time scale. Thus, at small and intermediate time scales (compared to τ_A), we get distinct non-Brownian behaviour in this model.

This difference is also seen in the probability distribution function $\mathcal{P}_{\sigma_f}(x,t|0,\sigma_0)$ of finding the particle at x at time t with velocity $\sigma_f v_0$ such that it was initially at the origin with velocity $\sigma_0 v_0$. Both σ_0 and σ_f can be either $+$ or $-$. To derive the master equation for the evolution of $\mathcal{P}_{\sigma_f}(x,t|0,\sigma_0)$, we first look at the contributions to $\mathcal{P}_{\sigma_f}(x,t+\delta t|0,\sigma_0)$ from various events for small δt. The first contribution is from those trajectories for which the RTP was at the position $(x - \sigma_f v_0 \delta t)$ at time t with velocity direction $\sigma(t) = \sigma_f$. In the further time δt, the RTP did not flip its velocity so that $\sigma(t+\delta t) = \sigma_f$ and also moved a distance $\sigma_f v_0 \delta t$ so that the final position becomes x. Note that the probability of these events is $(1 - \gamma\delta t)$ since the particle does not flip its velocity direction. The other contribution to $\mathcal{P}_{\sigma_f}(x,t+\delta t|0,\sigma_0)$ comes from those events where the RTP was at position x at time t with orientation $\sigma(t) = -\sigma_f$. In the next time interval $[t, t+\delta t]$, the RTP just flipped its velocity direction so that $\sigma(t+\delta t) = \sigma_f$. Such events

occur with a probability $\gamma\delta t$. Hence, the total contribution is given by

$$\mathcal{P}_{\sigma_f}(x,t+\delta t|0,\sigma_0) = (1-\gamma\delta t)\ \mathcal{P}_{\sigma_f}(x-\sigma_f v_0\delta t,t|0,\sigma_0) + \gamma\delta t\ \mathcal{P}_{-\sigma_f}(x,t|0,\sigma_0). \tag{1.9}$$

Finally expanding the distribution as a Taylor's series in δt and taking the $\delta t \to 0$ limit, we get

$$\begin{aligned}
\partial_t \mathcal{P}_+(x,t|0,\sigma_0) &= -v_0\partial_x\mathcal{P}_+(x,t|0,\sigma_0) - \gamma\mathcal{P}_+(x,t|0,\sigma_0) + \gamma\mathcal{P}_-(x,t|0,\sigma_0),\\
\partial_t \mathcal{P}_-(x,t|0,\sigma_0) &= \quad v_0\partial_x\mathcal{P}_-(x,t|0,\sigma_0) + \gamma\mathcal{P}_+(x,t|0,\sigma_0) - \gamma\mathcal{P}_-(x,t|0,\sigma_0).
\end{aligned} \tag{1.10}$$

These equations have the form of the Telegrapher's equations which have also appeared in several other contexts [109]. If the initial velocity direction σ_0 is chosen from ± 1 with equal probability $1/2$, then the solution $\mathcal{P}(x,t) = \frac{\mathcal{P}_+(x,t|0,\sigma_0)+\mathcal{P}_-(x,t|0,\sigma_0)}{2}$ of the master equation (1.10) is given by [70, 114]

$$\mathcal{P}(x,t) = \frac{e^{-\gamma t}}{2}\left[\delta(x-v_0t) + \delta(x+v_0t) + \frac{\gamma}{2v_0}\left\{I_0(\tilde{w}) + \frac{\gamma}{\tilde{w}}I_1(\tilde{w})\right\}\Theta\left(v_0t-|x|\right)\right], \tag{1.11}$$

where $\tilde{w} = \frac{\gamma}{v_0}\sqrt{v_0^2t^2-x^2}$, $I_\nu(z)$ is the modified Bessel function of the first kind and $\Theta(z)$ is the Heaviside theta function. Few remarks are in order. The distribution possesses two parts: two delta functions at $x = \pm v_0t$ and a non-delta function part. The δ-functions arise from those trajectories for which the RTP does not flip its velocity till time duration t: the probability of which is $e^{-\gamma t}$. Since the particle reaches either v_0t or $-v_0t$ depending on its initial σ_0, we get two δ-functions at $x = \pm v_0t$. On the other hand, when it flips its velocity, we get the non-delta function part in Eq. (1.11). The distance traversed in this case is always less than v_0t which gives rise to $\Theta\left(v_0t-|x|\right)$ in the expression. Observe that $P(x,t)$ has support over the finite interval $[-v_0t, v_0t]$ which is different than the Brownian motion where the Gaussian distribution has infinite support. Also the form of $\mathcal{P}(x,t)$ is clearly non-Gaussian. For $t\to\infty$ and $|x|\to\infty$ keeping $|x|/t$ finite, the distribution $\mathcal{P}(x,t)$ admits a large deviation form as shown in [114]. To see this, we use the asymptotic expression $I_\nu(z) \simeq e^z/\sqrt{2\pi z}$ for large z in Eq. (1.11) to obtain

$$\mathcal{P}(x,t) \sim \exp\left[-\gamma t\Psi\left(\frac{|x|}{v_0t}\right)\right], \quad \text{with} \tag{1.12}$$

$$\Psi(y) = 1-\sqrt{1-y^2}, \qquad -1\le y\le 1. \tag{1.13}$$

For $y\to 0$, we have $\Psi(y)\simeq y^2/2$ and the distribution converges to the Gaussian form $\mathcal{P}(x,t)\sim \exp\left(-x^2/4Dt\right)$ with $D = v_0^2/2\gamma$. This form is valid only for the central part of the distribution

which describes the typical fluctuations in x. For atypical fluctuations, one needs to look at the far tail of the distribution for which the full form of the rate function $\Psi(y)$ becomes important. As evident, this form is different than the Gaussian form.

1.2 Motivation and outline of the thesis

We saw that the position distribution of a free RTP has some key differences than that of a passive thermal particle. These differences become more potent at small and intermediate value of γt. On the other hand, at large γt, the effect of activity is seen only in the tails of the distribution. Another way to see this effect at large t is to put the RTP in a confining potential. The steady state distribution thus obtained is strictly non-Boltzmann and violates the detailed balance condition with a net non-zero entropy production. A natural question then is - How does activity affect the properties of a particle beyond position distributions and first-passage properties? Especially, with the current advancements in single active particle experiments [31–33,35–37], it becomes essential to develop theoretical frameworks that can corroborate with the experimental observations. Moreover, in some physical scenarios, the motion of an active particle takes in spatially heterogeneous medium where the motility parameters themselves depend on the position of the particle. For instance, during chemotaxis, the bacteria can sense the temporal signals to detect the presence of nutrient-gradient in the environment [115–119]. Depending on whether the chemo-attractant is near or far, it can modify its flagellar motion so that it spends more (less) time in the region of chemo-attractant (chemo-repellent). For instance when the bacteria are far from the chemo-attractant, they perform less tumbles and longer runs so that they can reach the site of chemo-attractant quickly [30,115]. Thus, studying heterogeneous active models is also important to account for these behaviours. In this thesis, we address the following three topics for active particles:

(a) Effect of activity on the extreme-value statistics and path functionals

(b) Role of spatial heterogeneity

(c) Properties of a tagged particle in a system of many active particles.

We now present an outline of the thesis. We have in total five chapters each based on five publications mentioned above. Each chapter begins with an introduction which gives the necessary background of the problem, explains the relevant mathematical framework and fixes the nota-

tions. Subsequent sections give a more rigorous treatment of the problem and contain most of the technical details with some being relegated to the Appendix. We also present extensive numerical verifications of all our analytical results. Each chapter then ends with a summary where we summarise our main findings of the chapter and their possible future extensions. Below, we discuss briefly the precise problems considered in each of these chapters.

Chapters (2) and (3) address the issues in topic (a) and demonstrate the effect of persistence on the statistics of the extremal quantities and path functionals [120, 121]. More specifically, chapter (2) looks at the *arcsine laws* and chapter (3) looks at the convex hull problem for a RTP. For a stochastic process of fixed duration t and starting from the origin in one dimension, the arcsine laws refer to the statistics of the following three observables: (i) the time t_m at which the particle reaches its maximum distance M, (ii) the time t_r spent on the positive side of the origin and (iii) the last time t_ℓ at which the particle crosses the origin. Interestingly, P. Lévy proved that the cumulative probabilities of these observables are all same for one dimensional Brownian motion and is given by the arcsine function [120]. Question is - How does activity ramify this universality and the three distributions? Chapter (2) addresses this question for a one dimensional RTP. By using the path decomposition technique for Markov processes [122] and the Feynman-Kac formalism [121, 123, 124], we show that the distributions of $t_m,\ t_r$ and t_ℓ depend on the initial velocity orientation $\sigma(0)$. For instance when $\sigma(0)$ is chosen between ± 1 with equal probability $1/2$, we find that the distributions of t_m and t_r are exactly same but the distribution of t_ℓ is slightly different. On the other hand, if $\sigma(0)$ is chosen asymmertically from ± 1, then all three distributions turn out to be different. Exact forms of these distributions are derived for all cases.

Continuing our study on topic (a), chapter (3) looks at the convex hull problem for a two dimensional isotropic RTP. Convex hull refers to the smallest convex polytope that encloses all points in the particle's trajectory [125, 126]. For a two dimensional Brownian motion, the mean area of the convex hull is given by $\langle A(t)\rangle_{BM} = \pi D t$ [127]. While the linear dependence of $\langle A(t)\rangle_{BM}$ on Dt can also be guessed from the dimensional analysis, the exact form can only be obtained by exploiting the connection of $\langle A(t)\rangle_{BM}$ with the statistics of the maximum M and the time t_m to reach this maximum. In chapter (3), we use this connection to demonstrate the effect of persistence on the mean area for a run and tumble particle. We find two different scaling behaviours of $\langle A(t)\rangle$ depending on the observation time t, namely $\langle A(t)\rangle \sim t^3$ for $t \ll \gamma^{-1}$ and $\langle A(t)\rangle \sim t$ for $t \gg \gamma^{-1}$. The crossover function connecting these two scaling regimes is also

derived analytically.

In chapters (4) and (5), we study problems related to topic (b). We look at the motion of a run and tumble particle with direction and position dependent rates of tumble. This means that the telegraphic noise $\sigma(t)$ in Eq. (1.7) changes from $+1$ to -1 with rate $R_1(x)$ and from -1 to $+1$ with another rate $R_2(x)$. For homogeneous case $R_1(x) = R_2(x) = \gamma$ (constant), we saw that the motion of a RTP at late times becomes indistinguishable from the Brownian motion. In chapter (4), we compute the late time behaviours of the free space position distributions, survival probabilities and the exit probabilities from a finite interval for $R_1(x) \neq R_2(x)$ and show that the spatial heterogeneity leads to strict non-Brownian forms even at late times. Chapter (5) then demonstrates the effect of the spatial heterogeneity on the statistics of a functional called *local time* (T_{loc}) which refers to the amount of time that the particle spends in the vicinity of a desired point (say x_{loc}) in the space [128, 129]. For the case when $R_1(x) = R_2(x) \sim |x|^\alpha \quad (\alpha \geq 0)$, we develop a 'path-counting method' which enables us to write the distribution of T_{loc} completely in terms of the probabilities of multiple visits to x_{loc}. Then exploiting this method, we obtain the statistics of T_{loc} both in free space as well as in presence of an absorbing wall.

Finally, we turn to the topic (c) in chapter (6). Motion of a tagged particle in an interacting multi-particle system is a classical problem in statistical physics. Paradigmatic example is the single-file diffusion where particles diffuse in one dimension but with the constraint that they cannot overtake the neighbouring particles [130, 131]. As a result, the order of a particle is maintained throughout its motion. Under this constraint, the mean squared-displacement (MSD) of the position of a tagged-particle grows sub-diffusively with time as $\sim \sqrt{t}$ for larger values of t [132]. In the context of active particles also, the MSD was shown to grow sub-diffusively as $\sim \sqrt{t}$ at late times similar to the single-file diffusion [133–136]. Numerically, it was found that the MSD possesses a scaling form in t/τ_A with τ_A being the activity timescale [136]. However, these studies are often numerical based and analytic calculations rely largely on hydrodynamic approximations or mean-field approximations [133–136]. Chapter (6) looks at a simple and analytically tractable model of N ($\gg 1$) active particles with nearest-neighbour harmonic interactions. Our main goal is to study the interplay of interaction and activity on the dynamics of tagged particles. For three models of active particles, namely RTP, AOUP and ABP, we obtain the exact variance and the two-point correlation functions from which we extract various scaling forms and scaling functions. For example, when the particles are interacting and $N \to \infty$, the variance has a crossover from $\sim t^\nu$ scaling at $t \ll \tau_A$ to $\sim \sqrt{t}$

scaling at $t \gg \tau_A$ where τ_A refers to the activity time scale. The value of the exponent ν and the crossover function connecting the two scaling regimes both depend on the choice of the model. In addition, we also find that the equal and unequal time autocorrelation and cross-correlations obey interesting scaling forms in the appropriate limits of the observation time t. The associated scaling functions are rigorously derived in all cases.

Chapter 2

Generalised 'Arcsine' laws for run-and-tumble particle in one dimension

The *arcsine laws* represent the interesting and counter-intuitive temporal behaviours of an one dimensional Brownian motion [137]. For a Brownian trajectory of duration t, these laws describe the probability distributions of the following three observables: (i) the time t_m to reach the maximum value M of the process, (ii) the residence time t_r spent on the positive (or the negative) semi axis and (iii) the last time t_ℓ that the process changes its sign (or crosses the origin). A schematic illustration of these observables for a trajectory $\{x(\tau)\}$ with $0 \leq \tau \leq t$ is shown in Figure 2.1. Remarkably for Brownian motion, it was shown by P. Lévy that the distributions of all three observables are exactly same and this universal distribution is given by [120]

$$P_{Br}(t_a, t) = \frac{1}{\pi} \frac{1}{\sqrt{t_a(t - t_a)}}, \qquad \text{with } t_a \in \{t_m, t_r, t_\ell\}. \tag{2.1}$$

The corresponding cumulative probability $F_c(\tau, t) = \text{Prob.}(t_a \leq \tau) = (2/\pi)\text{Arcsine}(\sqrt{\tau/t})$ has 'arcsine' form and hence the name arcsine laws. Over the years, the knowledge of these observables have been useful in various other contexts. For example, in convex hull problems, the mean area and the mean perimeter of the convex hull are related to the statistics of M and t_m [125]. Similarly, the knowledge of the residence time becomes useful in classifying the ergodic and non-ergodic phases of some systems [138]. As a result, these laws have been studied, either together or individually in various contexts like constrained Brownian motion [122, 139], random acceleration process [140, 141], stochastic thermodynamics [142], finance [143–145] and other Markov and non-Markov processes [146–160]. Extension to many diffusing particles has also been considered in [127, 161]. Quite remarkably, the statistics of t_m was recently used to detect whether a stationary process is equilibrium or not [162].

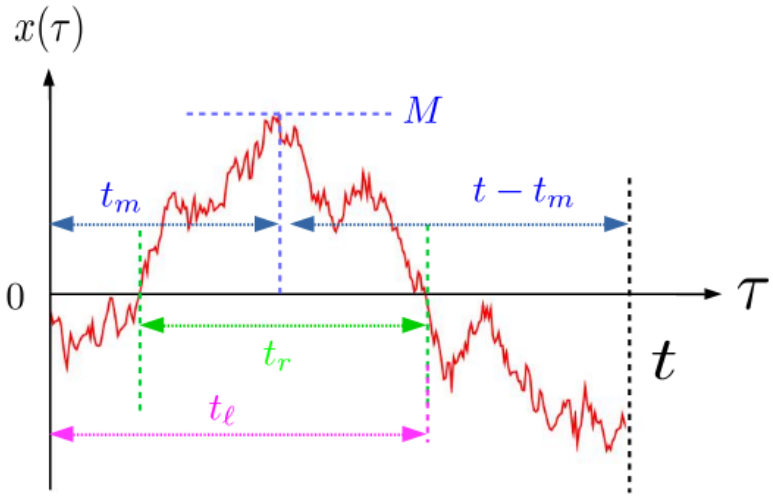

Figure 2.1: Schematic illustration of the arcsine laws for a stochastic trajectory of fixed duration t. The quantity t_m is the time at which the particle achieves its maximum displacement M within time interval $[0, t]$. The time duration t_r is the total time spent on the positive side of the origin over the duration t. Finally t_ℓ is the time that the particle crosses the origin for the last time.

While there has been a substantial amount of study on these observables for many stochastic processes, the effect of activity on their statistics has not yet been studied. This chapter aims to investigate the arcsine laws for active particles. Focus of our study will be the run and tumble particle in Eq. (1.7). As discussed before, these particles exhibit persistence behaviour at small and intermediate time scales which leads to distinct non-Brownian behaviours. Here, we demonstrate the effect of this persistence on the arcsine laws. More precisely, we look at a trajectory $\{x(\tau)\}$ of a RTP till fixed time t and compute the probability distributions of t_m, t_r and t_ℓ.

To derive these results, two essential quantities turn out to be (a) the time-dependent propagators of an one-dimensional RTP in presence of an absorbing wall at $x = M$ and (b) the (survival) probability that the RTP has not crossed the origin till time t. In the following, we calculate these propagators in Sec. 2.1 and the associated survival probabilities in the Sec. 2.2. We then use their expressions to calculate the joint distribution of M and t_m in Sec. 2.3. In the next two sections 2.4 and 2.5, we obtain the distributions of t_r and t_ℓ respectively which are then followed by a summary in Sec. 2.6

2.1 Propagator with absorbing barrier at $x = M$

Let us begin by computing the propagators for the RTP in presence of an absorbing wall at $x = M$ (≥ 0). We denote by $P_{\pm}(x, t|0, \sigma_0)$ the probability distribution to find the particle at x at time t with velocity direction $\pm v_0$ starting from the origin with direction $\sigma_0 \in \{+1, -1\}$ and with absorbing boundary at M. As illustrated later, these distributions become pertinent in deriving the results for arcsine laws. For RTP, the distributions $P_{\pm}(x, t|0, \sigma_0)$ satisfy the forward master equations

$$\begin{aligned} \partial_t P_+(x,t|0,\sigma_0) &= -v_0 \partial_x P_+(x,t|0,\sigma_0) - \gamma P_+(x,t|0,\sigma_0) + \gamma P_-(x,t|0,\sigma_0), \\ \partial_t P_-(x,t|0,\sigma_0) &= \quad v_0 \partial_x P_-(x,t|0,\sigma_0) + \gamma P_+(x,t|0,\sigma_0) - \gamma P_-(x,t|0,\sigma_0). \end{aligned} \tag{2.2}$$

These equations are derived in Appendix 8.2. In order to solve them, we have to supplement appropriate intial and boundary conditions. The initial conditions are $P_\sigma(x, 0|0, \pm) = a_\pm \delta(x)$ such that $a_+ + a_- = 1$ and $\sigma = \pm 1$. On the other hand, the boundary conditions are

$$P_{\pm}(x \to -\infty, t|0, \pm) = 0, \tag{2.3}$$

$$P_-(x \to M^-, t|0, \pm) = 0. \tag{2.4}$$

These boundary conditions can be understood as follows: For finite t, the RTP can at most have $x = -v_0 t$ and can never reach $x \to -\infty$. This gives boundary condition (2.3). Furthemore, for the particle to reach $x = M$ at time t with velocity $-v_0$, it should have crossed the barrier at some earlier time (since the particle is initially at the origin). However, such trajectories do not arise since there is absorbing condition at $x = M$. This leads to the second boundary condition (2.4). In appendix 8.2, we have explicitly solved the master equations (2.2) with boundary conditions (2.3) and (2.4). We find the following explicit expressions for the propagators for the four possible combinations of the initial and final velocity directions:

$$P_-(x,t|0,+) = \frac{\gamma}{2v_0}[\mathcal{I}(|x|, v_0, \gamma, t) - \mathcal{I}(2M - x, v_0, \gamma, t)], \tag{2.5}$$

$$P_+(x,t|0,+) = \frac{\gamma}{2v_0}[\mathcal{J}(|x|, v_0, \gamma, t) - \mathcal{J}(2M - x, v_0, \gamma, t)] - \Theta(x)\, \frac{d\mathcal{I}(x, v_0, \gamma, t)}{dx} \tag{2.6}$$

$$P_-(x,t|0,-) = \frac{\gamma}{2v_0}[\mathcal{J}(|x|, v_0, \gamma, t) - \mathcal{J}(2M - x, v_0, \gamma, t)] - \Theta(-x)\, \frac{d\mathcal{I}(|x|, v_0, \gamma, t)}{d|x|} \quad \text{and} \tag{2.7}$$

$$P_+(x,t|0,-) = \frac{\gamma}{2v_0}[\mathcal{I}(|x|, v_0, \gamma, t) - \mathcal{I}(2M - x, v_0, \gamma, t)] + \mathcal{T}(2M - x, v_0, \gamma, t) \tag{2.8}$$

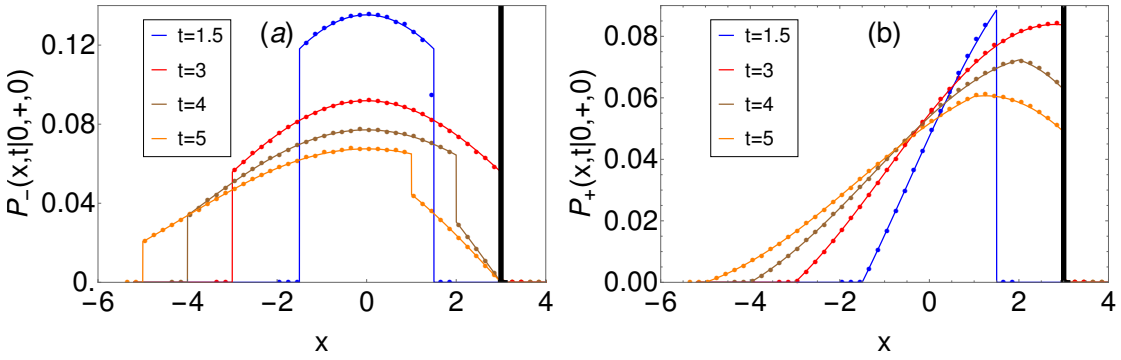

Figure 2.2: Time evolution of the propagators $P_{-}(x,t|0,+,0)$ and $P_{+}(x,t|0,+,0)$ given in Eqs. (2.5) and (2.6) respectively and their comparison with the numerical simulations. The solid lines represent the analytic formula and symbols are the simulation data. We have chosen the absorbing barrier at position $M = 3$ (shown by the thick black line). The delta function present in $P_{+}(x,t|0,+,0)$ is not shown in the plot. Other parameters of the plot are $v_0 = 1$ and $\gamma = 0.5$.

where the functions $\mathcal{I}(g,v_0,\gamma,t)$, $\mathcal{J}(\alpha,g,v_0,\gamma,t)$ and $\mathcal{T}(g,v_0,\gamma,t)$ (defined for $g>0$) are given by:

$$\mathcal{I}(g,v_0,\gamma,t) = \Theta\left(v_0 t - g\right) e^{-\gamma t} I_0\left(\gamma \frac{\sqrt{v_0^2 t^2 - g^2}}{v_0}\right), \tag{2.9}$$

$$\mathcal{J}(g,v_0,\gamma,t) = \Theta\left(v_0 t - g\right) e^{-\gamma t} \sqrt{\frac{v_0 t - g}{v t + g}} I_1\left(\gamma \frac{\sqrt{v_0^2 t^2 - g^2}}{v_0}\right), \tag{2.10}$$

$$\mathcal{T}(g,v_0,\gamma,t) = \Theta\left(v_0 t - g\right) \frac{e^{-\gamma t}}{v_0 t + g}\left[\frac{\gamma g}{v_0} I_0\left(\frac{\gamma\sqrt{v_0^2 t^2 - g^2}}{v_0}\right) + \sqrt{\frac{v_0 t - g}{v_0 t + g}} I_1\left(\frac{\gamma\sqrt{v_0^2 t^2 - g^2}}{v_0}\right)\right]. \tag{2.11}$$

In these equations, $I_\nu(z)$ stands for the modified Bessel function of first kind and $\Theta(z)$ is the Heaviside theta function. Note that the propagators $P^a_{\pm}(x,t|0,\pm)$ have term $\frac{d\mathcal{I}}{dx}$ which gives rise to terms like $e^{-\gamma t}\delta(x \pm v_0 t)$. Physically, such terms arise from those events for which RTP has not changed its velocity till time t. These events occur with probability $e^{-\gamma t}$. In Figures 2.2 and 2.3, we have shown the comparison of our analytic results with the numerical simulations for all four propagators in Eqs. (2.5)-(2.8). We observe excellent match for all of them. Finally, by using the large z asymptotic of $I_\nu(z) \simeq e^z/\sqrt{2\pi z}$ for both $\nu = 0$ and 1, we find that in the limit $v_0 \to \infty$ and $\gamma \to \infty$ keeping $v_0^2/(2\gamma) = D$ fixed, all four propagators reduce to

$$P_\sigma(x,t|0,\sigma_0) \xrightarrow[\gamma\to\infty,\ v_0\to\infty]{(v_0^2/2\gamma)=D} \frac{1}{\sqrt{4\pi D t}}\left[\exp\left(-\frac{x^2}{4Dt}\right) - \exp\left(-\frac{(2M-x)^2}{4Dt}\right)\right], \tag{2.12}$$

for $\sigma = \pm 1$, $\sigma_0 = \pm 1$ and for $x < M$. This is the propagator of a Brownian walker in presence of absorbing boundary at $x = M$ [163]. Therefore, we correctly recover the results for Brownian

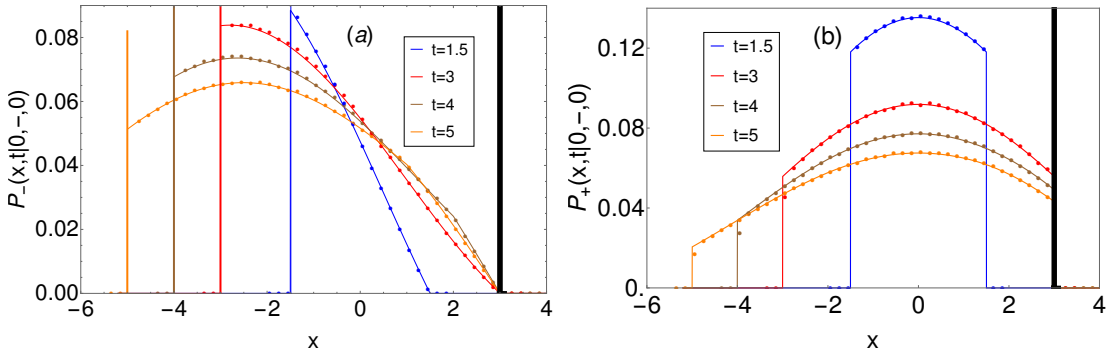

Figure 2.3: Time evolution of the propagators $P_-(x,t|0,-,0)$ and $P_+(x,t|0,-,0)$ given in Eqs. (2.7) and (2.8) respectively and their comparison with the numerical simulations. The solid lines represent the analytic formula and symbols are the simulation data. We have chosen the absorbing barrier at position $M = 3$ (shown by the thick black line). The delta functions present in $P_-(x,t|0,-,0)$ at different times are not shown completely. Other parameters of the plot are $v = 1$ and $\gamma = 0.5$.

motion in the limit $v_0 \to \infty,\ \gamma \to \infty$ keeping $D = v_0^2/2\gamma$ fixed. Howver for finite γ, the form of the propagators is different owing to the persistence nature of the RTPs.

In this section, we have so far looked at the propagators in presence of an absorbing boundary. Recall that our main goal is to derive the statistics of $t_m,\ t_r$ and t_ℓ for which these propagators will become useful. Another essential quantity for the arcsine laws is the survival probability $S_{\sigma_0}(x_0,t)$ which represents the probability that the RTP has not crossed $x = M$ till duration t starting from the position x_0 with velocity orientation σ_0. In the next section, we compute $S_{\sigma_0}(x_0,t)$ for a single RTP in one dimension.

2.2 Survival probability of the RTP

To get the survival probability $S_{\sigma_0}(x_0,t)$, one can, in principle, integrate the propagators obtained in the previous section over all final positions x [163]. However, it turns out more convenient and illustrative to solve the backward master equations to get the survival probabilities. These equations read [70]

$$\partial_t S_+(x_0,t) = v_0 \partial_{x_0} S_+(x_0,t) - \gamma S_+(x_0,t) + \gamma S_-(x_0,t), \tag{2.13}$$

$$\partial_t S_-(x_0,t) = -v_0 \partial_{x_0} S_-(x_0,t) + \gamma S_+(x_0,t) - \gamma S_-(x_0,t). \tag{2.14}$$

The derivation of these equations are provided in appendix 8.3. In order to solve these equations, we choose the initial condition $S_\pm(x_0,0) = 1$ since the particle will surely survive the wall initially for all $x_0 \neq M$. In addition, we consider the following boundary conditions: $S_\pm(x_0 \to -\infty, t) = 1$

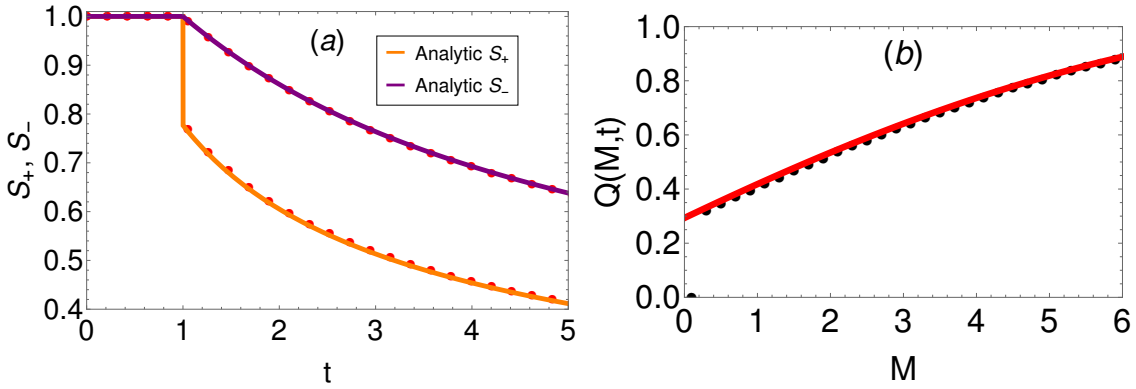

Figure 2.4: (a) Plot of the survival probabilities $S_{\pm}(x_0, t)$ given in Eqs.(2.15) and (2.16) and their comparison with simulation results (filled circles). The particle is initially chosen to be at position $x = 1$ with absorbing barrier at $M = 3$. (b) Numerical verification of the cumulative distribution $Q(M, t)$ in Eq. (2.33). The red solid line is the theoretical result and symbols represent the simulation data. We have chosen $t = 3$, $\gamma = 2.5, v_0 = 2$.

and $S_+(x_0 \to M^-, t) = 0$. The first boundary condition arises due to the fact that the particle, regardless of its initial velocity direction, will never reach $x = M$ at any finite time t if it starts initially from $x_0 \to -\infty$. On the other hand if the particle starts at $x_0 = M$ with positive velocity then the particle will immediately get absorbed leading to zero survival probability. With these conditions, backward equations (2.13) and (2.14) can be solved to obtain [70]

$$S_+(x_0, t) = 1 + v_0 \frac{d}{dM} \int_0^t d\tau\ \Theta\left(\tau - \frac{M - x_0}{v_0}\right) e^{-\gamma\tau}\ I_0\left(\frac{\gamma}{v_0}\sqrt{v_0^2\tau^2 - (M - x_0)^2}\right), \tag{2.15}$$

$$S_-(x_0, t) = 1 - \int_0^t d\tau\ \Theta\left(\tau - \frac{M - x_0}{v_0}\right) \frac{v_0 e^{-\gamma\tau}}{v_0\tau + (M - x_0)} \left[\frac{\gamma}{v_0}(M - x_0) I_0\left(\frac{\gamma}{v_0}\sqrt{v_0^2\tau^2 - (M - x_0)^2}\right) + \sqrt{\frac{v_0\tau - (M - x_0)}{v_0\tau + (M - x_0)}} I_1\left(\frac{\gamma}{v_0}\sqrt{v_0^2\tau^2 - (M - x_0)^2}\right)\right]. \tag{2.16}$$

Figure 2.4 presents the plots of these probabilities and also their comparison with the simulation. Due to the presence of Θ-functions, we notice in the figure that both $S_{\pm}$ remains 1 till a timescale $\tau_b = \frac{M - x_0}{v_0}$. This is because the RTPs, starting from x_0 ($< M$), will atleast take τ_b time to reach the barrier. After time τ_b, the particles can reach $x = M$ only with positive velocity. In the next instant, some particles flip their velocity from $+v_0$ to $-v_0$ and avoid getting absorbed by the wall. The remaining particles, however, do not change their velocity and get absorbed at time τ_b^+. This causes sudden drop in survival probability $S_+(x, \tau_b^+)$ as also seen in Fig. 2.4a. However, no sudden drop occurs in $S_-(x_0, t)$ since particles cannot reach the barrier at τ_b^- with $-v_0$ velocity. But, since the overall number of particles decreases, $S_-(x_0, t)$ also starts decreasing from value 1 after time τ_b but continuously.

Finally, in the limit $\gamma \to \infty$ and $v_0 \to \infty$ limit keeping $v_0^2/(2\gamma) = D$ fixed, we use the asymptotic

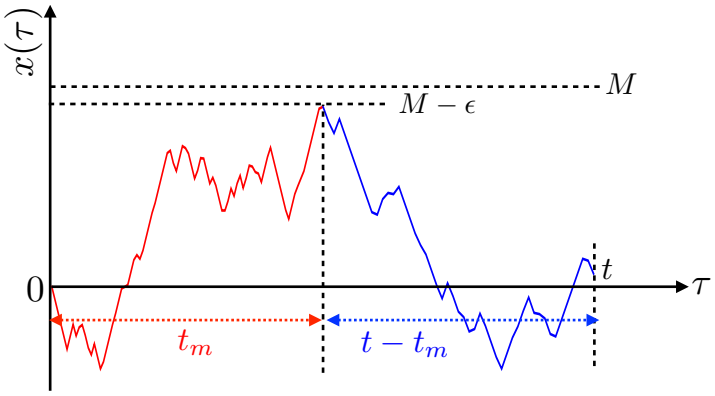

Figure 2.5: A typical trajectory of a RTP starting from the origin reaches the position $(M-\epsilon)$ at time t_m. In the remaining time $(t-t_m)$, the RTP, starting from $(M-\epsilon)$, does not hit the $x=M$ wall again. The trajectory is decomposed into two parts, from 0 to t_m (red part) and from t_m to t (blue part).

form of the Bessel functions $I_\nu(z) \simeq e^z/\sqrt{2\pi z}$ and plug it in Eqs. (2.15) and (2.16) to get

$$S_\pm(x_0,t) \xrightarrow[\gamma\to\infty,\ v_0\to\infty]{(v_0^2/2\gamma)=D} \text{erf}\left(\frac{M-x_0}{\sqrt{4Dt}}\right) \quad \text{where, } \text{erf}(z)=\frac{2}{\sqrt{\pi}}\int_0^z du\ e^{-u^2}. \tag{2.17}$$

which represents the survival probability of a Brownian particle [163].

2.3 Joint probability distribution $\mathcal{P}(M,t_m,t)$ of M and t_m

We now use the propagators and survival probabilities derived in the previous sections to calculate the joint distribution $\mathcal{P}(M,t_m,t)$ of the maximum M and time t_m at which this maximum is attained within the time interval $[0,t]$. For this, we decompose the trajectory $\{x(\tau)\}$ with $0\le\tau\le t$ in two parts (see Figure 2.5): (i) the first part is from $[0,t_m]$ and (ii) the second part from $[t_m,t]$. Let us now look at the contributions of each part to the distribution $\mathcal{P}(M,t_m,t)$. In the part (i), the particle, starting from the origin with direction $\sigma(t=0)=\sigma_0$, reaches $x=M$ at time t_m without crossing $x=M$ at any earlier time. The probability weight to $\mathcal{P}(M,t_m,t)$ in this part is just the propagator $P_{\sigma_m}(M,t_m|0,\sigma_0)$ to reach $x=M$ at time t_m with orientation $\sigma(t_m)=\sigma_m$ in presence of an absorbing wall at M. The absorbtion wall ensures that the particle has not crossed M at any earlier time. In part (ii), the particle remains below M in the interval $(t-t_m)$ such that it was at $x=M$ at time t_m with orientation σ_m. Hence, the weight to $\mathcal{P}(M,t_m,t)$ from this part is given by the probability $S_{\sigma_m}(M,t-t_m)$ to survive M till time $(t-t_m)$ given that it was initially at $x=M$ with orientation σ_m. Now, the RTP model is a Markov process in (x,σ) variables. This implies that the two parts are statistically independent. However, calculations in Eqs. (2.5-2.8) show that the quantities $P_{\sigma_m}(x,t_m|0,\sigma_0)$

and $S_{\sigma_m}(x, t-t_m)$ are exactly zero at $x = M$ for some values of σ_0 and σ_m. To circumvent this problem, we follow a technique from [140] where the propagators and survival probability are instead calculated at $x = (M - \epsilon)$ using which we compute the distribution of the required physical observable (which in our case is the joint distribution of M and t_m). Finally, we take the $\epsilon \to 0^+$ limit. Therefore, we calculate $P_{\sigma_m}(M-\epsilon, t_m|0, 0, \sigma_0)$ and $S_{\sigma_m}(M-\epsilon, t-t_m)$ for small ϵ. Furthermore, we take $\sigma_0 = \pm 1$ with equal probability. The joint distribution $\mathcal{P}(M, t_m, t)$ then reads

$$\mathcal{P}(M, t_m, t) = \lim_{\epsilon \to 0} \left[\frac{p_+(M-\epsilon, t_m|0) S_+(M-\epsilon, t-t_m) + p_-(M-\epsilon, t_m|0) S_-(M-\epsilon, t-t_m)}{\mathcal{Z}(\epsilon)} \right], \tag{2.18}$$

for $0 < M < v_0 t$ and $0 < t_m < t$ where $\mathcal{Z}(\epsilon, t)$ is a normalization factor and $p_\pm(M-\epsilon, t_m|0, 0) = \frac{1}{2}\left[P_\pm(M-\epsilon, t_m|0, +) + P_\pm(M-\epsilon, t_m|0, -)\right]$. Inserting the propagators from Eqs. (2.5)-(2.8) and the survival probabilities from Eqs.(2.15) and (2.16), we find

$$\left.\begin{aligned} S_-(M-\epsilon, t-t_m) &\approx \Theta(t-t_m)\, h(t-t_m) + O(\epsilon), \\ S_+(M-\epsilon, t-t_m) &\approx \frac{\gamma\, \epsilon}{v_0} h(t-t_m) + O(\epsilon^2), \end{aligned}\right\} \qquad h(t) = e^{-\gamma t}[I_0(\gamma t) + I_1(\gamma t)], \tag{2.19}$$

$$\left.\begin{aligned} p_+(M-\epsilon, t_m|0) &\approx -\frac{d}{dM}\left[\Theta(v_0 t_m - M)\; g(M, t_m)\right] + O(\epsilon), \\ p_-(M-\epsilon, t_m|0) &\approx -\frac{\gamma\, \epsilon}{v_0}\frac{d}{dM}\left[\Theta(v_0 t_m - M) g(M, t_m)\right] + O(\epsilon^2), \end{aligned}\right\} \qquad \text{where,} \tag{2.20}$$

$$g(M, t) = e^{-\gamma t}\left[I_0\left(\frac{\gamma}{v_0}\sqrt{v_0^2 t^2 - M^2}\right) + \sqrt{\frac{v_0 t - M}{v_0 t + M}} I_1\left(\frac{\gamma}{v_0}\sqrt{v_0^2 t^2 - M^2}\right)\right]. \tag{2.21}$$

Here $h(t)$ can be interpreted as the probability that the RTP, starting from the origin, has not crossed the origin till time t. Plugging these expansions in Eq. (2.18) gives the joint distribution $\mathcal{P}(M, t_m, t)$. However, the above derivation is valid only for $0 < t_m < t$. On the other hand, we anticipate non-zero contributions to $\mathcal{P}(M, t_m, t)$ for $t_m = 0$ and $t_m = t$ due to the persistence nature of the particle. Let us now calculate these contributions.

Note that $t_m = 0$ contribution arises from those events for which the RTP, starting with $-v_0$ velocity, remains in the negative side till time t. The probability of such events is $h(t)/2$ (the factor $1/2$ comes due to the symmetric inital condition). Moreover, the maximum distance then is $M = 0$. Therefore, the joint distribution for such events is

$$\underbrace{\mathcal{P}(M, t_m, t)}_{\text{contribution from paths with } t_m=0} = \frac{h(t)}{2}\delta(t_m)\; \delta(M) \tag{2.22}$$

On the other hand the contributions to $t_m = t$ event come from trajectories which starting from the origin reach the maximum displacement M at time $t_m = t$. The contribution of these paths

to the joint distribution $\mathcal{P}(M,t_m,t)$ is given by

$$\underbrace{\mathcal{P}(M,t_m,t)}_{\text{contribution from paths with } t_m=t} = \delta(t_m-t)\ \frac{[P_+(M,t|0,+,0)+P_+(M,t|0,-,0)]}{2}. \tag{2.23}$$

where $\frac{[P_+(M,t|0,+)+P_+(M,t|0,-)]}{2}$ is the probability density to find the particle at time t in position M. Inserting the explicit forms of these propagators from Eqs. (2.6) and (2.8), respectively, we get

$$\begin{aligned}\underbrace{\mathcal{P}(M,t_m,t)}_{\text{contribution from paths with } t_m=t} &= \delta(t_m-t)\ \frac{1}{2}\left[\mathcal{T}(M,v_0,\gamma,t)-\frac{d\mathcal{I}(M,v_0,\gamma,t)}{dM}\right]\\ &= -\frac{d}{dM}\left[\Theta(v_0t-M)\ g(M,t)\right], \end{aligned}\tag{2.24}$$

where $g(M,t)$ is given in Eq. (2.21). We now have all possible contributions to $\mathcal{P}(M,t_m,t)$. Adding all these contributions, we get

$$\begin{aligned}\mathcal{P}(M,t_m,t) =& \frac{h(t)}{2}\delta(M)\delta(t_m)-\frac{\delta(t_m-t)}{2}\frac{d}{dM}\left[\Theta(v_0t-M)\ g(M,t)\right]\\ &-\frac{\gamma\epsilon\ h(t-t_m)}{2v_0\ \mathcal{Z}(\epsilon)}\frac{d}{dM}\left[\Theta(v_0t_m-M)g(M,t_m)\right],\end{aligned}\tag{2.25}$$

where $h(t)$ and $g(M,t)$ are given in Eqs. (2.19) and (2.21). The only task left now is to calculate the factor $\mathcal{Z}(\epsilon)$ which is fixed from the normalisation condition

$$\int_0^t dt_m\int_0^{v_0t} dM\ \mathcal{P}(M,t_m,t)=1. \tag{2.26}$$

The integration of the first two terms in Eq. (2.25) is straightforward and we find both contributions give $h(t)/2$, i.e.

$$\text{Contribution from first/second term} = \int_0^t dt_m\int_0^{v_0t} dM\frac{h(t)}{2}\delta(M)\delta(t_m)=\frac{h(t)}{2}. \tag{2.27}$$

Similarly, for the third term, we find

$$\begin{aligned}\text{Contribution from the third term} &= -\frac{\gamma\epsilon}{2v_0\ \mathcal{Z}(\epsilon)}\int_0^t dt_m h(t-t_m)\int_0^{v_0t} dM\ \frac{d}{dM}\left[\Theta(v_0t_m-M)g(M,t_m)\right]\\ &= \frac{\epsilon}{2v_0\ \mathcal{Z}(\epsilon)}\ 2[1-h(t)].\end{aligned}\tag{2.28}$$

In moving to the second line, we have used the identity $\gamma\int_0^t dt' h(t-t')h(t')=2[1-h(t)]$ (see

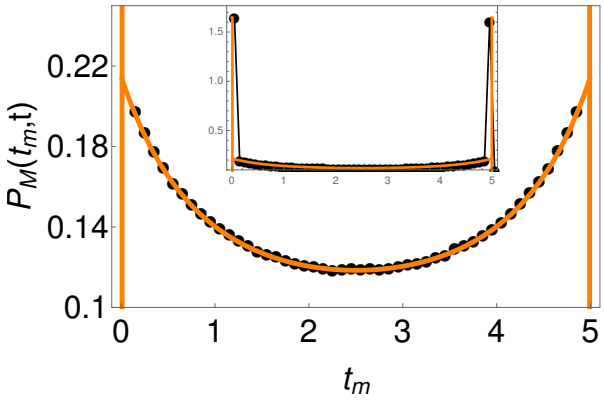

Figure 2.6: Plot of $P_M(t_m, t)$ in Eq. (2.34) and its comparison with numerical simulations for $v_0 = 1,\ \gamma = 1.5$ and $t = 5$. The solid orange line is the analytic result and the black dots are obtained in simulations. The inset shows the delta functions at $t_m = 0$ and $t_m = t$.

appendix 8.4 for the proof). Substituting all these contributions in Eq. (2.26), we get $\mathcal{Z}(\epsilon) = \frac{v_0}{\epsilon}$. Then the final form of $\mathcal{P}(M, t_m, t)$ follows from Eq. (2.25) to be

$$\mathcal{P}(M, t_m, t) = \frac{h(t)}{2}\delta(M)\delta(t_m) - \frac{\delta(t_m - t) + \gamma\ h(t - t_m)}{2}\frac{d\left[\Theta(v_0 t_m - M)\ g(M, t_m)\right]}{dM}. \tag{2.29}$$

To summarise, we have calculated the joint distribution of M and t_m for the case when the particle chooses $\sigma(0) = \pm 1$ initially with equal probability, i.e. $a_+ = a_- = 1/2$. Although we have presented our calculations for the symmetric initial condition, it can be easily extended to the asymmteric initial condition also where $a_+ \neq a_-$. Since the derivation for asymmetric case is a straightforward generalisation of Eq. (2.29), we have provided this derivation in appendix 8.5. In what follows, use the joint distribution $\mathcal{P}(M, t_m, t)$ to compute the marginal distributions of M and t_m.

2.3.1 Marginal probability distribution of M

We first integrate out the t_m variable from the joint distribution in Eq. (2.29) to get the marginal distribution $\mathcal{P}_M(M, t)$ for M:

$$\begin{aligned}\mathcal{P}(M, t) &= \int_0^t dt_m\ \mathcal{P}(M', t_m, t) \\ &= \frac{h(t)}{2}\delta(M) - \frac{1}{2}\frac{d}{dM}\left[\Theta(v_0 t - M)\ g(M, t)\right] \\ &\quad - \frac{\gamma}{2}\int_0^t dt_m h(t - t_m)\frac{d}{dM}\left[\Theta(v_0 t_m - M)\ g(M, t_m)\right].\end{aligned} \tag{2.30}$$

It turns out more convenient to compute the cumulative probability $Q(M,t) = \int_0^M dM'\, \mathcal{P}_M(M',t)$. Plugging $P(M,t)$ from Eq. (2.30) in this formula, we get the following terms:

$$\begin{aligned}\frac{1}{2}\int_0^M dM' \frac{d}{dM'}\left[\Theta(v_0 t - M')\; g(M',t)\right] &= \frac{1}{2}\left[\Theta(v_0 t - M')\; g(M',t)\right]\Big|_0^M, \\ &= \Theta\left(v_0 t - M\right)\frac{g\left(M,t\right)}{2} - \frac{h(t)}{2}. \end{aligned} \tag{2.31}$$

$$\begin{aligned}&\frac{\gamma}{2}\int_0^M dM' \int_0^t dt_m h(t-t_m)\frac{d}{dM}\left[\Theta(v_0 t_m - M)\; g(M,t_m)\right] \\ &\qquad = \frac{\gamma}{2}\int_0^t dt_m h(t-t_m)\left[\Theta\left(v_0 t_m - M\right) g\left(M,t_m\right) - h(t_m)\right], \\ &\qquad = \frac{\gamma}{2}\int_0^t dt_m \Theta\left(v_0 t_m - M\right) h(t-t_m) g\left(M,t_m\right) - \left[1-h(t)\right]. \end{aligned} \tag{2.32}$$

To perform algebraic simplifications in Eqs. (2.31) and (2.32), we have used the relations $g(0,t) = h(t)$ and $\gamma\int_0^t dt' h(t-t')h(t') = 2[1-h(t)]$. After these simplifications, the cumulative probability reads

$$Q(M,t) = 1 - \frac{1}{2}g(M,t)\Theta(v_0 t - M) - \frac{\gamma}{2}\int_0^t dt'\; \Theta(v_0 t' - M)\; h(t-t')\; g(M,t'), \tag{2.33}$$

where $h(t)$ and $g(M,t)$ are given in Eqs. (2.19) and (2.21). In Fig. 2.4b, we have compared our theoretical cumulative distribution $Q(M,t)$ against numerical simulation and we observe nice agreement. Note that the discontinuity at $M = 0$ and $M = v_0 t$ appear due to the presence of delta functions in the corresponding probability distribution function $\mathcal{P}_M(M,t)$ in Eq. (2.30). Finally, we remark that the cumulative probability $Q(M,t)$ represents simply the survival probability $S(0,t) = \left[S_+(0,t) + S_-(0,t)\right]/2$ where $S_\pm(0,t)$ are given in Eqs. (2.15) and (2.16). Our result in Eq. (2.33) is consistent with this expression of $S(0,t)$.

2.3.2 Marginal probability distribution of t_m

We now use the joint distribution $\mathcal{P}(M, t_m, t)$ in Eq. (2.29) to get the marginal distribution $P_M(t_m, t)$ of t_m. Performing integration over M, we get

$$\begin{aligned} P_M(t_m,t) &= \int_0^{v_0 t} dM\ \mathcal{P}(M,t_m,t), \\ &= \int_0^{v_0 t} dM \left[\frac{h(t)}{2}\delta(M)\delta(t_m) - \frac{\delta(t_m-t)+\gamma\ h(t-t_m)}{2}\frac{d}{dM}\left[\Theta(v_0 t_m - M)\ g(M,t_m)\right] \right], \\ &= \frac{h(t)}{2}\Big[\delta(t_m)+\delta(t-t_m)\Big] + \frac{\gamma}{2}h(t-t_m)h(t_m). \end{aligned} \tag{2.34}$$

Fig. 2.6 shows the comparison of $P_M(t_m, t)$ with the numerics. We observe an excellent agreement between them. Contrary to the Brownian motion [see Eq. (2.1)], we find that the distribution $P_M(t_m, t)$ for RTP possesses two delta-function terms at $t_m = 0$ and $t_m = t$. Below we argue that these terms arise due to the persistent nature of the RTPs. However, for $\gamma \to \infty$, we find $h(t) \simeq \frac{1}{\sqrt{\pi\gamma t}}$. Inserting this form in Eq. (2.34), the delta-function terms vanish and the non-delta function part converges to the result for Brownian motion in Eq. (2.1).

Let us now understand various terms in $P_M(t_m, t)$. The term proportional to $\delta(t_m)$ gets contributions from those trajectories for which particle, starting from the origin with $-v_0$, stays in the negative side within the interval $[0, t]$. The probability of such trajectories is just the survival probability $h(t)/2$. Similarly, the term proportional to $\delta(t_m - t)$ gets contributions from those trajectories which attain their maxima at the final time t. Interestingly, the probability of these events is also proportional to the survival probability $h(t)$. Heuristically, this can be understood by shifting the origin from $x = 0$ to the position of the maxima $x = M$ for every trajectory $\{x(\tau);\ 0 \le \tau \le t\}$ before performing the integration over M. Under the transformations $\bar{x} = M - x,\ \bar{\tau} = t - \tau$ and $\bar{\sigma} = \sigma$, the particle remains above the (new) origin throughout the duration $[0, t]$. Path probabilities for the original process and the transformed process are exactly identical which implies that their survival probabilities are also same. As a result the survival probability of the transformed trajectories is exactly $h(t)/2$. This gives rise to the prefactor $h(t)/2$ accompanying $\delta(t_m - t)$ term in Eq. (2.34).

We next turn to the non-delta function part. As clear from Eq. (2.34), this term is proportional to the product of $h(t_m)$ and $h(t - t_m)$, which are survival probabilities in the first and second durations t_m and $t - t_m$, respectively. To understand this form, we once again shift the origin to the position of the maxima. For the first part of the $[0, t_m]$, we consider the variable transformations $\bar{x} = M - x,\ \bar{\tau} = t_m - \tau$ while for second part $[t_m, t]$, we consider $\bar{x} = M - x,\ \bar{\tau} = \tau - t_m$. Under these transformations, once again, we find the contribution from each part is proportional to

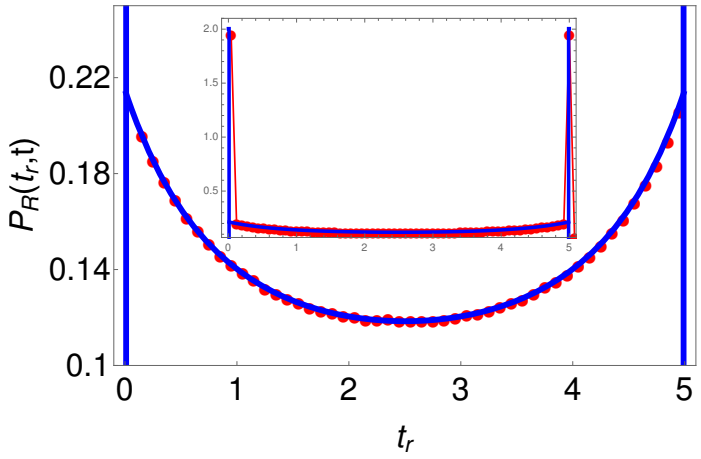

Figure 2.7: Plot of $P_R(t_r, t)$ in Eq. (2.56) and its comparison with numerical simulations. The solid blue line is the analytic result and the black dots are the simulation data. Parameters chosen are $v_0 =$, $\gamma = 1$ and $t = 5$. Inset shows the delta functions at $t_r = 0$ and $t_r = t$ for the same values of parameters.

the corresponding survival probabilities. And since the motion is Markovian in (x, σ) variables, the contributions from two parts appear as a product of their survival probabilities.

Recall that the distribution $P_M(t_m, t)$ in Eq. (2.34) is derived for symmetric initial condition whereby particle initially chooses $\pm v_0$ with equal probability ($a_+ = a_- = 1/2$). However, as mentioned before, it is easy to generalise this derivation for the asymmetric initial condition ($a_+ \neq a_-$) also. We refer to appendix 8.5 for a detailed derivation for the asymmetric case. Interestingly, in contrast to the symmetric case, we find that the distribution of t_m for $a_+ \neq a_-$ is asymmetric about $t_m = t/2$.

2.4 The residence time distribution $P_R(t_r, t)$

In the previous sections, we studied the statistics of M and t_m for a one dimensional run and tumble particle. Due to the persistence motion, we saw that the distribution of t_m in Eq. (2.34) possesses delta functions at $t_m = 0$ and $t_m = t$, which are otherwise not seen for Brownian motion. Importantly, for Brownian motion, Lévy proved that the distribution of t_m is exactly same as that of the residence time t_r which is defined as $t_r = \int_0^t d\tau \Theta\left(x(\tau)\right)$. In this section, we proceed to study the statistics of t_r for RTP and check if the distribution of t_r is also given by Eq. (2.34). In particular, we deine the distribution $P_R^{\pm}(t_r, t, x_0)$ of t_r for a given evolution time t when the RTP starts from the position x_0 with velocity $\pm v_0$. For this, it turns out useful to take the Laplace transform $Q^{\pm}(p, x_0, t) = \int_0^{\infty} dt_r \; e^{-pt_r} P_R^{\pm}(t_r, t, x_0)$ of the distributions with respect to t_r ($\to p$). Following the Feynman-Kac formalism [121, 123, 124], we find that these

Laplace transforms satisfy the backward master equations

$$\partial_t Q^+(p,x_0,t) = v_0\partial_{x_0}Q^+(p,x_0,t) - \gamma Q^+(p,x_0,t) + \gamma Q^-(p,x_0,t) - p\Theta(x_0)Q^+(p,x_0,t), \quad (2.35)$$

$$\partial_t Q^-(p,x_0,t) = -v_0\partial_{x_0}Q^-(p,x_0,t) + \gamma Q^+(p,x_0,t) - \gamma Q^-(p,x_0,t) - p\Theta(x_0)Q^-(p,x_0,t). \quad (2.36)$$

We have rigorously derived these equations in appendix 8.6. In order to solve them, we use the following initial and boundary conditions:

$$Q^{\pm}(p,x_0,t=0) = 1, \quad (2.37)$$

$$Q^{\pm}(p,x_0\to-\infty,t) = 1, \quad (2.38)$$

$$Q^{\pm}(p,x_0\to+\infty,t) = e^{-pt}. \quad (2.39)$$

Let us now try to understand these conditions. If the total duration $t = 0$, then the residence time $t_r = 0$ regardless of the initial orientation of the particle. This means that the distributions $P_R^{\pm}(t_r, t = 0, x_0) = \delta(t_r)$ which in terms of the Laplace transform translate to Eq. (2.37). Similarly if the initial postion $x_0 \to -\infty$, then the particle stays in the negative side of the origin for all finite t. This means that $t_r = 0$ and $Q^{\pm}(p, x_0 \to -\infty, t) = 1$ as indicated in Eq. (2.38). The same reasoning gives $t_r = t$ for $x_0 \to \infty$ which then leads to the boundary condition (2.39).

To solve Eqs. (2.35) and (2.36), we take another Laplace transformation with respect to t ($\to s$) as $\tilde{Q}^{\pm}(p,x_0,s) = \int_0^\infty dt e^{-st} Q^{\pm}(p,x_0,t)$. Rewriting the backward equations in terms of $\tilde{Q}^{\pm}(p,x_0,s)$, we get

$$\left[v_0\partial_{x_0} - \gamma - p\Theta(x_0) - s\right]\tilde{Q}^+(p,x_0,s) = -\gamma\tilde{Q}^-(p,x_0,s) - 1, \quad (2.40)$$

$$\left[v_0\partial_{x_0} + \gamma + p\Theta(x_0) + s\right]\tilde{Q}^-(p,x_0,s) = \gamma\tilde{Q}^+(p,x_0,s) + 1. \quad (2.41)$$

The boundary conditions (2.38) and (2.39) can also be translated in terms of $\tilde{Q}^{\pm}(p,x_0,s)$ as $\tilde{Q}^{\pm}(p,x_0\to-\infty,s) = \frac{1}{s}$ and $\tilde{Q}^{\pm}(p,x_0\to\infty,s) = \frac{1}{s+p}$. Let us first solve the Eqs.(2.40) and (2.41) for $x_0 > 0$ region where we put $\Theta(x_0) = 1$. We obtain

$$\left[v_0\partial_{x_0} - \gamma - p - s\right]\tilde{Q}^+(p,x_0,s) = -\gamma\tilde{Q}^-(p,x_0,s) - 1, \quad (2.42)$$

$$\left[v_0\partial_{x_0} + \gamma + p + s\right]\tilde{Q}^-(p,x_0,s) = \gamma\tilde{Q}^+(p,x_0,s) + 1. \quad (2.43)$$

Changing variable $Q^{\pm}(p,x_0,s)=\frac{1}{s}+Z^{\pm}(p,x_0,s)$ gives

$$[v_0\partial_{x_0}-\gamma-p-s]\,Z^{+}(p,x_0,s)=-\gamma Z^{-}(p,x_0,s)\,, \tag{2.44}$$

$$[v_0\partial_{x_0}+\gamma+p+s]\,Z^{-}(p,x_0,s)=\gamma Z^{+}(p,x_0,s)\,. \tag{2.45}$$

The boundary condition of $Q^{\pm}(p,x_0\to\infty,s+p)=\frac{1}{s+p}$ now becomes $Z^{\pm}(p,x_0\to-\infty,s)=0$. Proceeding similarly as done in appendix 8.2, we find that the solutions are given by

$$\tilde{Q}^{+}(p,x_0,s)=\frac{1}{s+p}+A(s,p)e^{-\frac{\lambda_p(s)x_0}{v_0}}, \tag{2.46}$$

$$\tilde{Q}^{-}(p,x_0,s)=\frac{1}{s+p}+\frac{A(s,p)}{\gamma}\left(s+p+\gamma+\lambda_p\right)e^{-\frac{\lambda_p(s)x_0}{v_0}}, \tag{2.47}$$

where $\lambda_p(s)=\sqrt{(s+p)\,(2\gamma+s+p)}$. Note that these solutions are derived for $x_0>0$. However, for $x_0<0$ also, one can put $\Theta(x_0)=0$ in Eqs. (2.40) and (2.41) and proceed similarly to yield

$$\tilde{Q}^{+}(p,x_0,s)=\frac{1}{s}+B(s,p)e^{\frac{\lambda_0(s)x_0}{v_0}}, \tag{2.48}$$

$$\tilde{Q}^{-}(p,x_0,s)=\frac{1}{s}+\frac{B(s,p)}{\gamma}\left(s+\gamma-\lambda_0(s)\right)e^{\frac{\lambda_0(s)x_0}{v_0}}. \tag{2.49}$$

Next to evaluate the constants $A(s,p)$ and $B(s,p)$ in the above expressions, we use the continuity of $\tilde{Q}^{\pm}(p,x_0,s)$ at $x_0=0$ which then gives

$$A(s,p)=\frac{p\left(\lambda_0(s)-s\right)}{s(s+p)(p+\lambda_0(s)+\lambda_p(s))}. \tag{2.50}$$

$$B(s,p)=-\frac{p\left(s+p+\lambda_p(s)\right)}{s(s+p)(p+\lambda_0(s)+\lambda_p(s))}, \tag{2.51}$$

Finally plugging these forms in Eqs. (2.46)-(2.49), we obtain the Laplace transforms $\tilde{Q}^{+}(p,x_0,s)$ for arbitrary x_0. However, we are interested in computing the statistics of residence time when the particle starts from the origin. Therefore, we provide below the expresions of $\tilde{Q}^{+}(p,x_0,s)$ for $x_0=0$:

$$\tilde{Q}^{+}(p,0,s)=-\frac{1}{2\gamma}\left(1+\frac{\lambda_0}{s}-\frac{\lambda_p}{s+p}-\frac{\lambda_0\lambda_p}{s(s+p)}\right), \tag{2.52}$$

$$\tilde{Q}^{-}(p,0,s)=-\frac{1}{2\gamma}\left(1-\frac{\lambda_0}{s}+\frac{\lambda_p}{s+p}-\frac{\lambda_0\lambda_p}{s(s+p)}\right). \tag{2.53}$$

Now if the particle initially chooses $\pm v_0$ with equal probability $1/2$, then the total probability is given by $P_R(t_r,t)=\frac{P_R^{+}(t_r,t)+P_R^{-}(t_r,t)}{2}$. Then the corresponding Laplace transform is $\tilde{Q}(p,0,s)=$

$\int_0^\infty dt e^{-st} \int_0^t dt_r e^{-pt_r} P_R(t_r,t) = \frac{\tilde{Q}^+(p,0,s)+\tilde{Q}^-(p,0,s)}{2}$. From Eqs. (2.52) and (2.53), it then follows

$$\tilde{Q}(p,0,s) = \frac{\tilde{Q}^+(p,0,s)+\tilde{Q}^-(s,0,p)}{2} = -\frac{1}{2\gamma}\left(1-\frac{\lambda_0(s)\lambda_p(s)}{s(s+p)}\right). \tag{2.54}$$

To get the distribution $P_R(t_r,t)$, we consider the inverse Laplace transformation

$$\int_0^\infty dt_r\ e^{-pt_r}\left[\delta(t_r)+\gamma e^{-st_r}e^{-\gamma t_r}\left\{I_0(\gamma t_r)+I_1(\gamma t_r)\right\}\right] = \frac{\lambda_p(s)}{s+p}, \tag{2.55}$$

and use this in Eq. (2.54). This results in the following explicit expression for the distribution of t_r spent by a RTP, starting form the origin, on the positive side over the duration t for the symmetric initial condition:

$$P_R\left(t_r,t\right) = \frac{h(t)}{2}\Big[\delta(t_r)+\delta(t_r-t)\Big] + \frac{\gamma}{2}h(t_r)h(t-t_r), \tag{2.56}$$

where $h(t)$ is given in Eq. (2.19). Note that just like in Brownian motion, for RTP also, the distribution of t_r is exactly same as that of t_m in Eq. (2.34). However, due to the persistence motion, the distribution of t_r gets delta-function contributions at $t_r = 0$ and $t_r = t$. Physically, these contributions arise from those trajectories which starting from the origin stay either to the $-$ve side or the $+$ve side throughout the entire duration of evolution t and probabilities of such events are $h(t)/2$ each. The analytic expression in Eq. (2.56) has been compared with simulation data in Figure 2.7 where we observe very good agreement.

Once again, we emphasize that the distribution of t_r in Eq. (2.56) is derived for symmetric initial condition, i.e., RTP initially chooses $\pm v_0$ with equal probability 1/2. However, it is easy to extend this derivation for asymmetric initial condition also. We refer the readers to appendix 8.7 for the details on this calculations. For the asymmetric case, we find that while the non-delta function part is exactly same as in the symmetric case in Eq. (2.56), the coefficients of the delta function parts depend on $a_\pm$. This dependence can be understood in the same way as for the symmetric case.

2.5 Last passage time distribution $P_L(t_\ell, t)$

We saw that for a RTP with symmetric initial condition, the distributions of time t_m to reach maxima and the residence time t_r are exactly same. We now look at the distribution $P_L(t_\ell,t)$ of the time t_ℓ at which the RTP, starting from the origin, crosses the origin for the last time. From Fig. 2.1, it is clear that one can break the trajectory from $[0,t]$ in two parts: (i) $[0,t_\ell]$

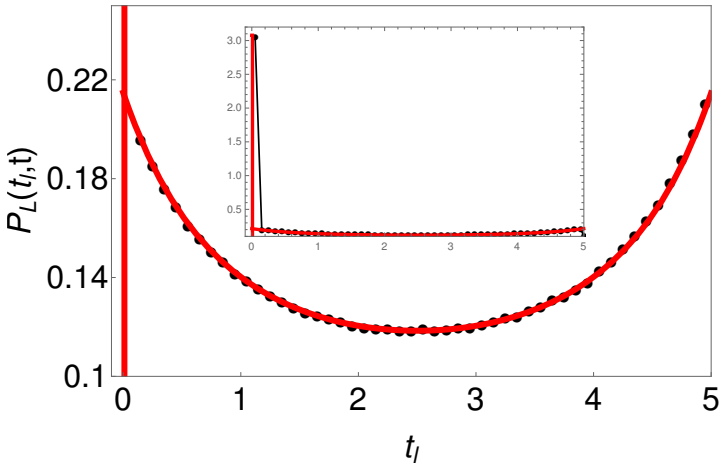

Figure 2.8: Plot of $P_L(t_\ell, t)$ in Eq. (2.60) and its comparison with numerical simulations for $\gamma = 1.5$, $v_0 = 1$ and $t = 5$. The solid red line is the analytic result and the black dots are simulation data. The inset shows the delta function at $t_\ell = 0$.

part and (ii) $[t_\ell, t]$ part. In first part, the particle reaches the origin at time t_ℓ with orientation σ_ℓ given that it was initially at the origin with orientation σ_0. The probability of such events is $P_{\sigma_\ell}(0, t_\ell|0, \sigma_0)v_0 dt_\ell$ where the notation $P_{\sigma_\ell}(0, t_\ell|0, \sigma_0)$ denotes the aforementioned probability distribution in an infinite line. In second part, the particle, starting from the origin, does not return the origin in the remaining interval $(t-t_\ell)$; the probability of which is $h(t-t_\ell)$. Therefore, we have

$$P_L(t_\ell, t)dt_\ell = \sum_{\sigma_\ell=\pm} v_0 dt_\ell P_{\sigma_\ell}(0, t_\ell|0, \sigma_0)\ h(t - t_\ell). \tag{2.57}$$

To write the distribution in infinite line, we use the following results of [70, 114]:

$$P_{\sigma_\ell}(0, t_\ell|0, \sigma_0) = \frac{\delta(t_\ell)}{2v_0} + \frac{\gamma\ e^{-\gamma t_\ell}}{4v_0}[I_0(\gamma t_\ell) + I_1(\gamma t_\ell)], \tag{2.58}$$

$$= \frac{\delta(t_\ell)}{2v_0} + \frac{\gamma\ h(t_\ell)}{4v_0}, \tag{2.59}$$

where $h(t)$ is given in Eq. (2.19). Inserting this expression in Eq. (2.57), we get

$$P_L(t_\ell, t) = \delta(t_\ell)h(t) + \frac{\gamma}{2}h(t_\ell)h\left(t - t_\ell\right), \tag{2.60}$$

Note that the result in Eq. (2.59) is independent of σ_0. Therefore, Eq. (2.60) also holds for asymmetric initial condition. In Figure 2.8, we compare the analytic expression with numerical simulations. We observe nice agreement between them. Finally, we observe that distribution $P_L(t_\ell, t)$ is almost same as the other two distributions $P_M(t_m, t)$ and $P_R(t_r, t)$ except that $P_L(t_\ell, t)$ has only one delta function at $t_\ell = 0$. Presence of this δ-function at $t_\ell = 0$ stems

from the same reasons with which they appear in the cases of t_m and t_r. This represents the contribution from those trajectories which starting from the origin, go in either +ve or −ve direction and stays in that region for the entire duration of evolution t.

2.6 Summary

In this chapter, we examined the statistics of the following three quantities for a one dimensional RTP starting from the origin: (i) the time t_m taken to achieve the maximum displacement M, (ii) the residence time t_r on the positive (or equivalently negative) semi-axis and (iii) the last time t_ℓ that the particle crosses the origin. For Brownian motion, the distributions of these three quantities turn out to be exactly same as shown by P. Lévy in [120]. Herein, we studied their statistics for a single RTP. By focusing on a simple run and tumble particle, our study illustrated the effect of persistence on the distributions of these quantities. We find that all three distributions possess the delta-function part and a non-delta function part. While for t_m and t_r, the distribution has two delta functions at $t_m = 0$ and $t_m = t$ (and same for t_r), one finds only one delta function at $t_\ell = 0$ for the last passage time. Moreover, if the RTP initially chooses $\pm v_0$ velocity with equal probability 1/2, then the non-delta function part in all three cases are exactly same. For this case, exact expressions of these three distributions are given in Eq. (2.34) for t_m, in Eq. (2.56) for t_r and in Eq. (2.60) for t_ℓ. On the other hand, if $\pm v_0$ velocities are initially chosen with probability $a_\pm$ where $a_+ \neq a_- \neq 1/2$, then the non-delta function parts are also different.

Interestingly it turns out that although we have considered a simple one dimensional run and tumble particle in this chapter, recent studies have revealed that our results on t_m and t_r in Eqs. (2.34) and (2.56) respectively are true even for d-dimensional run and tumble motion [92, 93]. While for t_m this can be analytically proved, it remains still an open problem to prove this for t_r. Furthermore, analysing arcsine laws for other models of active particles like active Brownian particle and active Ornstein-Uhlenbeck particle are interesting future directions. At the end, we remark that some of our results may be verified experimentally using E. Coli in an isotropic medium. Especially, our result for t_m in Eq. (2.34) is valid even in higher dimensions. Therefore, it would be interesting to analyze the space-time trajectories of an E. Coli and compare the results on extreme-value statistics with our analytical results.

Chapter 3

Convex hull of a run and tumble particle in two dimensions

In the previous chapter, one of the problems that we considered was the statistics of the maximum displacement M of the 1-d RTP and the time t_m taken to reach this maximum displacement. Interestingly, the knowledge of these two quantities play a pertinent role in calculating the statistical properties of the convex hull of a general 2-d stochastic process. To define a convex hull, let us assume that $(\vec{r}_1, \vec{r}_2, ..., \vec{r}_N)$ represent the position of a particle in two dimensions at various instances of time. Then, convex hull refers to the smallest convex polygon that encloses all these points [125–127]. We refer to Figure 3.1 for a schematic illustration of a convex hull. Geometrically, it gives a measure of the spatial extent over which the particle has moved in a given duration of time. As such, convex hull has been useful in ecology in estimating the home-range size of foraging animals from their locational data [164]. In the random walk literature, the mean perimeter and the mean area of the convex hull were found to have connections with the subject of the extreme-value statistics (see [161] for a review and also discussion below) which has lead to the computation of these quantities for a wide variety of processes [165–177]. For a two dimensional RTP also, this connection was instrumental in computing the mean perimeter exactly in [178]. Here, we present a study on its mean area. Our aim is to demonstrate how it gets modified due to the persistence motion of the RTP. From an experimental point of view, since the RTP is an emblematic model for the bacterial motion [29, 30], we expect our study to be useful in estimating the spatial extent over which the bacteria move during their (food) search activities. This, in turn, may find application in designing and demarcating their mobility territory.

The rest of this chapter is organised as follows: We first discuss precise run and tumble model in two dimensions in Sec. 3.1. Then, in Sec. 3.2, we briefly discuss the central idea for computing the mean area of the convex hull for a general two dimensional stochastic process. We then use

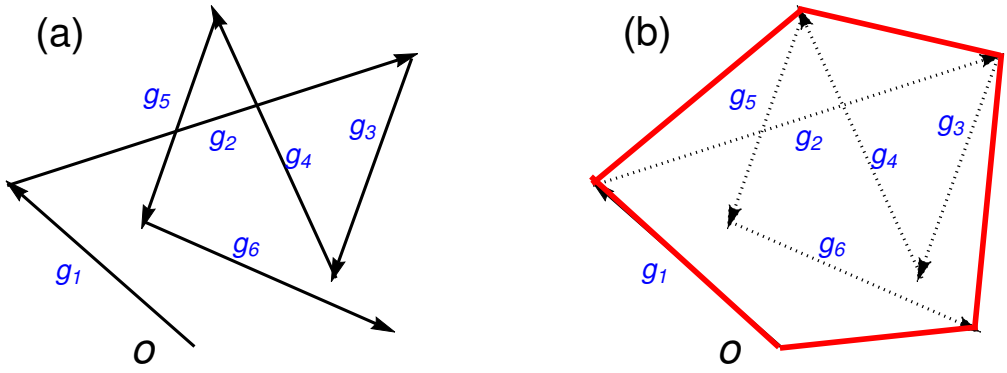

Figure 3.1: Panel (a) shows a typical trajectory of a RTP in two dimensions with $n = 6$ number of runs. The corresponding convex hull is shown in red in panel (b). Here $\vec{g_i} = (x_i, y_i)$ is the increment in the position in i-th run.

this idea to demonstrate the mean area for RTP in Secs. 3.3 and 3.4. Finally, we summarise in Sec. 3.5.

3.1 Model

We first discuss the run and tumble model in two dimensions and introduce the notations that will be useful in the subsequent sections. Starting from the origin, the particle chooses a random direction ϕ_1 measured with respect to the x-axis and drawn uniformly between $[0, 2\pi)$. It then performs a ballistic run along this direction for a random time τ_1 drawn from the exponential distribution $\rho(\tau) = \gamma e^{-\gamma\tau}$. After this, the particle tumbles instantaneously to choose another direction ϕ_2 uniformly between $[0, 2\pi)$ for the next run. The next run lasts for another random time τ_2 drawn independently from $\rho(\tau)$. In this way, the particle moves in a series of runs and tumbles. During the i-th run, the increment $\vec{g_i} = (x_i, y_i)$ in the position of the RTP is given by

$$x_i = v_0 \tau_i \cos(\phi_i), \tag{3.1}$$

$$y_i = v_0 \tau_i \sin(\phi_i). \tag{3.2}$$

Then, the position of the RTP at the end of the i-th run reads

$$X_i = X_{i-1} + x_i, \tag{3.3}$$

$$Y_i = Y_{i-1} + y_i, \tag{3.4}$$

where $i = 1, 2, ...$ Note that the particle is initially located at the origin which gives $(X_0, Y_0) = (0, 0)$. In this chapter, we consider this model in two different statistical ensembles depending on whether (i) the number of tumbles n or (ii) the total observation time t is fixed. In case (i), the number of tumbles n is held fixed but the total observation time t varies from realisation to realisation. On the other hand, for case (ii), the number of tumbles fluctuates from sample to sample and we stop the process once the total observation time t has elapsed. We will refer to (i) as fixed-n ensemble and (ii) as fixed-t ensemble. For these two ensembles, we analytically compute the mean area by using the relevant connection to the extreme-value statistics. Below, we briefly discuss the key idea to compute the mean area of the convex hull for a general two dimensional stochastic process. A more rigorous account of this idea can be found in [161].

3.2 Mean area of the convex hull

Consider a closed curve $\mathcal{C}$ in two dimensions parametrised by points $\{(\mathcal{X}(s), \mathcal{Y}(s))\}$ on its boundary where s represents the arc length. Given this curve $\mathcal{C}$, its maximum extension $\mathcal{M}(\theta)$ along the direction θ (with respect to the x-axis) is given by

$$\mathcal{M}(\theta) = \max_{s \in \mathcal{C}} \left[\mathcal{X}(s) \cos\theta + \mathcal{Y}(s) \sin\theta\right]. \tag{3.5}$$

According to Cauchy's formulae, the perimeter L and the area A of the domain bounded by $\mathcal{C}$ are given in terms of $\mathcal{M}(\theta)$ as [179]

$$L = \int_0^{2\pi} d\theta\ \mathcal{M}(\theta), \tag{3.6}$$

$$A = \frac{1}{2} \int_0^{2\pi} d\theta \left[\mathcal{M}^2(\theta) - \left(\mathcal{M}'(\theta)\right)^2\right], \tag{3.7}$$

where $\mathcal{M}'(\theta) = \frac{d\mathcal{M}(\theta)}{d\theta}$. To proceed further, we consider a two dimensional discrete time process of n time-steps whose positions at successive times are denoted by $\{(X_i, Y_i)\}$ with $1 \leq i \leq n$. Moreover, the curve $\mathcal{C}$ now represents the convex hull for the points $\{(X_i, Y_i)\}$. As evident from Eq. (3.7), one then needs to construct the support function $\mathcal{M}(\theta)$ in order to compute the area of the convex hull $\mathcal{C}$. Now to construct this support function, one needs the knowledge of the points $\{(\mathcal{X}(s), \mathcal{Y}(s))\}$ which is a difficult task. Fortunately, as shown in [127, 161], $\mathcal{M}(\theta)$ also represents the maximum of the projections of all $\{(X_i, Y_i)\}$ along the direction θ. The support function then becomes

$$\mathcal{M}(\theta) = \max_{1 \leq i \leq n} \left[X_i \cos\theta + Y_i \sin\theta\right], \tag{3.8}$$

and the mean area of the convex hull for this n-stepped stochastic process is given by

$$\langle A_n \rangle = \frac{1}{2} \int_0^{2\pi} d\theta \left[\langle \mathcal{M}^2(\theta) \rangle - \langle \left(\mathcal{M}'(\theta) \right)^2 \rangle \right]. \tag{3.9}$$

To construct $\mathcal{M}(\theta)$, we assume that the maximum in Eq. (3.8) is reached at k^* step which then gives

$$\mathcal{M}(\theta) = X_{k^*} \cos\theta + Y_{k^*} \sin\theta, \tag{3.10}$$

$$\mathcal{M}'(\theta) = -X_{k^*} \sin\theta + Y_{k^*} \cos\theta. \tag{3.11}$$

These two equations in conjunction with Eq. (3.9) give the mean area of the convex hull for a general discrete-time stochastic process. However, for isotropic processes, we can further simplify this formula by noting that both $\langle \mathcal{M}^2(\theta) \rangle$ and $\langle \mathcal{M}'^2(\theta) \rangle$ are independent of the direction θ. We then just consider the direction $\theta = 0$ and rewrite Eq. (3.9) as

$$\langle A_n \rangle = \pi \left[\langle M_n^2 \rangle - \langle Y_{k^*}^2 \rangle(n) \right]. \tag{3.12}$$

Here $M_n = \max[X_1, X_2, ..., X_n]$ is the maximum displacement along the x-axis achieved at k^* time-step and Y_{k^*} is the corresponding abscissa. Eq. (3.12) will be instrumental in calculating the mean area in the fixed-n ensemble. While Eq. (3.12) has been obtained for discrete time isotropic stochastic process, it is straightforward to extend this analysis for continuous time case also. For this case, the mean area is given by [161]

$$\langle A(t) \rangle = \pi \left[\langle M^2(t) \rangle - \langle Y(t_m)^2 \rangle(t) \right], \tag{3.13}$$

where $M(t) = \max[\{X(\tau)\},\ \forall\ 0 \leq \tau \leq t]$ is the maxima along x-axis, t_m is the time at which this maximum is reached and $Y(t_m)$ is the corresponding y-coordinate. Once again Eq. (3.13) will be useful in computing the mean area for the fixed-t ensemble. In the following sections, we proceed to calculate the mean area of the convex hull for a RTP in the fixed-n and the fixed-t ensembles separately.

3.3 Mean area for fixed-n ensemble

We first consider the mean area in the fixed-n ensemble. As clear from Eq. (3.12), this problem reduces to the computation of the statistics of the maximum M_n of the x-coordinate and the corresponding y-coordinate $Y_{k^*}(n)$ where k^* denotes the time-step at which M_n is achieved. To

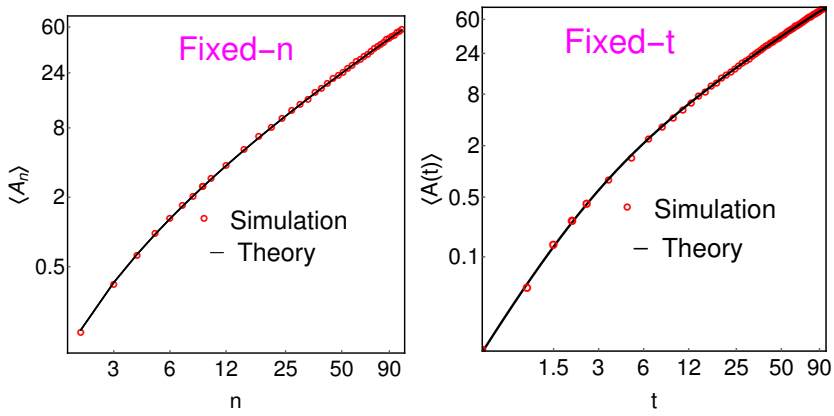

Figure 3.2: Log-Log plot of the mean area of the convex hull of a RTP in fixed-n ensemble (left) and fixed-t ensemble (right). We have also performed a comparison with the numerics. The corresponding analytic expressions are derived in Eqs. (3.35) and (3.59) respectively. For both plots, parameters chosen are $v_0 = 1$, $\gamma = 1.5$.

this end, we calculate the joint probability distribution $p(x_i, y_i, \tau_i)$ of the increments (x_i, y_i) and the run duration τ_i. Since, the RTP moves ballistically during i-th run, one has $x_i^2 + y_i^2 = v_0^2 \tau_i^2$ with the run time τ_i drawn from the exponential distribution. Hence the joint probability distribution $p(x, y, \tau)$ of the increments $x_i = x,\ y_i = y$ and $\tau_i = \tau$ is given by

$$p(x, y, \tau) = \frac{\gamma e^{-\gamma \tau}}{\pi}\ \delta(v_0^2 \tau^2 - x^2 - y^2). \tag{3.14}$$

The factor $1/\pi$ is the normalisation constant. Marginalising $p(x, y, \tau)$ over τ gives the joint distribution of the increments as

$$p(x, y) = \frac{\gamma}{2\pi v_0\ \sqrt{x^2 + y^2}}\ \exp\left(-\frac{\gamma}{v_0}\sqrt{x^2 + y^2}\right). \tag{3.15}$$

From Eqs. (3.3) and (3.4), we see that the run and tumble motion with fixed number of tumbles is equivalent to a random walker in two dimensions with increments (x, y) drawn from the joint distribution $p(x, y)$ in Eq. (3.15). In what follows, we use this mapping to an isotropic random walker in two dimensions to compute the quantities $\langle M_n^2 \rangle$ and $\langle Y_{k^*}^2 \rangle(n)$ and then insert them in Eq. (3.12) to calculate the mean area.

3.3.1 Computation of $\langle M_n^2 \rangle$

We first compute the second moment of the maximum M_n along x-axis of the random walker whose positions at different time steps are denoted by $\{X_0, X_1, X_2, ...X_n\}$. These positions evolve according to the update rule given in Eq. (3.3) with increments $\{x_i\}$ drawn independently from the distribution $p_1(x)$. This probability distribution is obtained by integrating $p(x, y)$ in Eq.

(3.15) over y:

$$p_1(x) = \int_{-\infty}^{\infty} dy\ p(x,y) = \frac{\gamma}{\pi v_0} K_0\left(\frac{\gamma|x|}{v_0}\right). \tag{3.16}$$

Here $K_0(z)$ denotes the zeroth order modified Bessel function of second kind. Note that $p_1(x)$ is continuous and symmetric function of x. Therefore, the auxillary random walker is characterised by independent and identical jump increments that are drawn from continuous and symmetric distribution. This enables us to use the Pollaczek-Spitzer formula which specifies the maximum of a random walker with independent and identical increments drawn from continuous and symmetric distribution [180]. This formula gives the cumulative probability $Q_n(M) = \text{Prob}[M_n \leq M]$ of the maximum M_n as [180, 181]

$$\sum_{n=0}^{\infty} z^n \langle e^{-\lambda M_n}\rangle = \sum_{n=0}^{\infty} z^n \int_0^{\infty} dM e^{-\lambda M} Q_n'(M) = \frac{\phi(z,\lambda)}{\sqrt{1-z}}, \tag{3.17}$$

where $0 \leq z \leq 1$ and $\lambda \geq 0$ and the function $\phi(z,\lambda)$ is defined as

$$\phi(z,\lambda) = \exp\left(-\frac{\lambda}{\pi}\int_0^{\infty} d\xi\ \frac{\ln(1-z\hat{p}_1(\xi))}{\lambda^2+k^2}\right). \tag{3.18}$$

Here $\hat{p}_1(\xi)$ is the Fourier transform of $p_1(x)$ which from Eq. (3.16) can be written as

$$\hat{p}_1(\xi) = \int_{-\infty}^{\infty} dx\ e^{i\xi x} p_1(x)\ = \frac{1}{\sqrt{1+\xi^2\bar{\sigma}^2}}, \qquad \text{with } \bar{\sigma} = \frac{v_0}{\gamma} \tag{3.19}$$

Finally, expanding Eq. (3.17) in λ, we see that the generating functions of the first two moments of M_n are [182]

$$h^{(1)}(z) = \sum_{n=0}^{\infty} z^n \langle M_n\rangle = \frac{1}{\pi(1-z)}\int_0^{\infty}\frac{d\xi}{\xi^2}\ \ln\left(\frac{1-z\hat{p}_1(\xi)}{1-z}\right), \tag{3.20}$$

$$h^{(2)}(z) = \sum_{n=0}^{\infty} z^n \langle M_n^2\rangle = (1-z)\left[h^{(1)}(z)\right]^2 + \frac{\bar{\sigma}^2 z}{2(1-z)^2}. \tag{3.21}$$

Next, we expand the right hand side of Eq. (3.21) in z and the coefficient of z^2 term gives $\langle M_n^2\rangle$. Interestingly, $\langle M_n^2\rangle$ can be expressed in terms of $\langle M_n\rangle$ and the variance of jumps as

$$\langle M_n^2\rangle = \sum_{m=1}^{n-1}\langle M_m\rangle\left[\langle M_{n-m}\rangle - \langle M_{n-m-1}\rangle\right] + \frac{n\bar{\sigma}^2}{2}. \tag{3.22}$$

Hence we need the expression of mean $\langle M_n\rangle$ to obtain the second moment $\langle M_n^2\rangle$. This can, in principle, be done by differentiating the right hand side of Eq. (3.20) with respect to z. This

has been computed in [178] exactly and we use this expression here as

$$\langle M_n \rangle = \frac{\bar{\sigma}}{2\sqrt{\pi}} \sum_{j=1}^{n} \frac{\Gamma\left(\frac{j+1}{2}\right)}{\Gamma\left(\frac{j+2}{2}\right)}. \tag{3.23}$$

From this expression, it then follows

$$\langle M_{n-m} \rangle - \langle M_{n-m-1} \rangle = \frac{\bar{\sigma}}{2\sqrt{\pi}} \frac{\Gamma\left(\frac{n-m+1}{2}\right)}{\Gamma\left(\frac{n-m+2}{2}\right)}, \quad n > 1. \tag{3.24}$$

which we plug in Eq. (3.22) to obtain

$$\langle M_n^2 \rangle = \frac{v_0^2}{2\gamma^2} \left(\frac{\mathcal{S}_n}{\pi} + n \right), \quad n > 1 \tag{3.25}$$

where the quantity $\mathcal{S}_n$ is defined as

$$\mathcal{S}_n = \frac{\sqrt{\pi}}{\sigma} \sum_{m=1}^{n-1} \frac{\Gamma\left(\frac{n-m+1}{2}\right)}{\Gamma\left(\frac{n-m+2}{2}\right)} \langle M_m \rangle. \tag{3.26}$$

$$= \frac{2+\pi}{\sqrt{\pi}} \left[\frac{\Gamma\left(\frac{n-1}{2} - \lfloor \frac{n-3}{2} \rfloor\right)}{\Gamma\left(\frac{n}{2} - 1 + \lceil \frac{3-n}{2} \rceil\right)} + \frac{\Gamma\left(\frac{n}{2} + 1 - \lfloor \frac{n}{2} \rfloor\right)}{\Gamma\left(\frac{n+1}{2} - \lfloor \frac{n}{2} \rfloor\right)} - \frac{\Gamma\left(\frac{n+2}{2}\right)}{\Gamma\left(\frac{n+1}{2}\right)} - \frac{\Gamma\left(\frac{n+1}{2}\right)}{\Gamma\left(\frac{n}{2}\right)} \right] \Theta(n-1)$$

$$+ \sum_{m=1}^{n-1} \frac{\Gamma\left(\frac{n-m+1}{2}\right)}{\Gamma\left(\frac{n-m+2}{2}\right)} \left[\frac{\Gamma\left(2 + \lfloor \frac{m-1}{2} \rfloor\right)}{\Gamma\left(\frac{3}{2} + \lfloor \frac{m-1}{2} \rfloor\right)} + \frac{\Gamma\left(\frac{3}{2} + \lfloor \frac{m}{2} \rfloor\right)}{\Gamma\left(1 + \lfloor \frac{m}{2} \rfloor\right)} \right]. \tag{3.27}$$

For large n, one can simplify this expression as

$$\mathcal{S}_n \simeq \pi n, \quad \text{as } n \to \infty. \tag{3.28}$$

The details of this calculation are given in appendix 8.9. To summarise, we have obtained the exact form of $\langle M_n^2 \rangle$ which will be useful to compute the mean area in Eq. (3.12).

3.3.2 Computation of $\langle Y_{k^*}^2 \rangle(n)$

We now calculate the second quantity $\langle Y_{k^*}^2 \rangle(n)$ required to compute the mean area in Eq. (3.12). For this, we first construct the grand joint distribution $\mathscr{P}(M, Y, k^*|n)$ of the maximum $M_n = M$ along x-axis reached at k^* time-step with the corresponding displacement along y-axis being $Y_{k^*} = Y$. We then use it to calculate the second moment of Y. Formally, this grand joint distribution can be written as

$$\mathscr{P}(M, Y, k^*|n) = \int \vec{dx}\ \vec{dy}\ \mathcal{Z}_{k^*}\big(M, Y, \{x_i\}, \{y_i\}\big) \prod_{j=1}^{n} p(x_j, y_j), \tag{3.29}$$

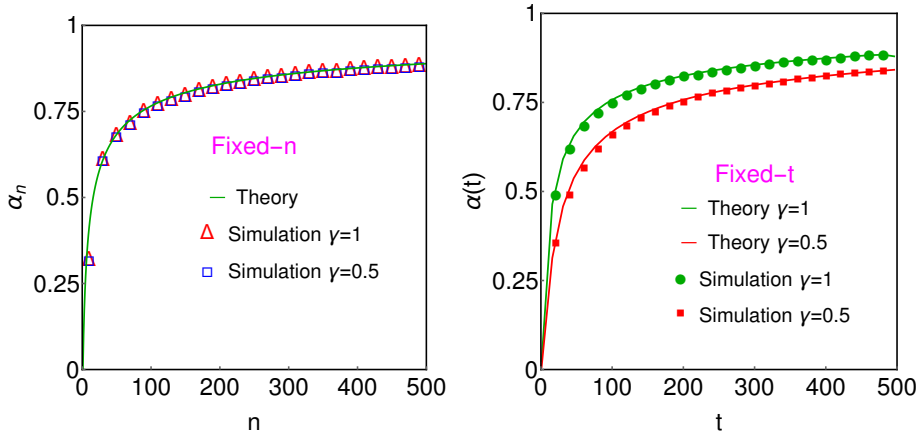

Figure 3.3: Plot of α_n vs. n (left panel) and $\alpha(t)$ vs. t (right panel) for two different values of γ and $v_0 = 1$ and their comparison with the numerics. The corresponding expressions of α_n and $\alpha(t)$ are, respectively, given in Eqs. (3.38) and (3.63).

with the short-hand notation $\vec{dx} = dx_1 dx_2 ... dx_n$ and $\vec{dy} = dy_1 dy_2 ... dy_n$. Also, the function $\mathcal{Z}_{k^*}\left(M, Y, \{x_i\}, \{y_i\}\right)$ is defined as

$$\mathcal{Z}_{k^*}\left(M, Y, \{x_i\}, \{y_i\}\right) = \left[\prod_{j\neq k^*, j=0}^{n} \Theta\left(M - X_j\right)\right] \delta\left(M - X_{k^*}\right)\ \delta\left(Y - Y_{k^*}\right). \tag{3.30}$$

Let us try to understand various terms appearing in Eq. (3.29). Recall that $X_i = \sum_{j=1}^{i} x_j$ and $Y_i = \sum_{j=1}^{i} y_j$ with $X_0 = Y_0 = 0$. The δ-functions in Eq. (3.30) then ensure that $X_{k^*} = M$ and $Y_{k^*} = Y$ while Θ-functions ensure that all other $\{X_i\}$ are below M. We then integrate over all increments $\{x_i, y_i\}$ with appropriate probability weight $\prod_{i=1}^{n} p(x_i, y_i)$.

Since, we are interested in the statistics of Y and k^*, we integrate $\mathscr{P}(M, Y, k^*|n)$ over M to obtain the joint distribution of Y and k^* as

$$\mathcal{P}(Y, k^*|n) = \int_0^\infty dM\ \mathscr{P}(M, Y, k^*|n). \tag{3.31}$$

Taking the Fourier transformation of this with respect to Y ($\to \xi$) and performing some algebraic simplications (see appendix 8.8), we get

$$\bar{\mathcal{P}}\left(\xi, k^*|n\right) = q_{k^*} q_{n-k^*}\ \left[\hat{p}_2(\xi)\right]^{k^*}, \tag{3.32}$$

where $\bar{\mathcal{P}}\left(\xi, k^*|n\right)$ denotes the Fourier transform of $\mathcal{P}(Y, k^*|n)$ and $\hat{p}_2(\xi)$ is the Fourier transformation of the marginal distribution of y-increment and is given by

$$\hat{p}_2(\xi) = \int_{-\infty}^{\infty} dy\ e^{i\xi y} \int_{-\infty}^{\infty} dx\ p(x, y) = \frac{1}{\sqrt{1 + \xi^2 \bar{\sigma}^2}}, \tag{3.33}$$

with $\bar{\sigma} = v_0/\gamma$. The other term q_n in Eq. (3.32) is the Sparre-Andersen survival probability of a random walker in one dimension starting from the origin and characterised by independent and identical increments drawn from symmetric and continuous distribution [183]. It is given by $q_n = \binom{2n}{n} 2^{-2n}$. Now to calculate $\langle Y^2 \rangle$, we differentiate Eq. (3.32) appropriately with respect to ξ and also use the relation $\sum_{k^*} k^* q_{k^*} q_{n-k^*} = n/2$ [181] to get

$$\langle Y^2_{k^*} \rangle(n) = \langle Y^2 \rangle = \frac{v_0^2}{2\gamma^2} n. \tag{3.34}$$

3.3.3 Mean area $\langle A_n \rangle$

We now have both quantities required to compute the mean area in Eq. (3.12). Plugging $\langle Y^2_{k^*} \rangle(n)$ from Eq. (3.34) along with $\langle M_n^2 \rangle$ from Eq. (3.25), the mean area of the convex hull of a 2-d isotropic RTP in the fixed-n ensemble is given by

$$\langle A_n \rangle = \frac{v_0^2}{2\gamma^2} \mathcal{S}_n, \quad n > 1 \tag{3.35}$$

where the term $\mathcal{S}_n$ is given in Eq. (3.27). In Figure 3.2, we have compared our analytic formula with the numerical simulations and we find excellent agreement between them. To construct convex hull numerically, we deploy the *Andrew's monotone chain algorithm* [184] which is further expedited with Akl's heuristic [185]. To calculate the area, we denote the m vertices of the convex hull as $\{\bar{X}_i, \bar{Y}_i\},\ 1 \leq i \leq m$ in order of their Cartesian coordinates and use

$$A = \frac{1}{2} \sum_{i=0}^{m-1} \left(\bar{Y}_i + \bar{Y}_{i+1} \right) \left(\bar{X}_i - \bar{X}_{i+1} \right), \tag{3.36}$$

with $(\bar{X}_0, \bar{Y}_0) = (\bar{X}_m, \bar{Y}_m)$. Finally, we estimate the mean area using the *simple sampling* where we generate 10^4 realisations of RTP, construct area of each of them using Eq. (3.36) and then take the average.

One can further simplify the expression of the mean area for large n. We have shown in (3.28) that $\mathcal{S}_n \simeq \pi n$ for larger values of n and using this in Eq. (3.35), we get

$$\langle A_n \rangle \simeq \frac{n\pi}{2} \frac{v_0^2}{\gamma^2}, \qquad \text{as } n \to \infty. \tag{3.37}$$

For better visibility of the mean area for different parameters, we define the following quantity

$$\alpha_n = \frac{2\langle A_n \rangle}{n\pi\sigma^2}, \tag{3.38}$$

and plot it as a function of n. From Eq. (3.35), we anticipate it to be independent of both v_0 and γ and also α_n should saturate to value 1 for $n \to \infty$. In Figure 3.3 (left panel), we have plotted α_n for different values of γ. We observe that the simulation data for all γ converge to the analytical result and also saturate to value 1 for large n. This also provides an additional verification of our result in Eq. (3.35).

3.4 Mean area for fixed-t ensemble

In the previous sections, we calculated the mean area in the fixed-n ensemble. Here, we look at the RTP in the fixed-t ensemble where the total observation time t is fixed while the number of tumbles n varies from realisation to realisation. As illustrated below, the results derived for the fixed-n ensemble before will be useful to derive the mean area for this case. The mean perimeter of the convex hull for this case was studied in [178]. Here, we study the mean area.

Let us consider a realisation of the RTP where it encounters n tumbles. Remeber that n fluctuates from sample to sample. Now after every run except the last one, the particle experiences a tumbling event. This implies that all run times $\{\tau_i\}$ for $1 \leq i \leq n-1$ are independently drawn from the exponential distribution $\rho(\tau) = \gamma e^{-\gamma \tau}$. Hence, the joint distribution $p(x_i, y_i, \tau_i)$ for the first $(n-1)$ runs is still given by Eq. (3.14). However, in the last run of duration τ_n, the particle is yet to experience a tumble: the probability of which is $e^{-\gamma \tau_n}$. Hence, the joint distribution for the last run is

$$p_{\rm last}(x_n, y_n, \tau_n) = \frac{e^{-\gamma \tau_n}}{\pi}\ \delta(v_0^2 \tau_n^2 - x_n^2 - y_n^2) = \frac{1}{\gamma}\ p(x_n, y_n, \tau_n), \tag{3.39}$$

with $p(x_n, y_n, \tau_n)$ is given by Eq. (3.14). Note that unlike in the fixed-n case, the total time t is fixed here, i.e. $\sum_{i=1}^{n} \tau_i = t$. Therefore, the grand joint distribution of the increments $\{x_i\},\ \{y_i\}$ and n reads

$$P\big(\{x_i\}, \{y_i\}, n|t\big) = \int_0^t d\tau_1 \int_0^t d\tau_2 .... \int_0^t d\tau_n\ \frac{1}{\gamma} \left[\prod_{i=1}^{n} p(x_i, y_i, \tau_i)\right] \delta\left(\sum_{i=1}^{n} \tau_i - t\right). \tag{3.40}$$

Taking Laplace transformation with respect to t ($\to s$) gets rid of the δ-function

$$\int_0^\infty dt\ e^{-st}\ P\big(\{x_i\}, \{y_i\}, n|t\big) = \frac{1}{\gamma} \left[\prod_{i=1}^{n} \frac{\gamma\ \exp\left(-\frac{(\gamma+s)}{v}\sqrt{x_i^2 + y_i^2}\right)}{2\pi v_0\ \sqrt{x_i^2 + y_i^2}}\right]. \tag{3.41}$$

Rewriting this equation as

$$\int_0^\infty dt\ e^{-st}\ P\big(\{x_i\},\{y_i\},n|t\big) = \frac{1}{\gamma}\left(\frac{\gamma}{\gamma+s}\right)^n\ \left[\prod_{i=1}^n g_s(x_i,y_i)\right], \tag{3.42}$$

$$\text{with} \qquad g_s(x,y) = \frac{(\gamma+s)\ \exp\left(-\frac{(\gamma+s)}{v}\sqrt{x_i^2+y_i^2}\right)}{2\pi v_0\sqrt{x^2+y^2}}, \tag{3.43}$$

we perform the inverse Laplace transformation to get

$$P\big(\{x_i\},\{y_i\},n|t\big) = \int_\Gamma \frac{ds}{2\pi i}\ e^{st}\ \frac{1}{\gamma}\left(\frac{\gamma}{\gamma+s}\right)^n\ \left[\prod_{i=1}^n g_s(x_i,y_i)\right], \tag{3.44}$$

where Γ is the Bromwich contour in the complex s plane. Now the function $g_s(x,y)$ in this equation is positive over all (x,y) and is also normalised to unity. Hence, we can interpret it as a probability distribution. This enables us to think of the term inside the square bracket in Eq. (3.44) as the joint distribution of the increments x_i and y_i of an auxillary isotropic random walker with correlated jumps and total time steps n. Such mapping of RTP to random walk has also been considered in [92] to study the survival probability. Here, we exploit this mapping to compute the mean area $\langle A(t)\rangle$ of the convex hull by using the Cauchy's formula in Eq. (3.13). This, in turn, reduces to calculating $\langle M^2(t)\rangle$ and $\langle Y(t_m)^2\rangle(t)$ which we consider below:

3.4.1 Computation of $\langle M^2(t)\rangle$

Let us calculate the first quantity $\langle M^2(t)\rangle$ needed for the mean area in Eq. (3.13). Recall that $M(t)$ is the maximum displacement along x-direction of the RTP till duration t. The joint distribution of the increments $\{x_i\}$ along x-direction and n is obtained by integrating $P\big(\{x_i\},\{y_i\},n|t\big)$ in Eq. (3.44) over all $\{y_i\}$:

$$P_x\big(\{x_i\},n|t\big) = \int_{-\infty}^\infty dy_1 dy_2..dy_n\ P\big(\{x_i\},\{y_i\},n|t\big), \tag{3.45}$$

$$= \int_\Gamma \frac{ds}{2\pi i}\ e^{st}\ \frac{1}{\gamma}\left(\frac{\gamma}{\gamma+s}\right)^n\ \left[\prod_{i=1}^n g_s(x_i)\right], \tag{3.46}$$

$$\text{with} \qquad g_s(x) = \int_{-\infty}^\infty dy\ g_s(x,y) = \frac{(\gamma+s)}{\pi v_0} K_0\left(\frac{(\gamma+s)|x|}{v_0}\right). \tag{3.47}$$

We use this expression of $P_x\big(\{x_i\},n|t\big)$ to obtain the statistics of $M(t)$. For this, we define $Q(M,n|t)$ as the probability that the x-position of the RTP is smaller than M, i.e. $X_i < M$ for $1 \le i \le n$, where $X_i = \sum_{j=1}^i x_j$. As done for the fixed-n ensemble, this (survival) probability

can be formally written as

$$Q(M,n|t) = \int_{-\infty}^{\infty} dx_1 ... \int_{-\infty}^{\infty} dx_n \text{ Prob.}\left[X_1 < M, X_2 < M, ..., X_n < M, n|t\right], \tag{3.48}$$

$$= \int_{-\infty}^{\infty} dx_1 ... \int_{-\infty}^{\infty} dx_n \; \Theta(M - X_1)..\Theta(M - X_n) \; P_x\big(\{x_i\}, n|t\big) \tag{3.49}$$

After performing some straightforward calculations, the second moment $\langle M^2(t)\rangle$ turns out to be

$$\langle M^2(t)\rangle = \sum_{n=1}^{\infty} \int_0^{\infty} dM \; M^2 \; \partial_M Q(M,n|t), \tag{3.50}$$

$$= \sum_{n=1}^{\infty} \int_{\Gamma} \frac{ds}{2\pi i} \; e^{st} \; \frac{1}{\gamma} \left(\frac{\gamma}{\gamma + s}\right)^n \; \langle M_s^2(n)\rangle. \tag{3.51}$$

Here we have summed over all possible n and defined $\langle M_s^2(n)\rangle$ as

$$\langle M_s^2(n)\rangle = \int_0^{\infty} dM \; M^2 \; \partial_M Q_s(M,n), \qquad \text{with} \tag{3.52}$$

$$Q_s(M,n) = \int_{-\infty}^{\infty} dx_1 ... \int_{-\infty}^{\infty} dx_n \; \Theta(M - X_1)..\Theta(M - X_n) \; \left[\prod_{i=1}^{n} g_s(x_i)\right]. \tag{3.53}$$

Note that $g_s(x)$ is normalised to unity and can be interpretated as the probability distribution of x. Hence, from Eq. (3.53), we can decipher $Q_s(M,n)$ as the cumulative probability that the maximum is below M for a random walker with n steps and independent and identical jumps characterised by symmetric and continuous distribution $g_s(x)$. This enables us to use the Pollaczek Spitzer formulae in Eqs. (3.20) and (3.21) to calculate $\langle M_s^2(n)\rangle$ (as done for the fixed-n ensemble) [180]. Proceeding exactly as before, we get

$$\langle M_s^2(n)\rangle = \frac{v_0^2}{2(\gamma + s)^2} \left(\frac{\mathcal{S}_n}{\pi} + n\right), \tag{3.54}$$

where $\mathcal{S}_n$ is given in Eq. (3.27). Substituting this form of $\langle M_s^2(n)\rangle$ in Eq. (3.51) and performing the inverse Laplace transformation, we get

$$\langle M^2(t)\rangle = \frac{v_0^2}{2\gamma^2} \left[e^{-\gamma t} - 1 + \gamma t + \frac{e^{-\gamma t}}{\pi} \sum_{n=1}^{\infty} \frac{\mathcal{S}_n}{\Gamma(n+2)} (\gamma t)^{n+1}\right]. \tag{3.55}$$

3.4.2 Computation of $\langle Y(t_m)^2\rangle(t)$

We next calculate the other quantity $\langle Y(t_m)^2\rangle(t)$ for the mean area $\langle A(t)\rangle$ in Eq. (3.13). Note that $Y(t_m|t)$ is the displacement along y-direction at time t_m when the RTP achieves maximum

along x-direction. We first notice that the maximum along x-axis will be reached at the end of some complete jump, say k^* which gives $Y(t_m) = \sum_{i=1}^{k^*} y_i$. Therefore, from the joint distribution $P(\{x_i\}, \{y_i\}, n|t)$ in Eq. (3.44) of the random walker, we have

$$\langle Y(t_m)^2 \rangle(t) = \int_\Gamma \frac{ds}{2\pi i}\ e^{st}\ \frac{1}{\gamma}\ \sum_{n=1}^{\infty} \left(\frac{\gamma}{\gamma+s}\right)^n\ \langle Y_{k^*}^2 \rangle_s(n), \tag{3.56}$$

where Y_{k^*} is the y-displacement of the random walker in Eq. (3.44) at the end of k^* time step during which maximum along x-axis is reached. Following the procedure given in sec. 3.3.2, we get

$$\langle Y_{k^*}^2 \rangle_s(n) = \frac{v_0^2}{(\gamma+s)^2}\frac{n}{2}. \tag{3.57}$$

Plugging this in Eq. (3.56) and performing the inverse Laplace transformation and then summing over n, we get

$$\langle Y(t_m)^2 \rangle(t) = \frac{v_0^2}{2\gamma^2}\left(\gamma t - 1 + e^{-\gamma t}\right). \tag{3.58}$$

3.4.3 Mean area $\langle A(t) \rangle$

We now have obtained both terms required for the mean area in Eq. (3.13). Substituting $\langle M^2(t) \rangle$ from Eq. (3.55) and $\langle Y(t_m)^2 \rangle(t)$ from Eq. (3.58) in Eq. (3.13), we find that $\langle A(t) \rangle$ possesses the scaling form

$$\langle A(t) \rangle = \frac{v_0^2}{2\gamma^2}\mathcal{J}(\gamma t), \tag{3.59}$$

with the scaling function $\mathcal{J}(w)$ is given by

$$\mathcal{J}(w) = e^{-w}\sum_{n=2}^{\infty}\frac{\mathcal{S}_n}{\Gamma(n+2)}w^{n+1}. \tag{3.60}$$

In Figure 3.2 (right panel), we have compared our analytic expression with the numerical simulation. We observe nice agreement between them. To contrast our result with that of the Brownian motion, we look at the asymptotic forms of $\langle A(t) \rangle$ in Eq. (3.59). For large t, we anticipate the number of tumbles n also to be large for which we have $\mathcal{S}_n \simeq \pi n$. Using this form gives the large-γt asymptotic form of $\langle A(t) \rangle$. On the other hand, for small γt, we simply consider the first few terms of the summation in $\mathcal{J}(w)$. The final asymptotic expressions of

$\langle A(t)\rangle$ are:

$$\langle A(t)\rangle \simeq \frac{\gamma v_0^2 t^3}{6\pi} + O(t^4), \qquad \text{for } t \ll \gamma^{-1} \tag{3.61}$$

$$\simeq \frac{\pi v_0^2}{2\gamma} t + O(\sqrt{t}), \qquad \text{for } t \gg \gamma^{-1}. \tag{3.62}$$

Indeed, for $t \gg \gamma^{-1}$, the leading order term matches with that of the Brownian motion with effective diffusion coefficient $v_0^2/2\gamma$ [127]. However, at small times, the behaviour of $\langle A(t)\rangle$ is quite different as indicated by the cubic ($\sim t^3$) growth. To understand this behaviour, we recall that the minimum number of tumbles experienced by the RTP is two (counting the starting point as a tumble). Under this circumstance, the convex hull is essentially a triangle with two sides of length $v_0\tau$ and $v_0(t-\tau)$ and angle ϕ between them chosen uniformly from $[0, 2\pi)$. Also note that the run time τ is exponentially distributed, i.e. $\rho(\tau) = \gamma e^{-\gamma\tau}$. Then, the area is given by $A(t) = |\frac{v_0^2\tau(t-\tau)\sin\zeta}{2}|$ whose mean grows as $\sim t^3$ with time. Hence, even though, we recover the Brownian motion result at large times, the short time behaviour of the mean area is rather different. Another way to see this difference is to define the quantity

$$\alpha(t) = \frac{2\langle A(t)\rangle}{\gamma t \pi \bar{\sigma}^2}, \qquad \text{with } \bar{\sigma} = \frac{v_0}{\gamma}. \tag{3.63}$$

Then, from Eq. (3.62), it follows that $\alpha(t)$ saturates to the value 1 as $t \to \infty$. Figure 3.3 (right panel) illustrates this fact where we plot $\alpha(t)$ versus t for two different values of γ and also compare with the numerics. For both cases, we observe excellent agreement of numerical data with our analytic expressions. Also, in both cases, $\alpha(t)$ approaches the value 1. This provides an additional verfication of our analytic formula in Eq. (3.59).

3.5 Summary

This chapter dealt with the mean area of the convex hull problem for a 2-d isotropic run and tumble motion. Motivated by the biological applicability of the RTP model to the bacterial motion, we computed the mean area exactly in two different statistical ensembles namely, (i) fixed-n ensemble and (ii) fixed-t ensemble. For both cases, we saw that the effect of persistence is sharply seen in the expression of the mean area at small and intermediate times. In fact, for fixed-t ensemble, we saw that $\langle A(t)\rangle$, at small times, has $\sim t^3$ scaling with time which is different than the Brownian behaviour (linear scaling) at large times. The crossover function connecting these two scaling regimes has been explicitly derived in Eq. (3.60).

We end this chapter by mentioning a few open directions. While the mean area and the mean

perimeter can be analytically calculated (thanks to their connection to the extreme-value statistics), obtaining analytic results for higher moments and probability distribution is still an open problem even for the simple Brownian motion. We believe that our work may have potential biological applications in estimating the spatial extent over which bacteria like E. Coli move, since they exhibit the run and tumble dynamics. Given that E. Coli inhabits the lower intestine of warm-blooded animals, this, in turn, may find application in designing and demarcating their mobility territory. However here, we have looked at the simple version of the RTP model where tumbles are instantaneous. On the other hand, experimentally, the bacteria spends small but non-zero time (~ 0.1s) during tumbling events. It would be an interesting future direction to extend our results to the realistic run and tumble model where tumbles are non-instantaneous as observed experimentally [29, 30]. We anticipate the results for fixed-n case to be same as our simple model with instantaneous tumbles. However, for fixed-t ensembles, the results will be different atleast at small and intermediate times. Furthermore, it also remains an open problem to study the convex hull problem for other models of active particles like active Brownian motion and active Ornstein-Uhlenbeck motion.

Chapter 4

Run-and-Tumble particle in inhomogeneous media in one dimension

Up to this point in the thesis, we have considered the run and tumble particle in homogeneous medium such that the motility parameters like v_0 and γ are constant both in space and time. However, experiments reveal that the run time for some species of bacteria like E Coli strongly depends on the concentration of the nutrient and its gradient [115–119]. Moreover, the run time also depends on whether the bacteria are moving along or opposite to the nutrient concentration gradient even though the run time is still exponentially distributed [30, 115]. Motivated from these observations, we study here a one dimensional run and tumble particle in heterogeneous medium where the flip from $+1 \to -1$ occurs with a rate $R_1(x)$ that is different than rate $R_2(x)$ with which flip from $-1 \to +1$ occur. Note that both $R_1(x)$ and $R_2(x)$ are functions of the position x and we consider the following forms in this chapter:

$$\begin{aligned} R_1(x) &= \left(\frac{|\, x \,|}{l}\right)^{\alpha} \left[\gamma_1\ \theta(x) + \gamma_2\ \theta(-x)\right], \\ R_2(x) &= \left(\frac{|\, x \,|}{l}\right)^{\alpha} \left[\gamma_2\ \theta(x) + \gamma_1\ \theta(-x)\right], \end{aligned} \tag{4.1}$$

where $\alpha \geq 0$, $\theta(x)$ is the Heaviside function and, γ_1 and γ_2 (both positive) are position independent rates. The constant l sets the length scale over which the rate functions vary. Given these rate functions, we compute, for different values of α, γ_1 and γ_2, the probability distribution function $P(x,t)$ in an infinite space, the survival probability in a semi-infinite line and the exit probability from a finite interval. Similar studies of RTP in heterogeneous settings have also been considered in [186] with position dependent speed $v_0(x)$, in [187] with inhomogeneous force field, in [188] with stochastic input signal, in Markov robots [189], in active gels [190, 191], in chemotaxis [192, 193] and quorum sensing [194, 195].

The rest of the chapter is structured as follows: In Sec. 4.1, we calculate the probability distribution $P(x,t)$ of finding the particle at position x at time t for different values of α. We then demonstrate the survival probability in Sec. 4.2 and the exit probability in Sec. 4.3. Finally, we summarise in Sec. 4.4

4.1 The probability density function $P(x,t)$

We first look at the probability distributions $P_{\pm}(x,t)$ of finding the RTP at position x at time t with velocity $\pm v_0$. We assume that the particle was initially located at the origin and can have velocity $\pm v_0$ with equal probability 1/2, i.e. $P_{\pm}(x,0) = \frac{1}{2}\delta(x)$. Following the Langevin equation (1.7) along with rates in Eq. (4.1), the distributions $P_{\pm}(x,t)$ satisfy the following Fokker-Planck equation:

$$\begin{aligned} \partial_t P_+(x,t) &= -v_0 \partial_x P_+(x,t) - R_1(x) P_+(x,t) + R_2(x) P_-(x,t), \\ \partial_t P_-(x,t) &= \quad v_0 \partial_x P_-(x,t) + R_1(x) P_+(x,t) - R_2(x) P_-(x,t). \end{aligned} \tag{4.2}$$

Our aim is to solve these coupled differential equations for different α. For this, we take the Laplace transformation of the distributions with respect to t ($\to s$) as

$$\bar{P}_{\pm}(x,s) = \int_0^{\infty} dt e^{-st} P_{\pm}(x,t). \tag{4.3}$$

The master equations (4.2) then become

$$\big(v_0 \partial_x + R_1(x) + s\big)\bar{P}_+ = R_2(x)\bar{P}_- + \frac{1}{2}\delta(x), \tag{4.4}$$

$$\big(-v_0 \partial_x + R_2(x) + s\big)\bar{P}_- = R_1(x)\bar{P}_+ + \frac{1}{2}\delta(x). \tag{4.5}$$

We next define the new variables

$$\bar{P}(x,s) = \bar{P}_+(x,s) + \bar{P}_-(x,s), \tag{4.6}$$

$$\bar{Q}(x,s) = \bar{P}_+(x,s) - \bar{P}_-(x,s), \tag{4.7}$$

and rewrite the above equations in terms of $\bar{P}(x,s)$ and $\bar{Q}(x,s)$ as

$$v_0 \partial_x \bar{P} + s\bar{Q} + \frac{2\,\mathrm{sgn}(x)\Delta \mid x \mid^{\alpha}}{l^{\alpha}}\bar{P} + \frac{2\gamma \mid x \mid^{\alpha}}{l^{\alpha}}\bar{Q} = 0, \tag{4.8}$$

$$s\bar{P} + v_0 \partial_x \bar{Q} = \delta(x), \tag{4.9}$$

with the notation $\Delta = \frac{\gamma_1 - \gamma_2}{2}$ and $\gamma = \frac{\gamma_1 + \gamma_2}{2}$. The signum function sgn(x) in Eq. (4.8) takes values -1 for $x < 0$, 0 for $x = 0$ and 1 for $x > 0$. Eliminating $\bar{P}(x, s)$ from Eq. (4.8) gives a closed equation for $\bar{Q}(x, s)$ which for $x \neq 0$ reads

$$\partial_x^2 \bar{Q} + \frac{2 \text{ sgn}(x) \Delta \mid x \mid^{\alpha}}{v_0 \ l^{\alpha}} \partial_x \bar{Q} - \left(\frac{2\gamma \ s \mid x \mid^{\alpha}}{v_0^2 \ l^{\alpha}} + \frac{s^2}{v_0^2} \right) \bar{Q} = 0. \tag{4.10}$$

We can, similarly, eliminate $\bar{Q}(x, s)$ from Eq. (4.9) and get a closed equation for $\bar{P}(x, s)$ as

$$s\bar{P}(x, s) - \delta(x) = \partial_x \left(\frac{v_0^2}{s + \frac{2\gamma \ |x|^{\alpha}}{l^{\alpha}}} \right) \left[\partial_x \bar{P}(x, s) + \frac{2\Delta \text{ sgn}(x) |x|^{\alpha}}{v_0 l^{\alpha}} \bar{P}(x, s) \right]. \tag{4.11}$$

One can, in principle, solve this equation and then perform the inverse Laplace transformation to obtain the distribution $P(x, t)$. However, it turns out convenient to solve Eq. (4.10) first and then use it to obtain $\bar{P}(x, s)$ from Eq. (4.9).

To simplify Eq. (4.10) further, we make the transformation

$$\bar{Q}(x, s) = e^{-\frac{\Delta |x|^{\alpha+1}}{v(\alpha+1) l^{\alpha}}} G(x, s), \tag{4.12}$$

and use it in Eq. (4.10) to get

$$\partial_x^2 G - \left[\frac{\Delta\alpha \mid x \mid^{\alpha-1}}{v_0 \ l^{\alpha}} + \frac{2\gamma s \mid x \mid^{\alpha}}{v_0^2 \ l^{\alpha}} + \frac{\Delta^2 \mid x \mid^{2\alpha}}{v_0^2 \ l^{2\alpha}} + \frac{s^2}{v_0^2} \right] G = 0. \tag{4.13}$$

We have finally reduced the coupled master equations (4.2) to this second-order differential equation. But solving this equation for arbitrary values of α is a challenging task. However for some specific values of α, we can solve it exactly. In what follows, we solve Eq. (4.13) separately for $\alpha = 0$ and $\alpha = 1$ and present some approximate results for general α.

4.1.1 Case I: $\alpha = 0$

For $\alpha = 0$, Eq. (4.13) takes the form

$$\partial_x^2 G - \lambda^2 G = 0, \tag{4.14}$$

where $\lambda(s) = \frac{1}{v_0} \sqrt{\Delta^2 + 2\gamma s + s^2}$. The boundary conditions to solve this equation are $G(x \to \pm\infty, s) = 0$ which stem due to the fact that the distributions $P_{\pm}(x \to \pm\infty, t) = 0$. It is

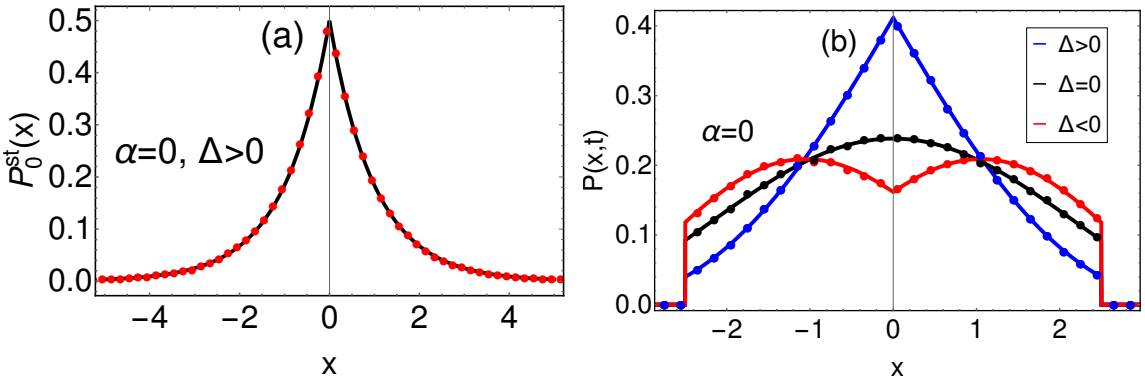

Figure 4.1: (a) Steady-state distribution $P_0^{st}(x)$ for $\alpha = 0$. The black solid line is the analytic expression given in Eq.(4.17) while the symbols are the simulation data for $v_0 = 1, \gamma_1 = 2$ and $\gamma_2 = 1$. (b) Comparison of the time dependent distribution $P(x,t)$ given in Eq. (4.19) for $\alpha = 0$ with the numerical simulations for $v_0 = 1$ and $t = 2.5$. The solid line is the analytic expression while the symbols are the simulation data. Parameters chosen are (i) $\gamma_1 = 1.5, \gamma_2 = 1$ (Blue) (ii) $\gamma_1 = \gamma_2 = 1$ (Black) and (iii) $\gamma_1 = 1, \gamma_2 = 1.5$ (Red). For better demonstration of the bulk part, we have not shown δ-functions in this plot.

straightforward to solve Eq. (4.14) to get

$$G(x,s) = \begin{cases} A_+ e^{-\lambda(s)x}, & \text{if } x > 0 \\ A_- e^{\lambda(s)x}, & \text{if } x < 0 \end{cases} \tag{4.15}$$

with $A_\pm$ are being position independent constants. Substituting this solution in Eq. (4.12) gives $\bar{Q}(x,s)$ which then gives $\bar{P}(x,s)$ from Eq. (4.9) in terms of $A_\pm$. To evaluate the constants $A_\pm$, one condition is obtained by noting the continuity of $\bar{P}(x,s)$ across $x = 0$. Another condition is obtained by integrating Eq. (4.9) from $-\epsilon$ to $+\epsilon$ and take $\epsilon \to 0$ which gives the discontinuity relation $\bar{Q}(x \to 0^+, s) - \bar{Q}(x \to 0^-, s) = \frac{1}{v_0}$. These two conditions then give $A_\pm$. The final expression of $\bar{P}(x,s)$ reads

$$\bar{P}(x,s) = \frac{1}{2s}\left(\lambda(s) + \frac{\Delta}{v_0}\right) e^{-\left(\lambda(s) + \frac{\Delta}{v_0}\right)|x|}. \tag{4.16}$$

The task now is to perform the inverse Laplace transformation to get the distribution in the time domain. First note that, for $\Delta > 0$ (*i.e.* $\gamma_1 > \gamma_2$), the RTP tumbles more frequently from $+1$ to -1 if $x > 0$ and from -1 to $+1$ if $x < 0$. This implies that the particle is drifted towards the origin from both sides of the origin for $\Delta > 0$. On the other hand, for $\Delta < 0$, the particle is drifted away from the origin. Hence, for $\Delta > 0$, we anticipate a stationary state distribution at

late times. Indeed, from Eq. (4.16), this stationary distribution is

$$P_0^{st}(x) = \lim_{s\to 0}\left[s\bar{P}(x,s)\right] = \frac{\Delta}{v_0}\, e^{-\frac{2\Delta}{v_0}|x|}, \tag{4.17}$$

which is the Laplace distribution characterised by the decay length $l_d = \frac{v_0}{2\Delta}$. Note that the decay length diverges as $\Delta \to 0$ implying no steady state for $\Delta = 0$ [70]. In Figure 4.1(a), we have compared this stationary distribution with the simulation data and we find excellent agreement between them. As mentioned before, the RTP experiences a drift away from the origin for $\Delta < 0$ which indicates no stationary distribution for this case. This can also be verified by noting that $\lim_{s\to 0}\left[s\bar{P}(x,s)\right] = 0$ for $\Delta < 0$.

Coming to the Laplace transform $\bar{P}(x,s)$ in Eq. (4.16), we use the following inverse Laplace transforms:

$$L_{s\to t}\left[e^{-\lambda(s)y}\right] = -\frac{d}{dy}\left[v_0 e^{-\gamma t} I_0\left(\sqrt{\gamma_1\gamma_2(t^2 - \frac{y^2}{v_0^2})}\right)\theta(v_0 t - y)\right]. \tag{4.18}$$

Here $L_{s\to t}[...]$ denotes the inverse Laplace transformation of $[...]$. Using this inversion in Eq. (4.16), we find the distribution $P(x,t)$ is given by

$$\begin{aligned} P(x,t) =& \frac{1}{2}e^{-\gamma_1 t}\delta(\mid x \mid - v_0 t) + \frac{\gamma_1}{2v_0}\left(1 + \frac{\gamma_2 \mid x \mid}{2v_0}\right) e^{-\frac{\gamma_1|x|}{2v_0}}\Theta\left(v_0 t - \mid x \mid\right) \\ & - \frac{\sqrt{\gamma_1\gamma_2}}{2v_0}\int_0^t d\tau\; e^{-\gamma\tau}\; \frac{d\,\mathcal{I}(\mid x \mid, \tau)}{d \mid x \mid}\Theta\left(v_0\tau - \mid x \mid\right), \end{aligned} \tag{4.19}$$

where $\mathcal{I}(x,t) = \frac{xe^{-\frac{\Delta x}{v_0}}}{v_0}\frac{I_1\left(\sqrt{\gamma_1\gamma_2(t^2-\frac{x^2}{v_0^2})}\right)}{\sqrt{t^2-\frac{x^2}{v^2}}}$ with $I_1(z)$ denoting the modified Bessel function of first kind. Let us now try to understand the distribution physically. Note that the distribution possesses δ-function terms at $x = \pm v_0 t$. They arise from those trajectories for which the RTP has not changed its velocity till duration t: the probability of which is $e^{-\gamma_1 t}$. The prefactor $1/2$ comes because the particle can choose $\pm v_0$ with equal probability $1/2$. Figure 4.1(b) shows the comparison of the distribution with the numerics for different values of Δ. For $\Delta < 0$, we observe that $P(x,t)$ has a dip at the origin while for $\Delta > 0$, $P(x,t)$ has a peak. This behaviour appears due to the fact that for $\Delta < 0$, there is a net drift away from the origin while for $\Delta > 0$, the drift is directed towards the origin. For $\Delta = 0$, our result is consistent with that in [70].

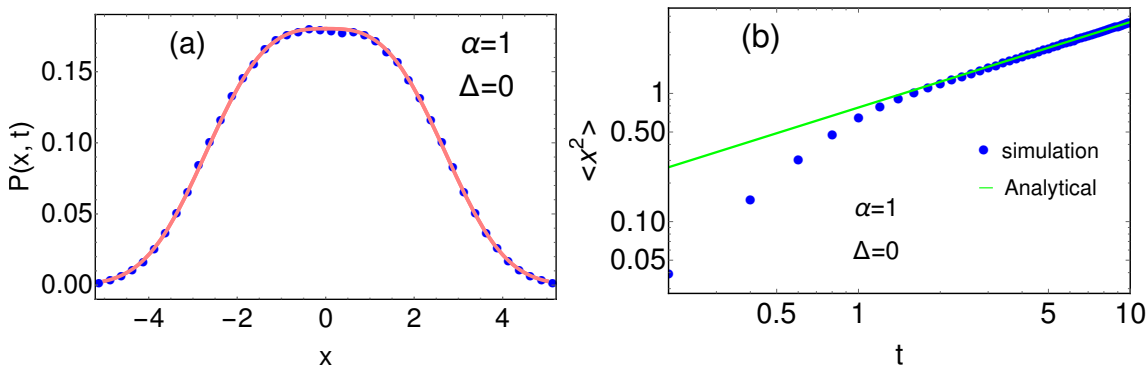

Figure 4.2: (a) Analytical expression of the distribution $P(x,t)$ given in Eq. (4.26) (solid line) for $\alpha = 1$ and $\Delta = 0$ is compared with the numerics (symbols) for $t = 10$. (b) Numerical verification of the scaling of the position as $x \sim t^{\frac{1}{3}}$ for $\alpha = 1$. For both plots, the chosen parameters are $v_0 = 1, \gamma_1 = \gamma_2 = 1.5$ and $l = 1$.

For large t, one can simplify the expression of the distribution in Eq. (4.19) as

$$P(x,t) \simeq \begin{cases} P_0^{st}(x) + \frac{e^{-t\left[\gamma-\sqrt{\gamma_1\gamma_2}\left(1-\frac{\bar{x}^2}{2}\right)+\Delta\bar{x}\right]}}{4|x|}\left[\sqrt{\frac{8t\sqrt{\gamma_1\gamma_2}}{\pi}}|\bar{x}| - te^{t\rho_-^2}\,\mathrm{Erfc}[\sqrt{t}\rho_-]\left(\Delta\bar{x}+\frac{\rho_+^2-\rho_-^2}{2}\right)\right. \\ \qquad \left. + te^{t\rho_+^2}\,\mathrm{Erfc}[\sqrt{t}\rho_+]\left(\Delta\bar{x}-\frac{\rho_+^2-\rho_-^2}{2}\right)\right], & \text{if } \gamma_1 > \gamma_2 \\ \frac{1}{\sqrt{4\pi D_0 t}}e^{-\frac{x^2}{4D_0 t}} & \text{if } \gamma_1 = \gamma_2 \\ \sqrt{\frac{\sqrt{\gamma^2-\Delta^2}}{2\pi t}}\frac{\bar{x}}{2v_0(1-\bar{x}^2)^{\frac{3}{4}}}\frac{\bar{x}\sqrt{\gamma^2-\Delta^2}+\Delta\sqrt{1-\bar{x}^2}}{\sqrt{\gamma^2-\Delta^2}-\gamma\sqrt{1-\bar{x}^2}}\,e^{-t\left[\Delta\bar{x}+\gamma-\sqrt{\gamma^2-\Delta^2}\sqrt{1-\bar{x}^2}\right]}, & \text{if } \gamma_1 < \gamma_2 \end{cases} \tag{4.20}$$

with $D_0 = \frac{v_0^2}{2\gamma}$, $\bar{x} = \frac{|x|}{v_0 t}$ and $\rho_\pm = \sqrt{\gamma - \sqrt{\gamma_1\gamma_2}} \pm \bar{x}\sqrt{\frac{\sqrt{\gamma_1\gamma_2}}{2}}$. A detailed derivation of these approximate expressions is given in appendix 8.10. For $\gamma_1 = \gamma_2$, we recover the Brownian motion limit and the distribution becomes Gaussian. However for $\gamma_1 \neq \gamma_2$, the distribution is strictly non-Gaussian. In fact for $\gamma_1 < \gamma_2$, the distribution has two symmetric moving peaks at $x = \pm\frac{|\Delta|}{\gamma}v_0 t$ which arises due to the effective drift that the particle experiences due to unequal rates.

4.1.2 Case II: $\alpha = 1$

Let us now consider the other analytically solvable case $\alpha = 1$. For this case, Eq. (4.13) becomes

$$\partial_x^2 G - \left[\frac{\Delta}{v_0 l} + \frac{2\gamma s \mid x \mid}{v_0^2 l} + \frac{s^2}{v_0^2} + \frac{\Delta^2 x^2}{v_0^2 l^2}\right] G = 0. \tag{4.21}$$

Below, we consider the $\Delta = 0$ case first and then $\Delta \neq 0$ case later.

4.1.2.1 $\Delta = 0$

For this case, Eq. (4.21) becomes

$$\partial_x^2 G(x,s) - \left[\frac{2\gamma s \mid x \mid}{v_0^2 l} + \frac{s^2}{v_0^2}\right] G(x,s) = 0. \tag{4.22}$$

The solution of this equation is given in terms of the Airy functions, i.e. $G(x,s) \sim \text{Ai}\left(\pm y + d_0\ s^{\frac{4}{3}}\right)$ with $y = c\ s^{\frac{1}{3}} \mid x \mid$ and $c = \left(\frac{2\gamma}{v_0^2 l}\right)^{\frac{1}{3}}$. Proceeding exactly in the same way as for $\alpha = 0$, we find that the Laplace transform $\bar{P}(x,s)$ for $\alpha = 1$ is given by

$$\bar{P}(x,s) = -\frac{c}{2s^{2/3}} \frac{\text{Ai}'\left(c\ s^{\frac{1}{3}} \mid x \mid + d_0\ s^{\frac{4}{3}}\right)}{\text{Ai}\left(d_0\ s^{\frac{4}{3}}\right)}, \tag{4.23}$$

where $d_0 = \frac{c\ l}{2\gamma}$. Now performing the inverse Laplace transformation of $\bar{P}(x,s)$ for arbitrary s turns out to be challenging. But for small s (which corresponds to large t in the time domain), we neglect $\sim O(s^{4/3})$ term in Eq. (4.23) and use $\text{Ai}(z) = \frac{\sqrt{z}}{\sqrt{3}\pi} K_{\frac{1}{3}}\left(\frac{2}{3} z^{\frac{3}{2}}\right)$. The resultant expression for $\bar{P}(x,s)$ for small s reads

$$\bar{P}(x,s) \simeq \frac{c^2 \mid x \mid}{2\sqrt{3}\pi \text{Ai}(0) s^{\frac{1}{3}}} K_{\frac{2}{3}}\left(\frac{2}{3}\left(c \mid x \mid\right)^{\frac{3}{2}} \sqrt{s}\right). \tag{4.24}$$

To perform the inverse Laplace transform of this equation, we use

$$L^{-1}_{s\to t}\left[2\sqrt{g}\ s^{m-1} K_{2\nu}\left(2\sqrt{gs}\right)\right] = t^{\frac{1}{2}-m} e^{-\frac{g}{2t}}\ W_{m-\frac{1}{2},\,\nu}\left(\frac{g}{t}\right), \quad \text{for } g > 0 \tag{4.25}$$

where $W_{m,\nu}(x)$ is the Whittaker function. Using this in Eq. (4.24), we find that the distribution $P(x,t)$ possess the scaling form

$$P(x,t) \simeq \frac{1}{t^{\frac{1}{3}}} f_1\left(\frac{|x|}{t^{\frac{1}{3}}}\right), \quad \text{for } \Delta = 0, \tag{4.26}$$

where the scaling function $f_1(y)$ is given by

$$f_1(y) = \frac{1}{4\pi \text{Ai}(0)} \sqrt{\frac{3c}{y}} e^{-\frac{y^3 c^3}{18}} W_{\frac{1}{6},\frac{1}{3}}\left(\frac{y^3 c^3}{9}\right). \tag{4.27}$$

The approximate equality in Eq. (4.26) indicates that the expression is valid only for large t. In Figure 4.2(a), we have plotted the distribution and compared it with the numerical simulations.

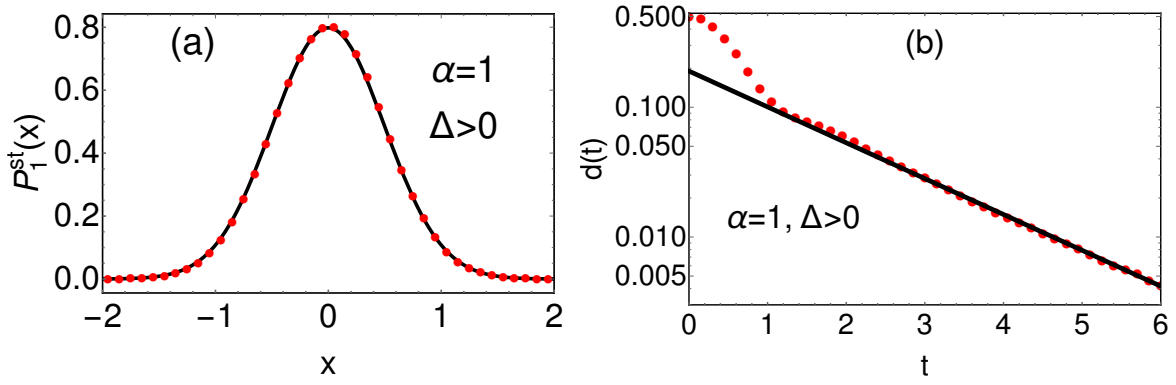

Figure 4.3: (a) Analytic expression of the stationary distribution $P_1^{st}(x)$ for $\alpha = 1$ given in Eq.(4.32) (solid line) is compared with the simulation of the Langevin equation (shown by filled circles). We have chosen are $v_0 = 1, l = 0.5, \gamma_1 = 3$ and $\gamma_2 = 1$. (b) We have shown the simulation data (filled circles) for $d(t) = \text{var}(\infty) - \text{var}(t)$ where $\text{var}(t) = \langle x(t)^2 \rangle - \langle x(t) \rangle^2$. As expected, we observe an exponential decay of the form $\sim e^{-\zeta t}$ of $d(t)$ at late times (shown by solid line) with $\zeta = 0.636$ obtained from the solution of Eq. (4.33) with largest real part. The parameters chosen are $\gamma_1 = 3.5, \gamma_2 = 1.5, v_0 = 1$ and $l = 1$.

We see excellent agreement between them. We get a further simplified expression of the scaling function $f_1(y)$ for smaller values of y by using $W_{\frac{1}{6},\frac{1}{3}}(y) \approx y^{\frac{1}{6}} e^{-\frac{y}{2}}$ for $y \to 0$ and $\text{Ai}(0) = \frac{\Gamma\left(\frac{1}{3}\right)}{2\pi 3^{\frac{1}{6}}}$ as

$$f_1(y) \simeq \frac{3^{\frac{1}{3}} c}{2\Gamma\left(\frac{1}{3}\right)} e^{-\frac{|y|^3 c^3}{9}}, \qquad \text{as } y \to 0. \tag{4.28}$$

From Eq. (4.26), we see that the position of the particle, for $\alpha = 1$, typically scales as $x \sim t^{\frac{1}{3}}$ which is different than the diffusive scaling of x for homogeneous case ($\alpha = 0$). Figure 4.2(b) illustrates this sub-diffusive scaling numerically. We finally remark that Eq. (4.28) describes the distribution only for typical fluctuations of x and fails as one moves towards the far tail of the distribution.

4.1.2.2 $\Delta \neq 0$

We next solve Eq. (4.21) for $\Delta \neq 0$. For this case, we make the transformation $\frac{z}{\sqrt{2}} = \frac{|\Delta|}{vl} x + \text{sgn}(x) \frac{\gamma s}{|\Delta|} \sqrt{\frac{l}{v|\Delta|}}$ Eq. (4.21) as

$$\partial_z^2 G - \left(\frac{z^2}{4} - \beta s^2 + \frac{\text{sgn}(\Delta)}{2} \right) G = 0 \tag{4.29}$$

where $\beta = \frac{l(\gamma^2-\Delta^2)}{2v_0|\Delta|^3}$. The solution of this equation is given in terms of the parabolic cylinder functions as

$$G(x,s) = \begin{cases} B_+ \; D_{\beta s^2 - \frac{1+\mathrm{sgn}(\Delta)}{2}} \left(\sqrt{\frac{2|\Delta|}{v_0 l}} \left(x + \frac{\gamma s l}{\Delta^2} \right) \right), & \text{if } x > 0 \\ B_- \; D_{\beta s^2 - \frac{1+\mathrm{sgn}(\Delta)}{2}} \left(\sqrt{\frac{2|\Delta|}{v_0 l}} \left(-x + \frac{\gamma s l}{\Delta^2} \right) \right), & \text{if } x < 0 \end{cases} \tag{4.30}$$

Substituting this solution in Eq. (4.12) gives $\bar{Q}(x,s)$ which then gives $\bar{P}(x,s)$ from Eq. (4.9) as

$$\bar{P}(x,s) = -\frac{1}{2s} \frac{d}{d \mid x \mid} \left[e^{-\frac{\Delta}{2v_0 l} x^2} \frac{D_{\beta s^2 - \frac{1+\mathrm{sgn}(\Delta)}{2}} \left(\sqrt{\frac{2|\Delta|}{v_0 l}} \left(\mid x \mid + \frac{\gamma s l}{\Delta^2} \right) \right)}{D_{\beta s^2 - \frac{1+\mathrm{sgn}(\Delta)}{2}} \left(\sqrt{\frac{2|\Delta|}{v_0 l}} \frac{\gamma s l}{\Delta^2} \right)} \right]. \tag{4.31}$$

As seen for $\alpha = 0$, for this case also, we anticipate a stationary distribution at large times for $\Delta > 0$. This can be obtained by taking the limit $\lim_{s\to 0} \left[s\bar{P}(x,s) \right]$. By noting $D_{-1}(z) = \sqrt{\frac{\pi}{2}} e^{\frac{z^2}{4}} \mathrm{Erfc}(\frac{z}{\sqrt{2}})$, we find

$$P_1^{st}(x) = \lim_{s\to 0} \left[s\bar{P}(x,s) \right] = \sqrt{\frac{\gamma_1 - \gamma_2}{2\pi v_0 l}} e^{-\frac{\gamma_1 - \gamma_2}{2v_0 l} x^2}, \tag{4.32}$$

with subscript 1 in $P_1^{st}(x)$ denoting $\alpha = 1$. In Figure 4.3(a), we have compared the stationary distribution with the direct numerical simulation and we find excellent agreement between them. While for $\alpha = 0$, the stationary distribution is the Laplace distribution, it is Gaussian for $\alpha = 1$.

Next, we study the relaxation to this steady state for $\Delta > 0$. Recall that the relaxation is controlled by the pole of $\bar{P}(x,s)$ with second largest real part (the largest pole is $s = 0$ which gives the steady state). If we denote this pole by ζ, then $|\zeta|^{-1}$ will set the timescale for the exponential relaxation. The pole ζ is obtained by solving

$$D_{\beta\zeta^2 - 1} \left(\sqrt{\frac{2 \mid \Delta \mid}{v_0 l}} \frac{\gamma \zeta l}{\Delta^2} \right) = 0. \tag{4.33}$$

We have verified this result in Figure 4.3(b) where we have plotted $d(t) = \mathrm{var}(\infty) - \mathrm{var}(t)$ as a function of t. Here $\mathrm{var}(t) = \langle x^2(t) \rangle - \langle x(t) \rangle^2$ is the variance of x. From the above discussion, we expect $d(t)$ to decay exponentially to zero as $d(t) \sim e^{-\zeta t}$ at large times. Indeed, in Figure 4.3(b), we numerically observe this exponential decay with timescale given by ζ^{-1}.

We next turn to $\Delta < 0$ case for which we have argued earlier there is no stationary state. In

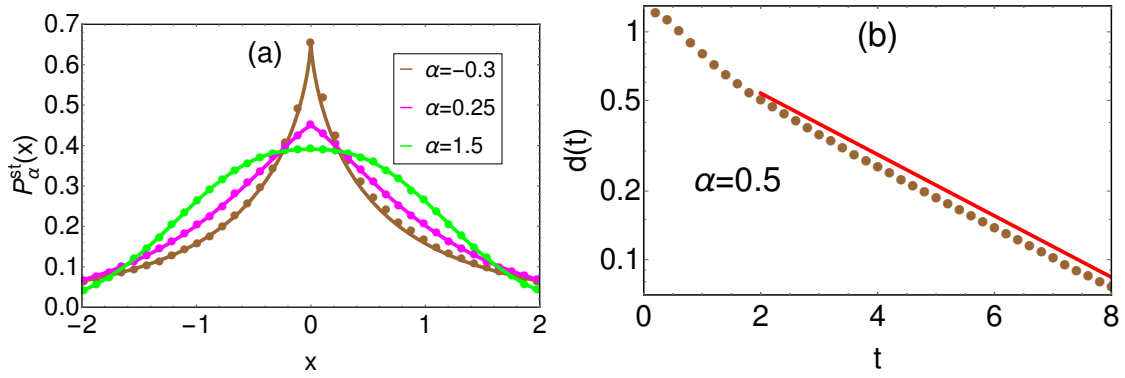

Figure 4.4: (a) Analytic expression of the stationary state distribution $P^{st}_{\alpha}(x)$ given in Eq. (4.37) (solid lines) is compared with the numerical simulation data (filled circles) for three values of α at $t = 15$. (b) Simulation data for $d(t) = \text{var}(\infty) - \text{var}(t)$, where $\text{var}(t) = \langle x^2(t)\rangle - \langle x(t)\rangle^2$. We see that $d(t)$ has an exponential decay of the form $\sim e^{-\zeta t}$ at late times. From the numerical fit (shown by red line), we get $\zeta = 0.31$. For both plots, we have taken $\gamma_1 = 2$, $\gamma_2 = 1$, $l = 1$ and $v_0 = 1$.

this case, the Laplace transform $\bar{P}(x,s)$ in Eq. (4.31) takes form

$$\bar{P}(x,s) = -\frac{1}{2s}\frac{d}{d\mid x\mid}\left[e^{-\frac{\Delta}{2vl}x^2}\frac{D_{\beta s^2}\left(\sqrt{\frac{2|\Delta|}{v_0 l}}\left(\mid x\mid +\frac{\gamma s l}{\Delta^2}\right)\right)}{D_{\beta s^2}\left(\sqrt{\frac{2|\Delta|}{v_0 l}}\frac{\gamma s l}{\Delta^2}\right)}\right], \tag{4.34}$$

where $\beta = \frac{l(\gamma^2-\Delta^2)}{2v|\Delta|^3}$. Performing the inverse Laplace transform analytically for this case turns out to be difficult. However, one can carry out the Bromwich integration numerically. However, in the next section, we show that the distribution possesses the scaling form $P(x,t) \simeq \frac{1}{2\sigma_1(t)}\mathcal{G}\left(\frac{|x|-\mu(t)}{\sigma_1(t)}\right)$ with $\mu(t) = \langle|x|\rangle = \frac{v_0|\Delta|}{\gamma}t$ and $\sigma_1^2(t) = \langle x^2\rangle - \langle|x|\rangle^2 = (v_0 l/|\Delta|)\ \ln(t)$. The scaling function $\mathcal{G}(u)$ is a mean zero and unit variance Gaussian.

4.1.3 Case III: General α

We now consider the distribution for general α (> 0) case. Unlike, in the previous two cases, making analytic progress for this case is harder. However, for large t, we present some results based on heuristic calculations. First, we rewrite Eq. (4.2) in terms of $P(x,t) = P_+(x,t) + P_-(x,t)$ and $Q(x,t) = P_+(x,t) - P_-(x,t)$ as

$$\partial_t P(x,t) = -v_0\ \partial_x Q(x,t), \tag{4.35}$$

$$\partial_t Q(x,t) = -R_+(x)Q(x,t) - R_-(x)P(x,t) - v_0\ \partial_x P(x,t), \tag{4.36}$$

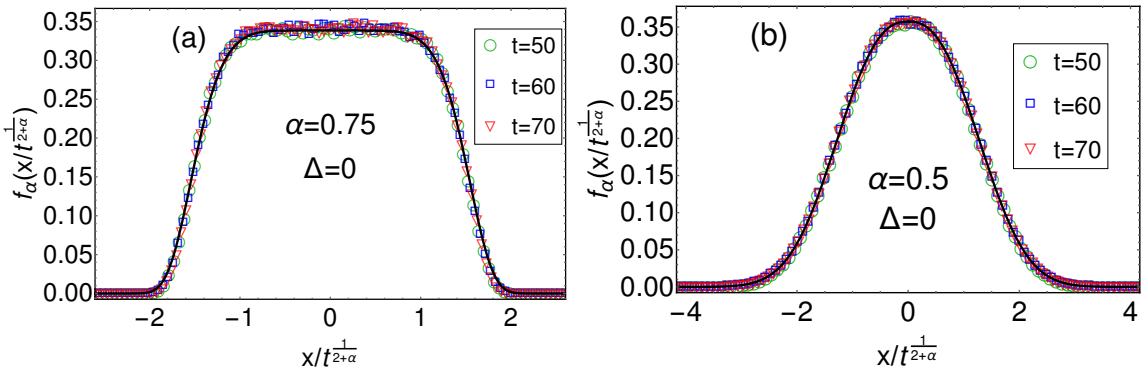

Figure 4.5: Numerical verification of the scaling function $f_\alpha(y)$ associated with the position distribution $P(x,t)$ for $\Delta = 0$ and two different values of α. For both plots, we have showed the analytic formula given in Eq. (4.42) by black solid line and simulation data by symbols. We have checked the scaling function for three different times with parameters $\gamma_1 = \gamma_2 = 1.5$, $v_0 = 1$ and $l = 1$.

where $R_\pm(x) = \frac{R_1(x) \pm R_2(x)}{2}$. Let us first solve this equation for $\Delta > 0$ for which we get steady state at late times.

4.1.3.1 $\Delta > 0$:

To get the stationary distribution $P^{st}_\alpha(x)$, we equate the time derivative on the left hand side of Eqs. (4.35) and (4.36) to zero and solve them with appropriate boundary conditions to yield

$$P^{st}_\alpha(x) = \frac{1}{2\,\Gamma\left(1+\frac{1}{\alpha+1}\right)} \left[\frac{(\gamma_1-\gamma_2)}{v_0\; l^\alpha\; (\alpha+1)}\right]^{\frac{1}{\alpha+1}} e^{-\frac{(\gamma_1-\gamma_2)}{v_0(\alpha+1)l^\alpha}|x|^{\alpha+1}}. \tag{4.37}$$

For $\alpha = 0$ and $\alpha = 1$, this expression matches with the Laplace and Gaussian distributions obtained in Eqs. (4.17) and (4.32) respectively. In Figure 4.4(a), we have numerically verified the stationary distribution for three different values of α other than $\alpha = 0$ and $\alpha = 1$. We observe excellent agreement for all of them. To get the relaxation behaviour for general α, one needs to solve Eqs. (4.35) and (4.36) which is a difficult task. However, numerically we find that the approach to steady state is still exponential for all α (which was analytically proved for $\alpha = 0$ and $\alpha = 1$). This has been illustrated in Figure 4.4(b) where we have plotted $d(t) = \text{var}(\infty) - \text{var}(t)$ as a function of t. We see that at late times $d(t) \sim e^{-\zeta t}$.

4.1.3.2 $\Delta \leq 0$:

As argued before the distribution $P(x,t)$ does not reach a stationary state for $\Delta \leq 0$. To get the large-t form of the distribution, we first note that the time evolution equation (4.35) of

$P(x,t)$ appear in the form of a continuity equation. On the other hand, the time evolution equation (4.36) for $Q(x,t)$ possesses decay terms proportional to the rates $R_+(x)$ which is a non-negative function. This implies that at large times $Q(x,t)$ will cease to possess its intrinsic time dependence and the only time dependence will come from $P(x,t)$. This enables us to drop $\partial_t Q$ term in Eq. (4.36) and rewrite it as $R_+(x)Q(x,t) = -R_-(x)P(x,t) - v_0\partial_x P(x,t)$. Plugging this in Eq. (4.35) gives

$$\partial_t P(x,t) \simeq \frac{v_0^2 l^\alpha}{2\gamma}\partial_x \left(\mid x \mid^{-\alpha} \partial_x P(x,t)\right) + \mathrm{sgn}(x)\frac{v_0\Delta}{\gamma}\partial_x P(x,t), \tag{4.38}$$

where approximate equality indicates that this equation is valid only in large t limit. Let us first analyse this equation for $\Delta = 0$. From numerical simulations, we find that the distribution $P(x,t)$, for this case, admits the scaling form (see Figure 4.5)

$$P(x,t) \simeq \frac{1}{t^{\frac{1}{2+\alpha}}} f_\alpha \left(\frac{|x|}{t^{\frac{1}{2+\alpha}}} \right). \tag{4.39}$$

For $\alpha = 0$ and $\alpha = 1$, we were able to derive the exact form of this scaling function $f_\alpha(z)$. To get $f_\alpha(z)$ for general α, we inject the scaling form (4.39) in Eq. (4.38) and obtain a differential equation for $f_\alpha(z)$ as

$$D_\alpha \frac{d}{dz}\left[z^{-\alpha}\frac{df_\alpha}{dz}\right] + \frac{1}{2+\alpha}\left(z\frac{df_\alpha}{dz} + f\right) = 0, \tag{4.40}$$

where $z = \frac{|x|}{t^{\frac{1}{2+\alpha}}}$ and $D_\alpha = \frac{v_0^2\ l^\alpha}{2\gamma}$. By changing variable $y = \frac{1}{(2+\alpha)^2 D_\alpha}\ z^{2+\alpha}$, the above equation gets further simplified as

$$y\frac{d^2 f_\alpha}{dy^2} + \left(\frac{1}{2+\alpha} + y\right)\frac{df_\alpha}{dy} + \frac{f_\alpha}{2+\alpha} = 0. \tag{4.41}$$

The solution of this equation is e^{-y} and $y^{\frac{1+\alpha}{2+\alpha}}\ {}_1F_1\left(\frac{1+\alpha}{2+\alpha}; 2 - \frac{1}{2+\alpha}; y\right)$, where ${}_1F_1$ stands for confluent hypergeometric function of first kind. The latter solution diverges as $y \to \infty$. Therefore, we keep only the first solution to finally get

$$f_\alpha(z) = \frac{(2+\alpha)^{\frac{\alpha}{2+\alpha}}}{2\Gamma\left(\frac{1}{2+\alpha}\right) D_\alpha^{\frac{1}{2+\alpha}}} e^{-\frac{z^{2+\alpha}}{(2+\alpha)^2 D_\alpha}}. \tag{4.42}$$

For $\alpha = 0$ and $\alpha = 1$ the scaling function $f_\alpha(z)$ correctly reduces to the expressions obtained in the previous sections. Figure 4.5 shows the comparison of the scaling function with the simulation data for two different values of α. For each α, we have performed the comparison for three different times and we see all simulation data converge to our analtical result. As remarked

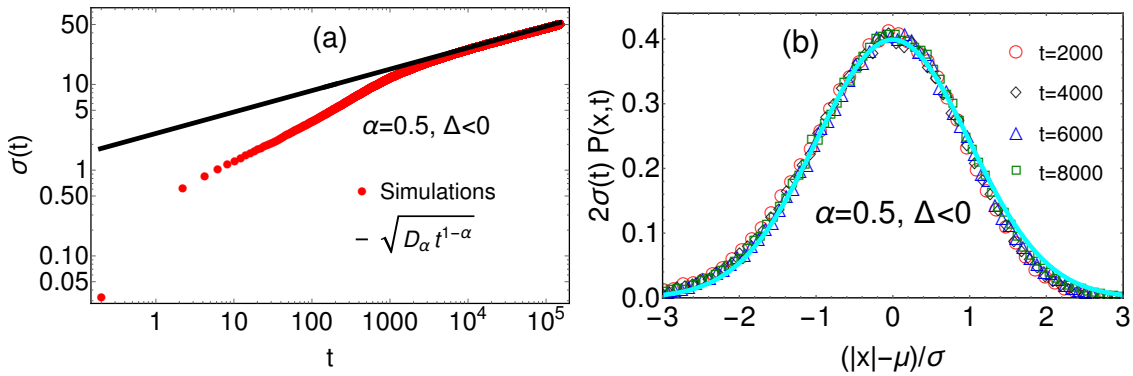

Figure 4.6: (a) Numerical verification of the variance $\sigma_\alpha^2(t)$ in Eq. (4.46) for $\alpha = 0.5$ and $\Delta < 0$. The black line corresponds to Eq. (4.46). (b) Numerical verification of the scaling behaviour of the distribution $P(x,t)$ in Eq. (4.44) for $\alpha = 0.5$ and $\Delta < 0$. The solid cyan line represents the analytic form $\mathcal{G}_\alpha(u) = e^{-u^2/2}/\sqrt{2\pi}$ while the symbols are simulation data for different times. For both plots, we have taken $\gamma_1 = 1.5,\ \gamma_2 = 1.6,\ l = 1$ and $v_0 = 1$.

for $\alpha = 1$, here also, the distribution $P(x,t)$ in Eq. (4.39) only describes the typical fluctuations of the position ($x \sim t^{\frac{1}{2+\alpha}}$) and it fails as one probes the far tails of the distribution.

We next analyse Eq. (4.38) for $\Delta < 0$. We saw before that due to the unequal rates, the particle experiences a drift away from the origin for $\Delta < 0$. Hence, we anticipate a distribution symmetric with respect to the origin and containing two moving peaks. This implies that the mean position of the particle is zero whereas the average value of the absolute position $\mu(t) = \langle |x| \rangle$ is not zero. In fact, the peaks of the distribution at two sides of the origin are situated at $x = \pm\mu(t)$. All these claims can be explicitly verified by simulating the Langevin equation for this case. Furthermore, numerically, we also find $\langle |x| \rangle = \mu(t) \sim \frac{v_0|\Delta|}{\gamma} t$. By changing the variables $|x| = \mu(t) + z$ and $\tau = t^{1-\alpha}$, we can reduce Eq. (4.38) at late times to

$$\partial_\tau P(z,\tau) = \mathcal{D}_\alpha \partial_z^2 P(z,\tau), \tag{4.43}$$

where $\mathcal{D}_\alpha = \frac{v_0^2 \ell^\alpha}{\gamma(1-\alpha)} \left(\frac{\gamma}{v_0|\Delta|}\right)^\alpha$ for $0 < \alpha < 1$. This immediately implies that for large t, the distribution $P(x,t)$ has the following scaling form

$$P(x,t) \simeq \frac{1}{2\sigma_\alpha(t)}\, \mathcal{G}\left(\frac{|x| - \mu(t)}{\sigma_\alpha(t)}\right) \tag{4.44}$$

where the scaling form $\mathcal{G}(u)$ satisfies

$$\partial_u^2 \mathcal{G}(u) + u \partial_u \mathcal{G}(u) + \mathcal{G}(u) = 0. \tag{4.45}$$

Also, in Eq. (4.44) $\sigma_\alpha^2(t) = \langle x^2 \rangle - \langle |x| \rangle^2$ is given by

$$\sigma_\alpha^2(t) \sim \mathcal{D}_\alpha t^{1-\alpha}, \qquad \text{for } 0 < \alpha < 1, \tag{4.46}$$

$$\sim (v_0 l/|\Delta|)\ \ln(t), \qquad \text{for } \alpha = 1. \tag{4.47}$$

We have numerically verified the form of $\sigma_\alpha^2(t)$ in Figure 4.6(a) for $\alpha = 0.5$. Coming back to Eq. (4.45), its solution is given by the zero mean and unit variance Gaussian $\mathcal{G}(u) = e^{-u^2/2}/\sqrt{2\pi}$. Verifying the scaling form in Eq. (4.44) numerically for arbitrary α (≤ 1) turns out to be difficult. For given v_0 and Δ, this scaling form becomes valid only at large times and this (large) time increases with decreasing α. Therefore, for small α, one has to go to very large times to observe Eq. (4.44) which is numerically expensive. On the other hand, for large α, the rates $\sim |x|^\alpha$ increases rapidly and to perform the simulatation with this large rate, we have to take a very small dt which, in turn, makes the numerics expensive. It turns out that the optimal value of α for numerical simulation is $\alpha = 0.5$. In Figure 4.6(b), we have illustrated the scaling function $\mathcal{G}(u)$ numerically for $\alpha = 0.5$ at different times.

Note that the scaling behaviour in Eq. (4.44) is valid for $0 < \alpha < 1$. For $\alpha > 1$, we numerically find that the variance $\sigma_\alpha(t)$ decreases with time and distribution $P(x,t)$, at large times, simply becomes a sum of two delta-functions at $x = \pm\mu(t)$.

4.2 Survival probability

So far, we studied the run and tumble particle in an infinite space and computed the position distribution for different values of α and Δ. Herein, we consider this system on a semi-infinite line and claculate the survival probability. Particularly, we compute the probability $S_\pm(x_0, t)$ that the particle, starting from x_0 with velocity $\pm v_0$, has not crosses the origin till time t. As in the homogeneous case, one can derive backward master equations satisfied by $S_\pm(x_0, t)$ for this case also:

$$\begin{aligned} \partial_t S_+(x_0,t) &= v_0 \partial_{x_0} S_+(x_0,t) - R_1(x_0) S_+(x_0,t) + R_1(x_0) S_-(x_0,t), \\ \partial_t S_-(x_0,t) &= -v_0 \partial_{x_0} S_-(x_0,t) + R_2(x_0) S_+(x_0,t) - R_2(x_0) S_+(x_0,t). \end{aligned} \tag{4.48}$$

Remember that the rates $R_1(x_0)$ and $R_2(x_0)$ are given in Eq. (4.1). In order to solve these equations, we use the initial and boundary conditions as done in Sec. 2.2. Recall that the boundary conditions are $S_\pm(x_0 \to \infty, t) = 1$ and $S_-(0,t) = 0$. The first boundary conditions arise because if the particle initially starts from infinity, then it will not reach the origin at any

finite t. Similarly, if the particle is initially at the origin and starts with the negative velocity then it will get absorbed at the very next instant. This gives rise to the second boundary condition. By same reasoning, we get the initial condition $S_{\pm}(x_0, 0) = 1$ for $x_0 \neq 0$.

Here also, to solve the backward equations (4.48), we first perform the Laplace transformation with respect to t as $\bar{S}_{\pm}(x_0, s) = \int_0^{\infty} dt e^{-st} S_{\pm}(x_0, t)$ and rewrite Eqs. (4.48) as

$$\begin{aligned} [-v_0 \partial_{x_0} + R_1(x_0) + s]\, \bar{S}_+(x_0, s) &= 1 + R_1(x_0) \bar{S}_-(x_0, s), \\ [\ v_0\ \partial_{x_0} + R_2(x_0) + s]\, \bar{S}_-(x_0, s) &= 1 + R_2(x_0) \bar{S}_+(x_0, s). \end{aligned} \tag{4.49}$$

To get rid of the inhomogeneous terms in this equation, we perform the transformations

$$\bar{S}_{\pm}(x_0, s) = \frac{1}{s} + \bar{U}_{\pm}(x_0, s), \tag{4.50}$$

which also simplifies the boundary conditions as $\bar{U}_{\pm}(x_0 \to \infty, s) = 0$. Eqs. (4.49) now become

$$\begin{aligned} [-v_0 \partial_{x_0} + R_1(x_0) + s]\, \bar{U}_+ &= R_1(x_0) \bar{U}_-, \\ [\ v_0\ \partial_{x_0} + R_2(x_0) + s]\, \bar{U}_- &= R_2(x_0) \bar{U}_+. \end{aligned} \tag{4.51}$$

We can further simplify these equations by defining

$$\begin{aligned} \bar{U}(x_0, s) &= \bar{U}_+(x_0, s) + \bar{U}_-(x_0, s), \\ \bar{H}(x_0, s) &= \bar{U}_+(x_0, s) - \bar{U}_-(x_0, s), \end{aligned} \tag{4.52}$$

which then gives

$$\partial_{x_0}^2 \bar{H} - \frac{2\Delta x_0^{\alpha}}{v_0 l^{\alpha}} \partial_{x_0} \bar{H} - \left[\frac{2\Delta \alpha x_0^{\alpha-1}}{v_0 l^{\alpha}} + \frac{2\gamma s x_0^{\alpha}}{v_0^2 l^{\alpha}} + \frac{s^2}{v_0^2} \right] \bar{H} = 0, \tag{4.53}$$

$$\text{and,} \qquad \bar{U}(x_0, s) = \frac{v_0}{s} \partial_{x_0} \bar{H} - \frac{2\Delta x_0^{\alpha}}{s\ l^{\alpha}} \bar{H}. \tag{4.54}$$

By making another transformation

$$\bar{H}(x_0, s) = e^{\frac{\Delta}{v_0(\alpha+1) l^{\alpha}} x_0^{\alpha+1}} F(x_0, s), \tag{4.55}$$

in Eq. (4.53), we get rid of the first order derivative to yield

$$\partial_{x_0}^2 F(x_0, s) - \left[\frac{\Delta \alpha x_0^{\alpha-1}}{v_0\ l^{\alpha}} + \frac{2\gamma s x_0^{\alpha}}{v_0^2\ l^{\alpha}} + \frac{\Delta^2 x_0^{2\alpha}}{v_0^2\ l^{2\alpha}} + \frac{s^2}{v_0^2} \right] F(x_0, s) = 0. \tag{4.56}$$

This is the main equation that we will solve for different values of α. Note that this equation is

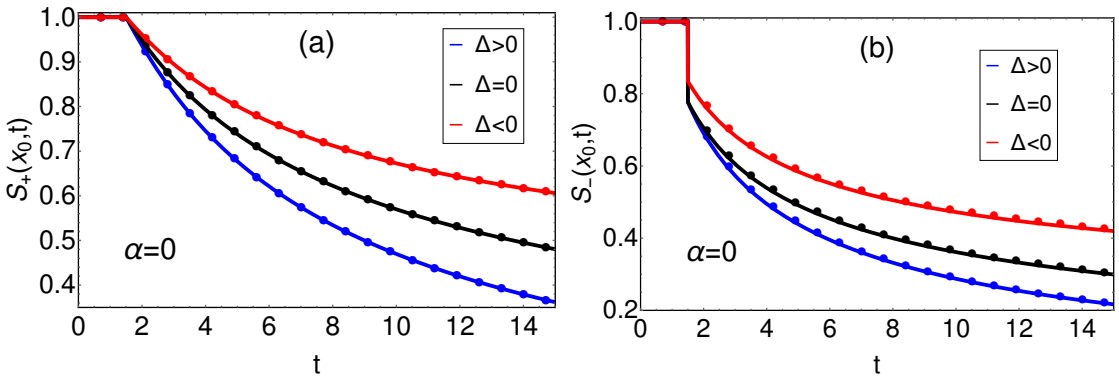

Figure 4.7: Numerical verification of the analytical expressions of $S_{\pm}(x_0,t)$ given in Eqs. (4.61) for $\alpha = 0$ and various signatures of Δ. In both (a) and (b), the solid lines correspond to the analytical expression and the symbols represent the simulation data. We have chosen (i) $\gamma_1 = 1.2$ $\gamma_2 = 1$ for blue, (ii) $\gamma_1 = \gamma_2 = 1$ for black and (iii) $\gamma_1 = 1$ $\gamma_2 = 1.2$ for red. Other parameters chosen are $x_0 = 1.5$, $v_0 = 1$ and $l = 1$.

identical to Eq. (4.13) for $G(x,s)$ obtained in the previous section for the distribution $P(x,t)$. However, the boundary conditions for two problems are different. Below, we solve Eq. (4.56) for $\alpha = 0$ and $\alpha = 1$ first and then for general α.

4.2.1 Case I: $\alpha = 0$

We first look at the survival problem for $\alpha = 0$. For $\Delta = 0$, the survival probability was computed exactly in [70]. Here, we are interested in this probability for $\Delta \neq 0$. Solving Eq. (4.56) for this case gives $F(x_0,s) \sim e^{-\lambda(s)x_0}$ where $\lambda(s) = \frac{1}{v_0}\sqrt{2\gamma s + s^2 + \Delta^2}$ which when inserted in Eqs. (4.54) and (4.55) yields

$$\bar{S}_{\pm}(x_0,s) = \frac{1}{s} + \frac{\mathcal{A}}{2s} e^{\left(\frac{\Delta}{v_0} - \lambda(s)\right)x_0} \left[-\Delta - v_0\lambda(s) \pm s\right], \tag{4.57}$$

where $\mathcal{A}$ is a constant independent of x_0. We use the boundary condition $\bar{S}_-(0,s) = 0$ to get $\mathcal{A}(s) = \frac{2}{\Delta + s + v_0\lambda(s)}$ which then gives

$$\bar{S}_-(x_0,s) = \frac{1}{s} - \frac{1}{s} e^{\left(\frac{\Delta}{v_0} - \lambda(s)\right)x_0}, \tag{4.58}$$

$$\bar{S}_+(x_0,s) = \frac{1}{s} - \frac{s + \gamma - v_0\lambda(s)}{s\gamma_2} e^{\left(\frac{\Delta}{v_0} - \lambda(s)\right)x_0}. \tag{4.59}$$

Next to get the survival probability in the time domain, we use the following inverse Laplace transformations:

$$
\begin{aligned}
L_{s\to t}\left[e^{-\lambda(s)x_0}\right] &= -v_0 e^{\frac{\Delta x_0}{v_0}}\frac{d}{dx_0}\left[e^{-\gamma t}I_0\left(\sqrt{\gamma_1\gamma_2\left(t^2-\frac{x_0^2}{v_0^2}\right)}\right)\Theta(v_0t-x_0)\right],\\
L_{s\to t}\left[(s+\gamma-v_0\lambda(s))e^{-\lambda(s)x_0}\right] &= \sqrt{\gamma_1\gamma_2}\frac{e^{-\gamma t+\frac{\Delta x_0}{v_0}}}{t+\frac{x_0}{v_0}}\left[\frac{x_0\sqrt{\gamma_1\gamma_2}}{v_0}I_0\left(\sqrt{\gamma_1\gamma_2\left(t^2-\frac{x_0^2}{v_0^2}\right)}\right)\right.\\
&\quad\left.+\sqrt{\frac{v_0t-x_0}{v_0t+x_0}}I_1\left(\sqrt{\gamma_1\gamma_2\left(t^2-\frac{x_0^2}{v_0^2}\right)}\right)\right]\Theta(v_0t-x_0)
\end{aligned}
\tag{4.60}
$$

Using these identities in Eqs. (4.58) and (4.59), we get

$$
\begin{aligned}
S_-(x_0,t) &= 1+v_0e^{\frac{\Delta x_0}{v_0}}\frac{d}{dx_0}\int_0^t d\tau e^{-\gamma\tau}I_0\left(\sqrt{\gamma_1\gamma_2\left(\tau^2-\frac{x_0^2}{v_0^2}\right)}\right)\Theta(v_0\tau-x_0),\\
S_+(x_0,t) &= 1-\sqrt{\frac{\gamma_1}{\gamma_2}}e^{\frac{\Delta x_0}{v_0}}\int_0^t d\tau\frac{e^{-\gamma\tau}}{\tau+\frac{x_0}{v}}\Theta(v_0\tau-x_0)\left[\frac{x_0\sqrt{\gamma_1\gamma_2}}{v_0}I_0\left(\sqrt{\gamma_1\gamma_2\left(\tau^2-\frac{x_0^2}{v_0^2}\right)}\right)\right.\\
&\quad\left.+\sqrt{\frac{v_0\tau-x_0}{v_0\tau+x_0}}I_1\left(\sqrt{\gamma_1\gamma_2\left(\tau^2-\frac{x_0^2}{v_0^2}\right)}\right)\right].
\end{aligned}
\tag{4.61}
$$

Our result is consistent with that of [70] for $\gamma_1=\gamma_2$. In Figure 4.7, we have checked our analytic expressions with the numerics for different Δ. We find excellent agreement for all cases. From Figure 4.7, we see that both $S_\pm(x_0,t)$ remains equal to unity till time $t_b=\frac{x_0}{v_0}$. This is because starting from x_0, the RTP will atleast take time t_b to reach the origin and therefore survives the origin till this time. Now when they reach the wall with $-v_0$ at time t_b^-, a fraction of particles will get absorbed which leads to a sudden jump in $S_-(x_0,t)$ (see Figure 4.7). However, this sudden jump does not appear for $S_+(x_0,t)$ since the particles cannot reach the wall with $+v_0$.

It is interesting to recall that the particle is drifted away from the origin for $\Delta<0$. This means it has a non-zero probability to avoid getting absorbed by the wall even at large times. In fact, by taking the $t\to\infty$ limit in Eqs. (4.61), we find that $\mathcal{S}_\pm(x_0)=S_\pm(x_0,t\to\infty)$ are given by

$$
\begin{aligned}
\mathcal{S}_+(x_0) &= 1-\frac{\gamma-|\Delta|}{\gamma+|\Delta|}e^{-\frac{2|\Delta|}{v_0}x_0},\\
\mathcal{S}_-(x_0) &= 1-e^{-\frac{2|\Delta|}{v_0}x_0}.
\end{aligned}
\tag{4.62}
$$

On the other hand, $\mathcal{S}_\pm(x_0)$ turns out to be zero for $\Delta\geq 0$ since the particle definitely reaches the origin after sufficient time.

We next analyse the expressions of $S_\pm(x_0,t)$ in Eqs. (4.61) for large times. For this, we first change the integration in Eqs. (4.61) as $\int_0^t=\int_0^\infty-\int_t^\infty$ and use $I_\nu(z)\simeq\frac{e^z}{\sqrt{2\pi z}}$ as $z\to\infty$. Note

that $S_{\pm}(x_0,t)$ for $t\to\infty$ becomes $\mathcal{S}_{\pm}(x_0)$ where $\mathcal{S}_{\pm}(x_0)$ are 0 for $\Delta\geq 0$ and are given by Eqs. (4.62) for $\Delta<0$. Defining $L_{\pm}(x_0,t)=S_{\pm}(x_0,t)-\mathcal{S}_{\pm}(x_0)$, we find

$$L_{+}(x_0,t)\approx\begin{cases}\sqrt{\frac{\gamma_1}{\gamma_2}}\left(\frac{x_0}{v_0}+\frac{1}{\sqrt{\gamma_1\gamma_2}}\right)\frac{(\gamma_1\gamma_2)^{\frac{1}{4}}e^{\frac{\Delta x_0}{v_0}}}{\sqrt{2\pi t^3}\left(\gamma-\sqrt{\gamma_1\gamma_2}\right)}e^{-t\left(\gamma-\sqrt{\gamma_1\gamma_2}\right)}, & \text{if } \gamma_1\neq\gamma_2\\ \frac{1}{\sqrt{\pi t}}\frac{\sqrt{2\gamma}}{v_0}\left(x_0+\frac{v_0}{\gamma}\right), & \text{if } \gamma_1=\gamma_2.\end{cases} \tag{4.63}$$

$$L_{-}(x_0,t)\approx\begin{cases}\frac{x_0}{v_0}\frac{(\gamma_1\gamma_2)^{\frac{1}{4}}e^{\frac{\Delta x_0}{v_0}}}{\sqrt{2\pi t^3}\left(\gamma-\sqrt{\gamma_1\gamma_2}\right)}e^{-t\left(\gamma-\sqrt{\gamma_1\gamma_2}\right)}, & \text{if } \gamma_1\neq\gamma_2\\ \frac{1}{\sqrt{\pi t}}\frac{x_0\sqrt{2\gamma}}{v_0}, & \text{if } \gamma_1=\gamma_2.\end{cases} \tag{4.64}$$

We see that while for $\Delta=0$, the survival probabilities decay as $\sim 1/\sqrt{t}$, they decay as $\sim t^{-\frac{3}{2}}e^{-t/\tau_r}$ (to $\mathcal{S}_{\pm}(x_0)$) for $\Delta\neq 0$ with timescale $\tau_r=\frac{1}{\gamma-\sqrt{\gamma_1\gamma_2}}$. Notice that this timescale diverges as $\Delta\to 0$ and one recovers the $\sim 1/\sqrt{t}$ decay.

4.2.2 Case II: $\alpha=1$

Let us now consider another analytically tractable case of $\alpha=1$. As shown later, the position dependence of the rates as $\sim|x|^{-1}$ gives rise to different large time behaviour of the survival probability than $\alpha=0$. We first look at $\Delta=0$.

4.2.2.1 $\Delta=0$

For this case, Eq. (4.56) becomes

$$\partial_{x_0}F(x_0,s)-\left(\frac{2\gamma s x_0}{v_0^2 l}+\frac{s^2}{v_0^2}\right)F(x_0,s)=0. \tag{4.65}$$

The solution of this is given in terms of the Airy functions [as seen in Eq. (4.22)]. Proceeding as in $\alpha=0$ case, we get

$$\bar{S}_{\pm}(x_0,s)=\frac{1}{s}-\frac{1}{s}\frac{v_0\ \mathrm{Ai}'\left(\frac{x_0 s^{\frac{1}{3}}}{\mathfrak{D}_1^{1/3}}+d_0 s^{\frac{4}{3}}\right)\pm s^{\frac{2}{3}}\ \mathfrak{D}_1^{1/3}\ \mathrm{Ai}\left(\frac{x_0 s^{\frac{1}{3}}}{\mathfrak{D}_1^{1/3}}+d_0 s^{\frac{4}{3}}\right)}{v_0\mathrm{Ai}'(0)-s^{\frac{2}{3}}\ \mathfrak{D}_1^{1/3}\ \mathrm{Ai}(0)}, \tag{4.66}$$

with $\mathfrak{D}_1=\frac{v_0^2 l}{2\gamma}$ and $d_0=\left(\frac{l}{2\gamma v_0}\right)^{\frac{2}{3}}$. Here also, we can obtain the analytical expressions only for small s (which corresponds to large t). Neglecting $O(s^{4/3})$ term in Eq. (4.66), we get for small

s

$$\bar{S}_{\pm}(x_0,s) \simeq \frac{1}{s} - \frac{1}{sv_0|\mathrm{Ai}'(0)|}\left[v\mathrm{Ai}'\left(\frac{x_0 s^{\frac{1}{3}}}{\mathfrak{D}_1^{1/3}}\right) \pm s^{\frac{2}{3}}\ \mathfrak{D}_1^{1/3}\ \mathrm{Ai}\left(\frac{x_0 s^{\frac{1}{3}}}{\mathfrak{D}_1^{1/3}}\right) - \frac{s^{\frac{2}{3}}\ \mathfrak{D}_1^{1/3}\ \mathrm{Ai}(0)}{|\mathrm{Ai}'(0)|}\mathrm{Ai}'\left(\frac{x_0 s^{\frac{1}{3}}}{\mathfrak{D}_1^{1/3}}\right)\right]. \tag{4.67}$$

Next we use $\mathrm{Ai}(z) = \frac{\sqrt{z}}{\sqrt{3\pi}}K_{\frac{1}{3}}\left(\frac{2}{3}z^{\frac{3}{2}}\right)$ and use the inverse Laplace transformation in Eq. (4.25) to obtain

$$S_{\pm}(x_0,t) \simeq 1 + \frac{e^{-\frac{x_0^3}{18\mathfrak{D}_1 t}}}{2\pi\sqrt{3g_1}v_0 \mid \mathrm{Ai}'(0) \mid}\left[\frac{x_0\mathrm{Ai}(0)}{\mid \mathrm{Ai}'(0) \mid \sqrt{t}}W_{\frac{1}{2},\frac{1}{3}}\left(\frac{x_0^3}{9\mathfrak{D}_1 t}\right) - \frac{v_0 x_0 t^{\frac{1}{6}}}{\mathfrak{D}_1^{1/3}}W_{-\frac{1}{6},\frac{1}{3}}\left(\frac{x_0^3}{9\mathfrak{D}_1 t}\right)\right.$$
$$\left. \pm \frac{\sqrt{x_0\ \mathfrak{D}_1^{1/3}}}{t^{\frac{1}{3}}}W_{\frac{1}{3},\frac{1}{6}}\left(\frac{x_0^3}{9\mathfrak{D}_1 t}\right)\right], \tag{4.68}$$

where $g_1 = \frac{x_0^3}{9\mathfrak{D}_1}$. Note that this solution is valid only at late times. In Figure 4.8(a), we have compared our analytical results with the numerical simulations. Although at small times our results deviate from the simulation data, the two match well at large times.

We can further simplify Eq. (4.68) for $t \to \infty$. Exploiting the relation $W_{k,m}(z) = e^{-\frac{z}{2}}z^{m+\frac{1}{2}}U(\frac{1}{2}+m-k, 1+2m, z)$, where $\mathcal{U}(a,b,z)$ is the confluent hypergeometric function of second kind and using the asymptotic form of $\mathcal{U}(a,b,z)$ for small z as $\mathcal{U}(a,b,z) \simeq \frac{\Gamma(b-1)}{\Gamma(a)}z^{1-b} + \frac{\Gamma(1-b)}{\Gamma(a-b+1)}$, we get

$$S_+(x_0,t) \approx \frac{1}{2\pi 3^{\frac{5}{6}}\ (\mathfrak{D}_1 t)^{\frac{2}{3}}}\left(-x_0^2\Gamma\left(-\frac{2}{3}\right) + \frac{6\ \mathfrak{D}_1\ \Gamma\left(\frac{1}{3}\right)}{v_0}\right),$$
$$S_-(x_0,t) \approx -\frac{1}{2\pi 3^{\frac{5}{6}}(\mathfrak{D}_1 t)^{\frac{2}{3}}}x_0^2\Gamma\left(-\frac{2}{3}\right). \tag{4.69}$$

Hence for $\alpha = 1$ also, both $S_{\pm}(x_0,t)$ possess power law decay with persistent exponent $\theta = 2/3$, which is different than $\theta = 1/2$ for $\alpha = 0$ case. Recall that for Brownian motion, the probability to survive the origin starting from the origin is precisely zero [163]. On the other hand, we see that the RTP has a non-zero probability to survive the origin even when $x_0 = 0$ [see $S_+(x_0,t)$ in Eq. (4.69)]. This happens because of the persistence nature of the RTPs, as previously observed in [70, 94] for $\alpha = 0$ and $\Delta = 0$.

4.2.2.2 $\Delta \neq 0$

For $\Delta \neq 0$ case, Eq. (4.56) takes the form

$$\partial_{x_0}^2 F - \left[\frac{\Delta}{v_0 l} + \frac{2\gamma s x_0}{v_0^2 l} + \frac{s^2}{v_0^2} + \frac{\Delta^2 x_0^2}{v_0^2 l^2}\right]F = 0. \tag{4.70}$$

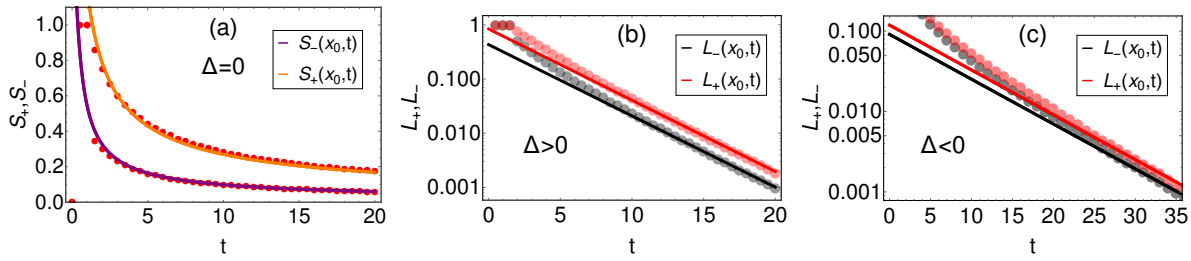

Figure 4.8: (a) Numerical verification of the analytical expressions of the survival probabilities $S_{\pm}(x_0,t)$ given in Eqs. (4.68) for $\alpha=1$ and $\Delta=0$. We have chosen $\gamma_1=\gamma_2=1$ and $x_0=1$. In panels (b) and (c), we have plotted the analytical form of $L_{\pm}(x_0,t)=S_{\pm}(x_0,t)-S_{\pm}(x_0,t\to\infty)$ given in Eqs. (4.73) as a function of t and compared them with the simulation. For these two cases, we have taken (b) $x_0=1.5,\gamma_1=2$ and $\gamma_2=1$ and (c) $x_0=1.5,\gamma_1=1$ and $\gamma_2=1.5$. For all three panels, the analytic results are shown by solid lines while the symbols correspond to the simulation data. Also $v_0=1$ and $l=1$ for all three panel.

This equation can also be transformed to Eq. (4.29) by performing the same variable transformations. The general solution is then given in terms of the parabolic cylinder functions. After using the boundary condition $\bar{S}_-(x_0\to 0,s)=0$, we get

$$\bar{S}_{\pm}(x_0,s)=\frac{1}{s}-\frac{1}{s}e^{\frac{\Delta x_0^2}{2v_0 l}}\frac{\mathcal{N}_{\pm}(x_0,s)}{\mathcal{N}_-(0,s)}, \tag{4.71}$$

where the functions $\mathcal{N}_{\pm}(x_0,s)$ are defined as

$$\begin{aligned}\mathcal{N}_{\pm}(x_0,s)=&\sqrt{\frac{2v_0\mid\Delta\mid}{l}}\left\{\beta s^2\Theta(-\Delta)+\Theta(\Delta)\right\}D_{\beta s^2-\Theta(-\Delta)}\left(\sqrt{\frac{2\mid\Delta\mid}{v_0 l}}\left(x_0+\frac{\gamma s l}{\Delta^2}\right)\right)\\&-s\frac{\gamma\pm\Delta}{\mid\Delta\mid}D_{\beta s^2-\Theta(\Delta)}\left(\sqrt{\frac{2\mid\Delta\mid}{v_0 l}}\left(x_0+\frac{\gamma s l}{\Delta^2}\right)\right),\end{aligned} \tag{4.72}$$

with $\beta=\frac{l(\gamma^2-\Delta^2)}{2v_0|\Delta|^3}$. Once again obtaining analytic expressions for arbitrary s turns out to be challenging and we proceed to analyse Eqs. (4.72) for small s. For $\Delta<0$, we anticipate a non-zero value of $S_{\pm}(x_0,t)$ as $t\to\infty$ which can be computed from the Laplace transforms $\bar{S}_{\pm}(x_0,s)$ as

$$\begin{aligned}\mathcal{S}_+(x_0)=\lim_{s\to 0}\left[s\bar{S}_+(x_0,s)\right]=&1-\frac{\gamma-\mid\Delta\mid}{\gamma+\mid\Delta\mid}e^{-\frac{|\Delta|x_0^2}{v_0 l}},\\ \mathcal{S}_-(x_0)=\lim_{s\to 0}\left[s\bar{S}_-(x_0,s)\right]=&1-e^{-\frac{|\Delta|x_0^2}{v_0 l}}.\end{aligned} \tag{4.73}$$

where we have used $D_0(z)=e^{-\frac{z^2}{4}}$. The same calculation for $\Delta\geq 0$ gives $\mathcal{S}_{\pm}(x_0)=0$ since the particle will definitely reach the origin after sufficient time. To get the approach to the stationary value $\mathcal{S}_{\pm}(x_0)$ for $\Delta<0$ and the decay to 0 for $\Delta>0$, at large t, we focus on the poles

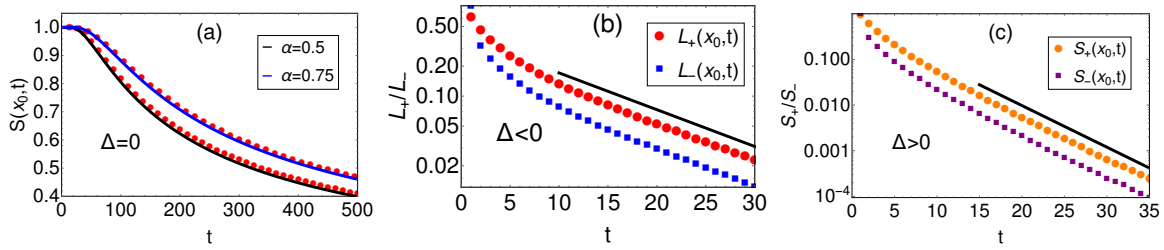

Figure 4.9: (a) Comparison of the analytic expression of the survival probability $S(x_0,t)$ given in Eq. (4.80) (shown by solid lines) with the simulation (shown by circles). We have chosen $\Delta = 0,\ \gamma_1 = \gamma_2 = 1,\ v_0 = 1,\ l = 1$ and $x_0 = 10$. (b) Simulation data (filled circles) for $L_\pm(x_0,t) = S_\pm(x_0,t) - \mathcal{S}_\pm(x_0)$ is shown for $\alpha = 0.5$. At late times, we observe an exponential decay of $L_\pm(x_0,t)$ of the form $\sim e^{-\zeta t}$. From exponential fit (shown by black line), we find that $\zeta = 0.085$. Parameters chosen for this plot are $\gamma_1 = 1.2,\ \gamma_2 = 1.5,\ v_0 = 1,\ x_0 = 1$, and $l = 1$. (c) Survival probabilities $S_\pm(x_0,t)$ are obtained from numerics for $\Delta > 0$ and $\alpha = 0.5$. Here also, we see an exponential decay of the form $\sim e^{-\zeta t}$ at late times and from exponential fit (shown by black line), we obtain $\zeta = 0.2097$. Values of parameters are $\gamma_1 = 2,\ \gamma_2 = 1,\ v_0 = 1,\ x_0 = 1$, and $l = 1$.

of $\bar{S}_\pm(x_0,s)$ in Eqs. (4.71). One pole is $s = 0$ which gives the stationary value for $\Delta < 0$. The other poles are obtained by solving the equation $\mathcal{N}_-(0,s) = 0$ in Eq. (4.71). The largest non-zero solution (say s^*) of this equation gives the large time behaviour of $S_\pm(x_0,t)$. Subtracting the stationary value from $S_\pm(x_0,t)$ as $L_\pm(x_0,t) = S_\pm(x_0,t) - S_\pm(x_0,t\to\infty)$, we get

$$L_\pm(x_0,t) \simeq -e^{\frac{\Delta x_0^2}{2v_0 l}} \frac{e^{s^* t}}{s^*} \frac{\mathcal{N}_\pm(x_0,s^*)}{\mathcal{N}'_-(0,s^*)}, \tag{4.74}$$

Figures 4.8(b) and 4.8(c) compare these asymptotic results with the numerical simulation and we observe excellent match.

4.2.3 Case III: General α

We now consider the general α case for which we solve Eqs. (4.51) directly. Once again, we analyse these equations for large times which necessarily requires large x_0 so that the particle survives for long times. With these approximations, we expect $U_+(x_0,t) = U_-(x_0,t)$ and the difference $H(x_0,t) = U_+(x_0,t) - U_-(x_0,t)$ in Eq. (4.52) should rapidly decay to zero. Then, the equation for $\bar{U}(x_0,s)$ in Eq. (4.52) becomes

$$s\bar{U}(x_0,s) \simeq \frac{v_0^2 l^\alpha}{2\gamma} \partial_{x_0}\left(\frac{1}{x_0^\alpha}\partial_{x_0}\bar{U}\right) - \frac{v_0\Delta}{\gamma}\partial_{x_0}\bar{U}. \tag{4.75}$$

We now solve this separately for $\Delta = 0$ and $\Delta \neq 0$ cases.

4.2.3.1 $\Delta = 0$:

For $\Delta = 0$, Eq. (4.75) becomes

$$s\bar{U}(x_0, s) \simeq \mathfrak{D}_\alpha \partial_{x_0}\left(\frac{1}{x_0^\alpha}\partial_{x_0}\bar{U}\right), \qquad \text{with } \mathfrak{D}_\alpha = \frac{v_0^2 l^\alpha}{2\gamma}. \tag{4.76}$$

This equation can be solved exactly and its general solution are given in terms of the Bessel functions as $|x_0|^{\frac{1+\alpha}{2}} I_{\frac{1+\alpha}{2+\alpha}}\left(\frac{2|x_0|^{\frac{2+\alpha}{2}}}{2+\alpha}\sqrt{\frac{s}{\mathfrak{D}_\alpha}}\right)$ and $|x_0|^{\frac{1+\alpha}{2}} K_{\frac{1+\alpha}{2+\alpha}}\left(\frac{2|x_0|^{\frac{2+\alpha}{2}}}{2+\alpha}\sqrt{\frac{s}{\mathfrak{D}_\alpha}}\right)$. But the first solution diverges as $|x_0| \to \infty$ and we take only the second solution. Therefore, we obtain

$$\bar{U}(x_0, s) = \mathcal{B}|x_0|^{\frac{1+\alpha}{2}} K_{\frac{1+\alpha}{2+\alpha}}\left(\frac{2|x_0|^{\frac{2+\alpha}{2}}}{2+\alpha}\sqrt{\frac{s}{\mathfrak{D}_\alpha}}\right). \tag{4.77}$$

Now to evaluate the constant $\mathcal{B}$, we translate the boundary condition $\bar{S}_-(0, s) = 0$ in terms of $\bar{U}(x_0, s)$ and write the final expression of $\bar{U}(x_0, s)$ as

$$\bar{U}(x_0, s) \simeq -\frac{4x_0^{1+\alpha}}{\Gamma\left(\frac{1+\alpha}{2+\alpha}\right)} \frac{s^{-\frac{\alpha+3}{2(2+\alpha)}}}{((2+\alpha)\sqrt{\mathfrak{D}_\alpha})^{\frac{1+\alpha}{2+\alpha}}} K_{\frac{1+\alpha}{2+\alpha}}\left(2\sqrt{g_\alpha s}\right), \tag{4.78}$$

To derive this solution, we have used the boundary condition $\bar{U}(x_0 \to \infty, s) = -2/s$. Finally the survival probability is given in terms of $\bar{U}(x_0, s)$ as

$$\begin{aligned} S(x_0, t) &= \frac{S_+(x_0, t) + S_-(x_0, t)}{2}, \\ &\simeq 1 - \frac{1}{2} L^{-1}_{s\to t}\left[\bar{U}(x_0, s)\right], \\ &\simeq 1 - \frac{e^{-\frac{x_0^{2+\alpha}}{2t\mathfrak{D}_\alpha(2+\alpha)^2}} \{\sqrt{\mathfrak{D}_\alpha}(2+\alpha)\}^{\frac{1}{2+\alpha}}\ x_0^{\frac{\alpha}{2}} t^{\frac{1}{2(2+\alpha)}}}{\Gamma\left(\frac{1+\alpha}{2+\alpha}\right)} W_{-\frac{1}{2(2+\alpha)}, \frac{1+\alpha}{2(2+\alpha)}}\left(\frac{x_0^{2+\alpha}}{\mathfrak{D}_\alpha(2+\alpha)^2 t}\right). \end{aligned} \tag{4.79}$$

In the last line, we have used Eq. (4.25) to perform the inverse Laplace transformation. To find asymptotics, we use the following representation of the Whittaker function $W_{m,k}(z) = e^{-\frac{z}{2}} z^{m+\frac{1}{2}} \mathcal{U}(\frac{1}{2} + m - k, 1 + 2m, z)$ in terms of the Tricomi confluent hypergeometric function $\mathcal{U}(a, b, z)$ of second kind whose asymptotic behaviour as $z \to 0$ is $\mathcal{U}(a, b, z) \approx \frac{\Gamma(b-1)}{\Gamma(a)} z^{1-b} + \frac{\Gamma(1-b)}{\Gamma(a-b+1)}$ which gives

$$S(x_0, t) \simeq \frac{|\ \Gamma\left(-\frac{1+\alpha}{2+\alpha}\right)\ |}{\Gamma\left(\frac{1+\alpha}{2+\alpha}\right)\Gamma\left(\frac{1}{2+\alpha}\right)} \frac{x_0^{1+\alpha}}{(2+\alpha)^{\frac{2(1+\alpha)}{2+\alpha}}} \frac{1}{(\mathfrak{D}_\alpha t)^{\frac{1+\alpha}{2+\alpha}}} \tag{4.80}$$

We see that the survival probability has the power-law decay with time with persistent exponent $\theta_\alpha = \frac{1+\alpha}{2+\alpha}$. It matches with the exponents obtained for $\alpha = 0$ and $\alpha = 1$ before. We have

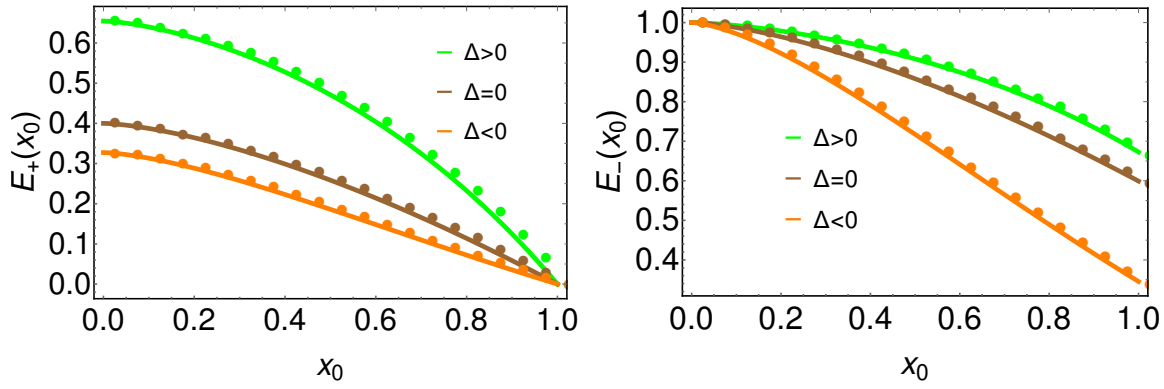

Figure 4.10: Numerical verification of the exit probability $E_{\pm}(x_0)$ given in Eqs. (4.85) and (4.86) for $\alpha = 0.5$. In both panels, the solid lines represent the analytic expression and the symbols correspond to the simulation. Parameters chosen are (i) Green: $\gamma_1 = 2,\ \gamma_2 = 1$, (ii) Brown: $\gamma_1 = 1,\ \gamma_2 = 1$ and (iii) Orange: $\gamma_1 = 1,\ \gamma_2 = 2$. Other common parameters are $v_0 = 1,\ l = 1$ and $\mathcal{M} = 1$

numerically verified our analytic result in Figure 4.9(a) and we observe nice agreement. We emphasize that our result is valid only for large x_0 and fails for small x_0 as can be verified numerically.

4.2.3.2 $\Delta < 0$:

Recall that for $\Delta < 0$, the RTP experiences a drift away from the origin. This gives rise to non-zero survival probability even for $t \to \infty$. Putting $\partial_t S_{\pm}(x_0, t)$ in Eqs. (4.48) gives the stationary form as

$$\mathcal{S}_+(x_0) = 1 - \frac{\gamma - \mid \Delta \mid}{\gamma + \mid \Delta \mid}\, e^{-\frac{2|\Delta|}{v_0 l^{\alpha}(\alpha+1)} x_0^{\alpha+1}}, \tag{4.81}$$

$$\mathcal{S}_-(x_0) = 1 - e^{-\frac{2|\Delta|}{v_0 l^{\alpha}(\alpha+1)} x_0^{\alpha+1}}. \tag{4.82}$$

To find the relaxation behaviour, we have to solve the full time dependent equations which for general α is difficult. As illustrated in Figure 4.9(b), we numerically find the approach to this steady value is exponential with same relaxation time for both $S_{\pm}(x_0, t)$. Similarly, for $\Delta > 0$, the survival probability exponentially decays to zero at large times. This has been numerically verified in Figure 4.9(c).

4.3 Exit probability of RTP from a finite interval for general α

After studying the RTP model in an infinite and semi-infinite space, we here study this model in a finite interval $[0, \mathcal{M}]$. We are interested in computing the probability $E_{\pm}(x_0)$ that the RTP,

starting from x_0 with velocity $\pm v_0$, will exit from $x = 0$ side without touching the boundary at $x = \mathcal{M}$. To derive differential equations for $E_\pm(x_0)$, we proceed as in [70] and consider a RTP that starts from x_0 with σv_0. In small time dt, the particle can either (i) change its velocity from σv_0 to $-\sigma v_0$ and move to new position $x_0' = x_0 - dx$ or (ii) continue moving with velocity σv_0 and move to $x_0' = x_0 + dx$. Events (i) occur with probability $R_\eta(x_0)\frac{dx}{v_0}$ while events (ii) occure with probability $1 - R_\eta(x_0)\frac{dx}{v_0}$ where $\eta = 1$ for $\sigma = +1$ and $\eta = 2$ for $\sigma = -1$. Starting from this new position x_0', the RTP then exits from $x = 0$ side without touching the side at $x = \mathcal{M}$. One can then write

$$\begin{aligned} E_+(x_0) &= \left[1 - R_1(x_0)\frac{dx}{v_0}\right] E_+(x_0 + dx) + R_1(x_0)\frac{dx}{v_0}E_-(x_0 - dx), \\ E_-(x_0) &= \left[1 - R_2(x_0)\frac{dx}{v_0}\right] E_-(x_0 - dx) + R_2(x_0)\frac{dx}{v_0}E_+(x_0 + dx). \end{aligned} \tag{4.83}$$

Keeping terms up to leading order in dx, we get the following differential equations for $E_\pm(x_0)$:

$$\begin{aligned} v_0\partial_{x_0}E_+ - R_1(x_0)E_+ + R_1(x_0)E_- &= 0, \\ -v_0\partial_{x_0}E_- + R_2(x_0)E_+ - R_2(x_0)E_- &= 0. \end{aligned} \tag{4.84}$$

To solve these equations, we need appropriate boundary conditions. These conditions are $E_+(x_0 = \mathcal{M}) = 0$ and $E_-(x_0 = 0) = 1$. Now if the particle is initially located at $x_0 = \mathcal{M}$ with $+v_0$ then it will definitely exit from $x = \mathcal{M}$ side giving rise to the zero exit probability from $x = 0$ side. Similarly, if it is at the origin initially with $-v_0$ then it will surely exit from $x = 0$ side and hence the second boundary condition. The task is to solve the coupled equations (4.84) with these conditions for general α. The calculation is fairly straightforward and we get

$$E_+(x_0) = \frac{e^{\bar{\Delta}\mathcal{M}^{1+\alpha}} - e^{\bar{\Delta}x_0^{1+\alpha}}}{e^{\bar{\Delta}\mathcal{M}^{1+\alpha}} - \frac{\gamma_2}{\gamma_1}}, \tag{4.85}$$

$$E_-(x_0) = \frac{e^{\bar{\Delta}\mathcal{M}^{1+\alpha}} - \frac{\gamma_2}{\gamma_1}e^{\bar{\Delta}x_0^{1+\alpha}}}{e^{\bar{\Delta}\mathcal{M}^{1+\alpha}} - \frac{\gamma_2}{\gamma_1}}, \tag{4.86}$$

where $\bar{\Delta} = \frac{2\Delta}{v_0(1+\alpha)l^\alpha}$. For $\alpha = 0$ and $\Delta = 0$, our results are consistent with previously obtained results in [70]. We have numerically verified these results in Figure 4.10 for different signatures of Δ and $\alpha = 0.5$. We observe excellent match for all cases. For a given α and x_0, we see that the exit probability is largest for $\Delta > 0$ and least for $\Delta < 0$. For $\Delta > 0$, the particle is drifted towards the origin which increases its chance to exit from $x = 0$ side. Similarly, for $\Delta < 0$, the particle is drifted away from the origin which decreases its likelihood to exit the interval from the origin.

4.4 Summary

We have investigated the run and tumble motion of a particle in a spatially heterogeneous medium in one dimension. More specifically, we studied the model where the telegraphic noise $\sigma(t)$ in Eq. (1.7) changes from $+1$ to -1 with rate $R_1(x)$ and from -1 to $+1$ with rate $R_2(x)$. These rates depend on the position x of the particle and their forms are given in Eqs. (4.1). This form may be motivated from the chemotaxis movement of the bacteria wherein they perform longer (shorter) runs in the direction of the chemo-attractant (chemo-repellent) and shorter (longer) runs away from it [115–119]. For instance, in Eqs. (4.1), $\gamma_1 > \gamma_2$ mimicks the presence of chemo-attractant at the origin and for this case, the RTP experiences a net drift towards the origin from both sides. Consequently, the probability distribution attains a steady state whose form is given in Eq. (4.37). Approach to this steady state was found to be exponential for all α. Contrarily, the distribution is always in the transient state for $\gamma_1 \leq \gamma_2$ case. While for $\gamma_1 = \gamma_2$, the distribution $P(x,t)$ has a peak at the origin [see Eq. (4.42)], we see in Eq. (4.44) that the distribution, for $\gamma_1 < \gamma_2$, has two moving symmetric peaks at $x = \pm\frac{v_0|\Delta|}{\gamma}t$ and a dip at the origin.

Next, we studied the survival probability $S(x_0,t)$ in a semi-infinite line for this model. For $\gamma_1 = \gamma_2$ and general α, we find that this probability possesses a power-law decay of the form $\sim 1/t^{\theta_\alpha}$ at large times with the exponent $\theta_\alpha = \frac{1+\alpha}{2+\alpha}$. On the other hand, $S(x_0,t)$ for $\gamma_1 < \gamma_2$ saturates to a non-zero value as $t \to \infty$ which is attributable to the drift that takes the particle away from the origin. Approach to this steady value is exponential as proved rigorously for $\alpha = 0$ and $\alpha = 1$ and verified numerically for other values of α. By the same line of reasoning, we also showed that $S(x_0,t)$ for $\gamma_1 > \gamma_2$ decays exponentially to zero at large times. Finally, we studied the RTP model in a finite interval and calculated the exit probability for all values of α.

Note that although we have focused on $\alpha \geq 0$, some of our results remain valid for negative α also. For example, the stationary distribution for $\gamma_1 > \gamma_2$ in Eq. (4.37) is valid for $-1 < \alpha < 0$ also and has been numerically verified in Figure 4.4a. Similarly, the scaling function $f_\alpha(z)$ of the distribution in Eq. (4.42) for $\gamma_1 = \gamma_2$ is also valid for $-2 < \alpha < 0$ (numerically checked but not shown here). Extending our study for negative α remains an interesting future direction. Also, the distribution $P(x,t)$ in Eq. (4.39) for $\gamma_1 = \gamma_2$ and general α is valid only for the typical fluctuations ($x \sim t^{\frac{1}{2+\alpha}}$) of the position and does not describe the far tails of the distribution. In particular, for homogeneous case ($\alpha = 0$), the distribution $P(x,t)$ for large (atypical) x admits a large deviation form as shown in [114]. It remains open to prove if such large deviation form also exists for the heterogeneous case. Lastly, it was recently shown in [92] that the survival probability for a RTP in d-dimension with $\alpha = 0$ and $\gamma_1 = \gamma_2$ has some universal features. It

would be interesting to see what happens to this universality when the rate becomes position dependent.

Chapter 5

Local time for run and tumble particle

The previous chapter demonstrated the consequence of the spatial heterogeneity on the motion of a run and tumble particle. Particularly, we examined how this heterogeneity ramifies the probability distribution and persistent properties of a RTP in one dimension. In this chapter, we continue our study on the heterogeneous RTP and look at the statistics of the local time. Local time (density) refers to the amount of time (per unit length) spent by the particle in the neighbourhood of a given point in space. Study of local time turns out to be useful in many interdisciplinary settings like in chemical reactions where the yield of a product is related to the amount of time that the reactants spent together [196–199]. Similarly, in biological settings, the action of a molecule in the interior of a cell depends on the time that it spends inside the cell [163, 200]. For stochastic processes, the local time properties can provide spatio-temporal properties of the particle's trajectory. Consequently, its statistics has been studied for a wide variety of stochastic processes [128,129,201–208]. So far, however, such studies have not yet been made in the context of active particles. This study is particularly relevant in the current day research where active particles are being used as nano-machines for various applications [38,39]. One quantity that may then estimate the efficiency of these nano-machines is the amount of time spent in the vicinity of the desired location. This potential application has motivated us to examine the statistical properties of the local time for active particles.

Focus of our study will again be the run and tumble particle in one dimension whose position evolves according to Eq. (1.7). Once again, we consider that the telegraphic noise $\sigma(t)$ in Eq. (1.7) changes from $1 \leftrightarrow -1$ with rate $R(x)$ defined as

$$R(x) = \gamma \frac{|x|^\alpha}{l^\alpha}, \qquad \text{with } \alpha \geq 0, \tag{5.1}$$

where γ is a positive constant that sets the timescale for the activity and l is the length over

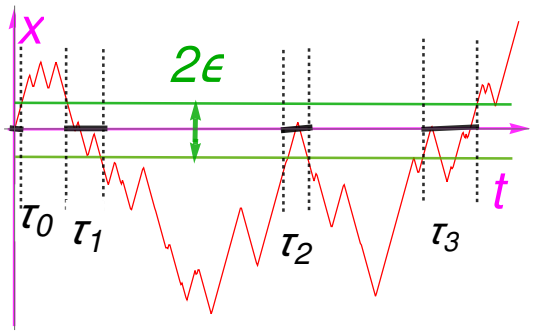

Figure 5.1: Schematic illustration of a typical trajectory (shown in red) of a RTP with observation time t. The interval $[-\epsilon, \epsilon]$ is shown in green and the particle spends $T_{2\epsilon} = \tau_0 + \tau_1 + \tau_2 + \tau_3$ amount of time inside this interval. This implies the local time (density) is given by $T_{loc} = \lim_{\epsilon \to 0} \left[\frac{\tau_0+\tau_1+\tau_2+\tau_3}{2\epsilon}\right]$.

which the rate varies. Note that unlike in the previous chapter, the rate of flip here only depends on the position of the particle and does not have any directional dependence. For this model, we are interested in the local time (density) T_{loc} which is formally defined as

$$T_{loc} = \int_0^t \delta(x(\tau))d\tau. \tag{5.2}$$

Notice that this quantity gives a measure of the amount of time (density) that the particle remains in the vicinity of the origin. We will demonstrate the effect of persistence on T_{loc} both in an infinite line and a semi-infinite line with an absorbtion wall. To derive the statistics of T_{loc}, we follow the Feynman-Kac's formalism [123, 124] as done for the residence time in Sec. 2.4. However, this formalism is analytically tractable only for $\alpha = 0$ and solving it for general α turns out to be difficult. Herein we develop an explicit path-counting method which gives us the exact forms of the distribution for all values of α.

In the rest of this chapter, we study the local time statistics in an infinite line in Sec. 5.1 with Sec. 5.1.1 containing discussions for $\alpha = 0$ and sec. 5.1.2 for general α. We then study T_{loc} in a semi-infinite line in Sec. 5.2 with Sec. 5.2.1 for $\alpha = 0$ and Sec. 5.2.2 for general α. We then summarise in Sec. 5.3.

5.1 Local time statistics in an infinite line

We first look at the statistical properties of T_{loc} for the RTP moving in an infinite line till time duration t. We denote by $P_{\pm}(T_{loc}, x_0, t)$ the probability distribution of T_{loc} given that the RTP was initially at x_0 with velocity $\pm v_0$. We also define the Laplace transformation of $P_{\pm}(T_{loc}, x_0, t)$

with respect to T_{loc} ($\to p$) as

$$Q_{\pm}(p,x_0,t)=\int_0^{\infty} dT_{loc}\; e^{-pT_{loc}}\; P_{\pm}\left(T_{loc},x_0,t\right). \tag{5.3}$$

To obtain the distribution of T_{loc}, it turns out more convenient to consider another intuitive definition of the local time due to P. Lévy [209]:

$$T_{loc}=\lim_{\epsilon\to 0^+}\frac{T_{2\epsilon}}{2\epsilon},\qquad \text{with}\qquad T_{2\epsilon}=\int_0^t \mathbb{I}_{\epsilon}\left(x(\tau)\right)d\tau, \tag{5.4}$$

where $\mathbb{I}_{\epsilon}\left(x(\tau)\right)=\Theta\left(x(\tau)+\epsilon\right)\Theta\left(\epsilon-x(\tau)\right)$. Then, the term $\mathbb{I}_{\epsilon}$ becomes $\mathbb{I}_{\epsilon}\left(x\right)=1$ for $-\epsilon<x<\epsilon$ and 0 otherwise. Physically $T_{2\epsilon}$ represents the amount of time that the particle remains inside a small but non-zero interval $[-\epsilon,\epsilon]$. In Figure 5.1, we have schematically illustrated the quantities $T_{2\epsilon}$ and T_{loc} for a trajectory of the RTP. In what follows, we first calculate the distribution of $T_{2\epsilon}$ and use transformation (5.4) to compute the distribution of T_{loc}.

Let the distribution of $T_{2\epsilon}$ be $G_{\pm}(T_{2\epsilon},x_0,t)$ with the initial position x_0 and initial velocity $\pm v_0$. The corresponding Laplace transformations with $T_{2\epsilon}$ ($\to q$) are

$$H_{\pm}(q,x_0,t)=\int_0^{\infty} dT_{2\epsilon}\; e^{-qT_{2\epsilon}}\; G_{\pm}\left(T_{2\epsilon},x_0,t\right). \tag{5.5}$$

From Feynman-Kac's formalism [121,123,124], we can write a set of coupled backward equations for $H_{\pm}(q,x_0,t)$ as (see appendix 8.6 for details)

$$\begin{aligned}\partial_t H_+ &= \;\; v_0\partial_{x_0}H_+ - R(x_0)H_+ + R(x_0)H_- - q\mathbb{I}_{\epsilon}\left(x_0\right)H_+,\\ \partial_t H_- &= -v_0\partial_{x_0}H_- + R(x_0)H_+ - R(x_0)H_- - q\mathbb{I}_{\epsilon}\left(x_0\right)H_-,\end{aligned} \tag{5.6}$$

We now proceed to solve these equations with rate $R(x_0)$ given in Eq. (5.1). To solve them, we use the following initial and boundary conditions:

$$H_{\pm}(q,x_0,t=0)=1, \tag{5.7}$$

$$H_{\pm}(q,x_0\to\pm\infty,t)=1. \tag{5.8}$$

Recall that if $t=0$ then the time spent in the interval $[-\epsilon,\epsilon]$ is also zero which gives $T_{2\epsilon}=0$. Therefore, the distribution is given by $G_{\pm}(T_{2\epsilon},x_0,t=0)=\delta\left(T_{2\epsilon}\right)$ which gives the initial condition in Eq. (5.7). Similarly, if the initial position is $x_0\to\pm\infty$, then also the particle will remain outside the interval $[-\epsilon,\epsilon]$ which finally gives the boundary conditions in Eq. (5.8).

As mentioned before, our main goal is to calculate the distribution $P_{\pm}\left(T_{loc},x_0,t\right)$ of the local

time. For this, we consider the definition of T_{loc} from Eq. (5.4) and use $P_{\pm}\left(T_{loc}, x_0, t\right) dT_{loc} = G_{\pm}(T_{2\epsilon}, x_0, t) dT_{2\epsilon}$ to get

$$Q_{\pm}\left(p, x_0, t\right) = \lim_{\epsilon \to 0} H_{\pm}\left(\frac{p}{2\epsilon}, x_0, t\right). \tag{5.9}$$

Therefore, the problem of deriving the statistics of T_{loc} reduces to calculating $H_{\pm}\left(q, x_0, t\right)$ for which we solve Eqs. (5.6). Taking Laplace transformation of $H_{\pm}(q, x_0, t)$ with respect to t in these equations gives

$$\bar{H}_{\pm}(q, x_0, s) = \int_0^{\infty} dt\ e^{-st}\ H_{\pm}(q, x_0, t). \tag{5.10}$$

The boundary conditions in Eq. (5.8) then become

$$\bar{H}_{\pm}(q, x_0 \to \pm\infty, s) = \frac{1}{s}. \tag{5.11}$$

Introducing two new functions

$$\bar{H}(q, x_0, s) = \frac{\bar{H}_{+}(q, x_0, s) + \bar{H}_{-}(q, x_0, s)}{2}, \tag{5.12}$$

$$\bar{Z}(q, x_0, s) = \frac{\bar{H}_{+}(q, x_0, s) - \bar{H}_{-}(q, x_0, s)}{2}, \tag{5.13}$$

we recast Eq. (5.6) in the Laplace space in terms of these functions as

$$s\bar{H} - 1 = v_0 \partial_{x_0} \bar{Z} - q\mathbb{I}_{\epsilon}\left(x_0\right) \bar{H}, \tag{5.14}$$

$$s\bar{Z} = v_0 \partial_{x_0} \bar{H} - 2R(x_0)\bar{Z} - q\mathbb{I}_{\epsilon}\left(x_0\right) \bar{Z}. \tag{5.15}$$

Using the second equation to write $\bar{Z}(q, x_0, s)$ completely in terms of $\bar{H}(q, x_0, s)$ and plugging it in the first equation, we get a closed-form differential equation for $\bar{H}(q, x_0, s)$ as

$$s\bar{H} - 1 = \frac{\partial}{\partial x_0}\left[\left(\frac{v_0^2}{s + 2R(x_0) + q\mathbb{I}_{\epsilon}}\right)\frac{\partial \bar{H}}{\partial x_0}\right] - q\mathbb{I}_{\epsilon}\left(x_0\right)\bar{H}. \tag{5.16}$$

This is the main equation that we will solve for general α. Below we solve it exactly for $\alpha = 0$ and then present an approximate solution for the general α case.

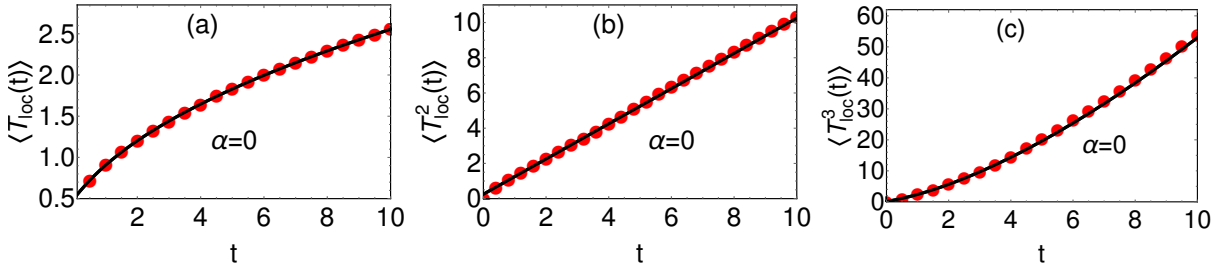

Figure 5.2: Moments of T_{loc} for $\alpha = 0$ given in Eq. (5.25) (shown by solid line) have been compared with the numerics (shown by red filled circles). We have taken $v_0 = 1$, $\gamma = 1$. For simulation, the interval $[-\epsilon, \epsilon]$ is chosen with $\epsilon = 0.001$.

5.1.1 Case I: $\alpha = 0$

For $\alpha = 0$, the rate $R(x_0)$ is just a constant and our model reduces to the usual homogeneous run and tumble motion. For this case Eq. (5.16) takes the form

$$s\bar{H} - 1 = \frac{\partial}{\partial x_0}\left(\frac{v_0^2}{s + 2\gamma + q\mathbb{I}_\epsilon}\frac{\partial \bar{H}}{\partial x_0}\right) - q\mathbb{I}_\epsilon(x_0)\,\bar{H}. \tag{5.17}$$

Solving this equation separately for regions inside and outside the interval $[-\epsilon, \epsilon]$ gives the exact solution of $\bar{H}(q, x_0, s)$. We then insert this solution in Eq. (5.15) to get $\bar{Z}(q, x_0, s)$. Finally substituting these solutions in Eqs. (5.12) and (5.13) results in the expressions of $\bar{H}_\pm(q, x_0, s)$ as

$$\bar{H}_+(q, x_0, s) = \begin{cases} \frac{1}{s} + \mathcal{A}_1(q,s)e^{\frac{\lambda_s x_0}{v_0}}, & \text{if } -\infty < x_0 < -\epsilon, \\ \frac{1}{s+q} + \mathcal{A}_2(q,s)e^{\frac{\lambda_q x_0}{v_0}} + \mathcal{A}_2(q,s)\left(\frac{-\lambda_q+\gamma+s+q}{\gamma}\right)e^{\frac{-\lambda_q x_0}{v_0}}, & \text{if } -\epsilon < x_0 < \epsilon, \\ \frac{1}{s} + \mathcal{A}_1(q,s)\left(\frac{-\lambda_s+\gamma+s}{\gamma}\right)e^{\frac{-\lambda_s x_0}{v_0}}, & \text{if } \epsilon < x_0 < \infty. \end{cases} \tag{5.18}$$

$$\bar{H}_-(q, x_0, s) = \begin{cases} \frac{1}{s} + \mathcal{A}_1(q,s)\left(\frac{-\lambda_s+\gamma+s}{\gamma}\right)e^{\frac{\lambda_s x_0}{v_0}}, & \text{if } -\infty < x_0 < -\epsilon, \\ \frac{1}{s+q} + \mathcal{A}_2(q,s)e^{-\frac{\lambda_q x_0}{v_0}} + \mathcal{A}_2(q,s)\left(\frac{-\lambda_q+\gamma+s+q}{\gamma}\right)e^{\frac{\lambda_q x_0}{v_0}}, & \text{if } -\epsilon < x_0 < \epsilon, \\ \frac{1}{s} + \mathcal{A}_1(q,s)e^{-\frac{\lambda_s x_0}{v_0}}, & \text{if } \epsilon < x_0 < \infty, \end{cases} \tag{5.19}$$

where $\lambda_s = \sqrt{s(s+2\gamma)}$, $\lambda_q = \sqrt{(s+q)(s+q+2\gamma)}$. In these solutions, the functions $\mathcal{A}_1(q,s)$ and $\mathcal{A}_2(q,s)$ do not depend on the initial position x_0. To evaluate these functions, we use the continuity of $\bar{H}_\pm(q, x_0, s)$ across $x_0 = \pm\epsilon$ which then completely specifies the Laplace transforms

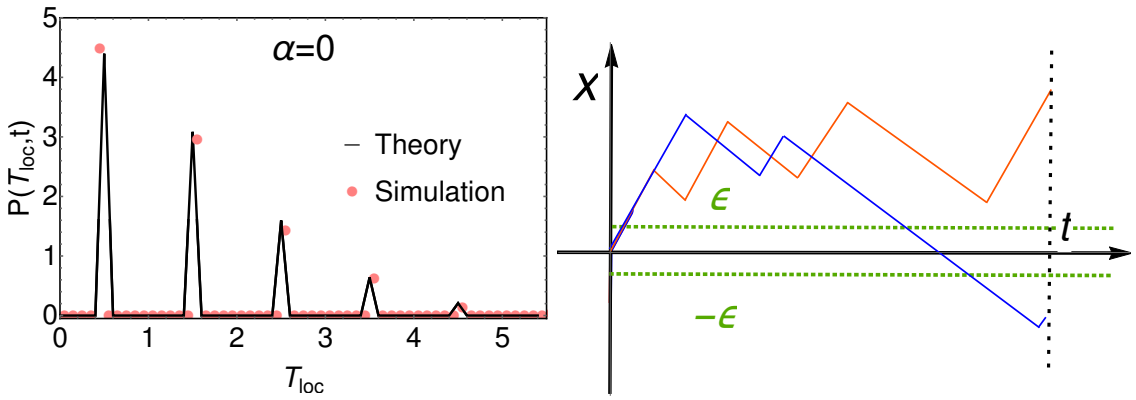

Figure 5.3: *Left panel:* Comparison of the distribution $P(T_{loc}, t)$ given in Eq. (5.31) for $\alpha = 0$ with the numerical simulations for $v_0 = 1$, $\gamma = 1$ and $t = 3$. In simulation, local time is measured inside the box $[-\epsilon, \epsilon]$ with $\epsilon = 0.01$. *Right panel:* Schematic trajectories of a RTP that give rise to different δ-function terms in Eq. (5.31). For example, the red trajectory contributes $T_{loc} = \frac{\epsilon}{2\epsilon v_0} = \frac{1}{2v_0}$ whereas the blue trajectory contributes $T_{loc} = \frac{3\epsilon}{2\epsilon v_0} = \frac{3}{2v_0}$ to $P(T_{loc}, t)$.

$\bar{H}_{\pm}(q, x_0, s)$. However, recall that, we are interested in the local time statistics for which we need to compute $\bar{H}_{\pm}(q, x_0, s)$ at $q = p/2\epsilon$ as clear from Eq. (5.9). Moreover, we are interested at $x_0 = 0$ and therefore provide only the form of $\mathcal{A}_2\left(\frac{p}{2\epsilon}, s\right)$ in the limit $\epsilon \to 0$ as

$$\lim_{\epsilon \to 0} \mathcal{A}_2\left(\frac{p}{2\epsilon}, s\right) = \frac{\lambda_s + s}{s\left(\lambda_s + s + \gamma - \gamma e^{-\frac{p}{v_0}}\right)} e^{-\frac{p}{2v_0}}. \tag{5.20}$$

Plugging this in the middle equation of set (5.18) then gives

$$Q_+(p, 0, t) = \lim_{\epsilon \to 0} H_{\pm}\left(\frac{p}{2\epsilon}, 0, t\right), \tag{5.21}$$

$$= \frac{(\lambda_s + s) e^{-\frac{p}{2v_0}}}{s\left(\lambda_s + s + \gamma - \gamma e^{-\frac{p}{v_0}}\right)}. \tag{5.22}$$

Since the initial position $x_0 = 0$, we expect $Q_+(p, 0, t) = Q_-(p, 0, t)$ by symmetry. This can also be verified by explicitly calculating $Q_-(p, 0, t)$ from Eq. (5.19). Dropping the subscript '$\pm$' from $Q_{\pm}(p, 0, t)$ and simply using the notation $\bar{Q}(p, s)$ instead of $\bar{Q}_{\pm}(p, 0, s)$, we get

$$\bar{Q}(p, s) = \frac{(\lambda_s + s) e^{-\frac{p}{2v_0}}}{s\left(\lambda_s + s + \gamma - \gamma e^{-\frac{p}{v_0}}\right)}. \tag{5.23}$$

To get the distribution $P(T_{loc}, t)$, the only task now is to perform the inverse Laplace transformation of $\bar{Q}(p, s)$. Before that, we use the Laplace transform $\bar{Q}(p, s)$ to compute few moments of T_{loc} which highlight some key differences from that of the Brownian motion.

5.1.1.1 Moments $\langle T_{loc}^n(t)\rangle$ for $\alpha = 0$

Following the definition of $\bar{Q}(p,s)$, the moments of T_{loc} are obtained by differentiating $\bar{Q}(p,s)$ with respect to p as

$$\langle T_{loc}^n(t)\rangle = L_{s\to t}\left[(-1)^n\left(\frac{\partial^n \bar{Q}(p,s)}{\partial p^n}\right)_{p=0}\right], \tag{5.24}$$

where $L_{s\to t}$, as before, denotes the inverse Laplace trasformation from $s \to t$. Substituting $\bar{Q}(p,s)$ from Eq. (5.23) in this equation yields the expressions of the general moments of T_{loc}. Obtaining closed-form expression for n-th order moment, however, turns out to be difficult. We below provide the expressions of the first three moments of T_{loc}:

$$\begin{aligned}
\langle T_{loc}(t)\rangle &= \frac{e^{-\gamma t}}{2v_0}\left[(1+2\gamma t)I_0(\gamma t) + 2\gamma t I_1(\gamma t)\right], \\
\langle T_{loc}^2(t)\rangle &= \frac{1}{4v_0^2}\left(1+4\gamma t\right), \\
\langle T_{loc}^3(t)\rangle &= \frac{e^{-\gamma t}}{8v_0^3}\left[(1+14\gamma t+16\gamma^2 t^2)I_0(\gamma t) + \left(6\gamma t + 16\gamma^2 t^2\right) I_1(\gamma t)\right],
\end{aligned} \tag{5.25}$$

Figure 5.2 shows the comparison of our result with the numerical simulations and we find excellent agreement for all three moments. For small γt, the RTP displays strong persistence effects as observed before for various quantities. Here also, we anticipate strong non-Brownian behaviour at small γt. To see this, we take the large s form of $\bar{Q}(p,s)$ in Eq. (5.23) by approximating $\lambda_s = \sqrt{s(2\gamma+s)} \simeq s$. This gives $\bar{Q}(p,s) \simeq \frac{e^{-\frac{p}{2v_0}}}{s}$ from which n-th order moment turns out to be

$$\langle T_{loc}^n(t)\rangle \simeq \frac{1}{(2v_0)^n}, \quad \text{as } \gamma t \to 0^+. \tag{5.26}$$

Interestingly, for small (but non-zero) times, the moments of T_{loc} become non-zero constants which is different than the Brownian motion for which the n-th moment scales as $\sim t^{\frac{n}{2}}$ with time [128]. As we show later that this difference essentially stems from the persistence nature of the RTPs at these timescales. On the other hand, for large times, we take the small-s form of the Laplace transform $\bar{Q}(p,s) \simeq \frac{2\mathfrak{D}_0}{\sqrt{s}(p+2\sqrt{s\mathfrak{D}_0})}$ with $\mathfrak{D}_0 = \frac{v_0^2}{2\gamma}$ and plugging this in Eq. (5.24), we get

$$\langle T_{loc}^n(t)\rangle \simeq \frac{n!}{\Gamma\left(\frac{n}{2}+1\right)}\left(\frac{t}{4\mathfrak{D}_0}\right)^{\frac{n}{2}}, \quad \text{as } \gamma t \to \infty \tag{5.27}$$

which expectedly matches with the results of Brownian motion [128].

5.1.1.2 $P\left(T_{loc}, t\right)$ for $\alpha = 0$

To compute the probability distribution $P(T_{loc}, t)$, we have to perform two inverse Laplace transformations of $\bar{Q}(p, s)$ in Eq. (5.23), namely one with respect to $p \to T_{loc}$ and the other with respect to $s \to t$. Therefore, we get

$$\begin{aligned} P\left(T_{loc}, t\right) &= L_{s\to t} \;\; L_{p\to T_{loc}} \left[\frac{(\lambda_s + s) e^{-\frac{p}{2v_0}}}{s\left(\lambda_s + s + \gamma - \gamma e^{-\frac{p}{v_0}}\right)} \right], \\ &= L_{s\to t} \;\; L_{p\to T_{loc}} \left[\frac{\lambda_s - s}{s\gamma} \sum_{m=0}^{\infty} \left(\frac{\gamma}{\lambda_s + s + \gamma} \right)^m e^{-\frac{(2m+1)p}{2v_0}} \right], \end{aligned} \tag{5.28}$$

The inversion with respect to p is easy and we have

$$P\left(T_{loc}, t\right) = L_{s\to t} \left[\frac{\lambda_s - s}{s\gamma} \sum_{m=0}^{\infty} \left(\frac{\gamma}{\lambda_s + s + \gamma} \right)^m \; \delta\left(T_{loc} - \frac{2m+1}{2v_0} \right) \right]. \tag{5.29}$$

Now to perform the inversion in s, we use the following result from [210]:

$$L_{s\to t} \left[\frac{\lambda_s - s}{s\gamma} \left(\frac{\gamma}{\lambda_s + s + \gamma} \right)^m \right] = e^{-\gamma t} \left[I_m(\gamma t) + I_{m+1}(\gamma t) \right], \tag{5.30}$$

and insert it in Eq. (5.29). The final expression of $P\left(T_{loc}, t\right)$ then follows to be

$$P\left(T_{loc}, t\right) = \sum_{m=0}^{\infty} \mathcal{S}_m(t) \; \delta\left(T_{loc} - \frac{2m+1}{2v_0} \right), \tag{5.31}$$

$$\text{with} \qquad \mathcal{S}_m(t) = e^{-\gamma t} \left[I_m(\gamma t) + I_{m+1}(\gamma t) \right]. \tag{5.32}$$

In simulation also, we see that the distribution $P\left(T_{loc}, t\right)$ appears as a series of δ-functions as indicated by Eq. (5.31). This comparison with the simulations has been shown in Figure 5.3 (left panel). Let us now try to understand physically how various δ-functions in Eq. (5.31) arise. Consider the red trajectory of the RTP in Figure 5.3 (right panel) where the particle, starting from the origin, does not cross the origin till time interval t. Here, the time spent by the particle inside the interval $[-\epsilon, \epsilon]$ is $T_{2\epsilon} = \frac{\epsilon}{v_0}$. Following the definition of local time in Eq. (5.4), we then get $T_{loc} = \frac{1}{2v_0}$. Such events give rise to the $m = 0$ term in Eq. (5.31). The corresponding coefficient $\mathcal{S}_0(t)$ then represents the probability that the particle, starting from the origin, has not crossed the origin till time t. Similarly, for the blue trajectory, the particle crosses the origin only once till time t with the initial position also being the origin. Here, $T_{2\epsilon} = \frac{3\epsilon}{v_0}$ and $T_{loc} = \frac{3}{2v_0}$. Therefore, these events contribute to the $m = 1$ term in Eq. (5.31) with the coefficient $\mathcal{S}_1(t)$ simply being the probability that the RTP, starting from the origin,

crosses the origin only once till time t. Extending this idea allows us to write the contribution $\mathcal{S}_m(t)\ \delta\left(T_{loc} - \frac{2m+1}{2v_0}\right)$ when the particle crosses the origin m-times till time t. The coefficient $\mathcal{S}_m(t)$ has the natural interpretation as the probability that the RTP crosses the origin m-times till time t starting from the origin. We have explicitly derived this in appendix 8.11.

Now to contrast $P\left(T_{loc}, t\right)$ in Eq. (5.31) with that of the Brownian motion, we analyse it in various limits for γt. Particularly for $\gamma t \to 0^+$, we have $I_m(\gamma t \to 0) = \delta_{m,0}$ which then makes the right hand side of Eq. (5.31) as

$$P\left(T_{loc}, t\right) \simeq \delta\left(T_{loc} - \frac{1}{2v_0}\right), \qquad \text{for } \gamma t \to 0. \tag{5.33}$$

This form also correctly recovers the moments of T_{loc} in Eq. (5.26) for small but non-zero γt. Next for $\gamma t \to \infty$, we also take the relevant scaling limit $v_0 T_{loc} \to \infty$ with $\frac{v_0 T_{loc}}{\sqrt{\gamma t}}$ fixed. One can then replace the summation in Eq. (5.26) by integration performing which gives $P(T_{loc}, t) \simeq v e^{-\gamma t} I_{v_0 T_{loc}}(\gamma t)$. Finally using the asymptotic expression $I_{v_0 T_{loc}}(\gamma t) \simeq \frac{e^{\gamma t}}{\sqrt{2\pi\gamma t}} e^{-\frac{v_0^2 T_{loc}^2}{2\gamma t}}$ for the aforementioned limits, we get the expression of $P(T_{loc}, t)$ as

$$P\left(T_{loc}, t\right) \simeq \sqrt{\frac{4\mathfrak{D}_0}{\pi t}} e^{-\frac{\mathfrak{D}_0 T_{loc}^2}{t}}, \qquad \text{as } \gamma t \to \infty, \tag{5.34}$$

with $\mathfrak{D}_0 = \frac{v_0^2}{2\gamma}$. As expected in this case, we recover the results of the Brownian particle in one dimension with diffusion constant $\mathfrak{D}_0$ [128].

5.1.2 Case II: General α

We now derive the statistics of T_{loc} for general α. Notice that the path-counting analysis used for $\alpha = 0$ in the previous section can also be applied for the general α case. So, for this case also, we expect the distribution $P\left(T_{loc}, t\right)$ to be given by Eq. (5.31) with $\mathcal{S}_m(t)$ being the probability for m returns to the origin till time t. But obtaining this probability $\mathcal{S}_m(t)$ for general α turns out to be challenging. Instead, we solve the backward master equations directly for this case.

From Eq. (5.15), we see that the backward equation for $\bar{Z}(q, x_0, s)$ has a decay term proportional to $2R(x_0)\bar{Z} + q\mathbb{I}_\epsilon\left(x_0\right)$ while for $\bar{H}(q, x_0, s)$ in Eq. (5.14), the decay term is only proportional to $q\mathbb{I}_\epsilon\left(x_0\right)$. So we expect $\bar{Z}(q, x_0, s)$ in the time domain to decay faster than $\bar{H}(q, x_0, s)$ which enables us to drop $s\bar{Z}$ term from Eq. (5.15) for small s (equivalently large t). Also, we are interested in the statistics of the local time T_{loc} which is related to the statistics of $T_{2\epsilon}$ via Eq. (5.9). By replacing q by $p/2\epsilon$ in Eq. (5.14) and using $\frac{p}{2\epsilon}\mathbb{I}_\epsilon\left(x_0\right) \to p\delta(x_0)$, we can transform Eq.

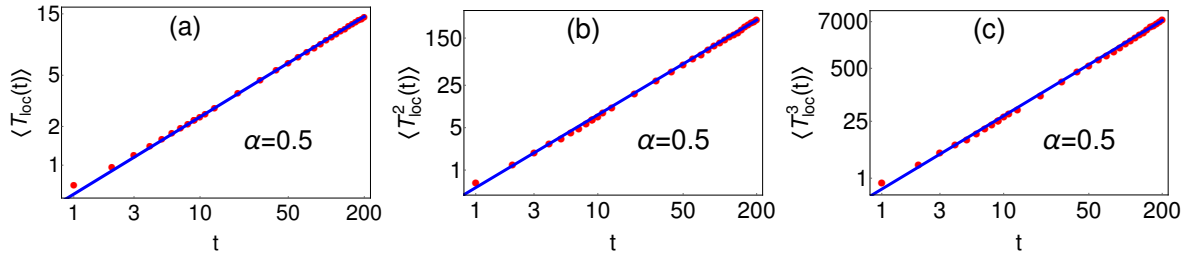

Figure 5.4: First three moments of T_{loc} in Eq. (5.39) have been compared with the numerical simulations for $\alpha = 0.5$. The analytic form is shown by solid blue lines and the symbols are the simulation data. Parameters chosen are $v_0 = 1,\ \gamma = 1,\ l = 1$. The slopes of the plots are (a) $\frac{3}{5}$, (b) $\frac{6}{5}$ and (c) $\frac{9}{5}$.

(5.14) for $\bar{H}(q, x_0, s)$ to a differential equation for $\bar{Q}(p, x_0, s)$ as

$$s\bar{Q} - 1 \simeq v_0^2 \frac{\partial}{\partial x_0}\left(\frac{1}{2R(x_0)}\frac{\partial \bar{Q}}{\partial x_0}\right) - p\delta(x_0)\bar{Q}. \tag{5.35}$$

Note that here $\bar{Q}(p, x_0, s) = \frac{\bar{Q}_+(p,x_0,s)+\bar{Q}_-(p,x_0,s)}{2}$ where $\bar{Q}_\pm(p, x_0, s)$ are the double Laplace transforms of the distribution $P_\pm\left(T_{loc}, x_0, t\right)$. The boundary condition for $\bar{Q}(p, x_0, s)$ is obtained from Eq. (5.11) as

$$\bar{Q}(p, x_0 \to \pm\infty, s) = \frac{1}{s}. \tag{5.36}$$

Once again to solve Eq. (5.35), we follow the route as done in Sec. 4.2.3. To avoid the repetition, we have relegated the details of this calculation to appendix 8.12. The final solution for $x_0 = 0$ reads

$$\bar{Q}(p, s) \simeq \frac{\mathcal{C}_\alpha}{s^{\frac{1}{2+\alpha}}\left(p + \mathcal{C}_\alpha s^{\frac{1+\alpha}{2+\alpha}}\right)}, \quad \text{with} \tag{5.37}$$

$$\mathcal{C}_\alpha = 2\left(\frac{\mathfrak{D}_\alpha}{(2+\alpha)^\alpha}\right)^{\frac{1}{2+\alpha}} \frac{\Gamma\left(\frac{1}{2+\alpha}\right)}{\Gamma\left(\frac{1+\alpha}{2+\alpha}\right)}. \tag{5.38}$$

Here $\mathfrak{D}_\alpha = \frac{v_0^2 l^\alpha}{2\gamma}$. Remember that this expression is valid only in the small-s limit. We now use it to compute the large-t behaviours of the moments and distribution separately.

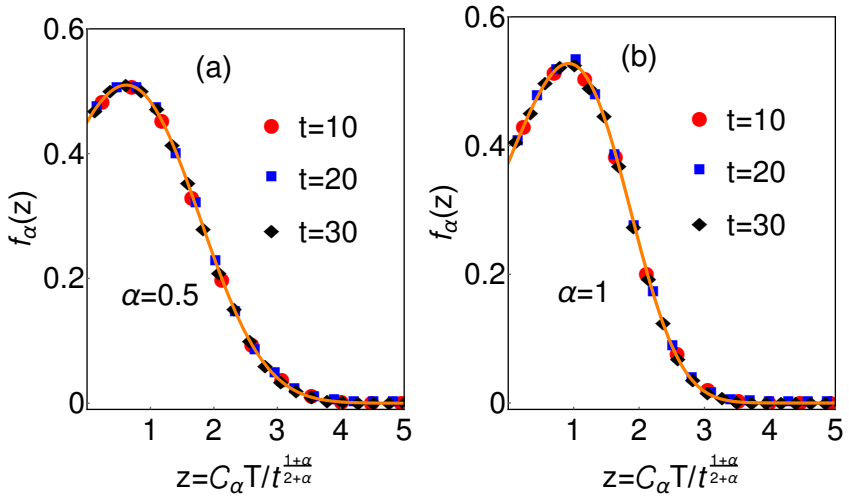

Figure 5.5: Comparison of the scaling function $f_\alpha(z)$ of T_{loc} in Eq. (5.43) (shown by solid line) with the numerical simulations (shown by different symbols) for $\alpha = 0.5$ and $\alpha = 1$. For each α, we have considered the simulation data for three different times. Parameters chosen are $v_0 = 1,\ \gamma = 1$ and $l = 1$.

5.1.2.1 Moments $\langle T_{loc}^n(t)\rangle$ for general α

Using the relation in Eq. (5.24), we can compute the moments of T_{loc} by plugging $\bar{Q}(p,s)$ from Eq. (5.37). The n-th order moment then reads

$$\langle T_{loc}^n(t)\rangle \simeq \frac{n!}{\mathcal{C}_\alpha^n \Gamma\left(\frac{1+(n+1)(1+\alpha)}{2+\alpha}\right)} t^{\frac{n(1+\alpha)}{2+\alpha}}. \tag{5.39}$$

Note that this equation gives the moments only at late times and ceases to be a good description at small and intermediate times. For $\alpha = 0$, it correctly gives the $\sim \sqrt{t}$ scaling of T_{loc} which was also observed before from the exact analysis. For general α, we find that the typical fluctuations of T_{loc} scale with time as $T_{loc} \sim t^{\frac{1+\alpha}{2+\alpha}}$ for large values of t. In Figure 5.4, we verify our results by comparing it with the numerical simulations for $\alpha = 0.5$. The deviation at small times is self-explanatory. The match becomes better as we go to higher values of t.

5.1.2.2 Scaling form of $P(T_{loc},t)$ at large t for general α

Let us now perform the double inverse Laplace transformation of $\bar{Q}(p,s)$ in Eq. (5.37) to find the distribution $P(T_{loc},t)$. Inversion of $\bar{Q}(p,s)$ with respect p is straightforward and we get

$$P(T_{loc},t) \simeq L_{s\to t}\left[\frac{\mathcal{C}_\alpha}{s^{\frac{1}{2+\alpha}}} e^{-\mathcal{C}_\alpha T_{loc} s^{\frac{1+\alpha}{2+\alpha}}}\right]. \tag{5.40}$$

To perform the other inverse Laplace transformation, we use the result from [211]

$$Ls \to t \left(\frac{e^{-ws^\beta}}{s^{1-\beta}} \right) = \frac{1}{\pi} \sum_{j=1}^{\infty} \frac{(-w)^{j-1}}{j!} \frac{\Gamma\left(1+j\beta\right)}{\beta\ t^{j\beta}} \sin\left(\pi j\beta\right), \quad \text{for } 0<\beta<1, \tag{5.41}$$

in Eq. (5.40), which then gives that the distribution $P(T_{loc},t)$ satisfies the scaling form

$$P(T_{loc},t) \simeq \frac{\mathcal{C}_\alpha}{t^{\frac{1+\alpha}{2+\alpha}}}\ f_\alpha\left(\frac{\mathcal{C}_\alpha T_{loc}}{t^{\frac{1+\alpha}{2+\alpha}}}\right), \tag{5.42}$$

where the scaling function $f_\alpha(z)$ is given by

$$f_\alpha(z) = \frac{1}{\pi} \sum_{j=1}^{\infty} \frac{(-z)^{j-1}}{j!} \frac{\Gamma\left(1+j\frac{1+\alpha}{2+\alpha}\right)}{\left(\frac{1+\alpha}{2+\alpha}\right)} \sin\left(\pi j \frac{1+\alpha}{2+\alpha}\right). \tag{5.43}$$

In Figure 5.5, we have numerically verified the expression of $f_\alpha(z)$ for $\alpha = 0.5$ and $\alpha = 1$. For each α, we have performed the simulations for three different values of t and we see nice agreement for all cases. For some values of α, we can perform the series summation in Eq. (5.43). For example, for $\alpha = 0$, the summation can be carried out and we recover the result in Eq. (5.34) for $P(T_{loc},t)$. For general α, it is difficult to carry out this sum analytically. However, one can get a simplified expression of $f_\alpha(z)$ for large z by using the saddle point method to evaluate the Bromwich integral in Eq. (5.40). We have derived this expression in appendix 8.13 and present only the final result here as

$$f_\alpha(z) \simeq \frac{z^{\frac{\alpha}{2}}}{\sqrt{2\pi}} \frac{(1+\alpha)^{\frac{\alpha}{2}}}{(2+\alpha)^{\frac{\alpha-1}{2}}}\ \exp\left(-\frac{(1+\alpha)^{1+\alpha}}{(2+\alpha)^{2+\alpha}}\ z^{2+\alpha}\right). \tag{5.44}$$

This expression is valid only for large z and breaks down for smaller values of z.

5.2 Local time in presence of an absorbing wall

Up to this point, we studied the moments and distribution of T_{loc} when the RTP moves in an infinite line till a fixed time duration t. But in many physical settings, particles move in a bounded domain in presence absorbtion boundary. For example, in chemical reactions taking place inside bounded domains, the time spent by a catalytic agent around the reactive points before coming out of the domain might be related to the efficiency of the reaction [196–199]. Similar examples might arise in biological settings, where the time spent by a protein molecule inside a cell before getting absorbed by a binding site might be useful [200]. Motivated from these examples, we proceed to study the statistics of the local time in presence of an absorbing

wall in this section.

More precisely, we consider a RTP in one dimension with the initial position x_0 and an absorbing wall at $x = M$ ($> x_0$). We follow its motion till it gets absorbed by the wall and denote the corresponding fisrt-passage time to M by t_f. The local time T_{loc} measured around the origin is then given by

$$T_{loc} = \int_0^{t_f} \delta\left(x(\tau)\right) d\tau. \tag{5.45}$$

This falls under a broad category of quantities called first passage functionals which have been studied in detail for Brownian motion [121]. For RTP, we denote the distribution of T_{loc} in Eq. (5.45) by $\mathcal{P}_{\pm}(T_{loc}, x_0)$ and their Laplace transforms with T_{loc} ($\to p$) by

$$\mathcal{Q}_{\pm}(p, x_0) = \int_0^{\infty} dT_{loc}\; e^{-pT_{loc}}\; \mathcal{P}_{\pm}(T_{loc}, x_0). \tag{5.46}$$

As done before, to derive the statistics of the local time, we follow another intuitive definition due to P. Lévy as [209]

$$T_{loc} = \lim_{\epsilon \to 0^+} \frac{T_{2\epsilon}}{2\epsilon}, \text{ with} \tag{5.47}$$

$$T_{2\epsilon} = \int_0^{t_f} \mathbb{I}_{\epsilon}\left(x(\tau)\right) d\tau, \tag{5.48}$$

where $T_{2\epsilon}$ is the time spent by the RTP inside a small but non-zero interval $[-\epsilon, \epsilon]$ till the first-passage time t_f. Once again, we will first derive the statistics of $T_{2\epsilon}$ and use it to obtain the properties of T_{loc} via Eq. (5.47).

Let $\mathbb{P}_{\pm}(T_{2\epsilon}, x_0)$ be the distribution of $T_{2\epsilon}$ and their Laplace transform with $T_{2\epsilon}$ ($\to q$) be

$$\mathbb{Q}_{\pm}(q, x_0) = \int_0^{\infty} dT_{2\epsilon}\; e^{-qT_{2\epsilon}}\; \mathbb{P}_{\pm}(T_{2\epsilon}, x_0). \tag{5.49}$$

Then using the definition of T_{loc} in Eq. (5.47), we get the relation

$$\mathcal{Q}_{\pm}(p, x_0) = \lim_{\epsilon \to 0} \mathbb{Q}_{\pm}\left(\frac{p}{2\epsilon}, x_0\right). \tag{5.50}$$

The Laplace transforms $\mathbb{Q}_{\pm}(q, x_0)$ satisfy the backward Fokker-Planck equations

$$v_0 \partial_{x_0} \mathbb{Q}_{+} - R(x_0)\mathbb{Q}_{+} + R(x_0)\mathbb{Q}_{-} - q\mathbb{I}_{\epsilon}(x_0)\mathbb{Q}_{+} = 0, \tag{5.51}$$

$$v_0 \partial_{x_0} \mathbb{Q}_{-} - R(x_0)\mathbb{Q}_{+} + R(x_0)\mathbb{Q}_{-} + q\mathbb{I}_{\epsilon}(x_0)\mathbb{Q}_{-} = 0. \tag{5.52}$$

with the following boundary conditions:

$$\mathbb{Q}_+(q, x_0 = M) = 1, \tag{5.53}$$

$$\mathbb{Q}_\pm(q, x_0 \to -\infty) < \infty. \tag{5.54}$$

To understand the first boundary condition, recall that if the particle starts from $x_0 = M^-$ initially with velocity $+v_0$ then it will instantly get absorbed by the wall. Consequently $T_{2\epsilon} = 0$ and $\mathbb{P}_+(T_{2\epsilon}, M^-) = \delta(T_{2\epsilon})$ which from Eq. (5.49) then gives the boundary condition in Eq. (5.53). Let us now understand the second boundary condition. If $x_0 \to -\infty$, then the first-passage time t_f also diverges. But the $T_{2\epsilon}$ spent inside the inteval $[-\epsilon, \epsilon]$ does not necessarily diverge. So, we anticipate the distribution to remain finite which in terms of $\mathbb{Q}_\pm(q, x_0)$ translate to Eq. (5.54).

In the following, we will solve the backward equations (5.51) and (5.52) and then use Eq. (5.50) to obtain $\mathcal{Q}_\pm(p, x_0)$ (as done for inifinite line case). For simplicity, here also, we consider $\alpha = 0$ and general α cases separately.

5.2.1 Case I: $\alpha = 0$

The backward equations in (5.51) and (5.52) for $\alpha = 0$ take the form

$$v_0 \partial_{x_0} \mathbb{Q}_+ - \gamma \mathbb{Q}_+ + \gamma \mathbb{Q}_- - q \mathbb{I}_\epsilon(x_0) \mathbb{Q}_+ = 0, \tag{5.55}$$

$$- v_0 \partial_{x_0} \mathbb{Q}_- + \gamma \mathbb{Q}_+ - \gamma \mathbb{Q}_- - q \mathbb{I}_\epsilon(x_0) \mathbb{Q}_- = 0. \tag{5.56}$$

Recall that $\mathbb{I}_\epsilon(x_0)$ is 1 if $-\epsilon < x_0 < \epsilon$ and 0 otherwise. As done for infinite line case, here also, we solve these equations in different regions of x_0 to get

$$\mathbb{Q}_+(q, x_0) = \begin{cases} \mathbb{B}(q), & \text{if } -\infty < x_0 < -\epsilon, \\ \mathbb{E}(q) e^{-\frac{\lambda(q) x}{v_0}} + \mathbb{F}(q) e^{\frac{\lambda(q) x}{v_0}}, & \text{if } -\epsilon < x_0 < \epsilon, \\ \mathbb{C}(q)(x_0 - M) + 1, & \text{if } \epsilon < x_0 < M. \end{cases} . \tag{5.57}$$

$$\mathbb{Q}_-(q, x_0) = \begin{cases} \mathbb{B}(q), & \text{if } -\infty < x_0 < -\epsilon, \\ \mathbb{E}(q) \frac{\lambda(q)+\gamma+q}{\gamma} e^{-\frac{\lambda(q) x}{v_0}} + \mathbb{F}(q) \frac{-\lambda(q)+\gamma+q}{\gamma} e^{\frac{\lambda(q) x}{v_0}}, & \text{if } -\epsilon < x_0 < \epsilon, \\ \mathbb{C}(q)(x_0 - M - \frac{v_0}{\gamma}) + 1, & \text{if } \epsilon < x_0 < M. \end{cases} . \tag{5.58}$$

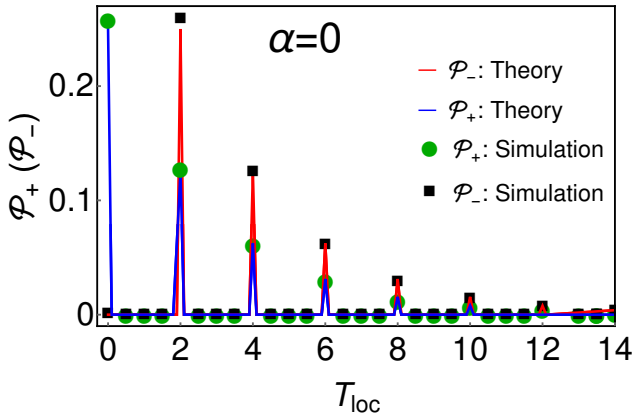

Figure 5.6: Numerical verification of the distributions $\mathcal{P}_{\pm}(T_{loc})$ in Eqs. (5.62) and (5.63) for $\alpha = 0$. We have taken $v_0 = 1$, $\gamma = 1$ and $M = 1$. In simulation, the local time is measured inside a box $[-\epsilon, \epsilon]$ with $\epsilon = 0.001$

To derive these solutions, we have used the boundary conditions in Eqs. (5.53) and (5.54). Also, here $\lambda(q) = \sqrt{q(q+2\gamma)}$ and $\mathbb{B}(q)$, $\mathbb{C}(q)$, $\mathbb{E}(q)$ and $\mathbb{F}(q)$ are functions independent of x_0 but depend on q. To compute these functions, we use the continuity of the solutions $\mathbb{Q}_{\pm}(q, x_0)$ across $x_0 = \pm\epsilon$ which then gives four linear equations involving $\mathbb{B}(q)$, $\mathbb{C}(q)$, $\mathbb{E}(q)$ and $\mathbb{F}(q)$. By solving these linear equations, we get the exact expressions of these functions. But here we are interested in $x_0 = \epsilon$ and therefore, need only the expression of $\mathbb{C}(q)$ as observed from Eqs. (5.57) and (5.58). Moreover, since we are ultimately interested in the statistics of the local time T_{loc}, we put $q = p/2\epsilon$ [see Eq. (5.50)] and obtain

$$\lim_{\epsilon\to 0} \mathbb{C}\left(\frac{p}{2\epsilon}\right) = \frac{\gamma\left(e^{\frac{2p}{v_0}} - 1\right)}{e^{\frac{2q}{v_0}}(v_0 + \gamma M) - \gamma M}. \tag{5.59}$$

Plugging this expression in Eqs. (5.57) and (5.58) and using the relation in Eq. (5.50), we write $\mathcal{Q}_{\pm}(p, \epsilon)$ in terms of $\mathbb{Q}_{\pm}(q, \epsilon)$ as

$$\mathcal{Q}_+(p) = \lim_{\epsilon\to 0} \mathbb{Q}_+\left(\frac{p}{2\epsilon}, \epsilon\right) = \frac{v_0}{v_0 + \gamma M - \gamma M e^{-\frac{2p}{v_0}}}, \tag{5.60}$$

$$\mathcal{Q}_-(p) = \lim_{\epsilon\to 0} \mathbb{Q}_-\left(\frac{p}{2\epsilon}, \epsilon\right) = \frac{v_0 e^{-\frac{2p}{v_0}}}{v_0 + \gamma M - \gamma M e^{-\frac{2p}{v_0}}}. \tag{5.61}$$

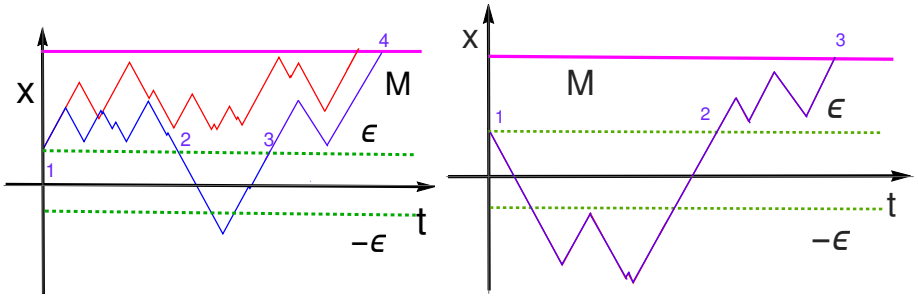

Figure 5.7: Schematic illustration of different trajectories of a RTP in presence of an absorbing wall at $x = M$ (shown in Magenta). The particle starts from $x_0 = \epsilon$ with velocity $+v_0$ for left panel and $-v_0$ for right panel and is evolved till it gets absorbed by the wall. Local time is then measured inside the interval $[-\epsilon, \epsilon]$ shown by dotted green lines.

Here $\mathcal{Q}_{\pm}(p)$ stand for $\mathcal{Q}_{\pm}(p, \epsilon)$. Performing the inverse Laplace transformation, we get the distribution $\mathcal{P}_{\pm}(T_{loc})$ as

$$\mathcal{P}_{+}(T_{loc}) = \sum_{m=0}^{\infty} \mathfrak{p}_0 \, (1-\mathfrak{p}_0)^m \, \delta\left(T_{loc} - \frac{2m}{v_0}\right), \tag{5.62}$$

$$\mathcal{P}_{-}(T_{loc}) = \sum_{m=1}^{\infty} \frac{\mathfrak{p}_0 \, (1-\mathfrak{p}_0)^m}{(1-\mathfrak{p}_0)} \delta\left(T_{loc} - \frac{2m}{v_0}\right), \tag{5.63}$$

where $\mathfrak{p}_0 = \frac{v_0}{v_0+\gamma M}$. In Figure 5.6, we have compared our analytic result with the numerical simulations. The agreement between them is excellent. Observe that the distributions $\mathcal{P}_{\pm}(T_{loc})$ appear as a series of δ-functions which is reminiscent about the infinite line case in Eq. (5.31). As we show next that the form of $\mathcal{P}_{\pm}(T_{loc})$ can be more easily derived by counting the number of paths that gives rise various delta function terms. Under this path-counting analysis, the prefactor accompanying $\delta\left(T_{loc} - \frac{2m}{v_0}\right)$ term in Eqs. (5.62) and (5.63) can be interpretated as the probability of m-visits to the origin by the RTP before getting absorbed at $x = M$ at time t_f.

5.2.1.1 Physical Derivation of $\mathcal{P}_{\pm}(T_{loc})$: Path Counting Analysis

Let us now try to understand various delta-function terms in Eqs. (5.62) and (5.63). We first focus on $\mathcal{P}_{+}(T_{loc})$. Figure 5.7 (left panel) schematically illustrates different trajectories of a RTP with initial position $x_0 = \epsilon$ and velocity $+v_0$. Notice that for the red trajectory, the particle gets absorbed by the wall $x = M$ without entering the $[-\epsilon, \epsilon]$ interval. Hence, the time $T_{2\epsilon}$ spent inside this interval is exactly zero which from Eq. (5.47) implies $T_{loc} = 0$. This gives rise to the $\delta(T_{loc})$ term corresponding to $m = 0$ in Eq. (5.62). The weight of this term will simply be the probability that the particle, starting from the origin, exits via $x = M$ without crossing the

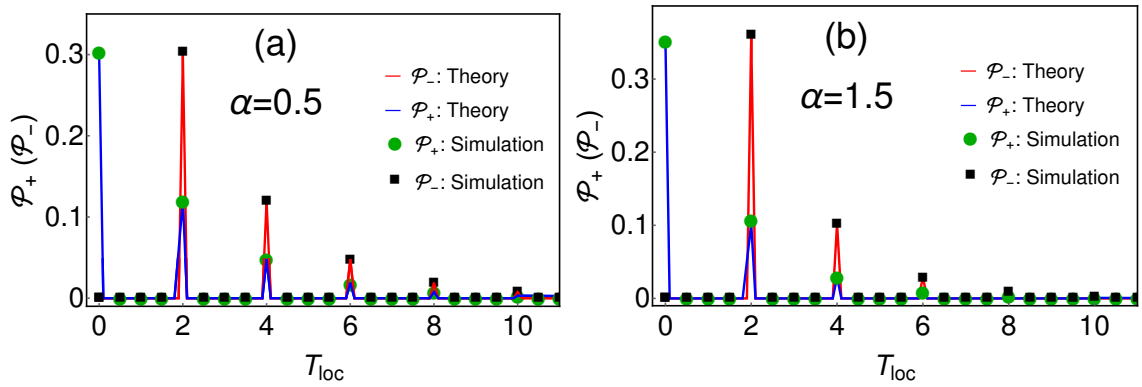

Figure 5.8: Analytical expressions of the distributions $\mathcal{P}_{\pm}(T_{loc})$ of the local time in Eqs. (5.66) and (5.67) have been compared with the numerical simulations for $\alpha = 0.5$ and $\alpha = 1.5$. Values of the parameters are $v_0 = 1,\ \gamma = 1,\ M = 1,\ l = 1$. For simulation, we have taken $\epsilon = 0.001$.

$x = 0$. This exit probability was exactly calculated in Sec. 4.3 to be $\mathfrak{p}_0 = \frac{v_0}{v_0+\gamma M}$. Consequently, we get the contribution $\mathfrak{p}_0\delta(T_{loc})$ in Eq. (5.62).

Similarly, for the blue trajectory in Figure 5.7 (left panel), the particle crosses the $[-\epsilon, \epsilon]$ interval twice before getting absorbed by the $x = M$ wall. Then the value of the local time is $T_{loc} = \frac{1}{2\epsilon}\left(\frac{2\epsilon}{v_0} + \frac{2\epsilon}{v_0}\right) = \frac{2}{v_0}$ which corresponds to the $m = 1$ term in Eq. (5.62). To understand its weight, we break the blue trajectory as $[1 \to 2] \bigoplus [2 \to 3] \bigoplus [3 \to 4]$. By following the same reasoning as for $m = 0$, we get the contributions of $1 - \mathfrak{p}_0$ and $\mathfrak{p}_0$ from parts $1 \to 2$ and $3 \to 4$ respectively. On the other hand, the RTP makes a first return to the origin in part $2 \to 3$ whose probability is unity (since the RTP motion is recurrent). The total contribution then becomes $\mathfrak{p}_0(1 - \mathfrak{p}_0)\delta\left(T_{loc} - \frac{2}{v_0}\right)$. Extending this rationale to the situation when the RTP crosses the $[-\epsilon, \epsilon]$ interval $2m$ times, we get $T_{loc} = \frac{2m}{v_0}$ and the corresponding weight $\mathfrak{p}_0(1 - \mathfrak{p}_0)^m$ in Eq. (5.62).

Let us now turn to $\mathcal{P}_-(T_{loc})$ in Eq. (5.63). From Figure 5.7 (right panel), we first notice that the particle will definitely enter the interval $[-\epsilon, \epsilon]$ when it starts from $x_0 = \epsilon$ with $-v_0$. Hence $T_{loc} = 0$ term does not appear in Eq. (5.63). However, other terms still appear. For example, in Figure 5.7 (right panel), we see the blue trajectory where the particle crosses the $[-\epsilon, \epsilon]$ interval twice before getting absorbed by the wall. As seen before, the particle will then contribute $T_{loc} = \frac{2}{v_0}$. To compute its weight, we once again break the trajectory as $[1 \to 2] \bigoplus [2 \to 3]$. The motion being recurrent, we get a contribution of unity in the part $1 \to 2$. On the other hand, the part $2 \to 3$ contributes $\mathfrak{p}_0$ since the particle exits from $x = M$. The total contribution then becomes $\mathfrak{p}_0\ \delta\left(T_{loc} - \frac{2}{v_0}\right)$. Similarly when the particle enters the interval $2m$ times, the total contribution to the distribution becomes $\mathfrak{p}_0(1 - \mathfrak{p}_0)^{m-1}\delta\left(T_{loc} - \frac{2m}{v_0}\right)$.

It is worth mentioning that although, we have focused on $x_0 = \epsilon$, the path-counting analysis

can be easily extended to arbitrary x_0. For example, for $x_0 = -\epsilon$ ($\to 0^-$) this analysis gives the distribution of T_{loc} as

$$\mathcal{P}_{\pm}(T_{loc}) = \sum_{m=0}^{\infty} \mathfrak{p}_0 (1-\mathfrak{p}_0)^m \delta\left(T_{loc} - \frac{2m+1}{v_0}\right), \tag{5.64}$$

and for $x_0 = 0$ the distribution is given by

$$\begin{aligned} \mathcal{P}_{+}(T_{loc}) &= \sum_{m=0}^{\infty} \mathfrak{p}_0 (1-\mathfrak{p}_0)^m \delta\left(T_{loc} - \frac{4m+1}{2v_0}\right), \\ \mathcal{P}_{-}(T_{loc}) &= \sum_{m=0}^{\infty} \mathfrak{p}_0 (1-\mathfrak{p}_0)^m \delta\left(T_{loc} - \frac{4m+3}{2v_0}\right). \end{aligned} \tag{5.65}$$

In fact, the path-counting method becomes easily adaptable to the general α case also. This is quite remarkable because solving the backward equations for arbitrary α and x_0 is analytically challenging as seen for the infinite line case. In the next section, we will use this path-counting analysis to obtain the exact distributions of T_{loc} for the arbitrary values of α.

5.2.2 Case II: General α

Let us now look at the distribution of T_{loc} for the general $\alpha \geq 0$ with an absorbing wall at $x = M$. Solving the backward equations (5.51) and (5.52) analytically for general α is difficult. However, the path-counting technique discussed in the previous section can be easily generalised to this case. Following the same physical arguments as before, the distributions $\mathcal{P}_{\pm}(T_{loc})$ for $x_0 = \epsilon$ ($\to 0^+$) can be found to be

$$\mathcal{P}_{+}(T_{loc}) = \sum_{m=0}^{\infty} \mathfrak{p}_\alpha \left(1-\mathfrak{p}_\alpha\right)^m \delta\left(T_{loc} - \frac{2m}{v_0}\right), \tag{5.66}$$

$$\mathcal{P}_{-}(T_{loc}) = \sum_{m=1}^{\infty} \mathfrak{p}_\alpha \left(1-\mathfrak{p}_\alpha\right)^{m-1} \delta\left(T_{loc} - \frac{2m}{v_0}\right), \tag{5.67}$$

where $\mathfrak{p}_\alpha$ denotes the probability that the RTP, starting from the origin, exits from $x = M$ side without crossing the origin. In Sec. 4.3, we have derived this exit probability exactly and its expression reads

$$\mathfrak{p}_\alpha = \frac{v_0(1+\alpha)l^\alpha}{\gamma M^{1+\alpha} + v_0(1+\alpha)l^\alpha}. \tag{5.68}$$

Figure 5.8 shows a comparison of our analytic results with the simulations for $\alpha = 0.5$ and $\alpha = 1.5$. We observe excellent match of our analytical results with the simulation data. Here also, one can extend these results for other initial positions as done for $\alpha = 0$ case.

5.3 Summary

Continuing our study on the heterogeneous RTP model, this chapter demonstrated the effect of the position dependent rate $R(x) \sim |x|^\alpha \quad (\alpha \geq 0)$ on the statistics of the local time T_{loc}. For the homogeneous case ($\alpha = 0$), we used the Feynman-Kac's formalism to compute the moments generating function of T_{loc} from which we exactly calculated the first three moments of T_{loc}. We then derived the distribution of T_{loc} for $\alpha = 0$ in Eq. (5.31) which appeared as a series summation of δ-functions with appropriate weights. By counting the number of paths, we argued that the term $\mathcal{S}_m(t)\delta\left(T_{loc} - \frac{2m+1}{2v_0}\right)$ in Eq. (5.31) arises when the RTP visits the origin m-times till time t. The weight $\mathcal{S}_m(t)$ is then interpretated as the probability of m-returns to the origin with starting position also being the origin.

While for general α, the distribution is still given by the series summation of δ-functions, calculating $\mathcal{S}_m(t)$ for this case turns out to be difficult. However for large t, we solved the backward equations to find that the typical fluctuations of T_{loc} scale with time as $T_{loc} \sim t^{\frac{1+\alpha}{2+\alpha}}$ and the distribution obeys the scaling form $P(T_{loc}, t) \simeq \frac{\mathcal{C}_\alpha}{t^{\frac{1+\alpha}{2+\alpha}}}\ f_\alpha\left(\frac{\mathcal{C}_\alpha T_{loc}}{t^{\frac{1+\alpha}{2+\alpha}}}\right)$. The corresponding scaling function $f_\alpha(z)$ is obtained explicitly in Eq. (5.43) for arbitrary values of $\alpha \geq 0$.

In the second part of this chapter, we considered the local time properties in presence of an absorbing wall at $x = M$ (> 0). By using the path-counting method, we showed that the distribution, for all values of $\alpha \geq 0$ and $x_0 = \epsilon$ ($\to 0^+$), is given as a series summation of δ-functions at $T_{loc} = \frac{2m}{v_0}$ where $m = 0, 1, 2, 3, ...$ The expressions of these distributions are given in Eqs. (5.66) and (5.67). Once again, these forms can be understood from the problem of m-visits to the origin (starting from the origin) for the RTP in presence of the absorbing boundary condition at $x = M$.

Although, throughout this chapter, we have focused on $\alpha \geq 0$ case, our result on $P(T_{loc}, t)$ in Eq. (5.43) is valid also for $-1 < \alpha < 0$. We have verified this numerically but not shown here. However, performing the local time study analytically in presence of an absorbing barrier for $\alpha < 0$ remains a direction yet to be explored. Finally, we end this chapter by noting that our results for T_{loc} in Eq. (5.31) (for infinite line) and in Eqs. (5.66) and (5.67) (with absorbing wall) for $\alpha = 0$ may be experimentally verified using granular self-propelled particles confined in a quasi one-dimensional channel [228]. In such a set-up, the RTP dynamics is generated by tuning the width of the channel and frequency of the thermal shaker above which the granular particles are placed.

Chapter 6

Crossover behaviours exhibited by fluctuations and correlations in a chain of active particles

In the previous chapters, we studied the motion of a single run and tumble particle and exemplified the effect of persistence on the statistical properties of different quantities like arcsine laws and convex hull problems. The last two chapters focused on the run and tumble motion in a spatially heterogeneous medium. But in all these studies, focus has been a single active particle's dynamics. However, various studies have shown that multi-particle interacting active systems exhibit different non-trivial features like flocking [40–43], motility-induced phase separation [44–47], non-existence of equation of state in pressure [48] and so on. Another interesting problem in this direction is the single-file motion of active particles in which the particles are constrained to move in one dimension such that they cannot overtake the surrounding particles [130, 131]. As a result, the order of a particle is maintained throughout its motion. In the context of diffusion, the single-file constraint gives rise to the sub-diffusive scaling of the mean squared displacement (MSD) of the tagged particle at large times as $\sim \sqrt{t}$ in contrast to the linear scaling seen in the ordinary diffusion [132]. The associated probability distribution with the tagged particle's position is also known for the single-file diffusion [212–214].

For active particles with inter-particle repulsive interaction, the MSD and the correlation of the positions of the tagged particles have been studied in [133–136] where the MSD was shown to grow sub-diffusively as $\sim \sqrt{t}$ at late times similar to the single-file diffusion. Numerically, it was found that the MSD possesses a scaling form in t/τ_A with τ_A being the activity (persistence) timescale [136]. However, these studies are often numerical based and analytic calculations rely largely on hydrodynamic approximations or mean-field approximations. A rigorous and systematic analytical treatment of the motion of a tagged particle in the interacting active particle systems has still been lacking. To address this problem, we consider a simple and

analytically tractable model of N active particles interacting via the nearest-neighbour harmonic interaction in this chapter. We focus on three models of active particles namely, run and tumble particle (RTP), active Ornstein-Uhlenbeck particle (AOUP) and active Brownian particle (ABP). While the first two models are considered in one dimension, we study the ABPs in two dimensions. For these three models, we compute different correlation functions of the positions and see how activity modifies them. Similar studies for RTPs have also been performed in [215]. Harmonic chain driven by active noises has also been studied in the context of polymers in [216–220]. It is worth mentioning that in the context of Brownian particles, the harmonic chain description has been used as an approximation of a system with fairly general class of two-body interaction [221]. Therefore, we hope that our study on the harmonic chain of active particles in this chapter might also be of interest in a more larger context.

The rest of this chapter is organized as follows: We begin with a basic preliminary of three models in Sec. 6.1 and then summarize our main findings in Sec. 6.2. For RTPs, we provide the derivation of various correlation functions in the limit $N \to \infty$ in Sec. 6.3 with variance in sec. 6.3.1, equal time correlation in Sec. 6.3.2, position autocorrelation in Sec. 6.3.3 and unequal time correlation in Sec. 6.3.4. For finite but large N, these correlations are calculated in Sec. 6.3.5. We then carry out this analysis for AOUPs in Sec. 6.4 and for ABPs in Sec. 6.5 which is followed by a summary in Sec. 6.6.

6.1 Models and preliminaries

Consider a chain of N active particles where every particle interacts with its nearest neighnour by harmonic interaction of spring constant K (see Figure 6.1). If $\vec{r}_\alpha(t)$ denotes the position (more precisely the displacement) of the α-th particle at time t with $\alpha = 0, 1, 2, ...N-1$, then it evolves according to the equations

$$\frac{d\vec{r}_\alpha}{dt} = -K\left(2\vec{r}_\alpha - \vec{r}_{\alpha+1} - \vec{r}_{\alpha-1}\right) + \vec{F}^A_\alpha(t), \qquad \text{for } \alpha = 0, 1, ..., N-1, \tag{6.1}$$

Throughout this chapter, we consider the periodic boundary condition where the 0-th and $(N-1)$-th particles interact with each other. Also, we consider RTPs and AOUPs in one dimension whereas the ABP model is considered in two dimensions. Hence, the position $\vec{r}_\alpha(t)$ for the first two models is $\vec{r}_\alpha(t) = (x_\alpha(t), 0)$ and it is $\vec{r}_\alpha(t) = (x_\alpha(t), y_\alpha(t))$ for ABP. The noise $\vec{F}^A_\alpha(t)$ in Eq. (6.1) is the force due to some non-equilibrium source which gives rise to the active nature of the particles. Its exact form depends on the choice of models. For example, for RTP,

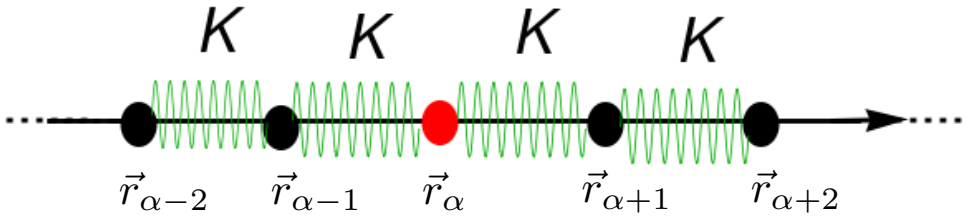

Figure 6.1: Schematic illustration of a chain of active particles with nearest-neighbour harmonic interaction with spring constant K. The tagged particle is shown in red.

$\vec{F}^A_\alpha(t) = (F^{RTP}_\alpha(t)\ ,\ 0)$ is given in terms of the telegraphic noise $\sigma_\alpha(t)$ as

$$F^{RTP}_\alpha(t) = v_0\ \sigma_\alpha(t), \qquad \text{for } \alpha = 0, 1, .., N-1, \tag{6.2}$$

$$\langle \sigma_\alpha(t)\sigma_\beta(t')\rangle = \delta_{\alpha,\beta}\ \exp\left(-2\gamma|t-t'|\right). \tag{6.3}$$

Similarly, for AOUPs, the noise is $\vec{F}^A_\alpha(t) = (F^{AOUP}_\alpha(t)\ ,\ 0)$ where $F^{AOUP}_\alpha(t)$ obeys the dynamics

$$F^{AOUP}_\alpha(t) = \lambda_\alpha(t), \quad \forall\alpha \qquad \text{with,}$$
$$\frac{d\lambda_\alpha}{dt} = -\zeta\lambda_\alpha + \sqrt{2D}\eta_\alpha(t), \tag{6.4}$$

where $\eta_\alpha(t)$ represents the Gaussian white noise with zero mean and correlation $\langle \eta_\alpha(t)\eta_\beta(t')\rangle = \delta_{\alpha,\beta}\ \delta(t-t')$. Finally, for ABPs, there is an internal orientational degree of freedom $\phi_\alpha(t)$ measured with respect to the x-axis that performs rotational diffusion. The noise $\vec{F}^A_\alpha(t)$ takes the form $\vec{F}^{ABP}_\alpha(t) = (\xi_\alpha(t), \psi_\alpha(t))$ where $\xi_\alpha(t)$ and $\psi_\alpha(t)$ evolve according to

$$\xi_\alpha(t) = v_A\cos\phi_\alpha(t), \quad \psi_\alpha(t) = v_A\sin\phi_\alpha(t), \tag{6.5}$$

$$\frac{d\phi_\alpha}{dt} = \sqrt{2D_{rot}}\ \eta_\alpha(t). \tag{6.6}$$

Here v_A (>0) is the speed of the particle and D_{rot} (>0) is the rotational diffusion constant which also sets the timescale for the activity. Once again, $\eta_\alpha(t)$ is the Gaussian white noise with zero mean and unequal-time correlation $\langle \eta_\alpha(t)\eta_\beta(t')\rangle = \delta_{\alpha,\beta}\ \delta(t-t')$. Furthermore, we assume that all ABPs are initially orientated along x-axis so that $\phi_\alpha(0) = 0$ for all α. For this particular choice of the initial orientation, the mean and correlations of $\xi_\alpha(t)$ and $\psi_\alpha(t)$ are given by [54]

$$\langle \xi_\alpha(t)\rangle = v_A e^{-D_{rot}t}, \quad \langle \psi_\alpha(t)\rangle = 0, \tag{6.7}$$

$$\langle \xi_\alpha(t)\xi_\beta(t')\rangle = \delta_{\alpha,\beta}\frac{v_A^2}{2}\left[e^{-D_{rot}|t-t'|} + e^{-D_{rot}\{t_1+t_2+2\min(t_1,t_2)\}}\right], \tag{6.8}$$

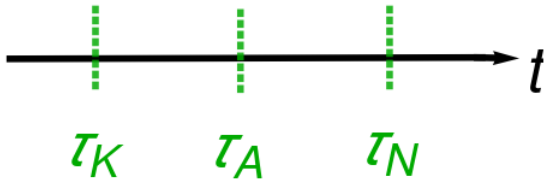

Figure 6.2: Schematics of three time scales in a harmonic chain of active particles. These time scales are (i) the interaction time scale $\tau_K = \frac{1}{K}$, (ii) the activity time scale $\tau_A = \frac{1}{\gamma}$ /$\frac{1}{\zeta}$ /$\frac{1}{D_{rot}}$ for RTP / AOUP /ABP and (iii) the relaxation time scale $\tau_N = \frac{N^2}{K}$ due to the finite ring size. We assume $\tau_K \ll \tau_A \ll \tau_N$.

$$\langle \psi_\alpha(t)\psi_\beta(t')\rangle = \delta_{\alpha,\beta}\frac{v_A^2}{2}\left[e^{-D_{rot}|t-t'|} - e^{-D_{rot}\{t_1+t_2+2\min(t_1,t_2)\}}\right], \tag{6.9}$$

$$\langle \xi_\alpha(t)\psi_\beta(t')\rangle = 0. \tag{6.10}$$

For these three models, we compute various two point correlation functions between the particles and demonstrate how activity and interaction ramify these quantities. Notice that there are three time scales in the problem: First is the interaction time scale $\tau_K = \frac{1}{K}$ which comes due to the inter-particle harmonic interaction. Second is the time scale τ_A due to the active nature of the particles. It is given by $\tau_A = \frac{1}{\gamma}$ for RTPs, $\tau_A = \frac{1}{\zeta}$ for AOUPs and $\tau_A = \frac{1}{D_{rot}}$ for ABPs. Third is the relaxation time scale $\tau_N = \frac{N^2}{K}$ due to the finite size of the ring. Later, we show that τ_N is the largest time scale that a particular Fourier mode will take to relax. Throughout this chapter, we consider $\tau_K \ll \tau_A \ll \tau_N$ as shown in Figure 6.2. Later, we illustrate that this order of time scales gives rise to interesting scaling behaviours of the correlation functions. The other case of $\tau_A \ll \tau_K \ll \tau_N$ only recovers the results of the Brownian motion with rescaled diffusion coefficient. Below, we use this order of τ_K, τ_A and τ_N to calculate various correlation functions for a chain of RTPs. We then perform this analysis for AOUPs and ABPs in the subsequent sections. We first summarise the main results of this chapter below.

6.2 Summary of the main results

Let us first summarise our main results on the variance $\langle x_\alpha^2(t)\rangle_c$ of the position of the tagged particle. We have schematically shown this in Figure 6.3. We obtain different scaling behaviours of the variance depending on where the observation time t lies. Recall that $\tau_K \ll \tau_A \ll \tau_N$. When $t \ll \tau_K$, then the tagged particle has not interacted with its neighbouring particles. We find that the variance for this case scales with time as $\langle x_\alpha^2(t)\rangle_c \sim t^b$, where the exponent b is same

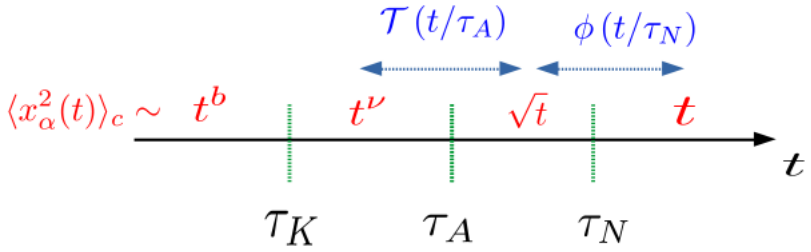

For RTP, $b = 2, \nu = 3/2$
For AOUP, $b = 3, \nu = 5/2$
For ABP, $b = 4, \nu = 7/2$ (x coordinate)
$b = 3, \nu = 5/2$ (y coordinate)

Figure 6.3: Summary of the main results on the variance $\langle x_\alpha^2(t)\rangle_c$ of the position of the tagged particle.

as the non-interacting case for all three models. On the other hand, when $\tau_K \ll t \ll \tau_A$, the tagged particle exhibits persistent motion and is also interacting with other particles. Here, we find a different growth behaviour of the variance as $\langle x_\alpha^2(t)\rangle_c \sim t^\nu$, where the value of ν depends on the model and is given in the figure. For $\tau_A \ll t \ll \tau_N$, the particle is indistinguishable from an interacting Brownian particle for all three models. In fact, we notice that the particle effectively performs the single-file diffusion at these time scales. Consequently, we recover the scaling behaviour $\langle x_\alpha^2(t)\rangle_c \sim \sqrt{t}$ (same as single-file diffusion) for all three models. Interestingly, we also analytically compute the scaling function $\mathcal{T}(t/\tau_A)$ (see Figure 6.3) that connects the scaling regime $\sim t^\nu$ with the single-file regime. The form of this scaling function depends on the model and is given in Eq. (6.37) for RTP, in Eq. (6.104) for AOUP and in Eqs. (6.136) and (6.137) for ABP. Finally for $t \gg \tau_N$, the tagged particle performs the normal diffusion and we obtain the diffusive scaling $\langle x_\alpha^2(t)\rangle_c \sim t$ for all three models. The associated scaling function $\phi(t/\tau_N)$ (see Figure 6.3) connecting the single-file regime and the diffusive regime is computed exactly and is given in Eq. (6.85). Analogous results are also obtained for the equal and unequal time correlation functions of the positions of two tagged particles. More precisely, we define the correlation function

$$\begin{aligned} C^1_{\alpha_1,\alpha_2}(t_1,t_2) &= \langle x_{\alpha_1}(t_1)x_{\alpha_2}(t_2)\rangle_c = \langle x_{\alpha_1}(t_1)x_{\alpha_2}(t_2)\rangle - \langle x_{\alpha_1}(t_1)\rangle\langle x_{\alpha_2}(t_2)\rangle, \\ C^2_{\alpha_1,\alpha_2}(t_1,t_2) &= \langle y_{\alpha_1}(t_1)y_{\alpha_2}(t_2)\rangle_c = \langle y_{\alpha_1}(t_1)y_{\alpha_2}(t_2)\rangle - \langle y_{\alpha_1}(t_1)\rangle\langle y_{\alpha_2}(t_2)\rangle. \end{aligned} \tag{6.11}$$

We emphasize that $\vec{r}_\alpha(t) = (x_\alpha(t), 0)$ for the RTPs and AOUPs, and $\vec{r}_\alpha(t) = (x_\alpha(t), y_\alpha(t))$ for the ABPs. Consequently, for the former two models, one has only the correlation $C^1_{\alpha_1,\alpha_2}(t_1,t_2)$,

while for ABPs, one has both $C^{1/2}_{\alpha_1,\alpha_2}(t_1,t_2)$. For the RTPs and AOUPs, we get

$$C^1_{\alpha,\alpha}(t,t) \propto t^{3/2}\ \mathcal{T}^{RT/OU}\left(\frac{t}{\tau_A}\right), \qquad \tau_K \ll t \ll \tau_N \tag{6.12}$$

$$C^1_{0,\beta}(t,t) \propto \begin{cases} t^{\nu}\ \Omega^{RT/OU}\left(\frac{\beta}{\sqrt{2Kt}}\right)\ ; & \tau_K \ll t \ll \tau_A \\ \sqrt{t}\ \mathcal{C}\left(\frac{\beta}{\sqrt{2Kt}}\right)\ ; & \tau_A \ll t \ll \tau_N, \end{cases} \tag{6.13}$$

$$C^1_{\alpha,\alpha}(t_1,t_2) \propto \begin{cases} t_1^{\nu}\ \mathcal{L}^{RT/OU}\left(\frac{t_2}{t_1}\right)\ ; & \tau_K \ll t_1 \ll \tau_A \\ \sqrt{t_1}\ \mathcal{M}\left(\frac{t_2}{t_1}\right)\ ; & \tau_A \ll t_1 \ll \tau_N \end{cases} \tag{6.14}$$

$$C^1_{\alpha_1,\alpha_2}(t_1,t_2) \propto \begin{cases} t_1^{\nu}\ \mathcal{P}^{RT/OU}\left(\frac{\beta}{\sqrt{2Kt_1}},\frac{t_2}{t_1}\right)\ ; & \tau_K \ll t_1 \ll \tau_A \\ \sqrt{t_1}\ \mathcal{Q}\left(\frac{\beta}{\sqrt{2Kt_1}},\frac{t_2}{t_1}\right)\ ; & \tau_A \ll t \ll \tau_N \end{cases} \tag{6.15}$$

where the value of ν is given in Figure 6.3 and $\mathcal{T},\ \Omega,\ \mathcal{C},\ \mathcal{L},\ \mathcal{M},\ \mathcal{P}$ and $\mathcal{Q}$ are the respective scaling functions. We provide the explicit expressions of these scaling functions in the respective sections where they are derived along with the proportionality constants. Similarly for the ABP, we get

$$C^p_{\alpha,\alpha}(t,t) \propto t^{3/2}\ \mathcal{T}^{AB}_p\left(\frac{t}{\tau_A}\right), \qquad \tau_K \ll t \ll \tau_N \tag{6.16}$$

$$C^p_{0,\beta}(t,t) \propto \begin{cases} t^{\nu}\ \Omega^{AB}_p\left(\frac{\beta}{\sqrt{2Kt}}\right)\ ; & \tau_K \ll t \ll \tau_A \\ \sqrt{t}\ \mathcal{C}\left(\frac{\beta}{\sqrt{2Kt}}\right)\ ; & \tau_A \ll t \ll \tau_N, \end{cases} \tag{6.17}$$

$$C^p_{\alpha,\alpha}(t_1,t_2) \propto \begin{cases} t_1^{\nu}\ \mathcal{L}^{AB}_p\left(\frac{t_2}{t_1}\right)\ ; & \tau_K \ll t_1 \ll \tau_A \\ \sqrt{t_1}\ \mathcal{M}\left(\frac{t_2}{t_1}\right)\ ; & \tau_A \ll t_1 \ll \tau_N \end{cases} \tag{6.18}$$

$$C^p_{\alpha_1,\alpha_2}(t_1,t_2) \propto \begin{cases} t_1^{\nu}\ \mathcal{P}^{AB}_p\left(\frac{\beta}{\sqrt{2Kt_1}},\frac{t_2}{t_1}\right)\ ; & \tau_K \ll t_1 \ll \tau_A \\ \sqrt{t_1}\ \mathcal{Q}\left(\frac{\beta}{\sqrt{2Kt_1}},\frac{t_2}{t_1}\right)\ ; & \tau_A \ll t \ll \tau_N \end{cases} \tag{6.19}$$

where $p = 1$ and 2 for x and y coordinates respectively. Again, the expressions of the scaling functions are provided later.

Previous results correspond to the $N \to \infty$ case for which $t \ll \tau_N$ since $\tau_N \to \infty$. These results get modified when $t \gg \tau_N$, i.e. for large but finite N. For this case, we find that the correlation function $C^p_{0,\beta}(t_1,t_2)$ for all three models takes the scaling form

$$C^p_{0,\beta}(t_1,t_2) \simeq \frac{2D_{eff}N}{K}\ \mathcal{W}\left(\frac{t_2}{t_1},\frac{\beta}{N},\frac{Kt_1}{N^2}\right), \quad t_1,t_2 \sim O(\tau_N) \tag{6.20}$$

where the scaling function $\mathcal{W}(t_r,z,y)$ is given in Eq. (6.82). Also, here D_{eff} is the effective

diffusion constants for the RTP ($D_{eff} = D_R = \frac{v_0^2}{2\gamma}$), AOUP ($D_{eff} = D_A = \frac{D}{\zeta^2}$) and ABP ($D_{eff} = D_{ABP} = \frac{v_A^2}{2D_{rot}}$) chains.

In what follows, we will rigorously derive these correlation functions. We first compute these quantities for RTP and then for AOUP and ABP in the subsequent sections.

6.3 Two-point correlation for RTP chain

We first calculate the equal time correlation function $\langle x_{\alpha_1}(t)x_{\alpha_2}(t)\rangle$ of the positions of the particles in a harmonic chain of RTPs. To this aim, we proceed to solve the Langevin equation (6.1) with $\vec{r}_\alpha(t) = (x_\alpha(t), 0)$ by taking its Fourier transform with respect to the index α. For a general function $g_\alpha(t)$, the Fourier transformation is defined as

$$g_\alpha(t) = \sum_{s=0}^{N-1} e^{\frac{2\pi i s}{N}\alpha}\ \bar{g}_s(t), \tag{6.21}$$

where $i^2 = -1$ and the inverse Fourier transformation as

$$\bar{g}_s(t) = \frac{1}{N}\sum_{\alpha=0}^{N-1} e^{-\frac{2\pi i s}{N}\alpha}\ g_\alpha(t). \tag{6.22}$$

Under Fourier transformation, Eqs. (6.1) become

$$\frac{d\bar{x}_s}{dt} = -a_s\bar{x}_s + \bar{F}_s^A(t)\ , \tag{6.23}$$

where we have used the notations

$$\bar{x}_s(t) = \frac{1}{N}\sum_{\alpha=0}^{N-1} e^{-\frac{2\pi i s}{N}\alpha}\ x_\alpha(t), \tag{6.24}$$

$$\bar{F}_s^A(t) = \frac{1}{N}\sum_{\alpha=0}^{N-1} e^{-\frac{2\pi i s}{N}\alpha}\ F_\alpha^A(t), \tag{6.25}$$

$$a_s = 4K\sin^2\left(\frac{\pi s}{N}\right). \tag{6.26}$$

Solving Eq. (6.23) for $\bar{x}_s(t)$, we get

$$\bar{x}_s(t) = e^{-a_s t}\ \bar{x}_s(0) + e^{-a_s t}\int_0^t d\tau\ e^{a_s\tau}\ \bar{F}_s^A(\tau). \tag{6.27}$$

Notice that $1/a_s$ here sets the decay time scale for the s-th mode. For fixed but large N, this time scale is of order $\sim O(N^2)$ with respect to the system size N. Later, we show that the

variance and the correlation functions exhibit different scaling behaviours depending on whether the observation time t is larger or smaller than the relaxation (decay) time scale τ_N.

From eQ. (6.27), the connected correlations turn out to be

$$\begin{aligned}\langle \bar{x}_s(t)\bar{x}^*_{s'}(t)\rangle_c &= \langle \bar{x}_s(t)\bar{x}^*_{s'}(t)\rangle - \langle \bar{x}_s(t)\rangle\langle \bar{x}^*_{s'}(t)\rangle \\ &= e^{-(a_s+a_{s'})t}\int_0^t d\tau_1\ d\tau_2\ e^{a_s\tau_1+a_{s'}\tau_2}\ \langle \bar{F}^A_s(\tau_1)\bar{F}^{A*}_{s'}(\tau_2)\rangle_c,\end{aligned} \tag{6.28}$$

where $\bar{x}^*_s(t)$ is the complex conjugate of $\bar{x}_s(t)$. Now, the noise $F^A_\alpha(t)$ for RTPs is just the telegraphic noise $\sigma_\alpha(t)$ whose exact correlation is given by Eq. (6.3). Using this equation to compute the correlation $\langle \bar{F}^A_s(\tau_1)\bar{F}^{A*}_{s'}(\tau_2)\rangle_c$ and plugging it in Eq. (6.28), we get

$$\langle \bar{x}_s(t)\bar{x}^*_{s'}(t)\rangle^{RTP}_c = \delta_{s,s'}\frac{v_0^2}{N}\ \mathcal{G}(2\gamma, a_s, t), \tag{6.29}$$

where the function $\mathcal{G}(u,w,t)$ is defined as

$$\mathcal{G}(u,w,t) = \frac{w\left[1+e^{-2wt}-2e^{-(u+w)t}\right]-u(1-e^{-2wt})}{w(w^2-u^2)}. \tag{6.30}$$

Since, our main aim is to calculate the two-point correlation $\langle x_{\alpha_1}(t)x_{\alpha_2}(t)\rangle_c$, we use the transformation in Eq. (6.24) to write

$$\langle x_{\alpha_1}(t)x_{\alpha_2}(t)\rangle_c = \sum_{s=0}^{N-1}\sum_{s'=0}^{N-1} e^{\frac{2\pi i s}{N}\alpha_1}e^{-\frac{2\pi i s'}{N}\alpha_2}\langle \bar{x}_s(t)\bar{x}^*_{s'}(t)\rangle_c. \tag{6.31}$$

Substituting the correlation $\langle \bar{x}_s(t)\bar{x}^*_{s'}(t)\rangle_c$ from Eq. (6.29) in this equation, we obtain the exact expression of the equal time correlation $\langle x_{\alpha_1}(t)x_{\alpha_2}(t)\rangle_c$ for all values of N. Below, we analyse this solution for $\alpha_1 = \alpha_2$ and $\alpha_1 \neq \alpha_2$ separately. We show that the correlations exhibit non-trivial scaling behaviours for $N \to \infty$ depending on where the observation time lies (see Figure 6.2).

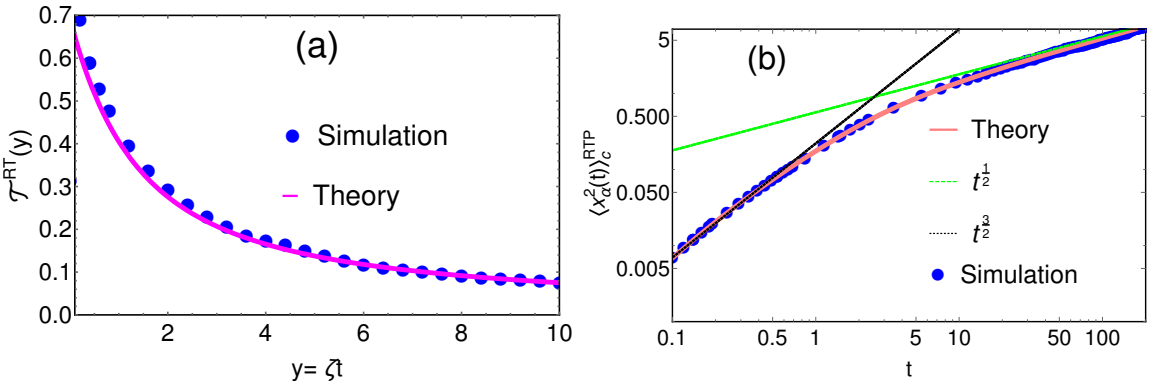

Figure 6.4: (a) Scaling function $\mathcal{T}^{RT}(y)$ in Eq. (6.37) for a chain of RTPs has been compared with the numerical simulations. (b) Asymptotic behaviour of $\langle x_\alpha^2(t)\rangle_c^{RTP}$ in the two regimes [as given in Eqs. (6.41)] has been numerically verified. For both plots, parameters chosen are $v_0 = 1,\ K = 2$, $\gamma = 0.5$ and $N = 100$ (for simulations).

6.3.1 Variance for RTP chain

Let us begin with the computation of the variance $\langle x_\alpha^2(t)\rangle_c^{RTP}$ for which we put $\alpha_1 = \alpha_2 = \alpha$ in Eq. (6.31). This gives

$$\begin{aligned}\langle x_\alpha^2(t)\rangle_c^{RTP} &= \langle x_\alpha^2(t)\rangle^{RTP} - \left(\langle x_\alpha(t)\rangle^{RTP}\right)^2 \\ &= \sum_{s=0}^{N-1} \langle |\bar{x}_s(t)|^2\rangle_c^{RTP}, \\ &= \frac{v_0^2}{N}\sum_{s=0}^{N-1} \mathcal{G}(2\gamma, a_s, t), \end{aligned} \tag{6.32}$$

where a_s and $\mathcal{G}(2\zeta, a_s, t)$ are given in Eqs. (6.26) and (6.30) respectively. Also, due to the translational symmetry of the problem, the expression of the variance is independent of the index α. We analyze it in the limit $N \to \infty$ for which we can change the summation over s in Eq. (6.32) to an integral as $\frac{1}{N}\sum_s \to \frac{1}{2\pi}\int_{-\pi}^{\pi} dq$ where $q = \frac{2\pi s}{N}$. The variance then reads

$$\langle x_\alpha^2(t)\rangle_c^{RTP} \simeq \frac{v_0^2}{2\pi}\int_{-\pi}^{\pi} dq\ \mathcal{G}\left(2\gamma, b_q, t\right), \tag{6.33}$$

$$\text{where}\quad b_q = 4K\sin^2(q/2). \tag{6.34}$$

As mentioned before, we are interested in $\tau_K \ll \tau_A$ (see Figure 6.2) with $\tau_A = \frac{1}{\gamma}$ for RTP (Note that $\tau_N \to \infty$ for $N \to \infty$). Let us now examine Eq. (6.33) in different temporal regimes.

For $t \ll \tau_K$, the observation time t is smaller than all time scales of the problem. This suggests us to directly take the small-t approximation of the function $\mathcal{G}\left(2\gamma, b_q, t\right)$ in Eq. (6.33). Following

the expression of $\mathcal{G}\left(2\gamma, b_q, t\right)$ in Eq. (6.30), one has $\mathcal{G}(2\gamma, b_q, t) \simeq t^2$ and inserting this in Eq. (6.33) gives

$$\langle x_\alpha^2(t)\rangle_c^{RTP} \simeq v_0^2 t^2, \qquad \text{for } t \ll \tau_K. \tag{6.35}$$

Since for small times, the particles do not feel the presence of the neighbouring particles, we reproduce the result for the non-interacting case where the RTPs move ballistically with speed v_0 [70]. Let us now analyze the variance in the other limit $t \gg \tau_K$. By plugging $\mathcal{G}\left(2\zeta, b_q, t\right)$ from Eq. (6.30) in Eq. (6.33), we find that $\langle x_\alpha^2(t)\rangle_c^{RTP}$ involves integrals of the form $\sim \int dq\ h(q)\ \exp\left[-Kt\sin^2(q/2)\right]$ where $h(q)$ is some function of q. In the limit $Kt \to \infty$, the leading contribution to these integrals will come from small values of q. This implies we can approximate $b_q \simeq Kq^2$ in Eq. (6.33). Using this approximation, we have calculated the variance for $t \gg \tau_K$ in appendix 8.14. Here, we quote only the final expression which obeys the scaling form

$$\langle x_\alpha^2(t)\rangle_c^{RTP} \simeq \frac{v_0^2 t^{\frac{3}{2}}}{\pi}\sqrt{\frac{2}{K}}\ \ \mathcal{T}^{RT}\left(\gamma t\right), \tag{6.36}$$

where the scaling function $\mathcal{T}^{RT}(y)$ is given by,

$$\mathcal{T}^{RT}(y) = \frac{1}{4}\int_{-\infty}^{\infty} dw\ \mathcal{G}\left(2y, \frac{w^2}{2}, 1\right), \qquad \text{for } t \gg \tau_K. \tag{6.37}$$

The function $\mathcal{G}\left(2y, \frac{w^2}{2}, 1\right)$ is given in Eq. (6.30). We have numerically verified this scaling function in Figure 6.4(a) and we see nice agreement of our analytic result with the numerics. To understand the asymptotic behaviour of the scaling function, we expand $\mathcal{G}\left(2y, \frac{w^2}{2}, 1\right)$ in Eq. (6.37) in different limits of y as follows:

$$\mathcal{T}^{RT}(y) \simeq \frac{2\sqrt{\pi}}{3}(2-\sqrt{2}) - \frac{4\sqrt{\pi}}{15}\left(8-5\sqrt{2}\right)y, \qquad \text{as } y \to 0, \tag{6.38}$$

$$\simeq \frac{\sqrt{\pi}}{2y} + O\left(\frac{1}{y^2}\right), \qquad \text{as } y \to \infty. \tag{6.39}$$

Plugging these asymptotic forms in Eq. (6.36), we find the simplified expression of $\langle x_\alpha^2(t)\rangle_c^{RTP}$ as

$$\langle x_\alpha^2(t)\rangle_c^{RTP} \simeq \frac{4(\sqrt{2}-1)}{3\sqrt{\pi K}} v_0^2 t^{\frac{3}{2}} + O\left(t^{5/2}\right), \qquad \text{for } t \ll \frac{1}{\gamma}, \tag{6.40}$$

$$\simeq \frac{v_0^2}{2\gamma}\sqrt{\frac{2t}{\pi K}} + O\left(t^{-1/2}\right), \qquad \text{for } t \gg \frac{1}{\gamma}. \tag{6.41}$$

Interestingly, we find that the variance exhibits a crossover behaviour from $t^{3/2}$ scaling for

$t \ll \frac{1}{\gamma}$ to $\sqrt{t}$ scaling for $t \gg \frac{1}{\gamma}$. Indeed, in simulations, we see two distinct scaling regimes of the variance as illustrated in Figure 6.4(b). These regimes are connected by the crossover function $\mathcal{T}^{RT}(y)$ given in Eq. (6.37). To understand these scaling behaviours physically, we recall that the typical fluctuations of $x_\alpha(t)$ for $t \gg \frac{1}{\gamma}$ are effectively described by that of the Brownian motion with diffusion coefficient $D_R = \frac{v_0^2}{2\gamma}$. Moreover, in simulations, we observe that the particles do not overtake other particles at these time scales. Hence, the motion of the tagged particle is effectively single-file diffusion for $t \gg \frac{1}{\gamma}$ which gives rise to the $\sim \sqrt{t}$ scaling of $\langle x_\alpha^2(t)\rangle_c^{RTP}$. On the other hand, for $t \ll \frac{1}{\gamma}$, the motion of the particle is highly persistent which in conjunction to the harmonic interaction leads to the $\sim t^{3/2}$ scaling. For a chain of RTPs, the $t^{3/2}$ behaviour for the variance was also obtained in [215] even though the crossover function was not obtained.

6.3.2 Covariance for RTP chain

We next calculate the equal time correlation function $\langle x_\alpha(t) x_{\alpha+\beta}(t)\rangle_c$ from Eq. (6.31). First note that due to the translational symmetry with respect to α, the correlation $\langle x_\alpha(t) x_{\alpha+\beta}(t)\rangle_c$ will be independent of α and we simply put $\alpha = 0$ without loss of generality. In Eq. (6.31), we get

$$\langle x_0(t) x_\beta(t)\rangle_c^{RTP} = \sum_{s,s'=0}^{N-1} e^{\frac{2\pi i s\beta}{N}} \langle \bar{x}_s(t) \bar{x}_{s'}^*(t)\rangle_c^{RTP}. \tag{6.42}$$

The correlation $\langle \bar{x}_s(t) \bar{x}_{s'}^*(t)\rangle_c^{RTP}$ is given in Eq. (6.29) and inserting this in Eq. (6.42), we find that the imaginary part of $\langle x_0(t) x_\beta(t)\rangle_c^{RTP}$ vanishes and we obtain

$$\langle x_0(t) x_\beta(t)\rangle_c^{RTP} = \frac{v_0^2}{N} \sum_{s=0}^{N-1} \cos\left(\frac{2\pi s\beta}{N}\right) \mathcal{G}(2\gamma, a_s, t). \tag{6.43}$$

As done for the variance, we again examine this equation in the limit $N \to \infty$ for which we change the summation in Eq. (6.43) by integral as $\frac{1}{N}\sum_s \to \frac{1}{2\pi}\int_{-\pi}^{\pi} dq$ with $q = \frac{2\pi s}{N}$. Eq. (6.43) then takes the form

$$\langle x_0(t) x_\beta(t)\rangle_c^{RTP} \simeq \frac{v_0^2}{2\pi} \int_{-\pi}^{\pi} dq \ \cos(q\beta) \ \mathcal{G}(2\gamma, b_q, t), \tag{6.44}$$

where $b_q = 4K \sin^2(q/2)$. As seen before, the variance $\langle x_0^2(t)\rangle_c^{RTP}$ shows interesting scaling behaviours depending on whether the observation time t is greater or smaller than τ_K. Here also, we study the correlation in Eq. (6.44) for $t \ll \tau_K$ and $t \gg \tau_K$ to reveal interesting scaling structures. Firstly for $t \ll \tau_K$, the motion of two particles being uncorrelated, we have

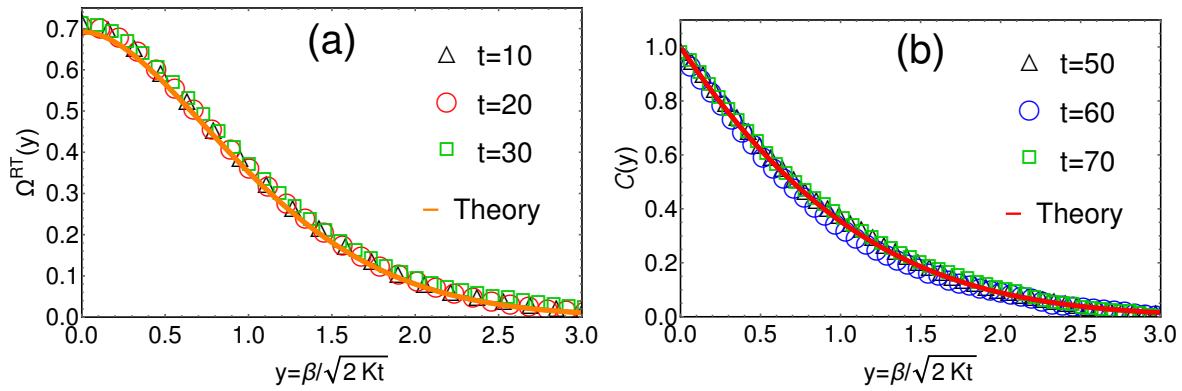

Figure 6.5: Scaling functions $\Omega^{RT}(y)$ and $\mathcal{C}(y)$ respectively in Eqs. (6.47) and (6.51) for the correlation $\langle x_0(t)x_\beta(t)\rangle_c^{RTP}$ are compared with the simulation data for three different observation times. Parameters chosen are (i) $K = 2,\ \gamma = 0.001$ and $v_0 = 1$ for left panel and (ii) $K = 2,\ \gamma = 2$ and $v_0 = 1$ for right panel. Simulation is conducted with $N = 200$ particles on a ring.

$\langle x_0(t)x_\beta(t)\rangle_c^{RTP} \simeq v_0^2 t^2\ \delta_{0,\beta}$. However, for $t \gg \tau_K$, we anticipate non-trivial correlation among the particles. To see this correlation, we proceed exactly same as in the case of variance. By plugging $\mathcal{G}(2\gamma, b_q, t)$ from Eq. (6.30) in Eq. (6.44), we see that $\langle x_0(t)x_\beta(t)\rangle_c^{RTP}$ has integrals like $\sim \int dq\ h(q)\ \exp\left[-Kt\sin^2(q/2)\right]$ which for $Kt \to \infty$ will be dominated by the small values of q. Performing approximations as for the variance, we get

$$\langle x_0(t)x_\beta(t)\rangle_c^{RTP} \simeq \frac{v_0^2}{4\pi}\sqrt{\frac{2t^3}{K}}\int_{-\infty}^{\infty} dw\ \cos\left(\frac{w\beta}{\sqrt{2Kt}}\right)\ \mathcal{G}\left(2\gamma t, \frac{w^2}{2}, 1\right). \tag{6.45}$$

Carrying out integral over w for general γt is difficult. However, one can perform this integral for different limits of γt. For example, for $\gamma t \to 0$, we approximate $\mathcal{G}\left(2\gamma t \to 0, \frac{w^2}{2}, 1\right) \simeq 4\left(\frac{1-e^{-\frac{w^2}{2}}}{w^2}\right)^2$ and perform the integration in Eq. (6.45) to find that $\langle x_0(t)x_\beta(t)\rangle_c^{RTP}$ obeys the scaling form

$$\langle x_0(t)x_\beta(t)\rangle_c^{RTP} \simeq \frac{v_0^2}{\pi}\sqrt{\frac{2t^3}{K}}\ \Omega^{RT}\left(\frac{\beta}{\sqrt{2Kt}}\right), \qquad \text{for } \tau_K \ll t \ll \frac{1}{\gamma}, \tag{6.46}$$

with the scaling function $\Omega^{RT}(y)$ given by

$$\begin{aligned}\Omega^{RT}(y) =& \frac{\sqrt{\pi}}{6}\left[2e^{-\frac{y^2}{4}}\left(4+y^2\right) - 2\sqrt{2}e^{-\frac{y^2}{2}}\left(2+y^2\right)\right.\\ &\left. -\sqrt{\pi}y(6+y^2)\ \text{Erfc}\left(\frac{y}{2}\right) + 2\sqrt{\pi}y(3+y^2)\ \text{Erfc}\left(\frac{y}{\sqrt{2}}\right)\right].\end{aligned} \tag{6.47}$$

In Figure 6.5(a), we have compared our analytic result with the numerical simulations for three different times in the range $\tau_K \ll t \ll \frac{1}{\gamma}$. For all t, we see that the simulation data matches

with Eq. (6.47). The asymptotic forms of the scaling function $\Omega^{RT}(y)$ are given by

$$\Omega^{RT}(y) \simeq \frac{2\sqrt{\pi}}{3}(2-\sqrt{2}) - \sqrt{\pi}\left(\sqrt{2}-1\right) y^2 + O(y^3), \qquad \text{as } y \to 0, \tag{6.48}$$

$$\simeq \left(\frac{2\sqrt{\pi}}{y^4} + O\left(y^{-6}\right)\right) e^{-\frac{y^2}{4}}, \qquad \text{as } y \to \infty, \tag{6.49}$$

and using them, we find that $\langle x_0(t)x_\beta(t)\rangle_c^{RTP}$ for large β has faster than exponential decay as $\sim \beta^{-4}\exp\left(-\beta^2/l_d^2\right)$ decay length given by $l_d = 2\sqrt{2Kt}$.

Let us now look at the correlation $\langle x_0(t)x_\beta(t)\rangle_c^{RTP}$ in Eq. (6.45) in the limit $\gamma t \to \infty$. Approximating $\mathcal{G}\left(2\gamma t \to \infty, \frac{w^2}{2}, 1\right) \simeq \frac{1-e^{-w^2}}{\gamma t w^2}$, we can now perform the integration over w in Eq. (6.45). We then get a different scaling form of $\langle x_0(t)x_\beta(t)\rangle_c^{RTP}$ as

$$\langle x_0(t)x_\beta(t)\rangle_c^{RTP} \simeq D_R\sqrt{\frac{2t}{\pi K}}\,\mathcal{C}\left(\frac{\beta}{\sqrt{2Kt}}\right), \qquad \text{for } t \gg \frac{1}{\gamma}, \tag{6.50}$$

where $D_R = \frac{v_0^2}{2\gamma}$ and the scaling function $\mathcal{C}(y)$ is given by

$$\mathcal{C}(y) = e^{-\frac{y^2}{4}} - \frac{\sqrt{\pi}}{2} y\ \text{Erfc}\left(\frac{y}{2}\right). \tag{6.51}$$

The same scaling form has also been obtained in a variety of other interacting systems like random average process [222–224] and symmetric exclusion process [225,226]. Here, we derive it in the simple setting of a harmonic chain of active particles. In Figure 6.5(b), we have compared $\mathcal{C}(y)$ with the numerical simulations for three different values of t and we see excellent agreement for all of them. From the following asymptotic forms of the scaling function $\mathcal{C}(y)$

$$\mathcal{C}(y) \simeq 1 - \frac{\sqrt{\pi}}{2} y, \qquad \text{as } y \to 0, \tag{6.52}$$

$$\simeq \left(\frac{2}{y^2} + O\left(y^{-4}\right)\right) e^{-\frac{y^2}{4}}, \qquad \text{as } y \to \infty, \tag{6.53}$$

we see that for large β and $t \gg 1/\gamma$, $\langle x_0(t)x_\beta(t)\rangle_c^{RTP}$ decays as $\sim \beta^{-2}\exp\left(-\beta^2/l_d^2\right)$ with the decay-length $l_d = 2\sqrt{2Kt}$. On the other hand, for $\beta \to 0$, Eq. (6.50) correctly reduces to the variance in Eq. (6.41).

6.3.3 Position autocorrelation for RTP chain

We now turn to the autocorrelation $\langle x_\alpha(t_1)x_\alpha(t_2)\rangle_c$ between the positions of the α-th particle at two different times. For simplicity, we take $t_1 \le t_2$ without any loss of generality. To proceed,

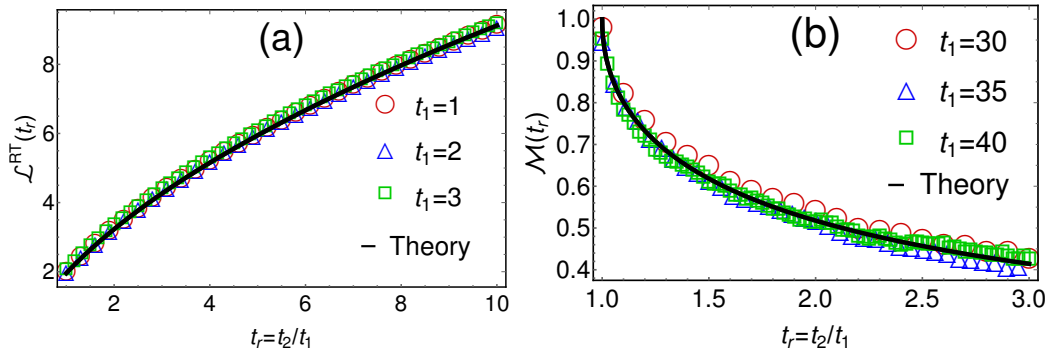

Figure 6.6: Scaling functions $\mathcal{L}^{RT}(t_r)$ and $\mathcal{M}(t_r)$ for the position autocorrelation in Eqs. (6.60) and (6.66) are compared with the numerical simulations for (a) $\gamma = 0.001$ and (b) $\gamma = 2$. For both panels, simulation is performed with $N = 200$, $K = 3$ and $v_0 = 1$.

we use the solution of $\bar{x}_s(t)$ in Eq. (6.27) to obtain the correlation $\langle \bar{x}_s(t_1)\bar{x}^*_{s'}(t_2)\rangle^{RTP}_c$ as

$$\langle \bar{x}_s(t_1)\bar{x}^*_{s'}(t_2)\rangle^{RTP}_c = \delta_{s,s'}\,\frac{v_0^2}{N}\mathcal{H}\left(2\gamma, a_s, t_1, t_2\right), \tag{6.54}$$

where a_s is given in Eq. (6.26) and the function $\mathcal{H}(u, w, t_1, t_2)$ is

$$\mathcal{H}(u,w,t_1,t_2) = -\frac{u}{w}\frac{e^{-w|t_1-t_2|}-e^{-w(t_1+t_2)}}{(w^2-u^2)} + \frac{e^{-u|t_1-t_2|}-e^{-(wt_1+ut_2)}}{(w^2-u^2)} - \frac{e^{-(ut_1+wt_2)}-e^{-w(t_1+t_2)}}{(w^2-u^2)}. \tag{6.55}$$

The autocorrelation $\langle x_\alpha(t_1)x_\alpha(t_2)\rangle^{RTP}_c$ can then be easily written in terms of $\langle \bar{x}_s(t_1)\bar{x}_{s'}(t_2)\rangle^{RTP}_c$ as

$$\langle x_\alpha(t_1)x_\alpha(t_2)\rangle^{RTP}_c = \sum_{s',s=0}^{N-1}\langle \bar{x}_s(t_1)\bar{x}^*_{s'}(t_2)\rangle^{RTP}_c, \tag{6.56}$$

$$= \frac{v_0^2}{N}\sum_{s=0}^{N-1}\mathcal{H}\left(2\gamma, a_s, t_1, t_2\right). \tag{6.57}$$

This equation provides the exact expression of the position autocorrelation valid for all values of N, t_1 and t_2. But to obtain non-trivial scaling behaviours, we again analyze $\langle x_\alpha(t_1)x_\alpha(t_2)\rangle^{RTP}_c$ in the limit $N \to \infty$. Changing the summation in Eq. (6.57) to integration as $\frac{1}{N}\sum_s \to \frac{1}{2\pi}\int_{-\pi}^{\pi} dq$ with $q = \frac{2\pi s}{N}$, we get

$$\langle x_\alpha(t_1)x_\alpha(t_2)\rangle^{RTP}_c \simeq \frac{v_0^2}{2\pi}\int_{-\pi}^{\pi} dq\ \mathcal{H}\left(2\gamma, b_q, t_1, t_2\right), \tag{6.58}$$

with $b_q = 4K\sin^2(q/2)$. As done in the previous two cases, we again examine this equation in various limits of t_1 and t_2 with respect to τ_K. For $t_1 \ll \tau_K$ and $t_2 \ll \tau_K$, the observation

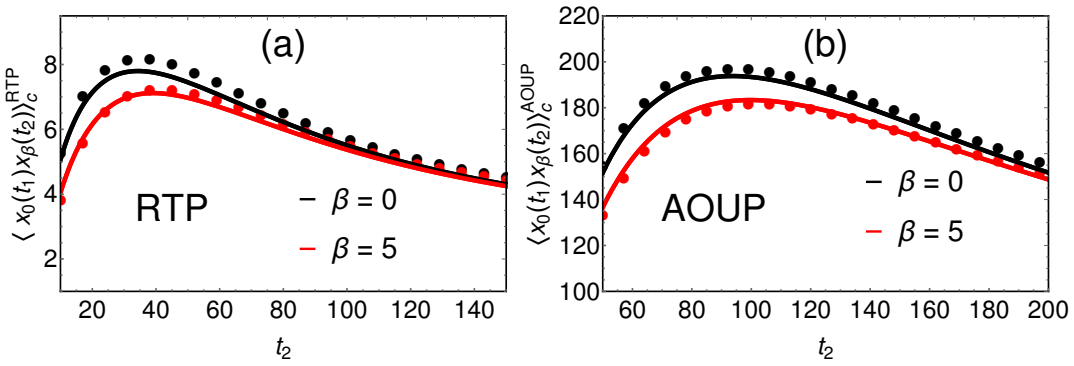

Figure 6.7: Illustration of the non-monotonic behaviour of $\langle x_0(t_1)x_\beta(t_2)\rangle_c$ for RTPs (left panel) and AOUPs (right panel). In both panels, solid curves represent the analytic results in Eqs. (6.74) and (6.100) and symbols are the simulation data. Values of parameters are (a) $K = 3,\ \gamma = 0.02,\ v_0 = 1,\ N = 200,\ t_1 = 10$ for left panel and (b) $D = 0.1,\ K = 2,\ \zeta = 0.02,\ N = 100,\ t_1 = 50$ for right panel.

times are smaller than all time scales present in the problem. This allows us to approximate $\mathcal{H}\left(2\gamma, b_q, t_1, t_2\right) \simeq t_1 t_2$ for both $t_1, t_2 \to 0$ using Eq. (6.55) and inserting this form in Eq. (6.58) gives $\langle x_\alpha(t_1)x_\alpha(t_2)\rangle_c^{RTP} = v_0^2 t_1 t_2$. Since the particles move ballistically and independently at this small time scale, we expect the autocorrelation to have this form.

For the other limit $t_1 \gg \tau_K,\ t_2 \gg \tau_K$ with fixed $\frac{t_2}{t_1}$, we perform similar approximations as for the variance and equal-time correlation function in the previous sections. Inserting $\mathcal{H}(2\gamma, b_q, t_1, t_2)$ from Eq. (6.55) in Eq. (6.58), we find that $\langle x_\alpha(t_1)x_\alpha(t_2)\rangle_c^{RTP}$ has terms like $\sim \int dq\ h(q)\ e^{-Kt\sin^2(q/2)}$ where $h(q)$ is some function of q. The predominant contribution to this integral for $Kt_1 \to \infty$ will come from the smaller values of q. Therefore, we approximate $b_q \simeq Kq^2$ and rewrite the autocorrelation in Eq. (6.58) as

$$\langle x_\alpha(t_1)x_\alpha(t_2)\rangle_c^{RTP} \simeq \frac{v_0^2}{2\pi}\sqrt{\frac{t_1^3}{K}}\int_{-\infty}^{\infty} dw\ \mathcal{H}\left(2\gamma t_1, w^2, 1, \frac{t_2}{t_1}\right), \qquad \text{for } t_1 \gg \tau_K. \tag{6.59}$$

We emphasize that this equation is derived assuming the ratio $\frac{t_2}{t_1}$ is fixed. Once again, it is analytically challenging to perform the integration over w in this equation. In this regard, we consider $\langle x_\alpha(t_1)x_\alpha(t_2)\rangle_c^{RTP}$ in different limits of γt_1 for which we can carry out the integration analytically.

For $\gamma t_1 \to 0$, we use $\mathcal{H}\left(2\gamma t_1 \to 0, w^2, 1, t_r\right) \simeq\ e^{-w^2(1+t_r)}\frac{(e^{t_r w^2}-1)(e^{w^2}-1)}{w^4}$ with $t_r = t_2/t_1$. Plugging this in Eq. (6.59), we get that $\langle x_\alpha(t_1)x_\alpha(t_2)\rangle_c^{RTP}$ has the scaling form

$$\langle x_\alpha(t_1)x_\alpha(t_2)\rangle_c^{RTP} \simeq \frac{v_0^2}{2\pi}\sqrt{\frac{t_1^3}{K}}\ \mathcal{L}^{RT}\left(\frac{t_2}{t_1}\right), \qquad \text{for } \tau_K \ll t_1 < t_2 \ll \frac{1}{\gamma}, \tag{6.60}$$

with the scaling function $\mathcal{L}^{RT}(t_r)$ defined as

$$\mathcal{L}^{RT}(t_r) = \frac{4\sqrt{\pi}}{3}\left[(1+t_r)^{3/2} - 1 - t_r^{3/2}\right]. \tag{6.61}$$

Figure 6.6(a) shows the numerical verification of $\mathcal{L}^{RT}(t_r)$ for different values of t_1. For each t_1, we plot $\mathcal{L}^{RT}(t_r)$ as a function of t_2. For all cases, we see that our analytic result is consistent with the simulations. Finally, by looking at the asymptotic forms of $\mathcal{L}^{RT}(t_r)$

$$\mathcal{L}^{RT}(t_r) \simeq \frac{8\sqrt{\pi}}{3}\left(\sqrt{2}-1\right) + 2\sqrt{\pi}\left(\sqrt{2}-1\right)(t_r - 1), \qquad \text{as } t_r \to 1, \tag{6.62}$$

$$\simeq 2\sqrt{\pi t_r} - \frac{4\sqrt{\pi}}{3}, \qquad \text{as } t_r \gg 1, \tag{6.63}$$

and substituting this in Eq. (6.60), we see a crossover of $\langle x_\alpha(t_1)x_\alpha(t_2)\rangle_c^{RTP}$ from $t_2^{3/2}$ to $\sqrt{t_2}$ as

$$\langle x_\alpha(t_1)x_\alpha(t_2)\rangle_c^{RTP} \simeq \frac{4(\sqrt{2}-1)}{3\sqrt{\pi K}} v_0^2\, t_1^{\frac{3}{2}} + O\left(t_2 - t_1\right), \qquad \text{for } t_2 \to t_1, \tag{6.64}$$

$$\simeq \frac{v_0^2 t_1}{\sqrt{\pi K}}\left(\sqrt{t_2} - \frac{2}{3}\sqrt{t_1}\right), \qquad \text{for } t_2 \gg t_1. \tag{6.65}$$

Quite remarkably, we see that when both t_1 and t_2 are smaller than $\tau_A = \frac{1}{\gamma}$, the autocorrelation increases with increasing time. This growth of $\langle x_\alpha(t_1)x_\alpha(t_2)\rangle_c^{RTP}$ with t_2 (for a fixed t_1) can also be seen in Figure 6.6(a).

Let us now look at the other limit $\gamma t_1 \to \infty$ of $\langle x_\alpha(t_1)x_\alpha(t_2)\rangle_c^{RTP}$ for which we can explicitly perform the integration in Eq. (6.59). Using the approximation $\mathcal{H}\left(2\gamma t_1 \to \infty, w^2, 1, t_r\right) \simeq \frac{1}{2\gamma t_1}\frac{e^{-w^2(t_r-1)} - e^{-w^2(t_r+1)}}{w^2}$ in Eq. (6.59), we obtain the scaling form

$$\langle x_\alpha(t_1)x_\alpha(t_2)\rangle_c^{RTP} \simeq D_R\sqrt{\frac{2t_1}{\pi K}}\,\mathcal{M}\left(\frac{t_2}{t_1}\right), \quad \text{for } t_2 > t_1 \gg \frac{1}{\gamma}, \tag{6.66}$$

where $D_R = \frac{v_0^2}{2\gamma}$ and the scaling function $\mathcal{M}(t_r)$ is given by

$$\mathcal{M}(t_r) = \frac{1}{\sqrt{2}}\left[\sqrt{t_r+1} - \sqrt{t_r-1}\right]. \tag{6.67}$$

Interestingly, by using the macroscopic fluctuation theory, this form of the position autocorrelation was also obtained for the single-file diffusion [132]. In Figure 6.6(b), we have plotted this scaling function and also compared it with the simulation for different values of times. The simulation data for all times converge to our analytical result. For $t_1 \ll 1/\gamma$, $t_2 \ll 1/\gamma$ but fixed t_1/t_2, we saw that the autocorrelation increases as a function of t_2 for a fixed t_1. To check the same for $t_1 \gg 1/\gamma$, $t_2 \gg 1/\gamma$, we look at the asymptotic forms of $\mathcal{M}(t_r)$ with respect to t_r.

These forms read

$$\mathcal{M}(t_r) \simeq 1 - \sqrt{\frac{t_r - 1}{2}}, \qquad \text{as } t_r \to 1, \tag{6.68}$$

$$\simeq \frac{1}{\sqrt{2t_r}} + \frac{1}{8\sqrt{2}\, t_r^{\frac{5}{2}}}, \qquad \text{as } t_r \gg 1, \tag{6.69}$$

from which we find the following asymptotic behaviours of $\langle x_\alpha(t_1)x_\alpha(t_2)\rangle_c^{RTP}$:

$$\langle x_\alpha(t_1)x_\alpha(t_2)\rangle_c^{RTP} \simeq D_R\sqrt{\frac{2t_1}{\pi K}} + O\left(\sqrt{t_2 - t_1}\right), \qquad \text{for } t_2 \to t_1, \tag{6.70}$$

$$\simeq \frac{D_R t_1}{\sqrt{\pi K t_2}} + O\left(\frac{t_1^3}{t_2^{5/2}}\right), \qquad \text{for } t_2 \gg t_1. \tag{6.71}$$

Unlike in the $t_1 \ll 1/\gamma$, $t_2 \ll 1/\gamma$ case, we find that $\langle x_\alpha(t_1)x_\alpha(t_2)\rangle_c^{RTP}$ for $t_1 \gg 1/\gamma$, $t_2 \gg 1/\gamma$ decreases with the increasing time [see Figure 6.6(b)]. This implies that $\langle x_\alpha(t_1)x_\alpha(t_2)\rangle_c^{RTP}$ has an overall non-monotonic dependence on t_2. For example, in Figure 6.7(a) ($\beta = 0$), we see that the autocorrelation first increases with time, attains a maximum value and then starts decreasing again for larger times. For small times $t_2 \ll \tau_K$, particles perform independent ballistic runs. As we increase t_2, the particles interact with the surrounding particles because of which their motions get correlated. However at large times, the particles are effectively like Brownian particles whose motions become less correlated as we increase time. Overall, we get a non-monotonic dependence. As we show later that this non-monotonic dependence of autocorrelation is seen for general $\langle x_0(t_1)x_\beta(t_2)\rangle_c^{RTP}$ with $\beta \neq 0$ and for other models of active particles also.

6.3.4 Unequal Time Position Correlations For RTP chain

We now compute the unequal time correlations $\langle x_\alpha(t_1)x_{\alpha+\beta}(t_2)\rangle_c^{RTP}$ for the chain of RTPs. Once again we take $t_1 \leq t_2$ and set $\alpha = 0$ since the correlation $\langle x_\alpha(t_1)x_{\alpha+\beta}(t_2)\rangle_c^{RTP}$ is independent of α due to the translational symmetry in α. Using the correlation $\langle \bar{x}_{s'}(t_1)\bar{x}_s^*(t_2)\rangle_c^{RTP}$ in Eq. (6.54), we can write the unequal time correlation in the positions of two different particles as

$$\langle x_0(t_1)x_\beta(t_2)\rangle_c^{RTP} = \sum_{s',s=0}^{N-1} e^{-\frac{2\pi i s\beta}{N}} \langle \bar{x}_{s'}(t_1)\bar{x}_s^*(t_2)\rangle_c^{RTP}, \tag{6.72}$$

$$= \frac{v_0^2}{N}\sum_{s=0}^{N-1} \cos\left(\frac{2\pi s\beta}{N}\right) \mathcal{H}\left(2\gamma, a_s, t_1, t_2\right). \tag{6.73}$$

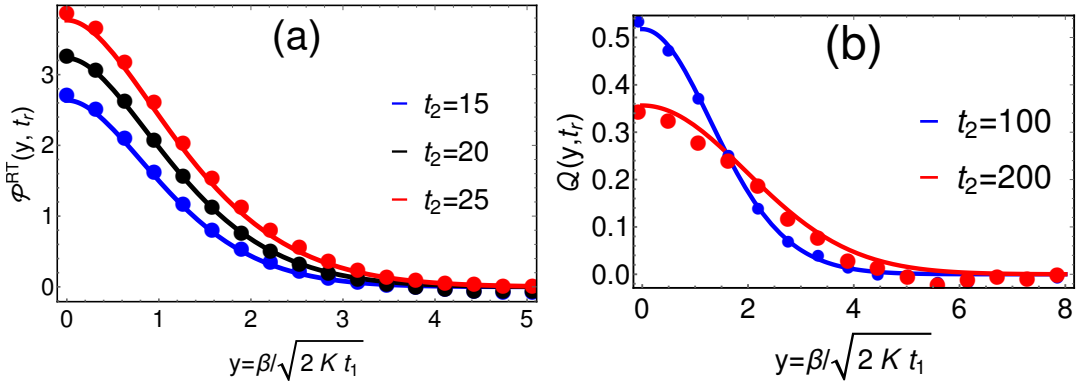

Figure 6.8: Scaling functions $\mathcal{P}^{RT}(y,t_r)$ and $\mathcal{Q}(y,t_r)$ for the unequal time correlation function $\langle x_0(t_1)x_\beta(t_2)\rangle_c^{RTP}$ of RTPs in Eqs. (6.76) and (6.78) are compared with the numerical simulations for (a) $t_1 = 10,\ \gamma = 0.001,\ N = 200$ and (b) $t_1 = 50,\ \gamma = 2,\ N = 500$. Common parameters for both plots are $v_0 = 1,\ K = 2$.

In the limit $N \to \infty$, this expression takes the form

$$\langle x_0(t_1)x_\beta(t_2)\rangle_c^{RTP} \simeq \frac{v_0^2}{2\pi}\int_{-\pi}^{\pi} dq\ \cos(q\beta)\ \mathcal{H}\left(2\gamma, b_q, t_1, t_2\right), \tag{6.74}$$

where $b_q = 4K\sin(q/2)$ and $\mathcal{H}\left(2\gamma, a_s, t_1, t_2\right)$ given in Eq. (6.55). Once again, we will compute this correlation for $t_1 \ll \tau_K$ and $t_1 \gg \tau_K$ keeping the ratio $\frac{t_2}{t_1}$ fixed. For $t_1 \ll \tau_K$, particles move independently and ballistically and the correlation takes the form $\langle x_0(t_1)x_\beta(t_2)\rangle_c^{RTP} \simeq v_0^2 t_1 t_2 \delta_{\beta,0}$. This can be easily proved by using the approximate form of $\mathcal{H}\left(2\gamma, a_s, t_1, t_2\right)$ for small t_1 and t_2 and performing the integration over q as done for the autocorrelation.

For the other limit $t_1 \gg \tau_K$, we take, as before, the small-q approximation of Eq. (6.74) and replace $b_q \simeq Kq^2$. Then the correlation can be rewritten as

$$\langle x_0(t_1)x_\beta(t_2)\rangle_c^{RTP} \simeq \frac{v_0^2}{2\pi}\sqrt{\frac{t_1^3}{K}}\int_{-\infty}^{\infty} dw\ \cos\left(\frac{w\beta}{\sqrt{Kt_1}}\right)\ \mathcal{H}\left(2\gamma t_1, w^2, 1, \frac{t_2}{t_1}\right), \quad \text{for } t_1 \gg \tau_K. \tag{6.75}$$

Once again we find that performing the integration over w is analytically difficult for general γt. But we can carry it out for different limits of γt. For example, for $\gamma t_1 \to 0$ with fixed $t_r = t_2/t_1$, we have $\mathcal{H}\left(2\zeta t_1, w^2, 1, \frac{t_2}{t_1}\right) \simeq e^{-w^2(1+t_r)}\frac{(e^{t_r w^2}-1)(e^{w^2}-1)}{w^4}$. Inserting this in Eq. (6.75) and performing the integration over w, we find that the correlation $\langle x_0(t_1)x_\beta(t_2)\rangle_c^{RTP}$ has the scaling form

$$\langle x_0(t_1)x_\beta(t_2)\rangle_c^{RTP} \simeq \frac{v_0^2}{2\pi}\sqrt{\frac{t_1^3}{K}}\ \mathcal{P}^{RT}\left(\frac{\beta}{\sqrt{2Kt_1}}, \frac{t_2}{t_1}\right), \quad \text{for } t_1 < t_2 \ll \frac{1}{\gamma}, \tag{6.76}$$

where the scaling function $\mathcal{P}^{RT}(y,t_r)$ is given by,

$$\mathcal{P}^{RT}(y,t_r) = \frac{\sqrt{\pi}}{3}\Bigg[2\sqrt{1+t_r}(2+2t_r+y^2)e^{-\frac{y^2}{2(1+t_r)}} - 2(2+y^2)e^{-\frac{y^2}{2}} - 2\sqrt{t_r}(2t_r+y^2)e^{-\frac{y^2}{2t_r}} + \sqrt{2\pi}(3+y^2)y\ \text{Erfc}\left(\frac{y}{\sqrt{2}}\right) + \sqrt{2\pi}(3t_r+y^2)y\ \text{Erfc}\left(\frac{y}{\sqrt{2t_r}}\right) - \sqrt{2\pi}(3+3t_r+y^2)y\ \text{Erfc}\left(\frac{y}{\sqrt{2(1+t_r)}}\right)\Bigg]. \tag{6.77}$$

In Figure 6.8(a), we have compared this scaling function with the numerics for three different values of t_r. For each t_r, we plot it as a function of β. We find excellent agreement between numerics and analytics in all cases. Analysing $\mathcal{P}^{RT}(y,t_r)$ further, we first observe that for $y \to 0$, we correctly reproduce the result for the autocorrelation in Eq. (6.60) as $\mathcal{P}^{RT}(y \to 0, t_r) = \mathcal{L}^{RT}(t_r)$. Similarly, for large β and fixed t_r, we see that $\langle x_0(t_1)x_\beta(t_2)\rangle_c$ decays as $\sim \beta^{-4}\exp\left(-\beta^2/\hat{l_d}^2\right)$ with the decay-length $\hat{l_d} = 2\sqrt{K(t_1+t_2)}$. Finally for $t_r = 1$, one gets $P^{RT}(y, t_r \to 1) = 2\sqrt{2}\Omega^{RT}(y)$ with $\Omega^{RT}(y)$ given in Eq. (6.47). Then it is easy to show that $\langle x_0(t_1)x_\beta(t_2)\rangle_c$ in Eq. (6.76) converges to the equal time corrrelation $\langle x_0(t)x_\beta(t)\rangle_c$ in Eq. (6.46).

Let us now consider the other limit $\gamma t_1 \to \infty$ in Eq. (6.75) for which we can perform the integration over w explicitly. Using the approximation $\mathcal{H}\left(2\gamma t_1 \to \infty, w^2, 1, \frac{t_2}{t_1}\right) \simeq \frac{e^{-w^2(t_r-1)} - e^{-w^2(t_r+1)}}{w^2}$ in this equation yields that $\langle x_0(t_1)x_\beta(t_2)\rangle_c^{RTP}$ obeys the scaling form

$$\langle x_0(t_1)x_\beta(t_2)\rangle_c^{RTP} \simeq D_R\sqrt{\frac{2t_1}{\pi K}}\ \mathcal{Q}\left(\frac{\beta}{\sqrt{2Kt_1}}, \frac{t_2}{t_1}\right), \qquad \text{for } t_1 \gg \frac{1}{\gamma}, \tag{6.78}$$

where $D_R = \frac{v_0^2}{2\gamma}$ and the scaling function $\mathcal{Q}(y,t_r)$ is given by

$$\mathcal{Q}(y,t_r) = \frac{1}{\sqrt{2}}e^{-\frac{y^2}{2(1+t_r)}}\left[\sqrt{t_r+1} - \sqrt{t_r-1}e^{-\frac{y^2}{(t_r^2-1)}}\right] + \frac{\sqrt{\pi}}{2}y\left[\text{Erf}\left(\frac{y}{\sqrt{2(t_r+1)}}\right) - \text{Erf}\left(\frac{y}{\sqrt{2(t_r-1)}}\right)\right]. \tag{6.79}$$

Figure 6.8(b) shows the comparison of our analytic result with the simulations. Excellent match between them validates our result in Eq. (6.79). Just like $t_1 \ll \tau_A$, $t_2 \ll \tau_A$ case, here also, it is straightforward to check that $\mathcal{Q}(y,t_r)$ reduces to appropriate scaling functions for $t_r = 1$ and $y = 0$. Also, for large β, the correlation decays as $\langle x_0(t_1)x_\beta(t_2)\rangle_c \sim \beta^{-2}\exp\left(-\beta^2/\hat{l_d}^2\right)$ with the decay-length $\hat{l_d} = 2\sqrt{K(t_1+t_2)}$

Another interesting point to note is that for a given β and t_1, we find that $\langle x_0(t_1)x_\beta(t_2)\rangle_c^{RTP}$ changes non-monotonically with t_2 where it initially increases with t_2, attains its maximum value and then decreases again with the further increase in t_2. Similar behaviour was also observed for

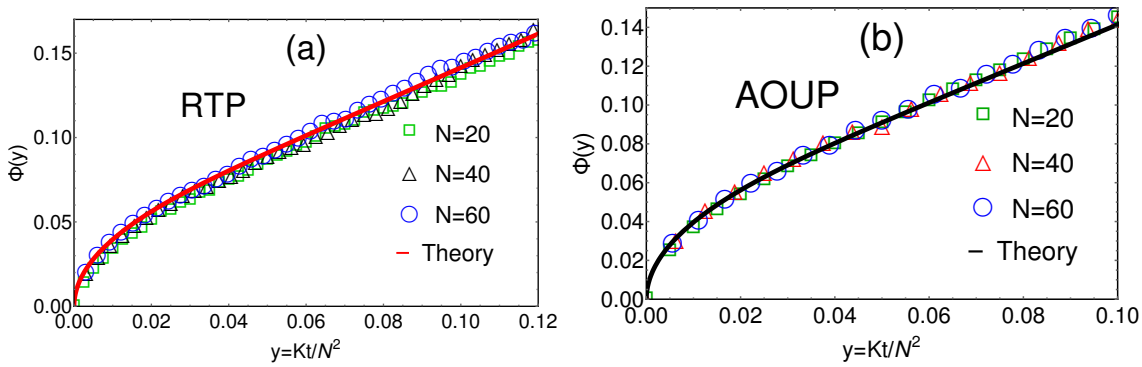

Figure 6.9: Scaling function $\Phi(y)$ in Eq. (6.85) for the variance $\langle x_\alpha^2(t)\rangle_c$ for large but finite N. Symbols are the simulation data for RTPs in the left panel and AOUPs in the right panel. We have chosen (a) $v_0=\sqrt{2},\ \gamma=1,\ K=2$ and (b) $D=0.6,\ \zeta=1,\ K=2$

the position autocorrelation ($\beta=0$) in the previous section. This non-monotonic dependence is illustrated in Figure 6.7(a) for different β. Physically, this behaviour can be understood by following the same reasoning as for the autocorrelation [see discussion below Eq. (6.71)].

6.3.5 Two-point correlation in RTP chain for large but finite N

Up to this point, we calculated the variance and correlation functions for $N\to\infty$ (equivalently $\tau_N\to\infty$) and found various scaling forms depending on where the observation time lies. Here we compute these quantities for large but finite N such that the relaxation time scale τ_N is finite. For this case, we consider the exact expression of $\langle x_0(t_1)x_\beta(t_2)\rangle_c^{RTP}$ in Eq. (6.73) and insert $\mathcal{H}\left(2\zeta,a_s,t_1,t_2\right)$ from Eq. (6.55) in this equation. After some straightforward algebraic simplifications for large N, we find

$$\begin{aligned}\langle x_0(t_1)x_\beta(t_2)\rangle_c^{RTP} &\simeq \frac{2D_Rt_1}{N}\\ &+\frac{D_RN}{2\pi^2K}\sum_{s=1}^{\infty}\cos\left(\frac{2\pi s\beta}{N}\right)\frac{e^{-\frac{4K\pi^2s^2}{N^2}(t_2-t_1)}+e^{-\frac{4K\pi^2s^2}{N^2}(t_2+t_1)}}{s^2}+O\left(\frac{1}{N}\right),\end{aligned}\tag{6.80}$$

where recall that $D_R=v_0^2/2\gamma$. Note that the first term in the right hand side can be order $\sim N$ (same as the second term) when t_1 is of order N^2. Therefore, we have retained it in the expression of $\langle x_0(t_1)x_\beta(t_2)\rangle_c^{RTP}$. Finally the correlation in Eq. (6.80) satisfies the scaling form

$$\langle x_0(t_1)x_\beta(t_2)\rangle_c^{RTP}\simeq\frac{2D_RN}{K}\,\mathcal{W}\left(\frac{t_2}{t_1},\frac{\beta}{N},\frac{Kt_1}{N^2}\right),\tag{6.81}$$

where the scaling function $\mathcal{W}(t_r, z, y)$ is

$$\mathcal{W}(t_r, z, y) = y + \frac{1}{2\pi^2} \sum_{s=1}^{\infty} \cos(2\pi s z) \, \frac{\sinh\left(4\pi^2 s^2 y\right)}{s^2} e^{-4\pi^2 s^2 t_r y}. \tag{6.82}$$

For large $y \to \infty$ keeping t_r fixed, the first term on the right hand side of this equation dominates and we get $\mathcal{W}(t_r, z, y) \simeq y$. This gives

$$\langle x_0(t_1) x_\beta(t_2) \rangle_c^{RTP} \simeq \frac{2D_R t_1}{N}, \qquad \text{for } Kt_1 \gg N^2. \tag{6.83}$$

On the other hand, for $Kt_1 \ll N^2$, $Kt_2 \ll N^2$ with fixed t_2/t_1, the summation in Eq. (6.82) can be recasted in the form of an integral performing which results in $\langle x_0(t_1) x_\beta(t_2) \rangle_c^{RTP}$ in Eq. (6.78). In what follows, we will use Eqs. (6.81) and (6.82) to compute the variance, covariance and autocorrelations for large but finite N.

6.3.5.1 Variance

Let us first compute the variance for which we put $\beta = 0$ and $t_1 = t_2 = t$ in Eqs. (6.81) and (6.82) and get

$$\langle x_\alpha^2(t) \rangle_c^{RTP} \simeq \frac{2D_R N}{K} \, \Phi\left(\frac{Kt}{N^2}\right), \tag{6.84}$$

with the scaling function $\Phi(y)$ defined as

$$\Phi(y) = y + \frac{1}{4\pi^2} \sum_{s=1}^{\infty} \frac{1 - e^{-8\pi^2 s^2 y}}{s^2}. \tag{6.85}$$

We have compared this scaling function with the simulations in Figure 6.9(a) for different values of N. We find an excellent agreement for all cases. To get different scaling behaviours of the variance, we look at the asymptotic forms of $\Phi(y)$ in different limits of y. For $y \to \infty$, the first term in Eq. (6.85) dominates to result in $\Phi(y \to \infty) \simeq y$. On the other hand, for $y \to 0$, the second term gives the dominant contribution to yield $\Phi(y \to 0) \sim \sqrt{y}$. Hence, we get the following asymptotic expressions for $\Phi(y)$:

$$\Phi(y) \simeq \sqrt{\frac{y}{2\pi}}, \qquad \text{as } y \to 0, \tag{6.86}$$

$$\simeq y + \frac{1}{24}, \qquad \text{as } y \to \infty. \tag{6.87}$$

Plugging these forms in Eq. (6.84), we obtain

$$\langle x_\alpha^2(t)\rangle_c^{RTP} \simeq D_R\sqrt{\frac{2t}{\pi K}}, \qquad \text{for } t \ll \frac{N^2}{K}, \tag{6.88}$$

$$\simeq \frac{2D_R}{N}t + O\left(t^0\right) \ , \qquad \text{for } t \gg \frac{N^2}{K}. \tag{6.89}$$

Therefore, the variance $\langle x_\alpha^2(t)\rangle_c^{RTP}$ has a crossover from $\sim \sqrt{t}$ scaling to $\sim t$ scaling and this crossover takes place at a time scale $t \sim \mathcal{O}\left(N^2\right)$. Since at this time scale, the motion of the RTP is indistinguishable from the Brownian motion, the scaling relation in Eq. (6.84) is valid for the harmonic chain of Brownian particles in a one dimensional ring.

6.3.5.2 Covariance

For the covariance, we replace $t_1 = t_2 = t$ in Eq. (6.81) and obtain the scaling form

$$\langle x_0(t)x_\beta(t)\rangle_c^{RTP} \simeq \frac{2D_R N}{K}\ \Psi\left(\frac{\beta}{N}, \frac{Kt}{N^2}\right), \tag{6.90}$$

where the scaling function $\Psi(z, y)$ is given by

$$\Psi(z, y) = y + \frac{1}{4\pi^2}\sum_{s=1}^{\infty}\cos\left(2\pi s z\right)\frac{1 - e^{-8\pi^2 s^2 y}}{s^2}. \tag{6.91}$$

For large y, we saw before that $\Psi(z, y) \simeq y$. Following Eq. (6.90), it then follows

$$\langle x_0(t)x_\beta(t)\rangle_c^{RTP} \simeq \frac{2D_R t}{N}, \qquad \text{for } Kt \gg N^2. \tag{6.92}$$

At this time scale $Kt \gg N^2$, the tagged particle has interacted with all other particles and consequently we get β independence of the covariance. On the other hand, for $Kt \ll N^2$ which corresponds to $y \to 0$ in Eq. (6.91), we can neglect the first term in the right hand side of this equation. Changing the summation over s in the second term to an integration and performing this intergration, we correctly reproduce the scaling results for $\langle x_0(t)x_\beta(t)\rangle_c^{RTP}$ in Eq. (6.50) for $t \gg \frac{1}{\gamma}$. Finally, we reiterate that the scaling results derived in this section remain valid also for the harmonic chain of the Brownian particles.

6.3.5.3 Autocorrelation

To get the autocorrelation, we put $\beta = 0$ in Eq. (6.81) and get the scaling form

$$\langle x_\alpha(t_1)x_\alpha(t_2)\rangle_c^{RTP} \simeq \frac{2D_R N}{K}\,\mathcal{R}\left(\frac{t_2}{t_1}, \frac{Kt_1}{N^2}\right), \tag{6.93}$$

where the scaling function $\mathcal{R}(t_r, z)$ is

$$\mathcal{R}(t_r, z) = z + \frac{1}{2\pi^2}\sum_{s=1}^{\infty}\frac{\sinh\left(4\pi^2 s^2 z\right)}{s^2}e^{-4\pi^2 s^2 t_r z}. \tag{6.94}$$

For $t_2 \to t_1$, this scaling form correctly reduces to that of the variance in Eq. (6.85). Also, for $Kt_1 \gg N^2$ but fixed t_2/t_1, following the same steps as for the covariance, we get

$$\langle x_\alpha(t_1)x_\alpha(t_2)\rangle_c^{RTP} \simeq \frac{2D_R t_1}{N}, \qquad \text{for } Kt_1 \gg N^2 \tag{6.95}$$

whereas for $Kt_1 \ll N^2$ and t_2/t_1 fixed, we reproduce the scaling result in Eqs. (6.66) and (6.67) for $t_1 \gg 1/\gamma$ and $t_2 \gg 1/\gamma$.

6.4 Variance, covariance and two-point correlation for AOUP chain

For a chain of RTPs, we saw that the correlations and flucuations of the positions of the tagged particles exhibit non-trivial scaling forms depending on the temporal regime that we are looking. We here devote this section to the study of the correlations in a chain AOUPs. For this, we turn to the solution of $\bar{x}_s(t)$ in Eq. (6.27) and insert $F_\alpha^{AOUP}(t)$ from Eq. (6.4) in this solution. Then the unequal time correlation for the Fourier variables $\bar{x}_s(t)$ as

$$\langle \bar{x}_s(t_1)\bar{x}^*_{s'}(t_2)\rangle_c^{AOUP} = \delta_{s,s'}\frac{D}{\zeta N}\,\mathcal{H}_1\left(\zeta, a_s, t_1, t_2\right), \tag{6.96}$$

where $t_1 \le t_2$ and a_s is given in Eq. (6.26). Also, $\mathcal{H}_1(u, w, t_1, t_2)$ is given in terms of $\mathcal{H}(u, w, t_1, t_2)$ in Eq. (6.55) as

$$\mathcal{H}_1(u, w, t_1, t_2) = \mathcal{H}(u, w, t_1, t_2) - \frac{\left(e^{-wt_1} - e^{-ut_1}\right)\left(e^{-wt_2} - e^{-ut_2}\right)}{(w-u)^2}. \tag{6.97}$$

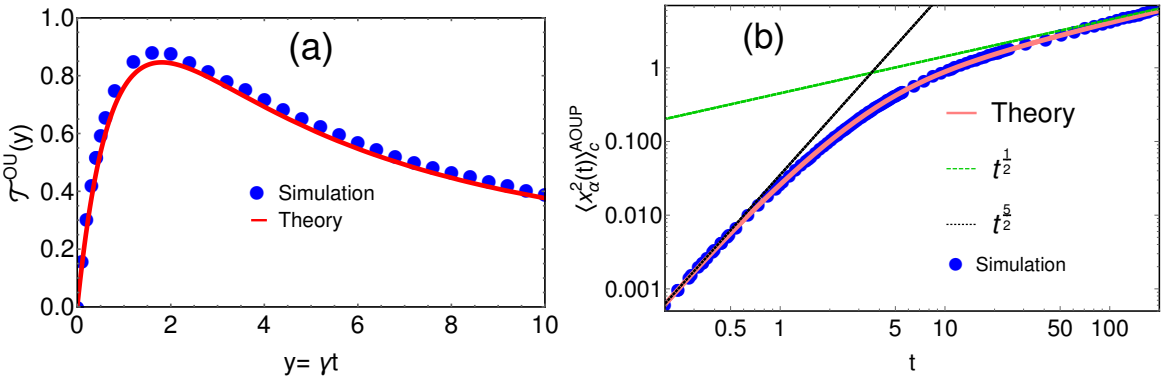

Figure 6.10: (a) Scaling function $\mathcal{T}^{OU}(y)$ in Eq. (6.104) for AOUPs is compared with the numerical simulation. (b) Illustration of different scaling regimes of $\langle x_\alpha^2(t)\rangle_c^{AOUP}$ for $\tau_k \ll t \ll \tau_A$ and $\tau_k \ll \tau_A \ll t$ [see Eqs. (6.107)]. For both plots, we have chosen $K = 2,\ \zeta = 0.5,\ D = 0.2$ and $N = 100$

We now use the inverse Fourier transformation to write the correlation function $\langle x_0(t_1)x_\beta(t_2)\rangle_c^{AOUP}$ in terms of $\langle \bar{x}_s(t_1)\bar{x}^*_{s'}(t_2)\rangle_c^{AOUP}$ in Eq. (6.96) as

$$\langle x_0(t_1)x_\beta(t_2)\rangle_c^{AOUP} = \sum_{s,s'=0}^{N-1} e^{-\frac{2i\pi\beta s}{N}} \langle \bar{x}_s(t_1)\bar{x}_{s'}(t_2)\rangle_c^{AOUP}, \tag{6.98}$$

$$= \frac{D}{\zeta N}\sum_{s=0}^{N-1} \cos\left(\frac{2\pi s\beta}{N}\right) \mathcal{H}_1\left(\zeta, a_s, t_1, t_2\right). \tag{6.99}$$

As done for the RTPs, we analyse this equation in the limit $N \to \infty$ to demonstrate various scaling behaviours of $\langle x_0(t_1)x_\beta(t_2)\rangle_c^{AOUP}$. For $N \to \infty$, we replace the summation in Eq. (6.99) by integral as $\frac{1}{N}\sum_s \to \frac{1}{2\pi}\int_{-\pi}^{\pi} dq$ where $q = \frac{2\pi s}{N}$. The two-point correlation then becomes

$$\langle x_0(t_1)x_\beta(t_2)\rangle_c^{AOUP} \simeq \frac{D}{2\pi\zeta}\int_{-\pi}^{\pi} dq \cos\left(q\beta\right)\ \mathcal{H}_1\left(\zeta, b_q, t_1, t_2\right), \tag{6.100}$$

where $b_q = 4K\sin^2\left(q/2\right)$. Once again, we will examine this expression for (i) $t_1 \ll \tau_k,\ t_2 \ll \tau_K$ and (ii) $t_1 \gg \tau_K,\ t_2 \gg \tau_K$ keeping the ratio $\frac{t_2}{t_1}$ fixed.

6.4.1 Case I: $t_1 \ll \tau_K,\ t_2 \ll \tau_K$

We first look at $\langle x_0(t_1)x_\beta(t_2)\rangle_c^{AOUP}$ for $t_1 \ll \tau_K$, $t_2 \ll \tau_K$ keeping the ratio $\frac{t_2}{t_1}$ fixed. Since τ_K is the smallest time scale in the problem, we see that t_1 and t_2 are smaller than all other time scales. Therefore, we expand $\langle x_0(t_1)x_\beta(t_2)\rangle_c^{AOUP}$ in Eq. (6.100) for $t_1 \to 0$ and $t_2 \to 0$. In these

limits, we approximate $\mathcal{H}_1(m,n,t_1,t_2) \simeq m t_1^2 \left(t_2 - \frac{t_1}{3}\right)$ and plugging this in Eq. (6.100), we find

$$\langle x_0(t_1) x_\beta(t_2)\rangle_c^{AOUP} \simeq D t_1^2 \left(t_2 - \frac{t_1}{3}\right) \delta_{\beta,0}, \qquad \text{as } t_1 \leq t_2 \ll \tau_K. \tag{6.101}$$

At these small time scales, particles move independently which leads to zero correlation between them. Also, for $\beta = 0$ and $t_1 = t_2 = t$, the variance $\langle x_0^2(t)\rangle_c^{AOUP} \simeq \frac{2D}{3} t^3$ simply represents the variance of a single AOUP.

6.4.2 Case II: $t_1 \gg \tau_K,\ t_2 \gg \tau_K$

Let us now consider $\langle x_0(t_1) x_\beta(t_2)\rangle_c^{AOUP}$ in the other limit where $t_1 \gg \tau_K$ and $t_2 \gg \tau_K$ keeping t_2/t_1 fixed. For this limit, we perform similar algebraic manipulations in Eq. (6.100) as done for the RTP [see discussion before Eq. (6.75)] to show that

$$\langle x_0(t_1) x_\beta(t_2)\rangle_c^{AOUP} \simeq \frac{D}{2\pi\zeta} \sqrt{\frac{t_1^3}{K}} \int_{-\infty}^{\infty} dw \cos\left(\frac{w\beta}{\sqrt{K t_1}}\right) \mathcal{H}_1\left(\zeta t_1, w^2, 1, \frac{t_2}{t_1}\right). \tag{6.102}$$

In the following, we will use this expression to calculate the variance, covariance and autocorrelation of the positions of tagged particles in a chain of AOUPs.

6.4.2.1 Variance

We first look at the variance $\langle x_0^2(t)\rangle_c^{AOUP}$ for which we put $\beta = 0$ and $t_1 = t_2 = t$ in Eq. (6.102). This leads to the scaling form

$$\langle x_0^2(t)\rangle_c^{AOUP} \simeq \frac{D t^{\frac{3}{2}}}{2\pi\zeta\sqrt{K}}\, \mathcal{T}^{OU}(\zeta t), \qquad \text{for } t \gg \tau_K, \tag{6.103}$$

with the scaling function $\mathcal{T}^{OU}(y)$ is given by

$$\mathcal{T}^{OU}(y) = \int_{-\infty}^{\infty} dw\ \mathcal{H}_1\left(y, w^2, 1, 1\right). \tag{6.104}$$

Figure 6.10(a) presents a comparison of the scaling function with the numerical simulation. Our analytic result is completely consistent with the simulation data. As we saw for the RTPs, the variance $\langle x_0^2(t)\rangle_c^{RTP}$ exhibit different scaling behaviours in different limits of t/τ_A. Recall that $\tau_A = \zeta^{-1}$ for AOUPs. To decipher these scaling behaviours for AOUPs, we look at the

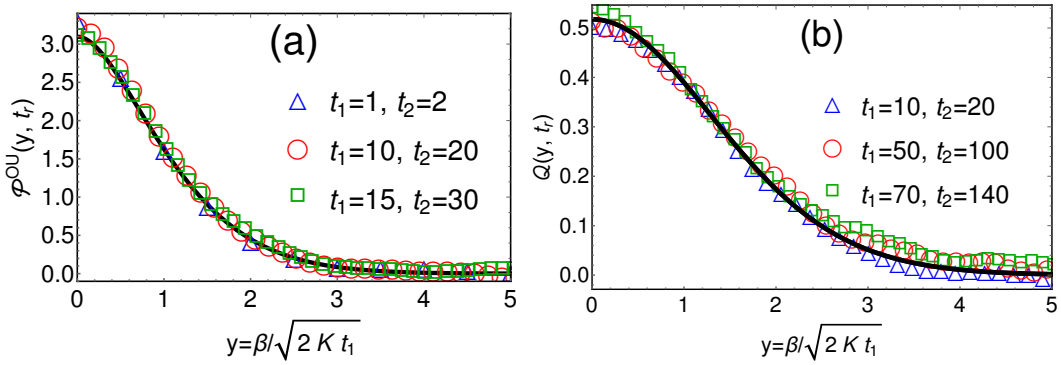

Figure 6.11: Scaling functions $\mathcal{P}^{OU}(y, t_r)$ and $\mathcal{Q}(y, t_r)$ in Eqs. (6.109) and (6.114) associated with $\langle x_0(t_1)x_\beta(t_2)\rangle_c^{AOUP}$ for $t_1 \ll 1/\zeta,\ t_2 \ll 1/\zeta$ and $t_1 \gg 1/\zeta,\ t_2 \gg 1/\zeta$ respectively have been compared with the numerical simulations. We have chosen (a) $D = 0.2$, $K = 2$, $\zeta = 0.001$ and $N = 100$ for left panel and (b) $D = 0.2$, $K = 2$, $\zeta = 1$ and $N = 200$ for right panel.

asymptotic forms of $\mathcal{T}^{OU}(y)$ for different y. By direct expansion, we get

$$\begin{aligned}\mathcal{T}^{OU}(y) &\simeq \frac{32\sqrt{\pi}}{15}\left(\sqrt{2}-1\right)y - \frac{32\sqrt{\pi}}{105}\left(8\sqrt{2}-9\right)y^2, \qquad \text{as } y \to 0,\\ &\simeq \frac{2\sqrt{2\pi}}{y} + O(y^{-2}), \qquad\qquad\qquad\qquad \text{as } y \to \infty. \end{aligned} \tag{6.105}$$

which then gives the crossover of $\langle x_0^2(t)\rangle_c^{AOUP}$ from $t^{\frac{5}{2}}$ to $\sqrt{t}$ at $t \sim \frac{1}{\zeta}$ as

$$\langle x_0^2(t)\rangle_c^{AOUP} \simeq \frac{16(\sqrt{2}-1)D}{15\sqrt{\pi K}}t^{\frac{5}{2}} + O\left(t^{\frac{7}{2}}\right), \qquad \text{for } t \ll \frac{1}{\zeta}, \tag{6.106}$$

$$\simeq \frac{D}{\zeta^2}\sqrt{\frac{2t}{\pi K}} + O\left(t^{-\frac{1}{2}}\right), \qquad \text{for } t \gg \frac{1}{\zeta}. \tag{6.107}$$

Interestingly, we find that the variance scales with time as $\langle x_0^2(t)\rangle_c^{AOUP} \sim t^{\frac{5}{2}}$ when time is much smaller than the activity time scale. Recall that the corresponding scaling for the RTP was $\langle x_0^2(t)\rangle_c^{RTP} \sim t^{\frac{3}{2}}$ in Eq. (6.40). Due to the inter-particle harmonic interaction, the motion of the tagged particle gets cagged. As a result of this caging effect, the scaling of the variance changes from $\sim t^3$ (non-interacting) to $\sim t^{\frac{5}{2}}$. On the other hand, for $t \gg 1/\zeta$, the motion is effectively like the single-file diffusion (as seen for RTPs) which leads to the $\sim \sqrt{t}$ scaling of the variance. In Figure 6.10(b), we have numerically illustrated this crossover behaviour along with the crossover function $\mathcal{T}^{OU}(\zeta t)$ that connects these two scaling regimes.

6.4.2.2 Covariance and unequal time correlations for $t_1 \ll \tau_A,\ t_2 \ll \tau_A$:

Drawing intuition from our study on RTPs, here also, we expect the correlation $\langle x_0(t_1)x_\beta(t_2)\rangle_c^{AOUP}$ obtained in Eq. (6.102) to possess different scaling forms for (i) $t_1 \ll \tau_A,\ t_2 \ll \tau_A$ and (ii)

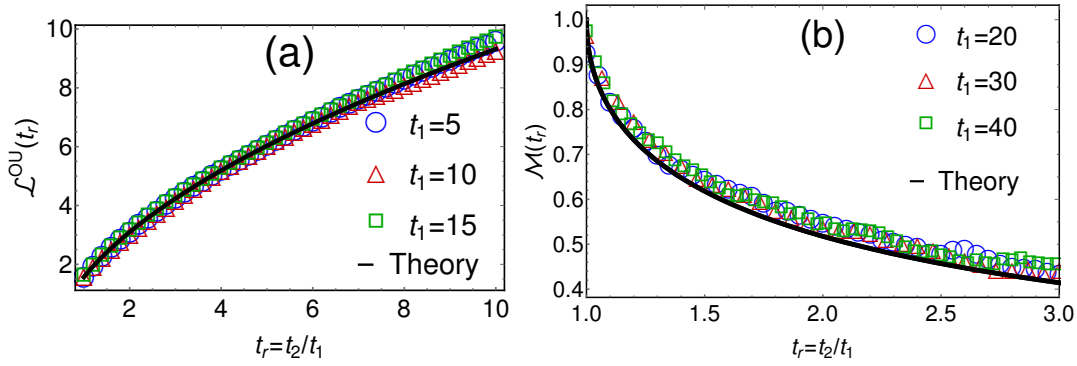

Figure 6.12: Scaling functions $\mathcal{L}^{OU}(t_r)$ and $\mathcal{M}(t_r)$ for the autocorrelation $\langle x_\alpha(t_1)x_\alpha(t_2)\rangle_c^{AOUP}$ in Eqs. (6.111) and (6.115) have been compared with the numerics. We have chosen (a) $D = 0.2$, $K = 2$, $\zeta = 0.001$ and $N = 100$ for left panel and (b) $D = 0.2$, $K = 2$, $\zeta = 1$ and $N = 200$ for right panel.

$t_1 \gg \tau_A,\ t_2 \gg \tau_A$. We consider case (i) in this section followed by a discussion on case (ii) in the next section.

For $\zeta t_1 \to 0$ with fixed $t_r = t_2/t_1$, we use the definition of $\mathcal{H}_1(\gamma t_1, w^2, 1, t_r)$ in Eq. (6.102) to expand $\mathcal{H}_1(\zeta t_1, w^2, 1, t_r) \simeq \frac{\zeta t_1}{w^6}\left[-2 + 2e^{-w^2} - e^{-(t_r+1)w^2} + 2e^{-t_r w^2} - e^{-(t_r-1)w^2} + 2w^2\right]$. Substituting this form in Eq. (6.102) and performing the integration over w, we find that $\langle x_0(t_1)x_\beta(t_2)\rangle_c^{AOUP}$ has the scaling form

$$\langle x_0(t_1)x_\beta(t_2)\rangle_c^{AOUP} \simeq \frac{D}{2\pi}\sqrt{\frac{t_1^5}{K}}\,\mathcal{P}^{OU}\left(\frac{\beta}{\sqrt{2Kt_1}}, \frac{t_2}{t_1}\right), \qquad \text{for } t_1 \le t_2 \ll \frac{1}{\zeta}, \tag{6.108}$$

with the scaling function $\mathcal{P}^{OU}(y, t_r)$ given by

$$\begin{aligned}
\mathcal{P}^{OU}(y,\ t_r) = \frac{\sqrt{\pi}}{30}\Bigg[&2\sqrt{1+t_r}\left(8+8t_r^2+9y^2+y^4+t_r(16+9y^2)\right)e^{-\frac{y^2}{2(t_r+1)}} - 30\sqrt{2\pi}y\,\mathrm{Erf}\left(\frac{y}{\sqrt{2}}\right)\\
&- 2(t_r-1)^{\frac{3}{2}}\left(7t_r-7+y^2\right)e^{-\frac{y^2}{2(t_r-1)}} - 4\left(8+9y^2+y^4\right)e^{-\frac{y^2}{2}} - 4\sqrt{t_r}\left(8t_r^2+9t_r y^2+y^4\right)e^{-\frac{y^2}{2t_r}}\\
&+\left(15+15t_r^2-10y^2+y^4+10t_r(-3+y^2)\right)\left\{2\sqrt{t_r-1}e^{-\frac{y^2}{2(t_r-1)}} + \sqrt{2\pi}y\,\mathrm{Erf}\left(\frac{y}{\sqrt{2(t_r-1)}}\right)\right\}\\
&+2\sqrt{2\pi}y^3\left(10+y^2\right)\mathrm{Erfc}\left(\frac{y}{\sqrt{2}}\right) - 2\sqrt{2\pi}y\left(15t_r^2+10t_r y^2+y^4\right)\mathrm{Erf}\left(\frac{y}{\sqrt{2t_r}}\right)\\
&+\sqrt{2\pi}y\left(15+15t_r^2+10y^2+y^4+10t_r(3+y^2)\right)\mathrm{Erf}\left(\frac{y}{\sqrt{2(t_r+1)}}\right)\Bigg].
\end{aligned} \tag{6.109}$$

In Figure 6.11(a), we have compared the scaling function $\mathcal{P}^{OU}(y, t_r)$ with the numerical simulations for three different sets of t_1 and t_2 but with constant $t_r = \frac{t_2}{t_1}$. For all cases, simulation data converge with Eq. (6.109). By expanding $\mathcal{P}^{OU}(y, t_r)$, we find that the correlation $\langle x_0(t_1)x_\beta(t_2)\rangle_c^{AOUP}$ in Eq. (6.108) for large β decays as $\sim \beta^{-6}\exp\left(\beta^2/\hat{l}_d^2\right)$ with decay length

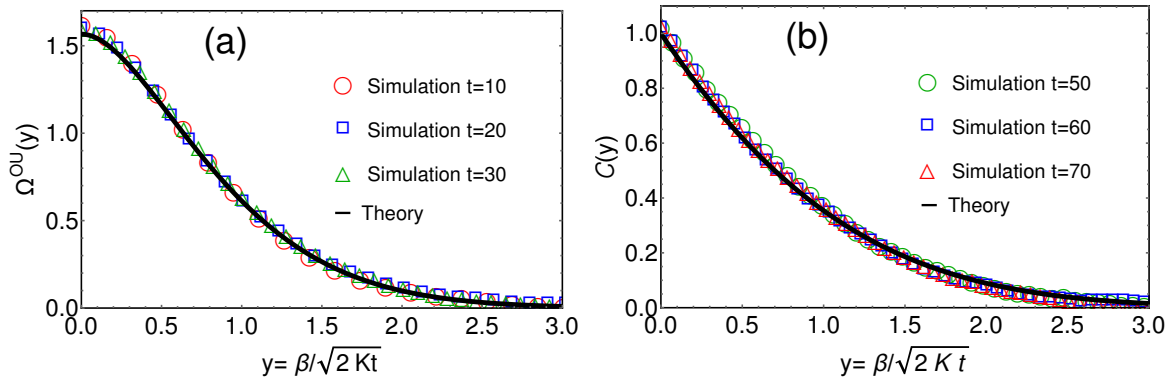

Figure 6.13: Numerical verification of the scaling function $\Omega^{OU}(y)$ in Eq. (6.113) and $\mathcal{C}(y)$ in Eq. (6.51) for the covariance $\langle x_0(t)x_\beta(t)\rangle_c^{AOUP}$. Parameters chosen are (a) $K = 2,\ \zeta = 0.00,$ $D = 0.5$ and $N = 150$ and (b) $K = 2,\ \gamma = 2,\ D = 1.7$ and $N = 150$.

$\hat{l}_d = 2\sqrt{K(t_1+t_2)}$. On the other hand, for $\beta = 0$, we get the position autocorrelation

$$\langle x_0(t_1)x_0(t_2)\rangle_c^{AOUP} \simeq \frac{D}{2\pi}\sqrt{\frac{t_1^5}{K}}\,\mathcal{L}^{OU}\left(\frac{t_2}{t_1}\right), \qquad \text{for } t_1 \le t_2 \ll \frac{1}{\zeta}, \tag{6.110}$$

with the scaling function $\mathcal{L}^{OU}(t_r) = \mathcal{P}^{OU}(y=0,t_r)$ given as

$$\mathcal{L}^{OU}(t_r) = \frac{8\sqrt{\pi}}{15}\left[(t_r+1)^{5/2} + (t_r-1)^{5/2} - 2(1+t_r^{5/2})\right]. \tag{6.111}$$

Numerical verification of this scaling function is shown in Figure 6.12(a) for different values of t_1. Finally, we look at the covariance $\langle x_0(t)x_\beta(t)\rangle_c^{AOUP}$ which is obtained by putting $t_1 = t_2 = t$ in Eq. (6.108). We find that the covariance satisfies the scaling

$$\langle x_0(t)x_\beta(t)\rangle_c^{AOUP} \simeq \frac{D\ t^{\frac{5}{2}}}{2\pi\sqrt{K}}\,\Omega^{OU}\left(\frac{\beta}{\sqrt{2Kt}}\right), \qquad \text{for } t \ll \frac{1}{\zeta}, \tag{6.112}$$

where the scaling function $\Omega^{OU}(y)$ can simply be written in terms of $\mathcal{P}^{OU}(y,t_r)$ in Eq. (6.109) as

$$\Omega^{OU}(y) = \mathcal{P}^{OU}(y,t_r=1). \tag{6.113}$$

Notice that this scaling function is different than the same obtained for the RTPs in Eq. (6.47). We have plotted the scaling function $\Omega^{OU}(y)$ in Figure 6.13(a) and also compared it with the numerical simulations for three different times. For each time, we observe excellent match of the numerics with the analytics. We end this section by noting that the covariance for large β decays as $\langle x_0(t)x_\beta(t)\rangle_c^{AOUP} \sim \beta^{-6}\exp\left(\beta^2/l_d^2\right)$ with decay length $l_d = 2\sqrt{K(t_1+t_2)}$ which is different than that of the RTPs where we saw $\langle x_0(t)x_\beta(t)\rangle_c^{RTP} \sim \beta^{-4}\exp\left(\beta^2/l_d^2\right)$.

6.4.2.3 Covariance and unequal time correlations for $t_1 \gg \tau_A,\ t_2 \gg \tau_A$:

We will now consider the correlation $\langle x_0(t_1)x_\beta(t_2)\rangle_c^{AOUP}$ in Eq. (6.102) in the other limit where the observation times t_1 and t_2 are greater than the activity time scale $\tau_A = 1/\zeta$. In the limit $\gamma t_1 \to \infty$ but fixed t_r, we can approximate the function $\mathcal{H}_1(\gamma t_1, w^2, 1, t_r)$ in Eq. (6.97) as $\mathcal{H}_1(\gamma t_1, w^2, 1, t_r) \simeq \frac{1}{\gamma t_1 w^2}\left(e^{-(t_r-1)w^2} - e^{-(t_r+1)w^2}\right)$ and plug it in Eq. (6.102) to yield the scaling form

$$\langle x_0(t_1)x_\beta(t_2)\rangle_c^{AOUP} \simeq D_A\sqrt{\frac{2t_1}{\pi K}}\ \mathcal{Q}\left(\frac{\beta}{\sqrt{2Kt_1}}, \frac{t_2}{t_1}\right), \qquad \text{for } \frac{1}{\gamma} \ll t_1 \le t_2, \tag{6.114}$$

where $D_A = \frac{D}{\zeta^2}$ and the scaling function $\mathcal{Q}(y, t_r)$ is given in Eq. (6.79). For AOUPs also, we obtain same result as for the RTPs in Eq. (6.78) since both models are indistinguishable from the Brownian motion in this time scale. In Figure 6.11(b), we have compared this scaling function with the same obtained from the simulation of AOUPs. We perform this comparison for three sets of t_1 and t_2 and we observe nice agreement for all of them. One can use $\langle x_0(t_1)x_\beta(t_2)\rangle_c^{AOUP}$ in Eq. (6.114) suitably to obtain the following scaling relation for the autocorrelation and covariance:

$$\langle x_0(t_1)x_0(t_2)\rangle_c^{AOUP} \simeq D_A\sqrt{\frac{2t_1}{\pi K}}\ \mathcal{M}\left(\frac{t_2}{t_1}\right), \qquad \text{for } \tau_A \ll t_1 \le t_2, \tag{6.115}$$

$$\langle x_0(t)x_\beta(t)\rangle_c^{AOUP} \simeq D_A\sqrt{\frac{2t}{\pi K}}\ \mathcal{C}\left(\frac{\beta}{\sqrt{2Kt}}\right), \qquad \text{for } t \gg \tau_A, \tag{6.116}$$

where the scaling functions $\mathcal{C}(y)$ and $\mathcal{M}(t_r)$ are given in Eqs. (6.51) and (6.67) respectively. These scaling functions are numerically illustrated in Figures 6.12(b) and 6.13(b) where we find excellent agreement between our analytic result and the simulations.

6.4.3 Large but finite N

We now look at the two-point correlation function $\langle x_0(t_1)x_\beta(t_2)\rangle_c^{AOUP}$ for AOUPs when N is large but finite. This means that the relaxation time scale $\tau_N \sim O(N^2)$ is now finite. For finite N, one needs to examine the exact expression of $\langle x_0(t_1)x_\beta(t_2)\rangle_c^{AOUP}$ Eq. (6.99). However, since we are looking at the time scales much larger than the activity time scale τ_A, we expect the two-point correlations for AOUP and RTP to be exactly same. Consequently, we get

$$\langle x_0(t_1)x_\beta(t_2)\rangle_c^{AOUP} \simeq \frac{2D_A N}{K}\ \mathcal{W}\left(\frac{t_2}{t_1}, \frac{\beta}{N}, \frac{Kt_1}{N^2}\right), \tag{6.117}$$

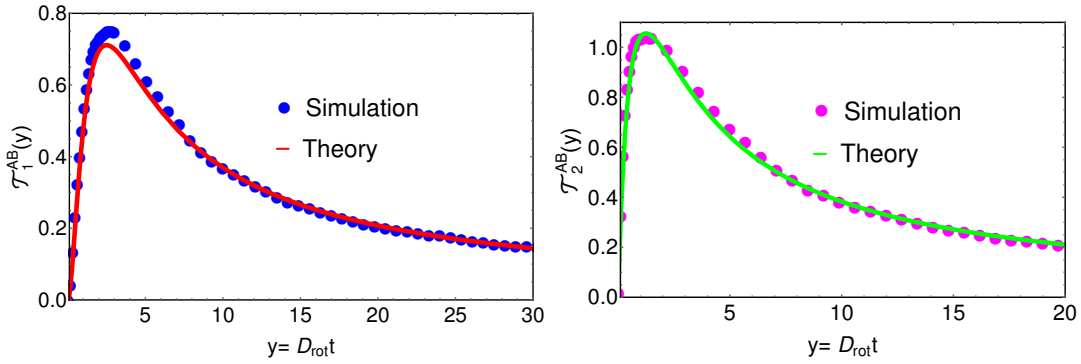

Figure 6.14: Scaling functions $\mathcal{T}_1^{AB}(y)$ and $\mathcal{T}_2^{AB}(y)$ in Eqs. (6.136) and (6.137) associated with the variance $\langle x_\alpha^2(t)\rangle_c^{ABP}$ and $\langle y_\alpha^2(t)\rangle_c^{ABP}$ have been compared with the numerical simulations for $K = 2,\ D_{rot} = 0.5,\ v_A = 1$ and $N = 100$.

where the scaling function $\mathcal{W}(t_r, z, y)$ is given in Eq. (6.82). From Eq. (6.117), it is easy to read the variance, covariance and autocorrelation as

$$\langle x_0(t_1)x_0(t_2)\rangle_c^{AOUP} \simeq \frac{2D_A N}{K}\ \mathcal{R}\left(\frac{t_2}{t_1}, \frac{Kt_1}{N^2}\right), \tag{6.118}$$

$$\langle x_0(t)x_\beta(t)\rangle_c^{AOUP} \simeq \frac{2D_A N}{K}\ \Psi\left(\frac{\beta}{N}, \frac{Kt}{N^2}\right), \tag{6.119}$$

$$\langle x_0^2(t)\rangle_c^{AOUP} \simeq \frac{2D_A N}{K}\Phi\left(\frac{Kt}{N^2}\right), \tag{6.120}$$

with the scaling functions $\Phi(y)$, $\Psi(z, y)$ and $\mathcal{R}(t_r, z)$ given respectively in Eqs. (6.85), (6.91) and (6.94). In Figure 6.9(b), we have shown a comparison of the scaling function $\Phi(y)$ with the numerical simulations for three different values of N. We see nice agreement for all cases.

6.5 Variance, covariance and two-point correlation for ABP chain

We now consider the third model of active particles called active Brownian particle and study the two-point correlation function for N active Brownian particles with nearest-neighbour harmonic interaction. We re-emphasize that this model is considered in two dimensions with $\vec{r}_\alpha(t) = (x_\alpha(t), y_\alpha(t))$ denoting the position of the α-th particle. Denoting its Fourier transformation with respect to α by $\vec{\tilde{r}}_s(t)$, we can rewrite the Langevin equation (6.1) as

$$\frac{d\vec{\tilde{r}}_s}{dt} = -a_s\vec{\tilde{r}}_s + \vec{\tilde{F}}_s^{ABP}(t), \tag{6.121}$$

where $\vec{\bar{F}}_s^{ABP}(t) = \left(\bar{\xi}_s(t), \bar{\psi}_s(t)\right)$. Using the correlations of the noise terms in Eqs. (6.7), (6.8) and (6.9), we obtain the connected correlations for $\bar{x}_s(t)$ and $\bar{y}_s(t)$ as

$$\langle \bar{x}_s(t_1)\bar{x}^*_{s'}(t_2)\rangle_c^{ABP} = \frac{v_A^2}{2N}\, \mathbb{H}_1\left(D_{rot}, a_s, t_1, t_2\right)\delta_{s,s'}, \tag{6.122}$$

$$\langle \bar{y}_s(t_1)\bar{y}^*_{s'}(t_2)\rangle_c^{ABP} = \frac{v_A^2}{2N}\, \mathbb{H}_2\left(D_{rot}, a_s, t_1, t_2\right)\delta_{s,s'}. \tag{6.123}$$

Once again we assume $t_1 \leq t_2$ without any loss of generality. Also, here a_s is defined in Eq. (6.26) and the functions $\mathbb{H}_{1/2}(m, n, t_1, t_2)$ are given by

$$\mathbb{H}_p(u, w, t_1, t_2) = \mathcal{H}(u, w, t_1, t_2) + (-1)^{p-1}\mathcal{V}(u, w, t_1, t_2) - 2\delta_{p,1}\frac{\left(e^{-ut_1} - e^{-wt_1}\right)\left(e^{-ut_2} - e^{-wt_2}\right)}{(w-u)^2}, \tag{6.124}$$

with $p \in \{1, 2\}$, $\mathcal{H}(a, b, t_1, t_2)$ is given in Eq. (6.55) and $\mathcal{V}(m, n, t_1, t_2)$ is defined as

$$\mathcal{V}(u, w, t_1, t_2) = \frac{ue^{-w|t_1-t_2|}\left(e^{-4ut_1} - e^{-2wt_1}\right)}{(w-u)(w-3u)(w-2u)} - \frac{e^{-wt_2}\left(e^{-ut_1} - e^{-wt_1}\right) - e^{-ut_2}\left(e^{-3ut_1} - e^{-wt_1}\right)}{(w-u)(w-3u)}. \tag{6.125}$$

Once we get the correlations of the Fourier variables $\bar{x}_s(t)$ and $\bar{y}_s(t)$ in Eqs. (6.122) and (6.123), we can transform them to get the position correlations as

$$\langle x_0(t_1)x_\beta(t_2)\rangle_c^{ABP} = \frac{v_A^2}{2N}\sum_{s=0}^{N-1}\cos\left(\frac{2\pi s\beta}{N}\right)\mathbb{H}_1\left(D_{rot}, a_s, t_1, t_2\right), \tag{6.126}$$

$$\langle y_0(t_1)y_\beta(t_2)\rangle_c^{ABP} = \frac{v_A^2}{2N}\sum_{s=0}^{N-1}\cos\left(\frac{2\pi s\beta}{N}\right)\mathbb{H}_2\left(D_{rot}, a_s, t_1, t_2\right). \tag{6.127}$$

which in the limit $N \to \infty$ takes the form

$$\langle x_0(t_1)x_\beta(t_2)\rangle_c^{ABP} \simeq \frac{v_A^2}{4\pi}\int_{-\pi}^{\pi} dq\ \cos(q\beta)\ \mathbb{H}_1\left(D_{rot}, b_q, t_1, t_2\right), \tag{6.128}$$

$$\langle y_0(t_1)y_\beta(t_2)\rangle_c^{ABP} \simeq \frac{v_A^2}{4\pi}\int_{-\pi}^{\pi} dq\ \cos(q\beta)\ \mathbb{H}_2\left(D_{rot}, b_q, t_1, t_2\right), \tag{6.129}$$

where $b_q = 4K\sin^2(q/2)$. As done for the other two models, we will, in the next two sections, analyze these correlations for (i) $t_1 \ll \tau_K,\ t_2 \ll \tau_K$ and (ii) $t_1 \gg \tau_K,\ t_2 \gg \tau_K$ with the ratio $\frac{t_2}{t_1}$ kept fixed. Finally, we then look at them for finite but large N.

6.5.1 Case I: $t_1 \ll \tau_K,\ t_2 \ll \tau_K$

Let us first examine Eqs. (6.128) and (6.129) when both observation times t_1 and t_2 are smaller than the interaction time scale τ_K. Then, we can use the approximation $\mathbb{H}_1(D_{rot}, a_s, t_1, t_2) \simeq$

$\frac{2}{3}D_{rot}^2 t_1^3(2t_2 - t_1)$ and $\mathbb{H}_2(D_{rot}, a_s, t_1, t_2) \simeq 2D_{rot}t_1^2\left(t_2 - \frac{t_1}{3}\right)$ for $t_1 \to 0$ and $t_2 \to 0$ and plug these forms in Eqs. (6.128) and (6.129) to obtain

$$\langle x_0(t_1)x_\beta(t_2)\rangle_c^{ABP} \simeq \frac{1}{3}v_A^2 D_{rot}^2 t_1^3(2t_2 - t_1)\delta_{\beta,0}, \qquad t_1 \leq t_2 \ll \tau_K, \tag{6.130}$$

$$\langle y_0(t_1)y_\beta(t_2)\rangle_c^{ABP} \simeq v_A^2 D_{rot}t_1^2\left(t_2 - \frac{t_1}{3}\right)\delta_{\beta,0}, \qquad t_1 \leq t_2 \ll \tau_K. \tag{6.131}$$

Since these particles move independently at these time scales, we generate uncorrelated motion between them as exemplified by $\delta_{\beta,0}$ term. Also, for $\beta = 0$ and $t_1 = t_2 = t$, both these equations reduce to the variance which are consistent with results from the previous study [54].

6.5.2 Case II: $t_1 \gg \tau_K,\ t_2 \gg \tau_K$

Let us consider the correlations $\langle x_0(t_1)x_\beta(t_2)\rangle_c^{ABP}$ and $\langle y_0(t_1)y_\beta(t_2)\rangle_c^{ABP}$ in the other limit where both t_1 and t_2 are larger than τ_K. Substituting $\mathbb{H}_{1/2}\left(D_{rot}, b_q, t_1, t_2\right)$ from Eq. (6.124) in Eqs. (6.128) and (6.129), we see that the correlations possess integrals like $\sim \int dq\, h(q) \exp\left[-Kt_1 \sin^2(q/2)\right]$ where $h(q)$ is some function of q. For large Kt_1, such integrals will be dominated by small values of q. This enables us to approximate $b_q \simeq Kq^2$ in Eqs. (6.128) and (6.129) and obtain the scaling relation

$$\langle x_0(t_1)x_\beta(t_2)\rangle_c^{ABP} \simeq \frac{v_A^2}{4\pi}\sqrt{\frac{t_1^3}{K}}\int_{-\infty}^{\infty} dw\ \cos\left(\frac{w\beta}{\sqrt{Kt_1}}\right)\ \mathbb{H}_1\left(D_{rot}t_1, w^2, 1, \frac{t_2}{t_1}\right), \tag{6.132}$$

$$\langle y_0(t_1)y_\beta(t_2)\rangle_c^{ABP} \simeq \frac{v_A^2}{4\pi}\sqrt{\frac{t_1^3}{K}}\int_{-\infty}^{\infty} dw\ \cos\left(\frac{w\beta}{\sqrt{Kt_1}}\right)\ \mathbb{H}_2\left(D_{rot}t_1, w^2, 1, \frac{t_2}{t_1}\right). \tag{6.133}$$

Below, we will use these expressions to demonstrate different scaling relations for the variance, covariance and autocorrelation.

6.5.2.1 Variance

Putting $\beta = 0$ and $t_1 = t_2 = t$ in Eqs. (6.132) and (6.133), we obtain the variance of $x_0(t)$ and $y_0(t)$ as

$$\langle x_0^2(t)\rangle_c^{ABP} \simeq \frac{v_A^2 t^{3/2}}{4\pi\sqrt{K}}\ \mathcal{T}_1^{AB}\left(D_{rot}t\right), \qquad t \gg \tau_K, \tag{6.134}$$

$$\langle y_0^2(t)\rangle_c^{ABP} \simeq \frac{v_A^2 t^{3/2}}{4\pi\sqrt{K}}\ \mathcal{T}_2^{AB}\left(D_{rot}t\right), \qquad t \gg \tau_K, \tag{6.135}$$

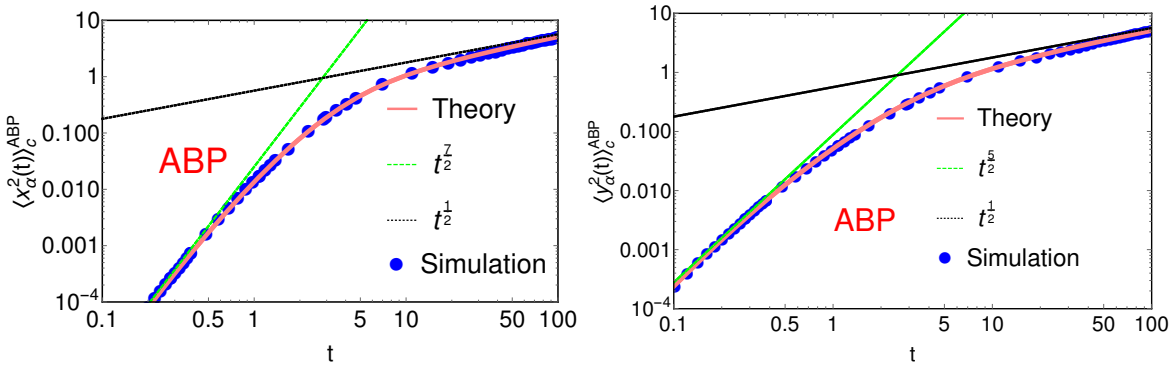

Figure 6.15: Plot of the asymptotic behaviours of $\langle x_\alpha^2(t)\rangle_c^{ABP}$ (left panel) and $\langle y_\alpha^2(t)\rangle_c^{ABP}$ (right panel) for $\tau_k \ll t \ll \tau_A$ and $\tau_k \ll \tau_A \ll t$ where $\tau_A = \frac{1}{D_{rot}}$ and $\tau_K = \frac{1}{K}$. Their analytic expressions are given in Eqs .(6.142) - (6.145) respectively. For both plots, we have chosen $K = 2,\ D_{rot} = 0.5$ and $v_A = 1$. Simulation is done with $N = 100$

where the scaling functions $\mathcal{T}_1^{AB}(y)$ and $\mathcal{T}_2^{AB}(y)$ are given by

$$\mathcal{T}_1^{AB}(y) = \int_{-\infty}^{\infty} dw\ \mathbb{H}_1(y, w^2, 1, 1), \tag{6.136}$$

$$\mathcal{T}_2^{AB}(y) = \int_{-\infty}^{\infty} dw\ \mathbb{H}_2(y, w^2, 1, 1). \tag{6.137}$$

Figure 6.14 compares this scaling relation with the results of the numerical simulations. We see a nice agreement between them. To decipher different scalings of the variance, we look at the asymptotic forms of the scaling functions $\mathcal{T}_1^{AB}(y)$ and $\mathcal{T}_2^{AB}(y)$ for which we directly expand $\mathbb{H}_{1/2}(y, w^2, 1, 1)$ in the above equations. The asymptotic forms then read

$$\mathcal{T}_1^{AB}(y) \simeq \frac{256(\sqrt{2}-1)\sqrt{\pi}}{105} y^2 - \frac{256\sqrt{\pi}\left(16\sqrt{2}-17\right)}{945} y^3, \qquad \text{as } y \to 0, \tag{6.138}$$

$$\simeq \frac{2\sqrt{2\pi}}{y} + O\left(y^{-2}\right), \qquad \text{as } y \to \infty, \tag{6.139}$$

$$\mathcal{T}_2^{AB}(y) \simeq \frac{64(\sqrt{2}-1)\sqrt{\pi}}{15} y - \frac{64\sqrt{\pi}}{105}\left(8\sqrt{2}-9\right) y^2, \qquad \text{as } y \to 0, \tag{6.140}$$

$$\simeq \frac{2\sqrt{2\pi}}{y} + O\left(y^{-2}\right), \qquad \text{as } y \to \infty. \tag{6.141}$$

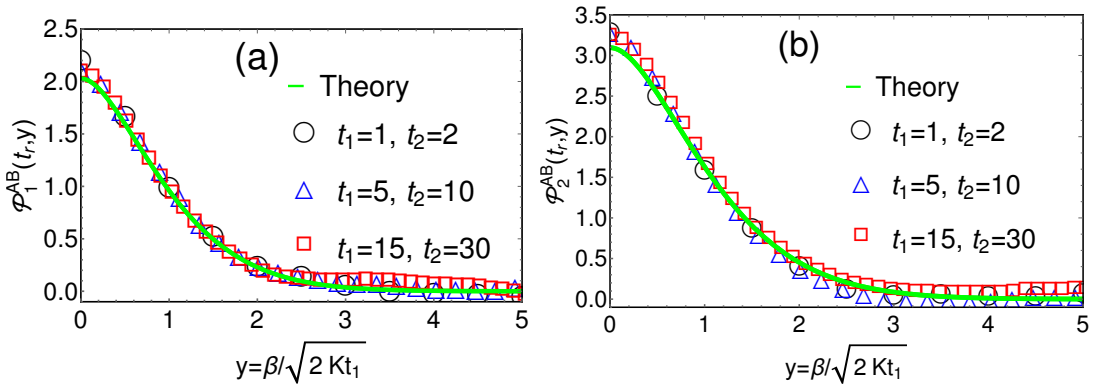

Figure 6.16: Scaling functions $\mathcal{P}_1^{AB}(y,t_r)$ and $\mathcal{P}_2^{AB}(y,t_r)$ in Eqs. (6.147) and (6.149) associated with $\langle x_0(t_1)x_\beta(t_2)\rangle_c^{ABP}$ and $\langle y_0(t_1)y_\beta(t_2)\rangle_c^{ABP}$ have been compared with the simulations for $K=2,\ D_{rot}=0.001,\ v_A=1.5$ and $N=100$.

Inserting these asymptotic forms in the expression of $\langle x_0^2(t)\rangle_c^{ABP}$ and $\langle y_0^2(t)\rangle_c^{ABP}$ in Eqs. (6.134) and (6.135), we get

$$\langle x_0^2(t)\rangle_c^{ABP} \simeq \frac{64(\sqrt{2}-1)}{105\sqrt{\pi}}\frac{v_A^2 D_{rot}^2}{\sqrt{K}}\ t^{7/2} + O\left(t^{9/2}\right), \qquad \text{for } \tau_K \ll t \ll \tau_A, \tag{6.142}$$

$$\simeq \frac{v_A^2}{2D_{rot}}\sqrt{\frac{2t}{\pi K}} + O\left(t^{-1/2}\right), \qquad \text{for } \tau_K \ll \tau_A \ll t, \tag{6.143}$$

$$\langle y_0^2(t)\rangle_c^{ABP} \simeq \frac{16(\sqrt{2}-1)}{15\sqrt{\pi}}\frac{v_A^2 D_{rot}}{\sqrt{K}}\ t^{5/2} + O\left(t^{7/2}\right), \qquad \text{for } \tau_K \ll t \ll \tau_A, \tag{6.144}$$

$$\simeq \frac{v_A^2}{2D_{rot}}\sqrt{\frac{2t}{\pi K}} + O\left(t^{-1/2}\right), \qquad \text{for } \tau_K \ll \tau_A \ll t. \tag{6.145}$$

We observe for $t \ll \tau_A$, the variance $\langle x_0^2(t)\rangle_c^{ABP}$ scales with time as $\sim t^{7/2}$ which is different than the $\sim t^{3/2}$ and $\sim t^{5/2}$ scalings for the RTP and AOUP respectively. The variance then crosses over to the $\sim \sqrt{t}$ scaling for $t \gg \tau_A$. On the other hand, for y-coordinate, we see a different crossover for the variance from $\sim t^{5/2}$ scaling at $t \ll \tau_A$ to the $\sim \sqrt{t}$ scaling at $t \gg \tau_A$. For both $\langle x_0^2(t)\rangle_c^{ABP}$ and $\langle y_0^2(t)\rangle_c^{ABP}$, these crossover behaviours have been numerically verified in Figure 6.15. Notice that for $\langle y_0^2(t)\rangle_c^{ABP}$, the $\sim t^{5/2}$ scaling at $t \ll \tau_A$ is same as that of the AOUP in Eq. (6.106). This stems from the fact that at this time scale, the dynamics of the y-coordinate of ABP and AOUP are exactly same.

We next use the unequal time position correlations in Eqs. (6.132) and (6.133) to obtain the covariance and autocorrelation. Since they possess different forms depending on whether (i) $\tau_K \ll t_1 \leq t_2 \ll \tau_A$ and (ii) $\tau_K \ll \tau_A \ll t_1 \leq t_2$, we proceed to analyze them separately for these two cases.

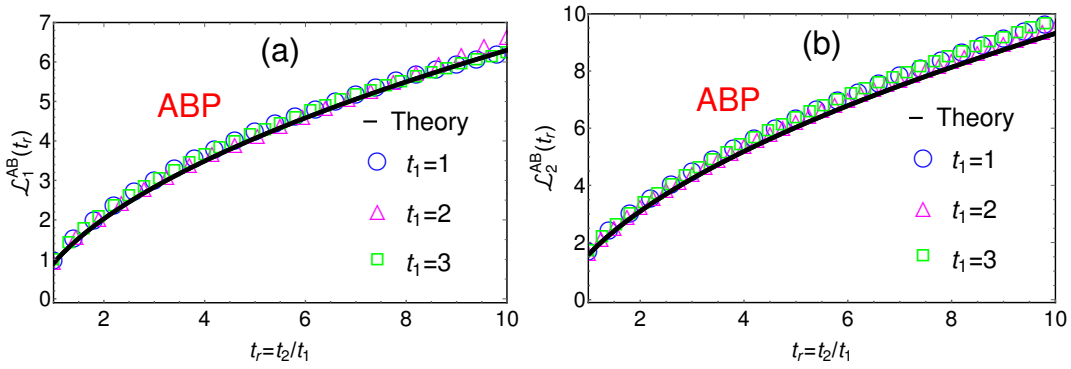

Figure 6.17: Numerical verification of the scaling functions $\mathcal{L}_1^{AB}(t_r)$ and $\mathcal{L}_2^{AB}(y,t_r)$ for the autocorrelations in Eqs. (6.152) and (6.153) for three different values of t_1. For both plots, parameters taken are $K=2,\ D_{rot}=0.0001,\ v_A=1$ and $N=100$ for the simulation.

6.5.2.2 Covariance and unequal time correlations for $t_1 \ll \tau_A,\ t_2 \ll \tau_A$

Here, we will compute the correlations $\langle x_0(t_1)x_\beta(t_2)\rangle_c^{ABP}$ and $\langle y_0(t_1)y_\beta(t_2)\rangle_c^{ABP}$ when both t_1 and t_2 are smaller than the activity time scale $\tau_A=\frac{1}{D_{rot}}$. Following Eq. (6.124), we approximate $\mathbb{H}_1\left(D_{rot}t_1,w^2,1,t_r\right)$ by

$$\mathbb{H}_1\left(D_{rot}t_1\to 0,w^2,1,t_r\right)\simeq\frac{2D_{rot}^2t_1^2}{w^8}\Big[e^{-w^2(1+t_r)}-4e^{-w^2t_r}-4e^{-w^2}\\ +(3-2w^2)e^{-w^2(t_r-1)}+4(2-2w^2+w^4)\Big],$$

and plug it in Eq. (6.132) to obtain the scaling form

$$\langle x_0(t_1)x_\beta(t_2)\rangle_c^{ABP}\simeq\frac{v_A^2D_{rot}^2t_1^{7/2}}{2\pi\sqrt{K}}\,\mathcal{P}_1^{AB}\left(\frac{\beta}{\sqrt{2Kt_1}},\frac{t_2}{t_1}\right),\qquad\text{for } t_1\le t_2\ll\tau_A, \tag{6.146}$$

where the scaling function $\mathcal{P}_1^{AB}(y,t_r)$ is given by

$$\mathcal{P}_1^{AB}(y,t_r)=\int_{-\infty}^{\infty}dw\,\frac{\cos\left(\sqrt{2}wy\right)}{w^8}\Big[e^{-w^2(1+t_r)}-4e^{-w^2t_r}-4e^{-w^2}\\ +(3-2w^2)e^{-w^2(t_r-1)}+4(2-2w^2+w^4)\Big]. \tag{6.147}$$

Same analysis for the y-coordinate yields

$$\langle y_0(t_1)y_\beta(t_2)\rangle_c^{ABP}\simeq\frac{v_A^2D_{rot}t_1^{5/2}}{2\pi\sqrt{K}}\,\mathcal{P}_2^{AB}\left(\frac{\beta}{\sqrt{2Kt_1}},\frac{t_2}{t_1}\right),\qquad\text{for } t_1\le t_2\ll\tau_A, \tag{6.148}$$

with the scaling function $\mathcal{P}_2^{AB}(y,t_r)$ given by

$$\mathcal{P}_2^{AB}(y,t_r)=\mathcal{P}^{OU}(y,t_r). \tag{6.149}$$

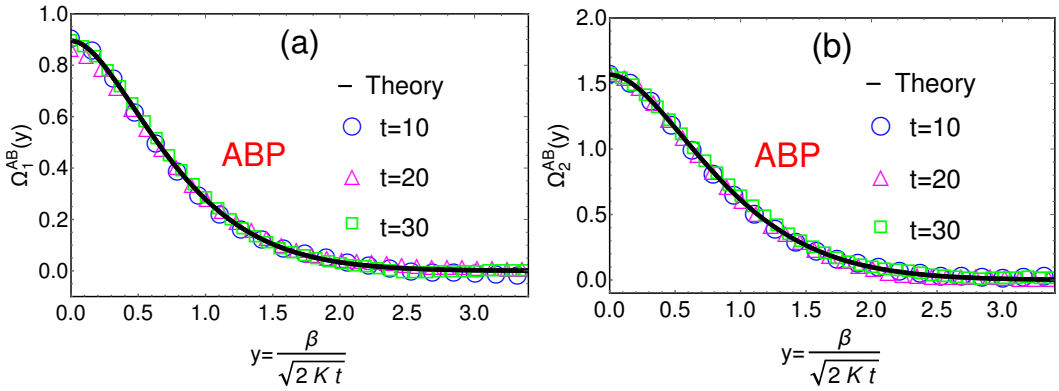

Figure 6.18: Numerical verification of the scaling functions $\Omega_1^{AB}(y)$ and $\Omega_2^{AB}(y)$ in Eqs. (6.156) and (6.157). For both plots, we have chosen $K = 2$, $D_{rot} = 0.001$, $v_A = 1.5$ and $N = 200$.

Here $\mathcal{P}^{OU}(y, t_r)$ represents the corresponding scaling function for AOUP in Eq. (6.109). Figure 6.16 compares the scaling functions $\mathcal{P}_1^{AB}(y, t_r)$ and $\mathcal{P}_2^{AB}(y, t_r)$ with the numerics for three sets of t_1 and t_2 with fixed t_2/t_1. We see that the simulation data collapse over our analytic results for all cases. To contrast the correlation $\langle x_0(t_1)x_\beta(t_2)\rangle_c^{ABP}$ in Eq. (6.146) from that of the RTPs and AOUPs, we look at its behaviour for large β. By direct expansion, we find that it decays as $\sim f(\beta)\, \exp\left(\beta^2/\hat{l}_d^2\right)$ where the decay length $\hat{l}_d = 2\sqrt{K(t_1+t_2)}$ and $f(\beta) = \beta^{-8}$. Recall that this correlation for RTPs and AOUPs also had a similar decay but with different $f(\beta)$, namely $f(\beta) = \beta^{-4}$ (RTP) and $f(\beta) = \beta^{-6}$ (AOUP). On the other hand, $\langle y_0(t_1)y_\beta(t_2)\rangle_c^{ABP}$ in Eq. (6.148) has exactly the same form as for AOUPs in Eq. (6.108). As mentioned before that the dynamics of the y-coordinate of the ABP and AOUP are essentially the same at these time scales.

Next, by putting $\beta = 0$ in Eqs. (6.146) and (6.148), we find that the autocorrelations have scaling form

$$\langle x_0(t_1)x_0(t_2)\rangle_c^{ABP} \simeq \frac{v_A^2 D_{rot}^2 t_1^{7/2}}{2\pi\sqrt{K}}\, \mathcal{L}_1^{AB}\left(\frac{t_2}{t_1}\right), \qquad \text{for } t_1 \le t_2 \ll \tau_A, \tag{6.150}$$

$$\langle y_0(t_1)y_0(t_2)\rangle_c^{ABP} \simeq \frac{v_A^2 D_{rot} t_1^{5/2}}{2\pi\sqrt{K}}\, \mathcal{L}_2^{AB}\left(\frac{t_2}{t_1}\right), \qquad \text{for } t_1 \le t_2 \ll \tau_A, \tag{6.151}$$

where the scaling functions $\mathcal{L}_{1,2}^{AB}(t_r)$ are given by

$$\mathcal{L}_1^{AB}(t_r) = \frac{16\sqrt{\pi}}{105}\left[(1+t_r)^{7/2} - 4\left(1+t_r^{7/2}\right) + \sqrt{t_r-1}\left(4 - 5t_r - 2t_r^2 + 3t_r^3\right)\right], \tag{6.152}$$

$$\mathcal{L}_2^{AB}(t_r) = \frac{8\sqrt{\pi}}{15}\left[(t_r+1)^{5/2} + (t_r-1)^{5/2} - 2(1+t_r^{5/2})\right]. \tag{6.153}$$

In Figure 6.17, we have plotted these two scaling functions and compared them against the numerical simulations for three different values of t_1. We find the convergence of the simulation

data with our analytic results for all cases.

Finally, we turn to the covariance $\langle x_0(t)x_\beta(t)\rangle_c^{ABP}$ and $\langle y_0(t)y_\beta(t)\rangle_c^{ABP}$ for which we put $t_1 = t_2 = t$ in Eqs. (6.146) and (6.148). This yields the scaling relation

$$\langle x_0(t)x_\beta(t)\rangle_c^{ABP} \simeq \frac{v_A^2 D_{rot}^2 t^{7/2}}{2\pi\sqrt{K}}\ \Omega_1^{AB}\left(\frac{\beta}{\sqrt{2Kt}}\right), \qquad \text{for } \tau_k \ll t \ll \tau_A, \tag{6.154}$$

$$\langle y_0(t)y_\beta(t)\rangle_c^{ABP} \simeq \frac{v_A^2 D_{rot} t^{5/2}}{2\pi\sqrt{K}}\ \Omega_2^{AB}\left(\frac{\beta}{\sqrt{2Kt}}\right), \qquad \text{for } \tau_k \ll t \ll \tau_A, \tag{6.155}$$

where the scaling functions $\Omega_{1/2}^{AB}(y)$ are given by

$$\Omega_1^{AB}(y) = \frac{\sqrt{\pi}}{630}\Big[2\sqrt{2}e^{-\frac{y^2}{4}}\left(384+348y^2+40y^4+y^6\right) - 16e^{-\frac{y^2}{2}}\left(48+87y^2+20y^4+y^6\right) \tag{6.156}$$
$$- \sqrt{2\pi}y\ \mathrm{Erfc}\left(\frac{y}{2}\right)\left(840+420y^2+42y^4+y^6\right) + 8\sqrt{2\pi}y\ \mathrm{Erfc}\left(\frac{y}{\sqrt{2}}\right)\left(105+105y^2+21y^4+y^6\right)\Big],$$

$$\Omega_2^{AB}(y) = \Omega^{OU}(y), \tag{6.157}$$

where $\Omega^{OU}(y)$ is given in Eq.(6.113). Figure 6.18 shows a comparison of these scaling functions with the numerical simulations for three different values of t. For all t, we see nice agreement of the numerical data with our analytic results.

6.5.2.3 Covariance and unequal time correlations for $t_1 \gg \tau_A,\ t_2 \gg \tau_A$

For times larger than the activity time scale τ_A, the motions of ABP, RTP and AOUP converge to that of the Brownian motion. Hence, we expect the results for $\langle x_0(t_1)x_\beta(t_2)\rangle_c^{RTP}$ derived in Eq. (6.78) for RTP to apply to both coordinates of ABP also. Consequently, we get

$$\langle x_0(t_1)x_\beta(t_2)\rangle_c^{ABP} \simeq \langle y_0(t_1)y_\beta(t_2)\rangle_c^{ABP} \simeq D_{ABP}\sqrt{\frac{2t_1}{\pi K}}\ \mathcal{Q}\left(\frac{\beta}{\sqrt{2Kt_1}}, \frac{t_2}{t_1}\right), \tag{6.158}$$

for $t_1 \gg \tau_A,\ t_2 \gg \tau_A$ with fixed t_2/t_1. The scaling fucntion $\mathcal{Q}(y, t_r)$ is given in Eq. (6.79). As done for RTP and AOUP, it is straightforward to obtain the expressions of the variance, covariance and position autocorrelations from Eq. (6.158). These expressions are given in Eqs. (6.115, 6.116) with D_A replaced by $D_{ABP} = v_A^2/(2D_{rot})$.

6.5.3 Large but finite N

For this case also, the observation time is much larger than the activity time scale. So the expressions derived in Eq. (6.81) for RTP and AOUP will also apply for this case:

$$\langle x_0(t_1)x_\beta(t_2)\rangle_c^{ABP} \simeq \langle y_0(t_1)y_\beta(t_2)\rangle_c^{ABP} \simeq \frac{2D_{ABP}N}{K}\ \mathcal{W}\left(\frac{t_2}{t_1}, \frac{\beta}{N}, \frac{Kt_1}{N^2}\right) \tag{6.159}$$

where $\mathcal{W}(t_r, y, z)$ is given in Eq. (6.82) and $D_{ABP} = \frac{v_A^2}{2D_{rot}}$. This solution then leads to the scaling relations for the variance, covariance and position autocorrelation as written in Sec. 6.4.3

6.6 Summary

Thus, we have studied a simple and analytically tractable model of N active particles with the nearest neighbour quadratic interaction. We considered three models of active particles namely, run and tumble particles and active Ornstein-Uhlenbeck particles in one dimension and active Brownian particles in two dimensions. This problem has three time scales - (i) the interaction time scale $\tau_K = \frac{1}{K}$, (ii) the activity time scale $\tau_A = \frac{1}{\gamma}$ / $\frac{1}{\zeta}$ / $\frac{1}{D_{rot}}$ for RTP / AOUP / ABP and (iii) the relaxation time scale $\tau_N = \frac{N^2}{K}$ due to the finite system size. We choose them such that $\tau_K \ll \tau_A \ll \tau_N$ [see Figure 6.2]. Our main quantities of interest were different two-point correlation functions of the positions of the tagged particles and see how they get modified due to the active nature of the particles.

We first computed the variance $\langle x_\alpha^2(t)\rangle_c$ of the position of the α-th particle. When $t \ll \tau_K$, the particles move independently so that we recover the scaling of $\langle x_\alpha^2(t)\rangle_c$ as in the non-interacting case. On the other hand, when $\tau_K \ll t \ll \tau_A$, the variance scales as $\sim t^\nu$ with exponent ν different than the non-interacting case. We calculated $\nu = \frac{3}{2}$ for RTP, $\nu = \frac{5}{2}$ for AOUP and $\nu = \frac{7}{2}$ $\left(= \frac{5}{2}\right)$ for x (y)-coordinate of ABP. Note that t^ν scaling of the MSD arises due to the interplay of the activity and caging effect due to the surrounding particles. Next, from this $\sim t^\nu$ scaling, the variance crosses over to $\sim \sqrt{t}$ scaling when $\tau_K \ll \tau_A \ll t$ for all three models with the corresponding crossover function derived rigorously in Eqs. (6.37) and (6.104) for the RTPs and AOUPs respectively and in Eqs. (6.136) and (6.137) for the ABPs. Similar crossover behaviour was also seen for the variance when the observation time t is of the order of $\sim \tau_N$. While for $t \ll \tau_N$, one gets $\sim \sqrt{t}$ scaling of $\langle x_\alpha^2(t)\rangle_c$ for all models, it scales diffusively when $t \gg \tau_N$. The associated crossover function is given in Eq. (6.85).

We next computed the equal time two-point correlation function $\langle x_0(t)x_\beta(t)\rangle_c$ for all three models. Once again, this correlation function displays different scaling behaviours depending on whether t is larger or smaller than the activity time scale. For example, when $\tau_K \ll t \ll \tau_N$, they exhibit scaling forms with respect to $y = \frac{\beta}{\sqrt{2Kt}}$ with distinct scaling functions $\Omega^{RT}(y)$, $\Omega^{OU}(y)$ and $\Omega_{1/2}^{AB}(y)$ which were derived in Eqs. (6.47), (6.113), (6.156) and (6.157) respectively. On the other hand, for $t \gg \tau_A$, we obtain the same scaling form for all models with the associated scaling function $\mathcal{C}(y)$ given in Eq. (6.51).

We then turned to the position autocorrelation $\langle x_\alpha(t_1)x_\alpha(t_2)\rangle_c$ and analyzed them in two limits - (A) $t_1 \ll \tau_A$, $t_2 \ll \tau_A$ and (B) $t_1 \gg \tau_A$, $t_2 \gg \tau_A$. In both these limits, the ratio $t_r = t_2/t_1$ is held fixed. For case (A), we derived distinct scaling forms of the autocorrelation in t_r and the corresponding scaling functions $\mathcal{L}^{RT}(t_r)$, $\mathcal{L}^{OU}(t_r)$ and $\mathcal{L}^{AB}_{1/2}(t_r)$ are calculated in Eqs. (6.61), (6.111), (6.152) and (6.153) respectively. For case (B), all models give rise to the same scaling function $\mathcal{M}(t_r)$ in Eq. (6.67). Quite remarkably, $\langle x_0(t)x_\beta(t)\rangle_c$ changes non-monotonically with t_2 (for a fixed t_1) where it first rises with t_2, attains a maximum value and then starts decreasing again. We reasoned that this non-monotonic nature arises due to the peristent nature of these particles.

We finally studied the unequal time correlation function $\langle x_0(t_1)x_\beta(t_2)\rangle_c$ ($t_1 \leq t_2$) and demonstrated different scaling behaviours depending on where t_1 and t_2 lie. For case (A), it has scaling form in two variables: $t_r = \frac{t_2}{t_1}$ and $y = \frac{\beta}{\sqrt{2Kt_1}}$ and the associated model-dependent scaling functions $\mathcal{P}^{RT}(y, t_r)$, $\mathcal{P}^{OU}(y, t_r)$ and $\mathcal{P}^{AB}_{1/2}(y, t_r)$ are calculated respectively in Eqs. (6.77), (6.109), (6.147) and (6.149). However for case (B), all models converge to the same scaling function $\mathcal{Q}(y, t_r)$ given in Eq. (6.79). As seen for the autocorrelation, $\langle x_0(t_1)x_\beta(t_2)\rangle_c$ also shows a non-monotonic dependence on t_2 for fixed β and t_1. Once again, this non-monotonic nature owes its origin to the persistent nature of these particles.

Chapter 7

Conclusion

Active matter is a class of driven non-equilibrium systems where the individual unit consumes the supplied energy and tranduces it into a systematic movement. While these systems typically appear in the biological context in the form of bacteria, cytoskeleton, tracer proteins, schools of fish and so on [5, 8, 26–29], recently active motion has also been realised in non-living settings like janus particles, vibrating granules and nano-robots [31–33,35]. The common feature of these systems is that their dynamics violates the time-reversal symmetry (at the local scale) and thus breaks the detailed balance condition [28, 83]. In fact, the dynamics of an active particle is a non-Markov process and the stochastic trajectory thus obtained represents a strongly correlated time series [70]. Obtaining exact analytical results on the extremal statistics and functional statistics for such correlated time series with history dependence is often a difficult task. In this thesis, we were able to obtain some exact results on the extremal statistics, convex hull and path functionals for a particular active model called run and tumble particle in Eq. (1.7). From this exact analysis, we were able to show how distinct non-Brownian behaviours arise at small and intermediate time scales.

In chapter (2), we looked at the arcsine laws for a single RTP in one dimension. For a stochastic trajectory of fixed duration t and starting from the origin in one dimension, the arcsine laws refer to the statistics of the following three observables: (i) the time t_m at which the particle reaches its maximum distance M, (ii) the time t_r spent on the positive side of the origin and (iii) the last time t_ℓ at which the particle crosses the origin. Interestingly, for Brownian motion, P. Lévy proved that the distributions of these three observable are exactly same and is given by Eq. (2.1) [120]. Contrarily, our study in chapter (2) showed that these three distributions and their universality for a RTP depend quite sensitively on its initial velocity direction σ_0. When

σ_0 is chosen between ± 1 with equal probability $1/2$, then one finds that the distributions of t_m and t_r are exactly same and this common distribution has two delta-functions at $t_m = 0$ and $t_m = t$ (same for t_r) and a non-delta function part. However, unlike in the Brownian motion, the distribution of t_ℓ for a RTP is slightly different with only one delta-function at $t_\ell = 0$ and the same non-delta function part as the other two observables. The expressions of these distributions are given in Eq. (2.34) for t_m, in Eq. (2.56) for t_r and in Eq. (2.60) for t_ℓ. Same analysis for the asymmetric initial condition (where σ_0 is chosen between ± 1 with unequal probability) gives that all three distributions are different. Interestingly, it turns out that our results on t_m and t_r for the symmetric case are valid even in higher dimensions [92]. While for t_m, this universality was proved in [92] by using the Sparre Andersen theorem [183], proving the same for t_r is still an open problem. Also, analysing the arcsine laws for other active models like active Brownian particle and active Ornstein-Uhlenbeck particle is an interesting future direction.

In chapter (3), we investigated the convex hull problem for a 2-d isotropic run and tumble motion. We studied this model in two different statistical ensembles depending on whether the number of tumbles (n) or the observation time (t) is fixed. Utilizing the connection of convex hull to the extreme-value statistics, we analytically computed its mean area for a single RTP in these two ensembles. These expressions are provided in Eq. (3.35) for the fixed-n ensemble and in Eq. (3.59) for the fixed-t ensemble. In particular we showed that the mean area $\langle A(t) \rangle$ for the fixed-t case exhibits two different scaling regimes depending on the observation time t, namely $\langle A(t) \rangle \sim t^3$ for $t \ll \gamma^{-1}$ and $\langle A(t) \rangle \sim t$ for $t \gg \gamma^{-1}$. This is different than the passive Brownian case where the mean area scales linearly with time as $\langle A(t) \rangle \sim t$ for all values of t [127]. We also derived the exact scaling function that connects the two scaling regimes in Eq. (3.60).

As a future direction, it would be interesting to study the convex hull problem for realistic run and tumble models where tumbles are not instantaneous. For fixed-n ensemble, we anticipate our results in Eq. (3.35) to be valid even for these realistic models. However, for fixed-t ensemble, the results will be different atleast at small and intermediate time scales. Also, going beyond the mean perimeter and the mean area, obtaining analytic results for the higher moments and probability distribution is an open problem even for the simple Brownian motion.

Note that the previous two chapters focused on the RTP model in a homogeneous setting where motility parameters like v_0 and γ are constant both in space and time. However, in many realistic scenarios, heterogeneous active models become more relevant specially when the particle is moving in a complex environment with an asymmetric distribution of the obstacles or

the nutrients in case of the bacteria [115–119]. This motivated us to consider, in chapter (4), the spatially heterogeneous run and tumble particle in one dimension with a position and direction dependent rate of tumbling. This means that the telegraphic noise $\sigma(t)$ in Eq. (1.7) flips from $+1 \to -1$ with a rate $R_1(x)$ that is different than rate $R_2(x)$ with which flip from $-1 \to +1$ occurs. The precise forms of these rates are given in Eqs. (4.1). We computed the late time behaviours of the position distributions, survival probabilities and exit probabilities from a finite interval and showed that the spatial heterogeneity leads to strict non-Brownian forms even at late times. One important point is that the position distribution in Eq. (4.39) describe only the typical fluctuations of the position and becomes invalid at the far tails of the distribution. In particular, for the homogeneous case, it was shown in [70, 114] that the distribution possesses a large deviation form at the tails. It remains an open direction to see if such large deviations forms exist even for the heterogeneous run and tumble model. Another interesting direction is to see if the universal features seen for the survival probability of a homogeneous RTP are also observed in the heterogeneous setting.

Next, we demonstrated the effect of the spatial heterogeneity on the statistics of the local time (density) in chapter (5). For the case when $R_1(x) = R_2(x) \sim |x|^\alpha$ ($\alpha \geq 0$), we developed a 'path-counting method' which enabled us to obtain the distribution of T_{loc} completely in terms of the probabilities of multiple visit to x_{loc}. Utilizing this method, we were able to derive the distribution of T_{loc} both in the free space and in presence of an absorbing wall. The analytic expressions of these distributions are given in Eq. (5.31) for $\alpha = 0$ in free space and in Eqs. (5.66) and (5.67) for general α with absorbing boundary condition. On the other hand, for $\alpha \neq 0$ and free space case, we showed that the typical fluctuations of T_{loc} scales with time as $T_{loc} \sim t^{\frac{1+\alpha}{2+\alpha}}$ and the distribution obeys the scaling form $P(T_{loc}, t) \simeq \frac{\mathcal{C}_\alpha}{t^{\frac{1+\alpha}{2+\alpha}}} f_\alpha\left(\frac{\mathcal{C}_\alpha T_{loc}}{t^{\frac{1+\alpha}{2+\alpha}}}\right)$. The corresponding scaling function $f_\alpha(z)$ is given in Eq. (5.43) for arbitrary values of $\alpha \geq 0$.

Although, in this chapter, we have focused only on $\alpha \geq 0$, some of our results are valid even for the negative values of α. For example, the scaling relation for the distribution in Eq. (5.42) is valid even for $-1 < \alpha < 0$. However, performing this study analytically in presence of an absorbing barrier for $\alpha < 0$ remains a direction yet to be explored. Also, studying the local time problem for other active models like active Brownian particle and active Ornstein-Uhlenbeck particle is a direction yet to be explored.

Finally in chapter (6), we studied a chain of N active particles with nearest-neighbour harmonic interactions. Our study demonstrated how exactly the activity (persistence) and interaction

affect the dynamics of tagged particles. In particular, we computed the variance and the two-point correlation functions of the positions of the tagged particles and showed that they exhibit interesting scaling forms depending on the observation time t. For instance, when the particles are interacting and $N \to \infty$, we found that the variance scales as $\sim t^{\nu}$ for $t \ll \tau_A$ (τ_A being the activity time scale) with exponent ν different than the non-interacting case. We calculated $\nu = \frac{3}{2}$ for RTP, $\nu = \frac{5}{2}$ for AOUP and $\nu = \frac{7}{2}$ $\left(= \frac{5}{2}\right)$ for x (y)-coordinate of ABP. The variance then crosses over to $\sim \sqrt{t}$ scaling for $t \gg \tau_A$ with the corresponding crossover function given in Eq. (6.37) for RTP, in Eq. (6.104) for AOUP and in Eqs. (6.136) and (6.137) for ABP. In addition, we also found that the equal and unequal time autocorrelation and cross-correlations obey interesting scaling forms in the appropriate limits of the observation time t. The associated scaling functions were rigorously derived in all cases. For future work, it would be interesting to develop fluctuating hydrodynamic frameworks for active models to study the single-file motion of tagged particles as done in [132]. Another interesting extension is to derive an effective time evolution equation for the position of a tagged particle. This will be useful in analysing how exactly the fluctuation-dissipation relation is broken in these models.

Chapter 8

Appendix

8.1 Equilibrium

In this section, we briefly discuss some features of an equilibrium system. Two important properties about a system in equilibrium are detailed balance and fluctuation-dissipation relation. While detailed balance is the statement about the probabilistic current balance between any two microscopic states, the fluctuation-dissipation relation tells how a system in equilibrium responds to a small external perturbation. In what follows, we discuss these two properites of an equilibrium system briefly. For concreteness, we present our analysis for a one dimensional diffusing particle whose position $x(t)$ evolves with time t as

$$\bar{\gamma}\frac{dx}{dt} = -\frac{dV(x)}{dx} + \sqrt{2D}\ \eta(t), \tag{8.1}$$

where $\bar{\gamma}$ is the friction coefficient, $V(x)$ is the confining potential and $D = \bar{\gamma}k_BT$ is the diffusion coefficient. Also, $\eta(t)$ is the Gaussian white noise with zero mean and delta correlation $\langle\eta(t)\eta(t')\rangle = \delta(t-t')$. For model (8.1), the probability to observe a trajectory $\{x(\tau)\}$ with $0 \le \tau \le t$ such that $x(0) = x_i$ and $x(t) = x_f$ is given by [21, 22]

$$P[\{x(\tau)\}] = \mathcal{N}e^{-\frac{1}{4D}\int_0^t d\tau\ [\bar{\gamma}\dot{x}+V'(x(\tau))]^2}. \tag{8.2}$$

Here $\mathcal{N}$ is the normalisation factor. Similarly, the probability to observe the time-reversed trajectory $\{\bar{x}(\tau)\}$ where $\bar{x}(\tau) = x(t-\tau)$ is [22]

$$P[\{\bar{x}(\tau)\}] = \mathcal{N} e^{-\frac{1}{4D}\int_0^t d\tau\ [-\bar{\gamma}\dot{x}+V'(x(\tau))]^2}. \tag{8.3}$$

Given these path probabilities, the equilibrium state satisfies the following conditions [11–16, 21–24]:

8.1.1 Detailed balance:

The first condition is the detailed balance condition which tells us about the time-reversibility between two states. To see this for the diffusion, let us take the ratio of two path probabilities in Eqs. (8.2) and (8.3) as

$$\frac{P[\{x(\tau)\}]}{P[\{\bar{x}(\tau)\}]} = e^{-\frac{1}{4D}\int_0^t d\tau\ 4\Gamma V'(x(\tau))\dot{x}}, \tag{8.4}$$

$$= e^{-\beta\left[V(x_f)-V(x_i)\right]}. \tag{8.5}$$

Identifying the steady-state distribution as $P_{st}(x) \propto e^{-V(x)/k_BT}$, it follows from Eq. (8.5) that

$$P_{st}(x_i)\ P[\{x(\tau)\}] = P_{st}(x_f)\ P[\{\bar{x}(\tau)\}]. \tag{8.6}$$

Next, we integrate over all intermediate $\{x(\tau)\}$ and get

$$P_{st}(x_i)\ W[x_f|x_i] = P_{st}(x_f)\ W[x_i|x_f], \tag{8.7}$$

where the quantity $W(x_a|x_b)$ defined as

$$W(x_a|x_b) = \int_{x(0)=x_b}^{x(t)=x_a} \mathcal{D}[x(\tau)]\ e^{-\frac{1}{4D}\int_0^t d\tau\ [\bar{\gamma}\dot{x}+V'(x(\tau))]^2}, \tag{8.8}$$

represents the transition probability distribution from position x_b to the position x_a. Eq. (8.7) implies that for diffusion, if the initial and the final states are drawn from the stationary distribution $P_{st}(x) \propto e^{-V(x)/k_BT}$, then the probabilities to observe a transition $x_i \to x_f$ and its time-reversed transition $x_f \to x_i$ are both same. This is the detailed balance condition. More generically, if $W(\Gamma_2|\Gamma_1)$ denotes the transition rate between two microscopic states Γ_1 and Γ_2 of a Markov process characterised by the steady-state distribution $P_{st}(\Gamma)$, then the detailed

balance condition is

$$P_{st}\left(\Gamma_1\right)\ W\left(\Gamma_2|\Gamma_1\right) = P_{st}\left(\mathcal{T}\ \Gamma_2\right)\ W\left(\mathcal{T}\ \Gamma_1|\mathcal{T}\ \Gamma_2\right), \tag{8.9}$$

where $\mathcal{T}$ is the time-reversal operator which inverts the time-sequence of the states and if the state involves velocities, changes the sign of the velocities.

Interestingly, the probabilities to observe a forward trajectory and its time-reversed trajectory are also related to the total entropy generated along a forward trajectory [21–23]. For a transition between states Γ_1 and Γ_2 in an infinitesimal time dt, the entropy generated can be formally written as

$$dS_{12} = k_B \log\left[\frac{P_{st}\left(\Gamma_1\right)\ W\left(\Gamma_2|\Gamma_1\right)}{P_{st}\left(\mathcal{T}\ \Gamma_2\right)\ W\left(\mathcal{T}\ \Gamma_1|\mathcal{T}\ \Gamma_2\right)}\right]. \tag{8.10}$$

Note that the detailed balance condition in Eq. (8.9) implies that no entropy is produced during a transition between two equilibrium states. Hence a non-zero value of dS_{12} is a clear signature of the departure from the equilibrium.

8.1.2 Fluctuation-dissipation relation:

Another property of an equilibrium system is the fluctuation-dissipation relation which tells how a system responds to a small external stimulus [14–16, 24, 25]. One of the early examples of this relation is the Einstein-Sutherland relation $D = \bar{\gamma} k_B T$ that relates the mobility $\bar{\gamma}$ of a diffusing particle to its diffusion coefficient D [17, 20]. Another example is the Kubo formula which gives the linear response of a system in thermal equilibrium to external perturbations in terms of the correlation functions in the unperturbed state [14]. Over the years, linear response has been studied in various cases that include Hamiltonian systems, open and chaotic systems, quantum systems, stochastic processes and random walks. We refer to [25, 227] for a detailed discussion on the response theory. Here, we briefly recall the central idea in the context of the diffusion [16].

Let us consider the Brownian motion in one dimension. At time $t = 0$, we turn on a small perturbation of the form $\epsilon f_p(t)$ with $\epsilon \to 0$. The time evolution equation then becomes

$$\bar{\gamma}\frac{dx}{dt} = -V'(x) + \sqrt{2D}\ \eta(t) + \epsilon f_p(t). \tag{8.11}$$

The effect of this perturbation on some observable $\mathcal{O}(x(t))$ up to linear order in ϵ can be written in terms of the response function $R(t,\tau)$ as

$$\langle \mathcal{O}(x(t))\rangle_\epsilon = \langle \mathcal{O}(x(t))\rangle_0 + \epsilon \int_0^t d\tau\ R(t,\tau) f_p(\tau), \tag{8.12}$$

from which the response function $R(t,\tau)$ follows to be

$$R(t,\tau) = \frac{\delta}{\delta\left[\epsilon f_p(\tau)\right]}\ \langle \mathcal{O}(x(t))\rangle_\epsilon \Big|_{\epsilon\to 0}. \tag{8.13}$$

Our aim is to calculate this response function for general observable $\mathcal{O}(x(t))$. To this aim, we first recall that the expectation of $\mathcal{O}(x(t))$ in presence of the perturbation reads

$$\langle \mathcal{O}(x(t))\rangle_\epsilon = \int \mathcal{D}[x(s)]\ \mathcal{O}(x(t))\ e^{-\frac{1}{4D}\int_0^t\ ds\ \left[\bar{\gamma}\dot{x}+V'(x(s))-\epsilon f_p(s)\right]^2}, \tag{8.14}$$

where $\langle..\rangle_\epsilon$ indicates average in presence of the perturbation. Taking the functional derivative like in Eq. (8.13) gives

$$R(t,\tau) = \frac{1}{2D}\langle \mathcal{O}(x(t))\left[\bar{\gamma}\dot{x}(\tau) + V'(x(\tau))\right]\rangle_0, \tag{8.15}$$

$$= \frac{\bar{\gamma}}{2D}\partial_\tau C(t,\tau) + \frac{1}{2D}\langle \mathcal{O}(x(t))V'(x(\tau))\rangle_0, \tag{8.16}$$

with $C(t,\tau) = \langle \mathcal{O}(x(t))x(\tau)\rangle_0$. At equilibrium, we anticipate this relation to obey the stationarity condition. This gives

$$R(t) = -\frac{\bar{\gamma}}{2D}\partial_t C(t) + \frac{1}{2D}\langle V'(x(0))\mathcal{O}(x(t))\rangle_0, \tag{8.17}$$

where we have used the short-hand notation $R(t) = R(t,0)$ and $C(t) = C(t,0)$. Next by changing $t \to -t$ in Eq. (8.17) and noting that the response function $R(-t) = 0$ (which follows from the causality condition as discussed in [16]), we get

$$\frac{\bar{\gamma}}{2D}\partial_t C(t) + \frac{1}{2D}\langle V'(x(t))\mathcal{O}(x(0))\rangle_0 = 0. \tag{8.18}$$

Adding Eqs. (8.17) and (8.18) gives

$$k_B T\ R(t) + \partial_t C(t) = \frac{k_B T}{4D}\left[\langle \mathcal{O}(x(t))V'(x(0))\rangle_0 - \langle \mathcal{O}(x(0))V'(x(t))\rangle_0\right]. \tag{8.19}$$

To calculate the right hand side of this equation, one can use the detailed balance condition in Eq. (8.7) and show

$$\langle \mathcal{O}(x(t))V'(x(0))\rangle_0 = \langle \mathcal{O}(x(0))V'(x(t))\rangle_0. \tag{8.20}$$

We refer to [16] for a proof of this relation. Finally, inserting this equation in Eq. (8.19), we get

$$k_B T\ R(t) = -\partial_t C(t), \quad \text{for } t > 0. \tag{8.21}$$

This is the celebrated fluctuation-dissipation relation which gives the response (up to linear order) of a system in thermal equilibrium to an external stimulus completely in terms of the equilibrium correlation functions. As clear from the derivation, this relation is valid only when the unperturbed state is an equilibrium state.

8.2 The propagator with an absorbing barrier at $x = M$

In this appendix, we derive and solve the master equations (2.2) satisfied by the propagators $P_\pm(x,t|0,\sigma_0)$ in presence of an absorbing boundary at $x = M$ (> 0). Let us consider the probability distribution $P_\sigma(x, t+\delta t|0,\sigma_0)$ for the particle to be at position x at time $t+\delta t$. This distribution gets contribution from two events: First, the particle was at position $(x - v_0\ \sigma\ \delta t)$ at time t with orientation σ and it did not flip σ in the interval $[t, t+\delta t]$, the probability of which is $(1-\gamma\delta t)$. Second, the particle was at position x at time t with orientation $-\sigma$ and it flips $\sigma \to -\sigma$ in the interval $[t, t+\delta t]$ whose probability is $\gamma\delta t$. Therefore, we have

$$P_\sigma(x, t+\delta t|0,\sigma_0) = (1-\gamma\delta t)P_\sigma(x - v_0\sigma\delta t, t|0,\sigma_0) + \gamma\delta t P_{-\sigma}(x,t|0,\sigma_0). \tag{8.22}$$

Expanding the propagator up to order $\sim \delta t$ and taking $\delta t \to 0$ limit gives the master equation (2.2) with $\sigma \in \{+,-\}$. Next, to solve these equations, we take Laplace transforms with respect to the time variable:

$$\bar{P}_\pm(x,s) = \int_0^\infty dt e^{-st} P_\pm(x,t). \tag{8.23}$$

which reduces Eqs. (2.2) to

$$\Big(v_0\partial_x+\gamma+s\Big)\bar{P}_+(x,s)=\ \gamma\bar{P}_-(x,s)+a_=\delta(x), \tag{8.24}$$

$$\Big(v_0\partial_x-\gamma-s\Big)\bar{P}_-(x,s)=-\gamma\bar{P}_+(x,s)+a_-\delta(x), \tag{8.25}$$

where the coefficients $a_\pm$ of the delta functions appear from the initial conditions $P_+(x,0|0,\sigma_0)=a_\pm\ \delta_{\sigma_0,\pm}\delta(x)$. For $x>0$, we can get rid of the $\delta(x)$ terms in Eqs.(8.24) and (8.25) and write

$$L_+\bar{P}_+(x,s)=\gamma\bar{P}_-(x,s),\ \text{with}\ \ L_+=\Big(v_0\partial_x+\gamma+s\Big), \tag{8.26}$$

and,

$$L_-\bar{P}_-(x,s)=-\gamma\bar{P}_+(x,s),\ \text{with}\ \ L_-=\Big(v_0\partial_x-\gamma-s\Big), \tag{8.27}$$

Multiplying both sides of Eqs. (8.26) and (8.27) by L_- and L_+ respectively, we obtain the following closed form equations:

$$\Big(v_0\partial_x-\gamma-s\Big)\Big(v_0\partial_x+\gamma+s\Big)\bar{P}_+(x,s)=-\gamma^2\bar{P}_+(x,s), \tag{8.28}$$

$$\Big(v_0\partial_x+\gamma+s\Big)\Big(v_0\partial_x-\gamma-s\Big)\bar{P}_-(x,s)=-\gamma^2\bar{P}_-(x,s). \tag{8.29}$$

To solve these equations, we try the solution $\bar{P}_+\sim e^{\beta x}$ and put this in Eq.(8.28) which gives $\beta=\pm\lambda(s)$ where $\lambda(s)=\frac{1}{v_0}\sqrt{s(2\gamma+s)}$. We then plug this solution in Eq.(8.26) to obtain the solution for $\bar{P}_-$. Finally, we get

$$\bar{P}_+(x,s)=\begin{cases}Ae^{\lambda(s)x}+Be^{-\lambda(s)x}, & \text{if } 0<x<M\\ Ce^{\lambda(s)x}, & \text{if } -\infty<x<0\end{cases} \tag{8.30}$$

$$\bar{P}_-(x,s)=\frac{1}{\gamma}\begin{cases}A(v_0\lambda(s)+\gamma+s)e^{\lambda(s)x}+B(-v_0\lambda(s)+\gamma+s)e^{-\lambda(s)x}, & \text{if } 0<x<M\\ C(v_0\lambda(s)+\gamma+s)e^{\lambda(s)x}, & \text{if } -\infty<x<0\end{cases} \tag{8.31}$$

where A, B and C are still unknown constants that need to be determined. For this, we integrate both sides of Eqs.(8.24) and (8.25) from $x=-\epsilon$ to $x=+\epsilon$ with $\epsilon\to 0^+$ to obtain the

discontinuity equations

$$\bar{P}_+(x \to 0^+, s) - \bar{P}_+(x \to 0^-, s) = \frac{a_+}{v_0}, \tag{8.32}$$

$$\bar{P}_-(x \to 0^+, s) - \bar{P}_-(x \to 0^-, s) = -\frac{a_-}{v_0}. \tag{8.33}$$

Another equation comes from the boundary condition $P_-(M,t) = 0$ in Eq. (2.4) which in the Laplace domain becomes

$$\bar{P}_-(M, s) = 0. \tag{8.34}$$

Next, we plug the solutions from Eqs. (8.30) and (8.31) in Eqs. (8.32), (8.33) and (8.34) to get three linear equations for the constants $A,\ B$ and C. Solving these equations yield the constants in terms of $s,\ \gamma,\ v_0$ for different choices of $a_\pm$. For example, when the RTP starts with $+v_0$ initially, then $a_+ = 1$ and $a_- = 0$. For this choice, we find

$$A(s) = -\frac{s + \gamma - v_0\lambda(s)}{2v_0^2\lambda(s)} e^{-2M\lambda(s)}, \tag{8.35}$$

$$B(s) = \frac{s + \gamma + v_0\lambda(s)}{2v_0^2\lambda(s)}, \quad \text{and,} \tag{8.36}$$

$$C(s) = \frac{s + \gamma - v_0\lambda(s)}{2v_0^2\lambda(s)} \Big(1 - e^{-2M\lambda(s)}\Big). \tag{8.37}$$

Using these expressions of the constants in Eqs. (8.30) and (8.31)

$$\bar{P}_+(x, s|0, +) = \frac{1}{2v_0^2\lambda(s)} \begin{cases} (s + \gamma + v_0\lambda(s))e^{-\lambda(s)x} - (s + \gamma - v_0\lambda(s))e^{\lambda(s)(x-2M)}, \\ \qquad\qquad \text{if } 0 < x < M \\ (s + \gamma - v_0\lambda(s))\Big(e^{\lambda(s)x} - e^{\lambda(s)(x-2M)}\Big), \\ \qquad\qquad \text{if } -\infty < x < 0 \end{cases} \tag{8.38}$$

$$\bar{P}_-(x, s|0, +) = \frac{\gamma}{2v_0^2\lambda(s)} e^{\lambda(s)|x|} - e^{\lambda(s)(x-2M)}. \tag{8.39}$$

Similarly, when the particle starts with $-v_0$ velocity, then $a_+ = 0$ and $a_- = 1$ and we get

$$\bar{P}_+(x,s|0,-) = \frac{\gamma}{2v_0^2\lambda(s)}\left(e^{-\lambda(s)|x|} - \frac{s+\gamma-v_0\lambda(s)}{s+\gamma+v_0\lambda(s)}\right)e^{\lambda(s)(x-2M)} \tag{8.40}$$

$$\bar{P}_-(x,s|0,-) = \frac{1}{2v_0^2\lambda(s)}\begin{cases} (s+\gamma-v_0\lambda(s))e^{-\lambda(s)x} - (s+\gamma-v_0\lambda(s)) & e^{\lambda(s)(x-2M)}, \\ & \text{if } 0<x<M \\ (s+\gamma+v_0\lambda(s))e^{\lambda(s)x} - (s+\gamma-v_0\lambda(s)) & e^{\lambda(s)(x-2M)}, \\ & \text{if } -\infty<x<0. \end{cases} \tag{8.41}$$

So far, we have obtained the exact form of the propagators corresponding to different initial conditions in terms of the Laplace variables s. To get the solutions in time domain, one need to perform inverse Laplace transforms $\bar{P}_\pm(x,s|0,\pm)$. Looking at the expressions in Eqs. (8.38-8.41), we need to know the following inverse Laplace transforms [210]

$$L^{-1}_{s\to t}\left[\frac{1}{\lambda(s)}e^{-g\lambda(s)}\right] = ve^{-\gamma t}I_0\left(\frac{\gamma}{v}\sqrt{v^2t^2-g^2}\right)\Theta(vt-g) \tag{8.42}$$

$$\begin{aligned} L^{-1}_{s\to t}\left[\frac{s+\gamma+\alpha\ v\lambda(s)}{\lambda(s)}e^{-\lambda(s)g}\right] &= \gamma v e^{-\gamma t}\sqrt{\frac{vt-g}{vt+g}}I_1\left(\frac{\gamma}{v}\sqrt{v^2t^2-g^2}\right)\Theta(vt-g) \\ &\quad - \frac{1+\alpha}{2}v^2\frac{d}{dg}\left[\Theta(vt-g)I_0\left(\frac{\gamma}{v}\sqrt{v^2t^2-g^2}\right)\right], \quad \text{for} \quad \alpha=\pm 1, \end{aligned} \tag{8.43}$$

$$\begin{aligned} L^{-1}_{s\to t}\left[(s+\gamma-v\lambda(s))e^{-\lambda(s)g}\right] &= \frac{\gamma v\ e^{-\gamma t}}{vt-g}\left[\frac{\gamma g}{v}I_0\left(\frac{\gamma}{v}\sqrt{v^2t^2-g^2}\right)\right. \\ &\quad \left. + \sqrt{\frac{vt-g}{vt+g}}I_1\left(\frac{\gamma}{v}\sqrt{v^2t^2-g^2}\right)\right]\Theta(vt-g). \end{aligned} \tag{8.44}$$

Inserting these inverse Laplace transforms in Eqs. (8.38-8.41), we arrive at the expressions of the propagators quoted in Eqs. (2.5-2.8).

8.3 Derivation of backward master equations for $S_\pm(x_0,t)$

In this appendix, we derive the backward master equations (2.13) and (2.14) satisfied by the survival probabilities $S_\pm(x_0,t)$. Let us first recall that $S_\sigma(x_0,t+dt)$ is the probability that the RTP with initial velocity direction σ survives from the absorbing wall at $x=0$ till time $t+dt$. We can break the entire trajectory into two parts: (i) $[0,dt]$ and (ii) $[dt,t+dt]$. In the first interval, the particle can do two things: (a) without changing σ, the particle moves to the new position $(x_0+\sigma v_0 dt)$ with probability $1-\gamma dt$ or (b) it changes its velocity direction from σ to $-\sigma$ and moves to the position $(x_0-\sigma v_0 dt)$ with probability γdt. After time dt, the RTP

survives the absorbing wall with the probability $S_\sigma(x_0 + \sigma v_0 dt, t)$ if event (a) occurs, and with probability $S_{-\sigma}(x_0 - \sigma v_0 dt, t)$ if event (b) occurs. Adding all these contributions, we get

$$S_\sigma(x_0, t + dt) = (1 - \gamma dt)\ S_\sigma(x_0 + \sigma v_0 dt, t) + \gamma dt\ S_{-\sigma}(x_0 - \sigma v_0 dt, t). \tag{8.45}$$

Performing Taylor's expansion for small dt, we get the following backward master equations:

$$\partial_t S_+(x_0, t) = v_0 \partial_{x_0} S_+(x_0, t) - \gamma S_+(x_0, t) + \gamma S_-(x_0, t), \tag{8.46}$$

$$\partial_t S_-(x_0, t) = -v_0 \partial_{x_0} S_-(x_0, t) + \gamma S_+(x_0, t) - \gamma S_-(x_0, t). \tag{8.47}$$

8.4 Proof of the identity

Here we prove the identity

$$\gamma \int_0^t dt' h(t - t') h(t') \stackrel{?}{=} 2[1 - h(t)]. \tag{8.48}$$

where $h(t) = e^{-\gamma t}[I_0(\gamma t) + I_1(\gamma t)]$. To prove this identity, we take Laplace transformation of the left hand side with respect to t and use its convolution form as follows:

$$\text{Laplace Transform}\left[\gamma \int_0^t dt' h(t - t') h(t')\right] = \gamma \tilde{h}(s)^2. \tag{8.49}$$

where $\tilde{h}(s)$ denotes the Laplace transform of $h(t)$ and is given by

$$\tilde{h}(s) = \text{Laplace Transform}[h(t)] = \frac{1}{\gamma}\left(\frac{\sqrt{s(2\gamma + s)}}{s} - 1\right). \tag{8.50}$$

Plugging this result in Eq. (8.49) and performing some algebraic simplifications, we get

$$\text{Laplace Transform}\left[\gamma \int_0^t dt' h(t - t') h(t')\right] = 2\left[\frac{1}{s} - \frac{1}{\gamma}\left(\frac{\sqrt{s(2\gamma + s)}}{s} - 1\right)\right]. \tag{8.51}$$

Finally, we perform the inverse Laplace transform on both sides with respect to s to get the identity in Eq. (8.48).

8.5 Probability distribution of t_m for general initial condition

In section (2.3.2), we derived the probability distribution of time t_m taken by the RTP to reach maximum M within the time duration $[0, t]$ given it was at the origin initially with velocity $\pm v_0$ chosen with equal probability, i.e. $a_+ = a_- = 1/2$. Herein, we extend this derivation to the asymmetric inital condition whereby it initially chooses $\pm v_0$ with different probabilities ($a_+ \neq a_-$). To this aim, we use the expressions for $P_\pm(M-\epsilon, t_m|0, \pm)$ obtained in section (2.1) to write $p_\pm(M-\epsilon, t_m|0) = a_+ P_\pm(M-\epsilon, t_m|0, +) + a_- P_\pm(M-\epsilon, t_m|0, -)$ for general initial conditions. After some simplifications, the expressions for $p_\pm(M-\epsilon, t_m|0, 0)$ read as,

$$\left.\begin{aligned} p_+(M-\epsilon, t_m|0) &\approx -\frac{d}{dM}\left[\Theta(v_0 t_m - M)\; g^{as}(M, t_m)\right] + O(\epsilon)\,, \\ p_-(M-\epsilon, t_m|0) &\approx -\frac{\gamma\,\epsilon}{v_0}\frac{d}{dM}\left[\Theta(v_0 t_m - M) g^{as}(M, t_m)\right] + O(\epsilon^2), \end{aligned}\right\} \tag{8.52}$$

where the function $g(M, t)$ in Eq. (2.21) is now changed to

$$g^{as}(M, t) = e^{-\gamma t}\left[a_+ I_0\left(\frac{\gamma}{v_0}\sqrt{v_0^2 t^2 - M^2}\right) + a_-\sqrt{\frac{v_0 t - M}{v_0 t + M}} I_1\left(\frac{\gamma}{v_0}\sqrt{v_0^2 t^2 - M^2}\right)\right]. \tag{8.53}$$

Inserting these expressions in Eq. (2.18), we get the part of the joint distribution $\mathcal{P}^{as}(M, t_m, t)$ of M and t_m for $0 < M < v_0 t$ and $0 < t_m < t$. Here the superscript 'as' in $\mathcal{P}^{as}(M, t_m, t)$ denotes the asymmetric initial condition. Note that the joint distribution thus obtained is valid only for $0 < t_m < t$. We now have to get the contributions from $t_m = 0$ and $t_m = t$. As seen for symmetric case, the contributions to $t_m = 0$ come from those events where the particle starts with $-v_0$ initially and stays on the negative side of the origin till duration t. Clearly, for such events $M = 0$. Consequently, we get

$$\underbrace{\mathcal{P}^{as}(M, t_m, t)}_{\text{contribution from paths with } t_m=0} = \delta(t_m)\delta(M) a_- h(t). \tag{8.54}$$

On the other hand the contributions to $t_m = t$ event come from events where the particle achieves its maximum at time $t_m = t$. Generalising Eq. (2.23) straightforwardly for general initial conditions, we find this contribution to be

$$\underbrace{\mathcal{P}^{as}(M, t_m, t)}_{\text{contribution from paths with } t_m=t} = \delta(t_m - t)\; [a_+ P_+(M, t|0, +) + a_- P_+(M, t|0, -)]. \tag{8.55}$$

Plugging the expressions of the propagators $P_+(M,t|0,\pm)$ from Eqs. (2.6) and (2.8) gives

$$\underbrace{\mathcal{P}^{as}(M,t_m,t)}_{\text{contribution from paths with } t_m=t} = -\frac{d}{dM}\left[\Theta(v_0 t - M)\; g^{as}(M,t)\right], \tag{8.56}$$

Finally adding all the three contributions and fixing the normalisation gives the exact form of the joint distribution $\mathcal{P}^{as}(M,t_m,t)$. Marginalising $\mathcal{P}^{as}(M,t_m,t)$ for t_m yields

$$\begin{aligned} P_M^{as}(t_m,t) &= \int_0^{vt} dM\; \mathcal{P}^{as}(M,t_m,t), \\ &= a_- h(t)\delta(t_m) + h^{as}(t)\delta(t-t_m) + \gamma h(t-t_m)h^{as}(t_m), \end{aligned} \tag{8.57}$$

where $h^{as}(t) = e^{-\gamma t}[aI_0(\gamma t) + bI_1(\gamma t)]$. Note that for $a_+ = a_- = \frac{1}{2}$, $h^{as}(t) = \frac{h(t)}{2}$ and Eq. (8.57) and we recover the results for symmetric case in Eq. (2.34). Also observe that for $a_+ \neq a_-$, the joint distribution $P_M^{as}(t_m,t)$ is different from Eq. (2.34).

8.6 Backward master equation for functional $Y\left[x\left(t\right)\right]$

Here we provide a derivation of the backward master equations which is useful in computing the statistics of a general functional $Y\left[x\left(t\right)\right]$

$$Y\left[x\left(t\right)\right] = \int_0^t d\tau\; U\left[x\left(\tau\right)\right], \tag{8.58}$$

where $\{x(\tau);\; 0 \leq \tau \leq t\}$ represents the trajectory of an one dimensional RTP of fixed duration t initially located at position x_0 and with initial orientation σ_0 that can take values ± 1. Let $P^{\sigma_0}(Y,x_0,t)$ be the probability density of Y. Then the corresponding characteristic function is given by

$$Q^{\sigma_0}(p,x_0,t) = \int_0^\infty dY e^{-pY} P^{\sigma_0}\left(Y,x_0,t\right) = \left\langle e^{-pY}\right\rangle_{(x_0,\sigma_0)}, \tag{8.59}$$

where $\langle ... \rangle_{(x_0,\sigma)}$ denotes the average over trajectories with initial position x_0 and velocity orientation σ. For a small time interval $[t, t+\delta t]$, we have

$$\begin{aligned} Q^{\sigma_0}(p, x_0, t+\delta t) &= \left\langle e^{-p\int_0^{t+\delta t} d\tau U[x(\tau)]} \right\rangle_{(x_0,\sigma_0)} \\ &= \left\langle e^{-p\int_0^{\delta t} d\tau U[x(\tau)]} e^{-p\int_{\delta t}^{t+\delta t} d\tau U[x(\tau)]} \right\rangle_{(x_0,\sigma_0)} \\ &= (1 - pU(x_0)\delta t) \left\langle e^{-p\int_{\delta t}^{t+\delta t} d\tau U[x(\tau)]} \right\rangle_{(x_0,\sigma_0)}. \end{aligned} \tag{8.60}$$

where (x_0, σ_0) is the initial configuration. In small time interval δt, the state (x_0, σ_0) of the RTP can change to $(x_0 + \sigma_0 v_0 \delta t, \sigma_0)$ with probability $(1 - \gamma\delta t)$ and to $(x_0 - \sigma_0 v_0 \delta t, -\sigma_0)$ with probability $\gamma\delta t$. We can write Eq.(8.60) as following:

$$\begin{aligned} Q^{\sigma_0}(p, x_0, t+\Delta t) = [1 - pU(x_0)\delta t] \Big[&(1-\gamma\delta t) \langle e^{-p\int_{\delta t}^{t+\delta t} d\tau U[x(\tau)]} \rangle_{(x_0+\sigma_0 v_0 \delta t, \sigma_0)} \\ &+ \gamma\delta t \left\langle e^{-p\int_{\delta t}^{t+\delta t} d\tau U[x(\tau)]} \right\rangle_{(x_0-\sigma_0 v_0\delta t, -\sigma_0)} \Big] \end{aligned} \tag{8.61}$$

$$= (1 - pU(x_0)\delta t) \left[(1-\gamma\delta t)\, Q^{\sigma_0}(p, x_0 + \sigma_0 v_0 \delta t, t) + \gamma\delta t Q^{-\sigma_0}(p, x_0, t) \right]. \tag{8.62}$$

Taking the $\delta t \to 0$ limit we obtain

$$\partial_t Q^{\sigma_0}(p, x_0, t) = \sigma_0 v_0 \partial_{x_0} Q^{\sigma_0}(p, x_0, t) - \gamma Q^{\sigma_0}(p, x_0, t) + \gamma Q^{-\sigma_0}(p, x_0, t) - pU(x_0) Q^{\sigma_0}(p, x_0, t). \tag{8.63}$$

For residence time t_r, we choose $U(x) = \Theta(x)$ and then Eq. (8.63) reduces to the backward master equations for t_r in Eqs.(2.35) and (2.36).

On the other hand, for $T_{2\epsilon}$ in Eq. (5.4), we have $U(x) = \mathbb{I}_\epsilon(x)$ and Eq. (8.63) reduces reduces to the backward master equations (5.6) with p replaced by q and $Q^{\sigma_0}(p, x_0, t)$ replaced by $H_{\sigma_0}(q, x_0, t)$.

8.7 Probability distribution for residence time t_r for general initial condition

In Sec. (2.4), we derived the distribution of the residence time t_r for symmetric initial condition where RTP initially chooses velocity $\pm v_0$ with equal probability 1/2. Herein we extend this

calculation for asymmetric initial condition for which we assume that the particle starts with $\pm v_0$ velocity with probability $a_\pm$ such that $a_+ + a_- = 1$. Let us denote the distribution of t_r by $P_R^{as}(t_r, t)$ and its double Laplace transform by $\tilde{Q}^{as}(p, s)$. Here 'as' in the superscript stands for asymmetric initial condition. Using the results in Eqs. (2.52) and (2.53) for this case, we have

$$\begin{aligned}\tilde{Q}^{as}(p,s) &= a_+\tilde{Q}_+(p,0,s) + a_-\tilde{Q}_-(p,0,s),\\ &= -\frac{1}{2\gamma}\left(1 - \frac{\lambda_0\lambda_p}{s(s+p)}\right) - \frac{a_+ - a_-}{2\gamma}\left(\frac{\lambda_0}{s} - \frac{\lambda_p}{s+p}\right).\end{aligned} \tag{8.64}$$

Now to get the distribution $P_R^{as}(t_r, t)$, we have to perform double inverse Laplace transformation. Comparing this expression with that of the symmetric case, we first observe that the first term in the right hand side of Eq. (8.64) is identical to Eq. (2.56). The inverse Laplace transformation of this term is given in Eq. (2.56). On the other hand, to invert second term, we use Eq. (2.55). Therefore the overall expression is given by

$$P_R^{as}(t_r, t) = h(t)\Big[a_-\delta(t_r) + a_+\delta(t_r - t)\Big] + \frac{\gamma}{2}h(t_r)h(t - t_r). \tag{8.65}$$

For $a_+ = a_- = \frac{1}{2}$, we recover the results for symmetric case in Eq. (2.56). Also note that asymmetry only changes the weights of the delta functions but does not alter the non-delta function part.

8.8 Derivation of $\bar{\mathcal{P}}\,(\xi, k^*|n)$ in Eq. (3.32)

Here, we provide a detailed derivation of the Fourier transform $\bar{\mathcal{P}}\,(\xi, k^*|n)$ in Eq. (3.32) which was instrumental in calculating the mean area of the convex hull in the fixed-n ensemble. To this end, we first write the expression of this Fourier-transform as

$$\bar{\mathcal{P}}\,(\xi, k^*|n) = \int_{-\infty}^{\infty} dY e^{i\xi Y} \int_0^{\infty} dM\ \mathscr{P}(M, Y, k^*|n). \tag{8.66}$$

Plugging $\mathscr{P}(M, Y, k^*|n)$ from Eq. (3.29), the Fourier transform can be rewritten as

$$\bar{\mathcal{P}}\,(\xi, k^*|n) = \int_0^{\infty} dM\ I_{\rm left}(M, \xi, k^*)\ I_{\rm right}(M, k^*, n), \tag{8.67}$$

with the functions $I_{\rm right}(M,k^*,n)$ and $I_{\rm left}(M,\xi,k^*)$ defined as

$$I_{\rm left}(M,\xi,k^*) = \int \prod_{i=1}^{k^*} dx_i\, \tilde{p}(x_i,\xi) \prod_{i=1}^{k^*-1} \Theta\left(M - \sum_{j=1}^{i} x_j\right) \delta\left(M - \sum_{j=1}^{k^*} x_j\right) , \tag{8.68}$$

$$I_{\rm right}(M,k^*,n) = \int \prod_{i=k^*+1}^{N} dy_i\, dx_i\, p(x_i,y_i)\, \Theta\left(M - \sum_{j=1}^{i} x_j\right) , \tag{8.69}$$

$$\text{with} \qquad \tilde{p}(x,\xi) = \int_{-\infty}^{\infty} dy e^{i\xi y} p(x,y)\,. \tag{8.70}$$

Let us first simplify the intergral $I_{\rm right}(M,k^*,n)$. By noting that $M = \sum_{i=1}^{k^*} x_i$ and $p_1(x) = \int_{-\infty}^{\infty} dy\; p(x,y)$, we have

$$I_{\rm right}(M,k^*,n) = \int \left[\prod_{i=k^*+1}^{n} dx_i p_1(x_i)\right] \prod_{i=k^*+1}^{n} \Theta\left(-\sum_{j=k^*+1}^{i} x_j\right) \tag{8.71}$$

Physically, this integral represents the probability that a random walker with identical and independent increments drawn from the symmetric and continuous probability distribution $p_1(x)$ remains below origin in $n-k^*$ time-steps given that it was initially at the origin. The Sparre-Andersen theorem tells that this (survival) probability is independent of $p_1(x)$ and is given by q_{n-k^*} where $q_n = \binom{2n}{n} 2^{-2n}$ [183]. Therefore

$$I_{\rm right}(M,k^*,n) = q_{n-k^*}\,. \tag{8.72}$$

Let us now look at the other term $I_{\rm left}(M,\xi,k^*)$ in the Fourier transform in Eq. (8.67). In Eq. (8.68), we first rewrite $\tilde{p}(x,\xi)$ as

$$\tilde{p}(x,\xi) = \frac{\tilde{p}(x,\xi)}{\int_{-\infty}^{\infty} dx\, \tilde{p}(x,\xi)} \times \tilde{p}_2(\xi) = f(x,\xi)\, \tilde{p}_2(\xi), \quad \text{with} \tag{8.73}$$

$$f(x,\xi) = \frac{\tilde{p}(x,\xi)}{\int_{-\infty}^{\infty} dx\, \tilde{p}(x,\xi)}, \text{ and } \tilde{p}_2(\xi) = \int_{-\infty}^{\infty} dx\, \tilde{p}(x,\xi). \tag{8.74}$$

Plugging this in Eq. (8.68), we get

$$I_{\rm left}(M,\xi,k^*) = [\tilde{p}_2(\xi)]^{k^*} \int \prod_{i=1}^{k^*} dx_i\, f(x_i,\xi) \prod_{i=1}^{k^*-1} \Theta\left(M - \sum_{j=1}^{i} x_j\right) \delta\left(M - \sum_{j=1}^{k^*} x_j\right). \tag{8.75}$$

With these simplifications, the Fourier transform $\bar{P}(\xi, k^*|n)$ in Eq. (8.67) becomes

$$\bar{P}(\xi, k^*|n) = q_{n-k^*} \, [\tilde{p}_2(\xi)]^{k^*} \int \left[\prod_{i=1}^{k^*} dx_i \, f(x_i, \xi) \right] \prod_{i=1}^{k^*} \Theta \left(\sum_{j=1}^{i} x_{k^*+1-j} \right) \tag{8.76}$$

Note that the function $f(x, \xi)$ in Eq. (8.74) is a symmetric and continuous function of x which is normalised to unity. Hence, it can be interpreted as a distribution of x parametrised by ξ. With this interpretation, the k^*-fold integral in Eq. (8.76) simply represents the Sparre-Andersen survival probability of a random walker with k^* steps. As mentioned before, this probability is given $q_{k^*} = \binom{2k^*}{k^*} 2^{-2k^*}$ Therefore, the final expression of $\bar{P}(\xi, k^*|n)$ reads

$$\bar{P}(\xi, k^*|n) = q_{k^*} \, q_{n-k^*} \, [\tilde{p}_2(\xi)]^{k^*} \, . \tag{8.77}$$

8.9 Proof $\mathcal{S}_n \simeq \pi n$ as $n \to \infty$

Here, we show that the term $\mathcal{S}_n$ in Eq. (3.26) becomes $\mathcal{S}_n \simeq \pi n$ for larger values of n. To this end, we cange the variable $m = zn$ in Eq. (3.26) and rewrite it as

$$\mathcal{S}_n = \frac{\sqrt{\pi}}{\sigma} \sum_{z=1/n}^{(n-1)/n} \frac{\Gamma\left(\frac{n(1-z)+1}{2}\right)}{\Gamma\left(\frac{n(1-z)+2}{2}\right)} \, \langle M_{nz} \rangle. \tag{8.78}$$

Note that $z \in \{\frac{1}{n}, \frac{2}{n}, ..., \frac{n-1}{n}\}$. For large n, we change the summation in Eq. (8.78) to integration as $\sum_{z=1/n}^{(n-1)/n} \to n \int_0^1 dz$ and rewrite it as

$$\mathcal{S}_n \simeq \frac{\sqrt{\pi}}{\sigma} n \int_0^1 dz \frac{\Gamma\left(\frac{n(1-z)+1}{2}\right)}{\Gamma\left(\frac{n(1-z)+2}{2}\right)} \, \langle M_{nz} \rangle, \qquad \text{as } n \to \infty. \tag{8.79}$$

We next use the result of [178] to write $\langle M_{nz} \rangle$ for large n as $\langle M_{nz} \rangle \simeq \sigma \sqrt{\frac{2zn}{\pi}}$. In addition, we approximate $\frac{\Gamma\left(\frac{n(1-z)+1}{2}\right)}{\Gamma\left(\frac{n(1-z)+2}{2}\right)} \simeq \sqrt{\frac{2}{n(1-z)}}$ as $n \to \infty$. Inserting these forms in Eq. (8.79) and performing the integration over z, we get

$$\mathcal{S}_n \simeq \pi n, \qquad \text{as } n \to \infty. \tag{8.80}$$

8.10 Derivation of the approximate expression of $P(x,t)$ given in Eq. (4.20) for $\alpha = 0$ at large t

8.10.1 $\Delta \geq 0$

We here provide a detailed derivation of the large-t expression of the distribution $P(x,t)$ which was written in Eq. (4.20). For this, we consider the exact expression Eq. (4.19) and change the time integral by $\int_0^t = \int_0^\infty - \int_t^\infty$. This gives

$$\begin{aligned} P(x,t) &= \frac{1}{2}e^{-\gamma_1 t}\delta(\mid x \mid -v_0 t) + \frac{\gamma_1}{2v_0}\left(1+\frac{\gamma_2 \mid x \mid}{2v_0}\right)e^{-\frac{\gamma_1|x|}{2v_0}}\Theta\left(v_0 t - \mid x \mid\right) \\ &- \frac{\sqrt{\gamma_1\gamma_2}}{2v_0}\int_0^\infty d\tau\ e^{-\gamma\tau}\ \frac{d\,\mathcal{I}(\mid x \mid,\tau)}{d \mid x \mid}\Theta\left(v_0\tau - \mid x \mid\right) \\ &+ \frac{\sqrt{\gamma_1\gamma_2}}{2v_0}\int_t^\infty d\tau\ e^{-\gamma\tau}\ \frac{d\,\mathcal{I}(\mid x \mid,\tau)}{d \mid x \mid}\Theta\left(v_0\tau - \mid x \mid\right). \end{aligned} \tag{8.81}$$

Now the particle attains a stationary distribution as $t \to \infty$. Also at large times, the coefficient of the δ-functions decay exponentially. Hence for large t, we get

$$P(x,t) - P_0^{st}(x) \simeq \frac{\sqrt{\gamma_1\gamma_2}}{2v_0}\int_t^\infty d\tau\ e^{-\gamma\tau}\ \frac{d\,\mathcal{I}(\mid x \mid,\tau)}{d \mid x \mid}. \tag{8.82}$$

Recall that $\mathcal{I}(x,t) = \frac{xe^{-\frac{\Delta x}{v_0}}}{v_0}\frac{I_1\left(\sqrt{\gamma_1\gamma_2(t^2-\frac{x^2}{v_0^2})}\right)}{\sqrt{t^2-\frac{x^2}{v_0^2}}}$ with I_1 being the modified Bessel function of first kind. Since t is large, the variable τ inside the integral in Eq. (8.82) is also large. This enables us to use the asymptotic form of the Bessel function as $I_\nu(z) \simeq \frac{e^z}{\sqrt{2\pi z}}$ for large z. For $v_0 t >> |x|$ alongwith the aforementioned approximations, we change the variable $\tau = tw$ to get

$$P(x,t) - P_0^{st}(x) \simeq \mathcal{C}_1\int_1^\infty dw\frac{e^{-t\left(\mathcal{C}_2 w + \frac{\mathcal{C}_3}{w}\right)}}{w^{3/2}}\left(1 - \frac{\Delta|x|}{v_0} - \frac{x^2\sqrt{\gamma_1\gamma_2}}{v_0^2 t w}\right), \tag{8.83}$$

where we have used the notation $\mathcal{C}_1 = \frac{(\gamma_1\gamma_2)^{1/4}}{2v_0\sqrt{2\pi t}}e^{-\frac{\Delta|x|}{v_0}}$, $\mathcal{C}_2 = \gamma - \sqrt{\gamma_1\gamma_2}$ and $\mathcal{C}_3 = \frac{x^2\sqrt{\gamma_1\gamma_2}}{2v_0^2 t^2}$. To obtain the distribution, we need the following integrals:

$$\int_1^\infty dw\frac{e^{-t\left(\mathcal{C}_2 w + \frac{\mathcal{C}_3}{w}\right)}}{w^{3/2}} = \sqrt{\frac{\pi}{\mathcal{C}_3 t}}e^{-2t\sqrt{\mathcal{C}_2\mathcal{C}_3}} - Z_{3/2}, \tag{8.84}$$

$$\int_1^\infty dw\frac{e^{-t\left(\mathcal{C}_2 w + \frac{\mathcal{C}_3}{w}\right)}}{w^{5/2}} = \frac{1}{2}\sqrt{\frac{\pi}{(\mathcal{C}_3 t)^3}}\left(1 + 2t\sqrt{\mathcal{C}_2\mathcal{C}_3}\right)e^{-2t\sqrt{\mathcal{C}_2\mathcal{C}_3}} - Z_{5/2} \tag{8.85}$$

where the term Z_μ is defined as,

$$Z_\mu = \int_0^1 dw \frac{e^{-t\left(\mathcal{C}_2 w + \frac{\mathcal{C}_3}{w}\right)}}{w^\mu} \tag{8.86}$$

Now the integral $Z_{1/2}$ can be easily performed to be

$$Z_{1/2} = \frac{1}{2}\sqrt{\frac{\pi}{\mathcal{C}_2 t}} e^{-2t\sqrt{\mathcal{C}_2\mathcal{C}_3}} \left[1 + \mathrm{Erf}\left(\sqrt{t\mathcal{C}_2} - \sqrt{t\mathcal{C}_3}\right) - e^{4t\sqrt{\mathcal{C}_2\mathcal{C}_3}}\ \mathrm{Erfc}\left(\sqrt{t\mathcal{C}_2} + \sqrt{t\mathcal{C}_3}\right)\right]. \tag{8.87}$$

From this, the integrals $Z_{3/2}$ and $Z_{5/2}$ follow to be $Z_{3/2} = -\frac{d}{d\mathcal{C}_3} Z_{1/2}$ and $Z_{5/2} = -\frac{d}{d\mathcal{C}_3} Z_{3/2}$. Finally, we obtain

$$\begin{aligned}
Z_{3/2} &= \frac{1}{2}\sqrt{\frac{\pi}{\mathcal{C}_3 t}} e^{-2t\sqrt{\mathcal{C}_2\mathcal{C}_3}} \left[2 - \mathrm{Erfc}\left(\sqrt{t\mathcal{C}_2} - \sqrt{t\mathcal{C}_3}\right) + e^{4t\sqrt{\mathcal{C}_2\mathcal{C}_3}}\ \mathrm{Erfc}\left(\sqrt{t\mathcal{C}_2} + \sqrt{t\mathcal{C}_3}\right)\right], \\
Z_{5/2} &= \frac{1}{2}\sqrt{\frac{\pi}{(\mathcal{C}_3 t)^3}} e^{-2t\sqrt{\mathcal{C}_2\mathcal{C}_3}} \left[1 + 2t\sqrt{\mathcal{C}_2\mathcal{C}_3} - \frac{1}{2}\left(1 + 2t\sqrt{\mathcal{C}_2\mathcal{C}_3}\right) \mathrm{Erfc}\left(\sqrt{t\mathcal{C}_2} - \sqrt{t\mathcal{C}_3}\right)\right. \\
&\quad \left. + \frac{1}{2}\left(1 - 2t\sqrt{\mathcal{C}_2\mathcal{C}_3}\right) e^{4t\sqrt{\mathcal{C}_2\mathcal{C}_3}}\ \mathrm{Erfc}\left(\sqrt{t\mathcal{C}_2} + \sqrt{t\mathcal{C}_3}\right)\right] + \frac{1}{\mathcal{C}_3 t} e^{-t(\mathcal{C}_2 + \mathcal{C}_3)}.
\end{aligned} \tag{8.88}$$

We have now all terms required to evaluate the integrals in Eqs. (8.84) and (8.85). Then plugging these integrals in Eq. (8.83), we obtain the result in Eq. (4.20) valid for large t. This derivation can also be used to evaluate the asymptotic form for $\gamma_1 = \gamma_2$.

8.10.2 $\Delta < 0$

After obtaining $P(x,t)$ for $\Delta > 0$, we now proceed to calculate the approximate expression of $P(x,t)$ for $\Delta \leq 0$. To this end, we perform the Bromwich integration of the Laplace transform $\bar{P}(x,s)$ in Eq. (4.16) as

$$P(x,t) = \frac{e^{-t\Delta\bar{x}}}{2\pi i} \int_{\gamma_0 - i\infty}^{\gamma_0 + i\infty} ds \left(\frac{\lambda(s) + \Delta}{2s}\right) e^{t\phi(s)}, \tag{8.89}$$

where $\bar{x} = \frac{|x|}{v_0 t}$, $\lambda(s) = \frac{1}{v_0}\sqrt{\Delta^2 + 2\gamma s + s^2}$ and the function $\phi(s)$ given by

$$\phi(s) = s - \bar{x} v_0 \lambda(s). \tag{8.90}$$

For large t, we expect the integration in Eq. (8.89) to be dominated by the saddle point of $\phi(s)$. The saddle point is obtained by setting $\frac{d\phi}{ds} = 0$ which gives

$$s_+ = -\gamma + \sqrt{\frac{\gamma^2 - \Delta^2}{1 - \bar{x}^2}}. \tag{8.91}$$

Now for $t \to \infty$, we expand the function $\phi(s)$ about $s = s_+$ and perform the integration as follows:

$$\begin{aligned} P(x,t) &\simeq \frac{e^{t[\phi(s_+) - \Delta\bar{x}]}}{2\pi i} \left(\frac{\lambda(s_+) + \Delta}{2s_+}\right) \int_{\gamma_0 - i\infty}^{\gamma_0 + i\infty} ds\ e^{t\frac{\phi''(s_+)}{2}(s-s_+)^2}, \\ &\simeq \frac{e^{t[\phi(s_+) - \Delta\bar{x}]}}{2\pi} \left(\frac{\lambda(s_+) + \Delta}{2s_+}\right) \int_{-\infty + i(s_+ + \gamma_0)}^{\infty + i(s_+ + \gamma_0)} dy\ e^{-t\frac{\phi''(s_+)}{2}y^2} \\ &\simeq \frac{e^{t[\phi(s_+) - \Delta\bar{x}]}}{2\pi} \left(\frac{\lambda(s_+) + \Delta}{2s_+}\right) \int_{-\infty}^{\infty} dz\ e^{-t\frac{\phi''(s_+)}{2}z^2}, \end{aligned} \tag{8.92}$$

where, we have used $\phi''(s_+) = \frac{d\phi}{ds}|_{s_+} = \frac{(1-\bar{x})^{3/2}}{\bar{x}^2\sqrt{\gamma^2 - \Delta^2}}$ is greater than zero. Performing the integration gives the asymptotic behaviour of $P(x,t)$ as written in Eq. (4.20).

8.11 Derivation of $\mathcal{S}_m(t)$

In this appendix, we derive the expression of the probability $\mathcal{S}_m(t)$ that the RTP, starting from the origin, returns to the origin m-times in time t. For simplicity, let us take the initial velocity direction to be $+v_0$. Formally $\mathcal{S}_m(t)$ can be written as

$$\begin{aligned} \mathcal{S}_m(t) = &\int_0^t d\tau_1 F_+(\tau_1) \int_0^{t-\tau_1} d\tau_2 F_-(\tau_1) ... \\ &\times \int_0^{t - \sum_{i=0}^{m-1}\tau_i} d\tau_m F_{(-1)^{m-1}}(\tau_m)\ S_{(-1)^{m-1}}\left(0, t - \sum_{i=1}^{m}\tau_i\right), \end{aligned} \tag{8.93}$$

Here $F_\sigma(\tau_i)$ is the distribution of the first return time τ_i to the origin with initial velocity direction $\sigma_0 v_0$ where $\sigma_0 \in [+,-]$. Also, $S_\sigma(0,t_i)$ is the probability that the RTP has not returned to the origin till time t_i starting from the origin. Rationale for writing Eq. (8.93) is as follows: The RTP makes a first passage to the origin in the time interval $[\tau_1, \tau_1 + d\tau_1]$ which $F_+(\tau_1)d\tau_1$ in Eq. (8.93). Now it can reach the origin only with $-v_0$. Starting from the origin with $-v_0$, it again makes another first-passage return to the origin in the time interval $[\tau_1 + \tau_2, \tau_1 + \tau_2 + d\tau_2]$. This gives rise to $F_-(\tau_2)d\tau_2$ term in Eq. (8.93). Similarly, between $(m-1)$-th and m-th visits of duration τ_m, the RTP makes a first-passage return to the origin with initial velocity $(-1)^{m-1}v_0$.

As a result, we get $F_{(-1)^{m-1}}(\tau_m)d\tau_m$ term in Eq. (8.93). Once it does this m-th visit, it will no longer cross the origin in the remaining time interval $t - \sum_{i=1}^{m} \tau_i$. Hence, we get the survival probability $S_{(-1)^{m-1}}\left(0, t - \sum_{i=0}^{m} \tau_i\right)$. Note that both $F_{\sigma_0}(\tau)$ and $S_{\sigma_0}(0,\tau)$ are insensitive to the initial velocity direction σ_0 (shown later).

The convolution structure of Eq. (8.93) suggests us to take the Laplace transform with respect to $t \to s$. This equation then simplifies to

$$\bar{\mathcal{S}}_m(s) = \left[\bar{F}_{\sigma_0}(s)\right]^m \bar{S}_{\sigma_0}(0,s). \tag{8.94}$$

Here $\bar{F}_{\sigma_0}(s)$ and $\bar{S}_{\sigma_0}(0,s)$ represent the Laplace transforms of $F_{\sigma_0}(\tau)$ and $S_{\sigma_0}(0,\tau)$ respectively. Since $\bar{F}_{+}(s) = \bar{F}_{-}(s)$ and $\bar{S}_{+}(0,s) = \bar{S}_{-}(0,s)$, we have replaced the subscript '$\pm$' by common σ_0 in Eq. (8.94). To write these Laplace transforms, we use the results of [210] as follows:

$$\bar{S}_{\sigma_0}(0,s) = \frac{\lambda(s) - s}{s\gamma}, \quad \text{and} \quad \bar{F}_{\sigma_0}(s) = \frac{\gamma}{s + \gamma + \lambda(s)}, \tag{8.95}$$

where $\lambda(s) = \sqrt{s(s+2\gamma)}$. As remarked before, both these Laplace transforms do not depend on σ_0. Plugging these expressions in Eq. (8.94) yields

$$\bar{\mathcal{S}}_m(s) = \left(\frac{\lambda(s) - s}{s\gamma}\right)\left(\frac{\gamma}{s + \gamma + \lambda(s)}\right)^m. \tag{8.96}$$

Next using Eq. (5.30) to perform the inverse Laplace transformation, we get

$$\mathcal{S}_m(t) = e^{-\gamma t}\left[I_m(\gamma t) + I_{m+1}(\gamma t)\right]. \tag{8.97}$$

This matches with the expression of $\mathcal{S}_m(t)$ quoted in Eq. (5.32).

8.12 Derivation of $\bar{Q}(p,s)$ in Eq. (5.37) for general α

This appendix provides a derivation of the solution of the Laplace transform $\bar{Q}(p,x_0,s)$ of the local time distribution $P\left(T_{loc},x_0,t\right)$ for general α. This solution has been written in Eq. (5.37). To begin with, we rewrite the backward equation for $\bar{Q}(p,x_0,s)$ in Eq. (5.35) as

$$s\bar{Q} - 1 \simeq \mathfrak{D}_\alpha \frac{\partial}{\partial x_0}\left(\frac{1}{|x_0|^\alpha}\frac{\partial \bar{Q}}{\partial x_0}\right) - p\delta(x_0)\bar{Q}, \tag{8.98}$$

which for $x_0 \neq 0$ becomes

$$s\bar{Q} - 1 \simeq \mathfrak{D}_\alpha \frac{\partial}{\partial x_0}\left(\frac{1}{|x_0|^\alpha}\frac{\partial \bar{Q}}{\partial x_0}\right), \tag{8.99}$$

The inhomogeneous part can be removed by defining a new function $\mathcal{U}(p, x_0, s)$

$$\bar{Q}(p, x_0, s) = \frac{1}{s} + \mathcal{U}(p, x_0, s), \tag{8.100}$$

and rewriting Eq. (8.99) in terms of $\mathcal{U}$ as

$$s\,\mathcal{U} \simeq \mathfrak{D}_\alpha \frac{\partial}{\partial x_0}\left(\frac{1}{|x_0|^\alpha}\frac{\partial \mathcal{U}}{\partial x_0}\right). \tag{8.101}$$

In terms of this new function, the boundary conditions in Eq. (5.36) take the form $\mathcal{U}(p, x_0 \to \pm\infty, s) = 0$. As seen in Sec. 4.2.3, the solution of this differential equation is given in terms of the Bessel function as

$$\mathcal{U}(p, x_0, s) \simeq \mathcal{B}(p, s)|x_0|^{\frac{1+\alpha}{2}} K_{\frac{1+\alpha}{2+\alpha}}\left(\frac{2|x_0|^{\frac{2+\alpha}{2}}}{2+\alpha}\sqrt{\frac{s}{\mathfrak{D}_\alpha}}\right), \tag{8.102}$$

where the function $\mathcal{B}(p, s)$ does not depend of x_0 and needs to be computed. Retracting this solution in terms of $\bar{Q}(p, x_0, s)$ from Eq. (8.100) gives

$$\bar{Q}(p, x_0, s) \simeq \frac{1}{s} + \mathcal{B}(p, s)|x_0|^{\frac{1+\alpha}{2}} K_{\frac{1+\alpha}{2+\alpha}}\left(\frac{2|x_0|^{\frac{2+\alpha}{2}}}{2+\alpha}\sqrt{\frac{s}{\mathfrak{D}_\alpha}}\right). \tag{8.103}$$

To evaluate the function $\mathcal{B}(p, s)$, we integrate Eq. (8.98) from $-\eta$ to η and take $\eta \to 0^+$ which then gives the discontinuity relation

$$\left(\frac{1}{|x_0|^\alpha}\frac{\partial \bar{Q}}{\partial x_0}\right)_{x_0=0^+} - \left(\frac{1}{|x_0|^\alpha}\frac{\partial \bar{Q}}{\partial x_0}\right)_{x_0=0^-} = \frac{p}{\mathfrak{D}_\alpha}\,\bar{Q}(p, 0, s). \tag{8.104}$$

Plugging $\bar{Q}(p, x_0, s)$ from Eq. (8.103) in this discontinuity relation gives the expression of $\mathcal{B}(p, s)$ as

$$\mathcal{B}(p, s) = \frac{1}{s} - \frac{\mathcal{C}_\alpha}{s^{\frac{1}{2+\alpha}}\left(p + \mathcal{C}_\alpha s^{\frac{1+\alpha}{2+\alpha}}\right)}, \tag{8.105}$$

$$\text{with} \qquad \mathcal{C}_\alpha = 2\left(\frac{\mathfrak{D}_\alpha}{(2+\alpha)^\alpha}\right)^{\frac{1}{2+\alpha}} \frac{\Gamma\left(\frac{1}{2+\alpha}\right)}{\Gamma\left(\frac{1+\alpha}{2+\alpha}\right)}. \tag{8.106}$$

Eqs. (8.103) and (8.105) completely specifies the Laplace transform $\bar{Q}(p, x_0, s)$ for any x_0. However, since we are interested in $x_0 = 0$, we provide here only the expression of $\bar{Q}(p, s) = \bar{Q}(p, 0, s)$ as

$$\bar{Q}(p,s) \simeq \frac{\mathcal{C}_\alpha}{s^{\frac{1}{2+\alpha}}\left(p + \mathcal{C}_\alpha s^{\frac{1+\alpha}{2+\alpha}}\right)}, \tag{8.107}$$

This result has been quoted in Eq. (5.37).

8.13 Derivation of $f_\alpha(z)$ for finite z

We here derive the expression of the scaling function $f_\alpha(z)$ in Eq. (5.43) for the local time when z is finite. For this, we take the Laplace transformation in Eq. (5.40) and write it in the form of Bromwich integral as

$$P(T_{loc}, t) \simeq \int_{-i\infty}^{+i\infty} \frac{ds}{2\pi i} \frac{\mathcal{C}_\alpha}{s^{\frac{1}{2+\alpha}}} e^{t\Phi\left(s, \frac{\mathcal{C}_\alpha T_{loc}}{t}\right)}. \tag{8.108}$$

The factor $\mathcal{C}_\alpha$ is given in Eq. (5.38) and the function $\Phi(s, w)$ is defined as

$$\Phi(s,w) = s - w s^{\frac{1+\alpha}{2+\alpha}}, \tag{8.109}$$

As $t \to \infty$, the integral in Eq. (8.108) will be dominated by the saddle point of $\Phi(s, w)$ in s. wThe saddle point is obtained by solving the equation $\left(\frac{d\phi}{ds}\right)_{s_*} = 0$ which gives the solution

$$s_* = \left(\frac{1+\alpha}{2+\alpha}\right)^{2+\alpha} w^{2+\alpha}. \tag{8.110}$$

We will assume w to be finite throughout. Expanding $\Phi(s, w)$ around $s = s_*$ and retaining terms up to order $(s - s_*)^2$ in Eq. (8.108), we get

$$\begin{aligned} P(T_{loc}, t) &\simeq \frac{e^{t\Phi(s_*,w)}}{2\pi i} \frac{\mathcal{C}_\alpha}{s_*^{\frac{1}{2+\alpha}}} \int_{-i\infty}^{i\infty} ds\ e^{t\frac{\Phi''(s_*,w)}{2}(s-s_*)^2}, \\ &\simeq \frac{e^{t\Phi(s_*,w)}}{2\pi} \frac{\mathcal{C}_\alpha}{s_*^{\frac{1}{2+\alpha}}} \int_{-\infty+i(s_*)}^{\infty+i(s_*)} dy\ e^{-t\frac{\Phi''(s_*,w)}{2}y^2}, \\ &\simeq \frac{e^{t\Phi(s_*,w)}}{2\pi} \frac{\mathcal{C}_\alpha}{s_*^{\frac{1}{2+\alpha}}} \int_{-\infty}^{\infty} du\ e^{-t\frac{\Phi''(s_*,w)}{2}u^2}. \end{aligned} \tag{8.111}$$

We have used the notation $w = \frac{\mathcal{C}_\alpha T_{loc}}{t}$ and $\Phi''(s,w) = \frac{d^2\Phi}{ds^2}$. Using $\Phi''(s_*,w) = \frac{(2+\alpha)^{1+\alpha}}{(1+\alpha)^{2+\alpha}} \frac{1}{w^{2+\alpha}}$, we perform the integration in the last line explicitly to get the distribution $P(T_{loc},t)$

$$P(t_{loc},t) \simeq \frac{\mathcal{C}_\alpha}{t^{\frac{1+\alpha}{2+\alpha}}}\ f_\alpha\left(\frac{\mathcal{C}_\alpha T_{loc}}{t^{\frac{1+\alpha}{2+\alpha}}}\right) \tag{8.112}$$

with the scaling function $f_\alpha(z)$ given by

$$f_\alpha(z) \simeq \frac{z^{\frac{\alpha}{2}}}{\sqrt{2\pi}} \frac{(1+\alpha)^{\frac{\alpha}{2}}}{(2+\alpha)^{\frac{\alpha-1}{2}}}\ \exp\left(-\frac{(1+\alpha)^{1+\alpha}}{(2+\alpha)^{2+\alpha}}\ z^{2+\alpha}\right). \tag{8.113}$$

This expression works only for finite z and it fails for small values of z. We have presented this result in Eq. (5.44).

8.14 Derivation of $\langle x_\alpha^2(t)\rangle_c^{RTP}$ when $t \gg \tau_K$

In this appendix, we will analyse the expression of $\langle x_\alpha^2(t)\rangle_c^{RTP}$ in Eq. (6.33) for $t \gg \tau_K$ to obtain a more simplified expression in Eq. (6.36). For this, we first define an integral

$$\mathcal{J}_0\left(a\right) = \int_{-\pi}^{\pi} dq\left[\mathcal{G}(a,b_q,t)\right]. \tag{8.114}$$

Then, from Eq. (6.33), it follows that the variance is given by

$$\langle x_\alpha^2(t)\rangle_c^{RTP} \simeq \frac{v_0^2}{2\pi}\ \mathcal{J}_0(2\gamma). \tag{8.115}$$

Let us look at $\mathcal{J}_0\left(a\right)$ for $t \gg \tau_K$. By inserting $\mathcal{G}(a,b_q,t)$ from Eq. (6.30) in Eq. (8.114), we can rewrite $\mathcal{J}_0\left(a\right)$ as

$$\mathcal{J}_0\left(a\right) = \underbrace{\int_{-\pi}^{\pi} e^{-b_q t}\left[\frac{b_q\left\{e^{-b_q t} - 2e^{-at}\right\} + a}{b_q\left(b_q^2 - a^2\right)}\right]}_{\text{first term}} + \underbrace{\int_{-\pi}^{\pi} \frac{dq}{b_q(b_q+a)}}_{\text{second term}}. \tag{8.116}$$

Let us first calculate the first term. Using $b_q = 4K\sin^2\left(q/2\right)$, we find that this term is possesses integrals of the form $\sim \int dq\, \exp\left[-Kt\sin^2(q/2)\right]$ which in the limit $Kt \to \infty$ will be dominated by the small values of q. Therefore, approximating $b_q \simeq Kq^2$ and making the transformation

$w = \sqrt{2Kt}\, q$, this term becomes

$$\text{first term } \simeq \sqrt{\frac{t^3}{2K}} \int_{-\infty}^{\infty} e^{-w^2/2} \left[\frac{\frac{w^2}{2}\left(e^{-w^2/2} - 2e^{-at}\right) + at}{\frac{w^2}{2}\left(\frac{w^4}{4} - a^2t^2\right)} \right]. \tag{8.117}$$

To evaluate the second term in Eq. (8.116), we rewrite it as

$$\text{second term } = \sqrt{\frac{t^3}{2K}} \int_{-\pi\sqrt{2Kt}}^{\pi\sqrt{2Kt}} \frac{dw}{\frac{w^2}{2}\left(\frac{w^2}{2} + at\right)} + \Delta(t). \tag{8.118}$$

where the function $\Delta(t)$ is given by

$$\Delta(t) = \text{second term } - \sqrt{\frac{t^3}{2K}} \int_{-\pi\sqrt{2Kt}}^{\pi\sqrt{2Kt}} \frac{dw}{\frac{w^2}{2}\left(\frac{w^2}{2} + at\right)}, \tag{8.119}$$

$$= \int_{-\pi}^{\pi} \frac{dq}{b_q(b_q + a)} - \sqrt{\frac{t^3}{2K}} \int_{-\pi\sqrt{2Kt}}^{\pi\sqrt{2Kt}} \frac{dw}{\frac{w^2}{2}\left(\frac{w^2}{2} + at\right)}. \tag{8.120}$$

Numerically by plotting $\Delta(t)$ as a function of t, we find that it is a decreasing function of t. On the other hand, the other term in Eq. (8.118) increases with time. Hence, for large t, we can neglect $\Delta(t)$ in Eq. (8.118) in comparison to the other term. With this approximation, the second term becomes

$$\text{second term } \simeq \sqrt{\frac{t^3}{2K}} \int_{-\infty}^{\infty} \frac{dw}{\frac{w^2}{2}\left(\frac{w^2}{2} + at\right)}. \tag{8.121}$$

Substituting these approximate expressions of the first and second terms from Eqs.(8.117) and (8.121) in Eq. (8.116) gives

$$\mathcal{J}_0(a) \simeq \sqrt{\frac{t^3}{2K}} \int_{-\infty}^{\infty} dw\ \mathcal{G}\left(at, \frac{w^2}{2}, 1\right), \tag{8.122}$$

and following the relation in Eq. (8.115), we obtain the scaling form of $\langle x_\alpha^2(t)\rangle_c^{RTP}$ for $t \gg \frac{1}{K}$ as quoted in Eq. (6.36).

Bibliography

[1] L. Berthier and G. Biroli, Theoretical perspective on the glass transition and amorphous materials, *Rev. Mod. Phys.* **83**, 587 (2011).

[2] A. Dhar, Heat transport in low-dimensional systems, *Advances in Physics* **57**, 457 (2008).

[3] F. Bonetto, J. L. Lebowitz, and L. Rey-Bellet, Fourier's law: a challenge to theorists, in *Mathematical Physics*, A. Fokas, A. Grigoryan, T. Kibble, and B. Zegarlinski, eds., Imperial College Press, London, 128 (2000).

[4] S. Lepri, R. Livi, and A. Politi, Thermal conduction in classical low-dimensional lattices, *Physics Reports* **377**, 1-80 (2003).

[5] S. Ramaswamy, The mechanics and statistics of active matter, *Annu. Rev. Condens. Matter Phys.* **1**, 323-45 (2010).

[6] P. Romanczuk, M. Bär, W. Ebeling, B. Lindner and L. Schimansky-Geier, Active Brownian particles, *Eur. Phys. J.: Spec. Top.* **202**, 1162 (2012).

[7] M. C. Marchetti, J. F. Joanny, S. Ramaswamy S, T. B. Liverpool, J. Prost, M. Rao and A. R. Simha, Hydrodynamics of soft active matter, *Rev. Mod. Phys.* **85**, 1143 (2013).

[8] S. Ramaswamy, Active matter, *J. Stat. Mech.* **054002** (2017).

[9] F. Schweitzer, Brownian Agents and Active Particles Collective Dynamics in the Natural and Social Sciences *(Berlin: Springer, 2003)*.

[10] C. Bechinger, R. Di Leonardo, H. Löwen, C. Reichhardt, G. Volpe and G. Volpe, Active particles in complex and crowded environments, *Rev. Mod. Phys.* **88**, 045006 (2016).

[11] C. Gardiner, Stochastic Methods, 4th ed. *(Berlin, Springer-Verlag, 2009)*.

[12] N. G. Van Kampen, Stochastic Processes in Physics and Chemistry, *(Elsevier, Amsterdam, 2007)*.

[13] H. B. Callen, Thermodynamics and an Introduction to Thermostatistics, 2nd ed. *(Wiley, New York, 1985)*.

[14] R. Kubo, The fluctuation-dissipation theorem, *Rep. Prog. Phys.* **29**, 255-84 (1966).

[15] R. Kubo, M. Toda and N. Hashitsume, Statistical Physics: Nonequilibrium Statistical Mechanics 2nd ed. *(Berlin: Springer, 1992)*

[16] H. K. Lee, S. Lahiri and H. Park, Nonequilibrium steady states in Langevin thermal systems, *Phys. Rev. E* **96**, 022134 (2017).

[17] A. Einstein, On the movement of small particles suspended in stationary liquids required by the molecular-kinetic theory of heat, *Annal. der Physik* **17**, 549-560 (1905).

[18] R. Brown, A Brief Account of Microscopical Observations Made on the Particles Contained in the Pollen of Plants, *Phil. Mag.* **4**, 161 (1828).

[19] P. Langevin, On the Theory of Brownian Motion, Comptes Rendues 146, 530-533 (1908).

[20] W. Sutherland, A dynamical theory of diffusion for nonelectrolytes and the molecular mass of albumin, *Phil. Mag. S.* **9**, 781 (1905).

[21] U. Seifert, Entropy production along a stochastic trajectory and an integral fluctuation theorem, *Phys. Rev. Lett.* **95**, 040602 (2005).

[22] U. Seifert, Stochastic thermodynamics, fluctuation theorems and molecular machines, *Rep. Prog. Phys.* **75**, 126001 (2012).

[23] C. Van den Broeck and M. Esposito, Ensemble and trajectory thermodynamics: A brief introduction, *Physica A: Statistical Mechanics and its Applications*, **418**, 6 (2015).

[24] M. Baiesi, C. Maes and B. Wynants, Fluctuations and response of nonequilibrium states, *Phys. Rev. Lett.* **103**, 010602 (2009).

[25] M. Baiesi and C. Maes, An update on the nonequilibrium linear response, *New J. Phys.* **15**, 013004 (2013).

[26] M. J. Schnitzer, S. M. Block, H. C. Berg and E. M. Purcell, Strategies for chemotaxis, *Symp. Soc. Gen. Microbiol.* **46**, 15 (1990).

[27] J. Tailleur and M. E. Cates, Statistical Mechanics of Interacting Run-and-Tumble Bacteria, *Phys. Rev. Lett.* **100**, 218103 (2008).

[28] J. O`Byrne, Y. Kafri, J. Tailleur, F. van Wijland, Time irreversibility in active matter, from micro to macro, *Nature Reviews Physics* **4**, 167-183 (2022).

[29] H. C. Berg, E. coli in Motion (New York: Springer, 2003).

[30] M. S. Kumar and P. Philominathan, The physics of flagellar motion of E. coli during chemotaxis, *Biophys Rev.* **2**, 13-20 (2010).

[31] J. R. Howse, R. A. L. Joners, A. J. Ryan, T. Gough, R. Vafabakhsh and R. Golestanian, Self-Motile Colloidal Particles: From Directed Propulsion to Random Walk, *Phys. Rev. Lett.* **99**, 048102 (2007).

[32] R. Golestanian, T. B. Liverpool and A. Ajdari, Propulsion of a molecular machine by asymmetric distribution of reaction products, *Phys. Rev. Lett.* **94**, 220801 (2005).

[33] D. Yamada, T. Hondou and M. Sano, Coherent dynamics of an asymmetric particle in a vertically vibrating bed, *Phys. Rev. E* **67**, 040301(R) (2003).

[34] L. Walsh, C. G. Wagner, S. Schlossberg, C. Olson, A. Baskaran and N. Menon, Noise and diffusion of a vibrated self-propelled granular particle, *Soft Matter* **13**, 8964-8968 (2017).

[35] N. Kumar, H. Soni, S. Ramaswamy and A. K. Sood, Flocking at a distance in active granular matter, *Nature Communications* **5**, 4688 (2014)

[36] R. Dreyfus, J. Baudry, M. L. Roper, M. Fermigier, H. A. Stone and J. Bibette, Microscopic artificial swimmers, *Nature* **437**, 862 (2005).

[37] H. Jiang, N. Yoshinaga and Masaki Sano, Active Motion of a Janus Particle by Self-Thermophoresis in a Defocused Laser Beam, *Phys. Rev. Lett.* **105**, 268302 (2010).

[38] G. Gompper et al, The 2020 motile active matter roadmap *J. Phys.: Condens. Matter* **32**, 193001 (2020).

[39] I. Santiago, Nanoscale active matter matters: Challenges and opportunities for self- propelled nanomotors, *Nano Today* **19**, 11 (2018).

[40] J. Toner, Y. Tu and S. Ramaswamy, Hydrodynamics and phases of flocks, *Ann. Phys.* **318**, 170 (2005).

[41] T. Vicsek, A. Czirók, E. Ben-Jacob, I. Cohen and O. Shochet, Novel Type of Phase Transition in a System of Self-Driven Particles, *Phys. Rev. Lett.* **75**, 1226 (2005).

[42] M. Ballerini et al, Interaction ruling animal collective behavior depends on topological rather than metric distance: evidence from a field study, *Proc. Natl Acad. Sci. USA* **105**, 1232-7 (2008).

[43] Y. Katz, K. Tunstrøm, C. C. Ioannou, C. Huepe and I. D. Couzin, Inferring the structure and dynamics of interactions in schooling fish, *Proc. Natl Acad. Sci. USA* **108** 18720-5 (2011).

[44] M. E. Cates and J. Tailleur, Motility-induced phase separation, *Annu. Rev. Condens. Matter Phys.* **6**, 219-44 (2015).

[45] G. Gonnella, D. Marenduzzo, A. Suma and A. Tiribocchi, Motility-induced phase separation and coarsening in active matter, *Comptes Rendus Physique* **16** 316-31 (2015).

[46] B. Partridge and C. F. Lee, Critical motility-induced phase separation belongs to the Ising universality class, *Phys. Rev. Lett.* **123** 068002 (2019).

[47] L. Caprini, U. Marconi and A. Puglisi, Spontaneous velocity alignment in motility-induced phase separation, *Phys. Rev. Lett.* **124** 078001 (2020).

[48] A. P. Solon, Y. Fily, A. Baskaran, M. E. Cates, Y. Kafri, M. Kardar and J. Tailleur, Pressure is not a state function for generic active fluids, *Nature Physics* **11**, 673678 (2015).

[49] H. H. Wensink, J. Dunkel, S. Heidenreich, K. Drescher, R. E. Goldstein, H. Löwen and J. M. Yeomans, Meso-scale turbulence in living fluids, *Proc. Natl Acad. Sci. USA* **109**, 14308-14313 (2012).

[50] S. Heidenreich, J. Dunkel, S. H. L. Klapp and M. Bär, Hydrodynamic length-scale selection in microswimmer suspensions, *Phys. Rev. E* **94**, 020601(R) (2016).

[51] S. Mukherjee, R. K. Singh, M. James and S. S. Ray, Anomalous diffusion and Lévy walks distinguish active from inertial turbulence, *Phys. Rev. Lett.* **127**, 118001 (2021).

[52] E. M. Purcell, Life at low Reynolds number, *American Journal of Physics* **45**, 3 (1977).

[53] U. Basu, S. N. Majumdar, A. Rosso and G. Schehr, Long-time position distribution of an active Brownian particle in two dimensions, *Phys. Rev. E* **100**, 062116 (2019).

[54] U. Basu, S. N. Majumdar, A. Rosso and G. Schehr, Active Brownian motion in two dimensions, *Phys. Rev. E* **98**, 062121 (2018).

[55] C. Kurzthaler, C. Devailly, J. Arlt, T. Franosch, W. C.K. Poon, V. A. Martinez and A. T. Brown, Probing the Spatiotemporal Dynamics of Catalytic Janus Particles with Single-Particle Tracking and Differential Dynamic Microscopy, *Phys. Rev. Lett.* **121**, 078001 (2018).

[56] P. Pietzonka, K. Kleinbeck, and U. Seifert, Extreme fluctuations of active Brownian motion, *New J. Phys.* **18**, 052001 (2016).

[57] T. GrandPre and D. T. Limmer, Current fluctuations of interacting active Brownian particles, *Phys. Rev. E* **98**, 060601(R) (2018).

[58] I. Santra, U. Basu and S. Sabhapandit, Active Brownian motion with directional reversals, *Phys. Rev. E* **104**, L012601 (2021).

[59] A. Shee, A. Dhar and D. Chaudhuri, Active Brownian particles: mapping to equilibrium polymers and exact computation of moments, *Soft Matter* **16**, 4776-4787 (2020).

[60] I. Santra, U. Basu and S. Sabhapandit, Run-and-tumble particles in two dimensions: Marginal position distributions, *Phys. Rev. E* **101**, 062120 (2020).

[61] W. Stadje, The exact probability distribution of a two-dimensional random walk, *J. Stat. Phys.* **46**, 207-216 (1987).

[62] K. Martens, L. Angelani, R. Di Leonardo and L. Bocquet, Probability distributions for the run-and-tumble bacterial dynamics: An analogy to the Lorentz model, *Eur. Phys. J. E* **35**, 84 (2012).

[63] A. Di Crescenzo, B. Martinucci and S. Zacks, Telegraph Process with Elastic Boundary at the Origin, *Methodology and Computing in Applied Probability* **20**, 333352 (2018).

[64] G. Gradenigo, and S. N. Majumdar, A first-order dynamical transition in the displacement distribution of a driven run-and-tumble particle, *J. Stat. Mech.* **053206** (2019).

[65] K. Proesmans, R. Toral and C. Van den Broeck, Phase transitions in persistent and run-and-tumble walks, *Physica A* **552**, 121934 (2020).

[66] F. Mori, P. Le Doussal, S. N. Majumdar, and G. Schehr, Condensation transition in the late-time position of a run-and-tumble particle, *Phys. Rev. E* **103**, 062134 (2021).

[67] C. Monthus, Large deviations at various levels for run-and-tumble processes with space-dependent velocities and space-dependent switching rates, *J. Stat. Mech.* **083212** (2021).

[68] V. Zaburdaev, M. Schmiedeberg and H. Stark, Random walks with random velocities, *Phys. Rev. E* **78**, 011119 (2008).

[69] F. Mori, G. Gradenigo and S. N. Majumdar, First-order condensation transition in the position distribution of a run-and-tumble particle in one dimension, *J. Stat. Mech.* **103208** (2021).

[70] K. Malakar, V. Jemseena, A. Kundu, K. Vijay Kumar, S. Sabhapandit, S. N. Majumdar, S. Redner and A. Dhar, Steady state, relaxation and first-passage properties of a run-and-tumble particle in one-dimension, *J. Stat. Mech.* **043215** (2018).

[71] T. Demaerel and C. Maes, Active processes in one dimension, *Phys. Rev. E* **97**, 032604 (2018).

[72] K. Malakar, A. Das, A. Kundu, K. V. Kumar and A. Dhar, Steady state of an active Brownian particle in a two-dimensional harmonic trap, *Phys. Rev. E* **101**, 022610 (2020).

[73] I. Santra, U. Basu, and S. Sabhapandit, Direction reversing active Brownian particle in a harmonic potential, *Soft Matter* **17**, 10108-10119 (2021).

[74] A. Pototsky and H. Stark, Active Brownian particles in two-dimensional traps, *Eur. Phys. Lett.* **98** 50004 (2012).

[75] S. C. Takatori, R. De Dier, J. Vermant and J. F. Brady, Acoustic trapping of active matter, *Nature Comm.* **7**, 10694 (2016).

[76] O. Dauchot and V. Démery, Dynamics of a Self-Propelled Particle in a Harmonic Trap, *Phys. Rev. Lett.* **122**, 068002 (2019).

[77] L. Caprini, E. Hernández-García, C. López and U. M. B. Marconi, A comparative study between two models of active cluster-crystals, *Sci. Rep.* **9**, 16687 (2019).

[78] D. Chaudhuri and A. Dhar, Active Brownian particle in harmonic trap: exact computation of moments, and re-entrant transition, *J. Stat. Mech.* **013207** (2021).

[79] A. Dhar, A. Kundu, S. N. Majumdar, S. Sabhapandit and G. Schehr, Run-and-tumble particle in one-dimensional confining potentials: Steady-state, relaxation, and first-passage properties, *Phys. Rev. E* **99**, 032132 (2019).

[80] F. J. Sevilla, A. V. Arzola and E. P. Cital, Stationary superstatistics distributions of trapped run-and-tumble particles, *Phys. Rev. E* **99**, 012145 (2019).

[81] U. Basu, S. N. Majumdar, A. Rosso, S. Sabhapandit and G. Schehr, Exact stationary state of a run-and-tumble particle with three internal states in a harmonic trap, *J. Phys. A: Math. Theor.* **53** 09LT01 (2020).

[82] N. R Smith, P. Le Doussal, S. N. Majumdar and G. Schehr, Exact position distribution of a harmonically-confined run-and-tumble particle in two dimensions, Preprint arXiv:2207.10445 (2022).

[83] E. Fodor, C. Nardini, M. E. Cates, J. Tailleur, P. Visco and F. van Wijland, How Far from Equilibrium Is Active Matter?, *Phys. Rev. Lett.* **117**, 038103 (2016).

[84] D. Frydel, Intuitive view of entropy production of ideal run-and-tumble particles, *Phys. Rev. E* **105**, 034113 (2022).

[85] R. Garcia-Millan and G. Pruessner, Run-and-tumble motion in a harmonic potential: field theory and entropy production, *J. Stat. Mech.* **063203** (2021).

[86] P. Padmanabha, D. M. Busiello, A. Maritan and D. Gupta, Fluctuations of entropy production of a run-and-tumble particle, Preprint arXiv:2207.12091 (2022).

[87] N. Razin, Entropy production of an active particle in a box, *Phys. Rev. E* **102**, 030103 (2020).

[88] D. Mandal, K. Klymko and M. R. DeWeese, Entropy production and fluctuation theorems for active matter, *Phys. Rev. Lett.* **119**, 258001 (2017).

[89] C. Ganguly and D. Chaudhuri, Stochastic thermodynamics of active Brownian particles, *Phys. Rev. E* **88**, 032102 (2013).

[90] D. Chaudhuri, Active Brownian particles: Entropy production and fluctuation-response, *Phys. Rev. E* **90**, 022131 (2014).

[91] L. Angelani, R. Di Leonardo and M. Paoluzzi, First-passage time of run-and-tumble particles, *Eur. Phys. J. E* **37**, 59 (2014).

[92] F. Mori, P. Le Doussal, S. N. Majumdar and G. Schehr, Universal survival probability for a d-dimensional run-and-tumble particle, *Phys. Rev. Lett.* **124** 090603 (2020).

[93] F. Mori, P. Le Doussal, S. N. Majumdar and G. Schehr, Universal properties of a run-and-tumble particle in arbitrary dimension, *Phys. Rev. E* **102**, 042133 (2020)

[94] P. Le Doussal, S. N. Majumdar and G. Schehr, Noncrossing run-and-tumble particles on a line, *Phys. Rev. E* **100**, 012113 (2019).

[95] J. F. Rupprecht, O. Bénichou and R. Voituriez, Optimal search strategies of run-and-tumble walks, *Phys. Rev. E* **94**, 012117 (2016).

[96] A. Scacchi and A. Sharma, Mean first passage time of active Brownian particle in one dimension, *Mol. Phys.* **116** 460-4 (2018).

[97] E. Woillez, Y. Zhao, Y. Kafri, V. Lecomte and J. Tailleur, Activated escape of a self-propelled particle from a metastable state, *Phys. Rev. Lett.* **122**, 258001 (2019).

[98] E. Woillez, Y. Kafri and N. S. Gov, Active trap model, *Phys. Rev. Lett.* **124**, 118002 (2020).

[99] D. Wexler, N. S. Gov, K. Ø. Rasmussen and G. Bel, Dynamics and escape of active particles in a harmonic trap, *Phys. Rev. Research* **2**, 013003 (2020).

[100] L. Caprini, F. Cecconi and U. M. B. Marconi, Correlated escape of active particles across a potential barrier, *J. Chem. Phys.* **155**, 234902 (2021).

[101] D. Martin, J. O´Byrne, M. E. Cates, E. Fodor, C. Nardini, J. Tailleur and F. van Wijland, Statistical Mechanics of Active Ornstein Uhlenbeck Particles, *Phys. Rev. E* **103**, 032607 (2021).

[102] R. Fürth, Schwankungserscheinungen in der Physik, *Sammlung Vieweg, Braunschweig* (1920).

[103] G. I. Taylor, Diffusion by Continous Movements, *Proc. London Math. Soc.* **20**, 196 (1920).

[104] S. Goldstein, On Diffusion by Discontinuous Movements, and on the Telegraph Equation, *Q. J. Mech. Appl. Math.* **4**, 129 (1951).

[105] M. Kac, A stochastic model related to the telegrapher‘s equation, *Mt. Rocky, J. Math.* **4** 497 (1974).

[106] J. Masoliver and G. H. Weiss, Transport Equations in Chromatography with a Finite Speed of Signal Propagation, *Sep. Sci. Tech.* **26**, 279 (1991).

[107] D. J. Durian and J. Rudnick, Photon migration at short times and distances and in cases of strong absorption, *J. Opt. Soc. Am.* **14**, 235 (1997).

[108] M. Boguñá, J. M. Porrá and J. Masoliver, Persistent random walk model for transport through thin slabs, *Phys. Rev. E* **59**, 6517 (1999).

[109] G. H. Weiss, Some applications of persistent random walks and the telegraphers equation, *Physica A* **311**, 381-410 (2002).

[110] J. Masoliver and K. Lindenberg and G. H. Weiss, Continuous time persistent random walk: a review and some generalizations, *Eur. Phys. J. B* **90**, 107 (2017).

[111] J. Masoliver and G. H. Weiss, On the maximum displacement of a one dimensional diffusion process described by the telegraphers noise, *Physica A* **195**, 93100 (1993).

[112] J. Masoliver, J. M. Porrá and G. H. Weiss, Solutions of the telegraphers equation in the presence of traps, *Phys. Rev. A.* **45**, 2222 (1992).

[113] J. Masoliver, J. M. Porrá and G. H. Weiss, Solution to the telegraphers equation in the presence of reflecting and partly reflecting boundaries, *Phys. Rev. E.* **48**, 939 (1993).

[114] D. S. Dean, S. N. Majumdar and Hendrik Schawe, Position distribution in a generalized run-and-tumble process, *Phys. Rev. E* **103**, 012130 (2021).

[115] H. C. Berg and D. A. Brown, Chemotaxis in Escherichia coli analysed by three-dimensional tracking, *Nature* **239** 500-4 (1972).

[116] L. Turner, W. S. Ryu and H. C. Berg, Real-time imaging of fluorescent flagellar filaments, *J. Bacteriol.* **182** 2793-801 (2000).

[117] P. G. de Gennes, Chemotaxis: the role of internal delays, *Eur. Biophys. J.* **33** 691-3 (2004).

[118] J. Adler, A method for measuring chemotaxis and use of the method to determine optimum conditions for chemotaxis by Escherichia coli, *J. Gen. Microbiol.* **74** 77-91 (1973).

[119] S. Chatterjee, R. Silveira and Y. Kafri, Chemotaxis when bacteria remember: drift versus diffusion, *PLoS Comput. Biol.* **7**, e1002283 (2011).

[120] P. Lévy, Sur certains processus stochastiques homogénes, *Compos. Math.* **7**, 283-339 (1939).

[121] S. N. Majumdar, Brownian functionals in physics and computer science, *Curr. Sci.* **89** 2076 (2005).

[122] S. N. Majumdar, J. Randon-Furling, M. J. Kearney and Y. Marc, On the time to reach maximum for a variety of constrained Brownian motions, *J. Phys. A: Math. Theor.* **41**, 365005 (2008).

[123] M. Kac, On distributions of certain Wiener functionals, *Trans. Am. Math. Soc.* **65**, 1 (1949).

[124] M. Kac, *in Proceedings of the Second Berkeley Symposium on Mathematical Statistics and Probability, Berkeley, Vol. 189 (1950)*, edited by J. Neyman (University of California Press, Berkeley, 1951).

[125] G. Letac and L. Takács, "6230", *Am. Math. Mon.* **87**, 142 (1980).

[126] D. Hug, Random polytopes Stochastic Geometry, Spatial Statistics and Random Fields, *(Heidelberg: Springer, 2013)*

[127] J. Randon-Furling, S. N. Majumdar and Alain Comtet, Convex Hull of N Planar Brownian Motions: Exact Results and an Application to Ecology, *Phys. Rev. Lett.* **103**, 140602 (2009).

[128] S. N. Majumdar and A. Comtet, Local and Occupation Time of a Particle Diffusing in a Random Medium, *Phys. Rev. Lett.* **89**, 060601 (2002).

[129] S. Sabhapandit, S. N. Majumdar and A. Comtet, Statistical properties of functionals of the paths of a particle diffusing in a one-dimensional random potential, *Phys. Rev. E* **73**, 051102 (2006).

[130] T. E. Harris, Diffusion with "collisions" between particles, *J. Appl. Probab.* **2**, 323 (1965).

[131] D. W. Jepsen, Dynamics of a Simple ManyBody System of Hard Rods, *J. Math. Phys.* **6**, 405 (1965).

[132] P. L. Krapivsky, K. Mallick and T. Sadhu, Dynamical properties of single-file diffusion, *J. Stat. Mech.*, **P09007** (2015).

[133] E. Teomy and R. Metzler, Transport in exclusion processes with one-step memory: density dependence and optimal acceleration, *J. Phys. A: Math. Theor.* **52**, 385001 (2019).

[134] E. Teomy and R. Metzler, Correlations and transport in exclusion processes with general finite memory, *J. Stat. Mech.* **103211** (2019).

[135] M. Galanti, D. Fanelli and F. Piazza, Persistent random walk with exclusion, *Eur. Phys. J. B* **86**, 456 (2013).

[136] P. Dolai, A. Das, A. Kundu, C. Dasgupta, A. Dhar and K. V. Kumar, Universal scaling in active single-file dynamics, *Soft Matter* **16** 7077-87 (2020).

[137] W. Feller, An Introduction to Probability Theory and its Applications (New York: Wiley, 1968).

[138] G. Bel and E. Barkai, Weak Ergodicity Breaking in the Continuous-Time Random Walk, *Phys. Rev. Lett.* **94**, 240602 (2005).

[139] J. Randon-Furling and S. N. Majumdar, Distribution of the time at which the deviation of a Brownian motion is maximum before its first-passage time, *J. Stat. Mech.* **P10008** (2007).

[140] S. N. Majumdar, A. Rosso and A. Zoia, Time to reach the maximum for a random acceleration process, *J. Phys. A: Math. Theor.* **43** 115001 (2010).

[141] H. Boutcheng, T. Bouetou, T. W. Burkhardt, A. Rosso, A. Zoia and K. T. Crepin, Occupation time statistics of the random acceleration model, *J. Stat. Mech.* **053213** (2016).

[142] A. C. Barato, E, Roldán, I. A. Martínez and S. Pigolotti, Arcsine laws in stochastic thermodynamics, *Phys. Rev. Lett.* **121**, 090601 (2018).

[143] D. Charles and W. Rosemari, The arcsine law and the treasury bill futures market, *Financ. Anal. J.* **36**, 71-4 (1980).

[144] A. N. Shiryaev, Quickest detection problems in the technical analysis of the financial data, *Mathematical Finance Bachelier Congress 2000* (New York: Springer 2002) p 487.

[145] S. N. Majumdar and J. P. Bouchaud, Optimal time to Sell a Stock in black-Scholes model, *Quant. Finance* **8**, 753 (2008).

[146] T. Sadhu, M. Delorme and K. J. Wiese, Generalized arcsine laws for fractional Brownian motion, *Phys. Rev. Lett.* **120**, 040603 (2018).

[147] G. Schehr and P. Le Doussal, Extreme value statistics from the real space renormalization group: Brownian motion, Bessel processes and continuous time random walks, *J. Stat. Mech.* **P01009** (2010).

[148] P. Singh and A. Pal, Extremal statistics for stochastic resetting systems, *Phys. Rev. E.* **103**, 052119 (2021).

[149] J. Rambeau and G. Schehr, Extremal statistics of curved growing interfaces in 1+ 1 dimensions, *Eur. Phys. Lett.* **91** 60006 (2010).

[150] P. Singh, Extreme value statistics and arcsine laws for heterogeneous diffusion processes, *Phys. Rev. E.* **105**, 024113 (2022).

[151] F. Mori, S. N. Majumdar and G. Schehr, Time between the maximum and the minimum of a stochastic process, *Phys. Rev. Lett.* **123**, 200201 (2019).

[152] F. Mori, S. N. Majumdar and G. Schehr, Distribution of the time between maximum and minimum of random walks, *Phys. Rev. E.* **101**, 052111 (2020).

[153] A. Baldassarri, J. P. Bouchaud, I. Dornic and C. Godréche, Statistics of persistent events: an exactly soluble model, *Phys. Rev. E* **59**, R20 (1999).

[154] C. Godréche and J. M. Luck, Statistics of the occupation time of renewal processes, *J. Stat. Phys.* **104**, 489-524 (2001).

[155] S. Burov and E. Barkai, Residence time statistics for N renewal processes, *Phys. Rev. Lett.* **107**, 170601 (2011).

[156] A. Dhar and S. N. Majumdar, Residence time distribution for a class of Gaussian Markov processes, *Phys. Rev. E* **59** 6413-8 (1999).

[157] Y. Kasahara, Limit theorems of occupation times for Markov processes, *Publ. RIMS, Kyoto Univ.* **12** 801-18 (1977).

[158] S. N. Majumdar and D. S. Dean, Exact occupation time distribution in a non-Markovian sequence and its relation to spin glass models, *Phys. Rev. E* **66** 041102 (2002).

[159] J. Lamperti, An occupation time theorem for a class of stochastic processes, *Trans. Am. Math. Soc.* **88** 380-7 (1958).

[160] A. Comtet, F. Cornu and G. Schehr, Last-Passage Time for Linear Diffusions and Application to the Emptying Time of a Box, *J. Stat. Phys.* **181**, 1565-1602 (2020).

[161] S. N. Majumdar, A. Comtet and J. Randon-Furling, Random convex hulls and extreme value statistics, *J. Stat. Phys.* **138**, 955 (2010).

[162] F. Mori, S. N. Majumdar and G. Schehr, Distribution of the time of the maximum for stationary processes, *Eur. Phys. Lett.* **135**, 30003 (2021).

[163] S. Redner, A Guide to First-Passage Processes *(Cambridge: Cambridge University Press, 2001).*

[164] B. J. Worton, A Convex Hull-Based Estimator of Home-Range Size, *Biometrics* **51**, 1206-15 (1995).

[165] A. Reymbaut, S. N. Majumdar and A. Rosso, The convex hull for a random acceleration process in two dimensions, *J. Phys. A: Math. Theor.* **44**, 415001 (2011).

[166] S. N. Majumdar, F. Mori, H. Schawe and G. Schehr, Mean perimeter and area of the convex hull of a planar Brownian motion in the presence of resetting, *Phys. Rev. E* **103**, 022135 (2021).

[167] D. S. Grebenkov, Y. Lanoiselée and S. N. Majumdar, Mean perimeter and mean area of the convex hull over planar random walks, *J. Stat. Mech.* **103203** (2017).

[168] G. Claussen, A. K. Hartmann and S. N. Majumdar, Convex hulls of random walks: Large-deviation properties, *Phys. Rev. E* **91**, 052104 (2015).

[169] H. Schawe, A. K. Hartmann and S. N. Majumdar, Large deviations of convex hulls of self-avoiding random walks, *Phys. Rev. E* **97**, 062159 (2018).

[170] H. Schawe and A. K. Hartmann, Large Deviations of Convex Hulls of the "True" Self-Avoiding Random Walk, *J. Phys.: Conf. Ser.* **1290**, 012029 (2019).

[171] M. Chupeau, O. Bénichou and S. N. Majumdar, Mean perimeter of the convex hull of a random walk in a semi-infinite medium, *Phys. Rev. E* **92**, 022145 (2015).

[172] J. Kampf, G. Last and I. Molchanov, On the convex hull of symmetric stable processes, *Proc. Am. Math. Soc.* **140**, 2527-35 (2012).

[173] M. Luković, T. Geisel and S. Eule, Area and perimeter covered by anomalous diffusion processes, *New J. Phys.* **15**, 063034 (2013).

[174] E. Dumonteil, S. N. Majumdar, A. Rosso and A. Zoia, Spatial extent of an outbreak in animal epidemics, *Proc. Natl Acad. Sci. USA* **110**, 4239-44 (2013).

[175] R. Eldan, Volumetric properties of the convex hull of an n-dimensional Brownian motion, *Electron. J. Probab.* **19**, 1-34 (2014).

[176] Z. Kabluchko and D. Zaporozhets, Intrinsic volumes of Sobolev balls with applications to Brownian convex hulls, *Trans. Am. Math. Soc.* **368**, 8873-99 (2016).

[177] H. Schawe, A. K. Hartmann and S. N. Majumdar, Convex hulls of random walks in higher dimensions: A large-deviation study, *Phys. Rev. E* **96**, 062101 (2017).

[178] A. K. Hartmann, S. N. Majumdar, H. Schawe and G. Schehr, The convex hull of the run-and-tumble particle in a plane, *J. Stat. Mech.* **053401** (2020).

[179] A. Cauchy, Mémoire sur la rectification des courbes et la quadrature des surfaces courbées, *(Paris: Chez de Bure fréres, 1832)*

[180] F. Pollaczek, Fonctions caractéristiques de certaines répartitions d'efinies au moyen de la notion d'ordre. Application á la théorie des attentes, *Comptes Rendus* **234**, 2334 (1952)

[181] S. N. Majumdar, Universal first-passage properties of discrete-time random walks and Lévy flights on a line: Statistics of the global maximum and records, *Physica A* **389** 4299 (2010).

[182] S. N. Majumdar and A. Comtet, Precise asymptotics for a random walker's maximum, *J. Stat. Mech.* **P06013** (2005).

[183] E. Sparre Andersen, On the fluctuations of sums of random variables II *Math. Scand.* **2**, 195-223 (1954).

[184] A. M. Andrew, Another efficient algorithm for convex hulls in two dimensions, *Inf. Process. Lett.* **9**, 216 (1979).

[185] S. G. Akl and G. T. Toussaint, A fast convex hull algorithm, *Inf. Process. Lett.* **7**, 219-22 (1978).

[186] L. Angelani and R. Garra, Run-and-tumble motion in one dimension with space-dependent speed, *Phys. Rev. E* **100**, 052147 (2019).

[187] P. Le Doussal, S. N. Majumdar and G. Schehr, Velocity and diffusion constant of an active particle in a one dimensional force field, *Eur. Phys. Lett.* **130**, 40002 (2020).

[188] S. Dev and S. Chatterjee, Run-and-tumble motion with steplike responses to a stochastic input, *Phys. Rev. E* **99** 012402 (2019).

[189] L. G. Nava, R. Großmann and F. Peruani, Markovian robots: minimal navigation strategies for active particles, *Phys. Rev. E* **97** 042604 (2018).

[190] N. Razin, R. Voituriez and N. S. Gov, Signatures of motor susceptibility to forces in the dynamics of a tracer particle in an active gel, *Phys. Rev. E* **99**, 022419 (2019).

[191] N. Razin, R. Voituriez, J. Elgeti and N. S. Gov, Generalized Archimedes' principle in active fluids, *Phys. Rev. E* **96**, 032606 (2017).

[192] M. A. Rivero, R. T. Tranquillo, H. M. Buettner and D. A. Lauffenburger, Transport models for chemotactic cell populations based on individual cell behavior, *Chem. Eng. Sci.* **44**, 2881-97 (1989).

[193] M. J. Schnitzer, Theory of continuum random walks and application to chemotaxis, *Phys. Rev. E* **48**, 2553 (1993).

[194] F. D. C. Farrell, C. Marchetti, D. Marenduzzo and J. Tailleur, Pattern formation in self-propelled particles with density-dependent motility, *Phys. Rev. Lett.* **108**, 248101 (2012).

[195] A. Solon, J. Stenhammar, M. E. Cates, Y. Kafri and J. Tailleur, Generalized thermodynamics of phase equilibria in scalar active matter, *Phys. Rev. E* **97**, 020602 (2018).

[196] G. Wilemski and M. Fixman, General theory of diffusioncontrolled reactions, *J. Chem. Phys.* **58**, 4009 (1973).

[197] O. Benichou, M. Coppey, J. Klafter, M. Moreau and G. Oshanin, Mean joint residence time of two Brownian particles in a sphere, *J. Phys. A: Math. Gen.* **38**, 7205 (2005).

[198] M. Doi, Theory of diffusion-controlled reaction between non-simple molecules. I, *Chem. Phys.* **11**, 107 (1975).

[199] S. I. Temkin and B. I. Yakobson, Diffusion-controlled reactions of chemically anisotropic molecules, *J. Phys. Chem.* **88**, 2679 (1984).

[200] A. Pal, I. P. Casuntilo and A. Kundu, Motion of a Brownian particle in the presence of reactive boundaries, *Phys. Rev. E* **100**, 042128 (2019).

[201] G. Kishore and A. Kundu, Local time of an OrnsteinUhlenbeck particle, *J. Stat. Mech.* **033218** (2021).

[202] S. Carmi, L. Turgeman and E. Barkai, On Distributions of Functionals of Anomalous Diffusion Paths, *J. Stat. Phys.* **141**, 1071 (2010).

[203] G. Louchard, Kac's formula, Levy's local time and Brownian excursion, *J. Appl. Probab.* **21**, 479 (1984).

[204] M. Csorgo, Z. Shi and M. Yor, Some Asymptotic Properties of the Local Time of the Uniform Empirical Process, *Bernoulli* **5**, 1035 (1999).

[205] D. S. Grebenkov, Residence times and other functionals of reflected Brownian motion, *Phys. Rev. E* **76**, 041139 (2007).

[206] A. Comtet, J. Desbois and S. N. Majumdar, The local time distribution of a particle diffusing on a graph, *J. Phys. A: Math. Gen.* **35**, L687 (2002).

[207] A. Pal, R. Chatterjee, S. Reuveni and A. Kundu, Local time of diffusion with stochastic resetting, *J. Phys. A: Math. Theor.* **52**, 264002 (2019).

[208] P. Singh and A. Pal, First-passage Brownian functionals with stochastic resetting, *J. Phys. A: Math. Theor.* **55**, 234001 (2022).

[209] A. A. Balkema and K. L. Chung, Seminar on Stochastic Processes, 1991, *Progress in Probability (Birkhuser, Boston, MA, 1992).*

[210] H. Bateman, Tables of Integral Transforms *(Mcgraw-Hill Book Company, New York, 1954).*

[211] E. W. Montroll and J. T. Bendler, On Lévy (or stable) distributions and the Williams-Watts model of dielectric relaxation, *J. Stat. Phys.* **34**, 129 (1984).

[212] C. Rödenbeck, J. Kärger and K. Hahn, Calculating exact propagators in single-file systems via the reflection principle, *Phys. Rev. E* **57**, 4382 (1998).

[213] E. Barkai and R. Silbey, Theory of Single File Diffusion in a Force Field, *Phys. Rev. Lett.* **102**, 050602 (2009).

[214] C. Hegde, S. Sabhapandit and A. Dhar, Universal Large Deviations for the Tagged Particle in Single-File Motion, *Phys. Rev. Lett.* **113**, 120601 (2014).

[215] S. Put, J. Berx and C. Vanderzande, Non-Gaussian anomalous dynamics in systems of interacting run-and-tumble particles, *J. Stat. Mech.* **123205** (2019).

[216] N. Samanta and R. Chakrabarti, Chain reconfiguration in active noise, *J. Phys. A: Math. Theor.* **49**, 195601 (2016).

[217] S. Chaki and R. Chakrabarti, Enhanced diffusion, swelling, and slow reconfiguration of a single chain in non-Gaussian active bath, *J. Chem. Phys.* **150**, 094902 (2019).

[218] H. Vandebroek and C. Vanderzande, Dynamics of a polymer in an active and viscoelastic bath, *Phys. Rev. E* **92** 060601 (2015).

[219] D. Osmanović and Y. Rabina, Dynamics of active Rouse chains, *Soft Matter* **13**, 963-8 (2017).

[220] D. Osmanović, Properties of Rouse polymers with actively driven regions, *J. Chem. Phys.* **149**, 164911 (2018).

[221] L. Lizana, T. Ambjörnsso, A. Taloni, E. Barkai and M. A. Lomholt, Foundation of fractional Langevin equation: Harmonization of a many-body problem, *Phys. Rev. E* **81**, 051118 (2010).

[222] R. Rajesh and S. N. Majumdar, Exact tagged particle correlations in the random average process, *Phys. Rev. E* **64**, 036103 (2001).

[223] J. Cividini, A. Kundu, S. N. Majumdar and D. Mukamel, Exact gap statistics for the random average process on a ring with a tracer, *J. Stat. Mech.* **053212** (2016).

[224] A. Kundu and J. Cividini, Exact correlations in a single-file system with a driven tracer, *Eur. phys. Lett.* **115**, 54003 (2016).

[225] A. Ponet, O. Bénichou, V. Démery and G. Oshanin, N-tag probability law of the symmetric exclusion process, *Phys. Rev. E* **97** 062119 (2018).

[226] A. Ponet, O. Bénichou, V. Démery and G. Oshanin, Bath-mediated interactions between driven tracers in dense single files, *Phys. Rev. Res.* **1** 033089 (2019).

[227] U. Basu and C. Maes, Nonequilibrium Response and Frenesy, *J. Phys.: Conf. Ser.* **638** 012001 (2015).

[228] A. Murali, P. Dolai, A. Krishna, K. Vijay Kumar and S. Thutupalli, arXiv:2101.00571 (2021).